Condensed Thiadiazoloquinoxalines (TQs) for Polymers and Small Molecules

Dissertation

Zur Erlangung des Grades

" Doktor der Naturwissenschaften"

am Fachbereich Chemie, Pharmazie und Geowissenschaften der

Johannes Gutenberg-Universität in Mainz

Cunbin An

Geboren in Henan Province, China

Mainz, 2015

Dekan: ████████████

1. Berichterstatter: ████████████████████

2. Berichterstatter: ████████████████

Tag der mündlichen Prüfung: 17.09.2015

Dedicated to my family

Table of Contents

Abbreviations

Å	angstrom
1,2-DCE	1,2-dichloroethane
1D	one-dimensional
2D	two-dimensional
2DWAXS	two-dimensional wide angle scattering
ΔE	energy gap
μ_h	hole mobility
μ_e	electron mobility
AcOH	acetic acid
a. u.	arbitrary unit
B3LYP	Becke, three-parameter, Lee-Yang-Parr
BLA	bond length alternation
br	broad (NMR signal)
CV	cyclic voltammetry
d	doublet (NMR signal)
dd	doublet of doublets (NMR signal)
DCM	dichloromethane
DFT	density functional theory
DMF	N,N-dimethylformamide
DSC	differential scanning calorimetry
EA	electron affinity
ESI+	electrospray positive ionization
eV	electron volt
Fc	ferrocene
FD-MS	field desorption mass spectrometry
FF	fill factor
FWHM	full width at half maximum
GIWAXS	grazing incident X-ray wide angle scattering
GPC	gel permeation chromatography

h	hour
HRMS	high resolution mass spectrometry
HMDS	hexamethyldisilazane
HOMO	highest occupied molecular orbital
ICT	intramolecular charge transfer
I_D	drain current
I_{on}/I_{off}	current on/off ratio
IP	ionization potential
I_{ph}	photocurrent
ITO	indium tin oxide
J_{sc}	short circuit current
LDA	lithium diisopropylamide
LEFET	light-emitting FET
LUMO	lowest unoccupied molecular orbital
m	multiplet (NMR signal)
M_n	number-average molecular weight
M_w	weight-average molecular weight
MW	microwace
NBS	N-bromosuucinimide
NIR	near infrared
nm	nanometer
OD	optical density
OFETs	organic field-effect transistors
OLEDs	organic light emitting diodes
OPTs	organic phototransistors
OPVs	organic photovoltaics
P3AT	poly (3-alkylthiophene)
P3HT	poly(3-hexylthiophene)
PCE	power conversion efficiency
PDI	polydispersity index
PL	photoluminescence

ppm	parts per million
PPV	poly(*para*-phenylene vinylene)
P_R	photoresponsivity
P_S	photosensitivity
q_{xy}	the in-plane scattering vector
q_z	the out-of-plane scattering vector
RFID	radio frequency identification tag
rpm	revolutions per minute
r.t.	room temperature
s	singlet (NMR signal)
SAM	self-assembled monolayers
SFM	scanning force microscopy
t	triplet (NMR signal)
TCB	1,2,4-trichlorobenzene
THF	tetrahydrofuran
TGA	thermogravimetric analysis
TIPS	triisopropylsilyl
TLC	thin layer chromatography
TMEDA	tetramethylethylenediamine
TQ	thiadiazoloquinoxaline
UV-vis-NIR	ultraviolet-visible-near infrared
V	volt
V_D	source-drain voltage
V_G	gate voltage
V_{oc}	open circuit voltage
V_T	threshold voltage

Chapter 1. Introduction

1.1 General background

Conjugated materials have been paid more and more attention in organic light-emitting diodes (OLEDs),[1] organic photovoltaic cells (OPVs)[2] and organic field-effect transistors (OFETs),[3] due to their potential applications in displays, energy storage and conversion, as well as radio frequency identification tags (RFID). In comparison with the traditional silicon based materials, organic conjugated materials provide many advantages including low cost, light weight and flexibility. Particularly important is the low-temperature solution processing, which is a crucial issue for the industrial interest of large-scale roll-to-roll electronic devices. Maybe the organic electronics don't completely replace the inorganic materials, but their multifunctional applications like light-emitting FETs (LEFETs) are real advantages over inorganic materials.

Since the first conjugated polymer poly(*para*-phenylene vinylene) (PPV) (**P1**, Chart 1) was reported as the active layer in OLEDs,[4] organic chemists have explored a tremendous amount of conjugated polymers for applications in OLEDs, OPVs and OFETs. They carefully adjusted molecular lowest unoccupied molecular orbital (LUMO), highest occupied molecular orbital (HOMO) and energy band gap. These factors play very important roles in different electronic devices. Some reasons are listed: (1) The HOMO levels determine the material ambient stability. (2) The energy band gap can change the emitting colors of polymers, which is very important for application in OLEDs. (3) Tuning the LUMO and HOMO energy levels of polymers to match their corresponding acceptors or donors can significantly influence power conversion efficiency (PCE) in OPVs. (4) LUMO energy level of polymers can determine material charge transport behavior (p-type, n-type, and ambipolar). (5) The very low band gap polymers are beneficial for transporting holes and electrons in OFETs but also as near-infrared dyes. Beside the above mentioned points, the modification of side chains is

also paid more attention, because they can significantly improve solubility, molecular weight and morphology, further enhancing device performance.

1.2 Strategies for tailoring polymer bandgaps

In order to develop the ideal materials for special applications, the LUMO and HOMO energy levels and energy band gaps of polymers need to be precisely tailored. However, the exact control of them is not a simple process, because many factors, which are related to each other, determine the final molecular bandgap. Herein several methods are summarized to discuss how to tune the band gap of polymers. The first one introduces aromatic backbone which can form the quinoid character in polymer chain. The second one optimizes the topology and geometry of polymers by tuning different linkage patterns and substituents in polymers, and the last method is fashion design at present, namely, alternating donor and acceptor (D-A) copolymer systems.

1.2.1 Resonance structures of polymeric units

The electron delocalization along the conjugated backbone converts the double bonds to single bonds, at the same time, transforms single bonds into double bonds, to form a resonance structure with quinoid character. The quinoid structures are less stable than aromatic structures. Formation of a quinoid structure requires destruction of the aromaticity and a loss in the stabilization energy, thereby narrowing the band gap. The bond length alternation (BLA) is the parameter to describe the ratio of the aromatic to quinoid population. It needs to be mentioned that the quinoid character increases with reducing BLA value.[5] Chart 1.1 presents five polymers, which have two possible resonance structures (aromatic and quinoid structures) in the ground state. Poly(*para*-phenylene) (**P1**) has a large energy band gap between 3.0 and 3.5 eV,[6] due to the large BLA between the benzene units. After introducing ethylene spacers between benzene units to reduce the aromatic stabilization energy, the band gap of poly(*para*-phenylenevinylene) (**P2**) decreases to 2.5 eV.[5] When the benzene unit is replaced by thiophene in **P1**, which has a lower aromaticity than benzene, the

band gap of polythiophene (**PT**, **P3**) is further reduced to 2.0 eV.[7] The aromatic structures of three polymers as above mentioned provide more contribution than quinoid structures. As a breakthrough work in developing low band gap polymers, Wudl and coworkers reported a poly(isothianaphthene) (**P4**) with a band gap of ~1 eV due to efficient increase of the quinoid character.[8] Heterocyclic unit replacement in **P4**, on the other hand, a slightly lower band gap of 0.95 eV was achieved in poly(thieno[3,4-b]pyrazine) (**P5**), due to the formation of more stabilized quinoid structure.[9]

P1 (PPP)	ΔE ~ 3.0 - 3.5 eV
P2 (PPV)	ΔE ~ 2.5 eV
P3 (PT)	ΔE ~ 2.0 eV
P4 (PITN)	ΔE ~ 1.0 eV
P5 (PDHTP)	ΔE ~ 0.95 eV
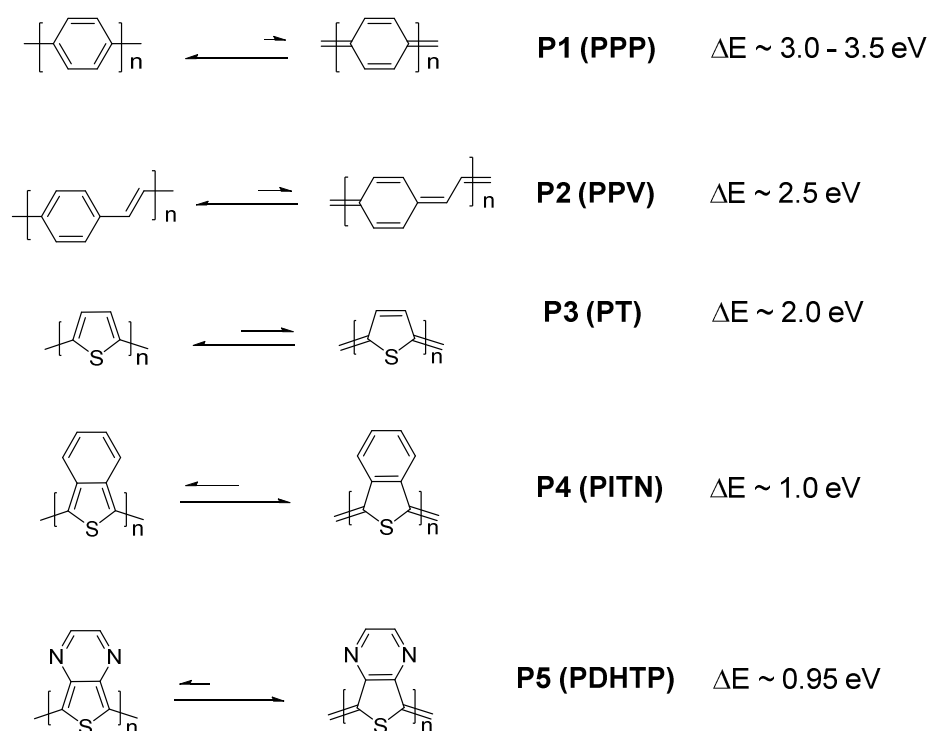
Chart 1.1 Aromatic and quinoid resonance structures for low band gap polymers.

1.2.2 Topology and geometry

The band gaps of polymers are significantly affected by their topologies. Three different linkages (*ortho*, *meta* and *para* positions) of poly(phenylenevinylene)s are shown in Chart 1.2. **P6-P8** were early studied by theoretical calculations[10] and their band gaps were measured as shown in Figure 1.1. For the same repeating unit of polymer, the order of the band gap is **P8**

(*p*-polymer) < **P7** (*o*-polymer) < **P6** (*m*-polymer). The corresponding soluble polymers **P9-P11** with different linkages were synthesized by Wittig reaction.[11] The UV-vis spectra showed the maximum absorption wavelength (λ_{max}) at 330, 340 and 380 nm, for **P9**, **P10** and **P11**, respectively. Their optical bandgaps enlarged with **P11** (*p*-polymer) < **P10** (*o*-polymer) < **P9** (*m*-polymer), which was in agreement with **P6-P8**. These theoretical calculations and experiment results confirmed that *para* linkages of polymers were beneficial for π electron delocalization in the conjugated backbone, yielding a lower bandgap, while *meta* linkages strongly interrupt π electron delocalization, leading to large bandgap. It should be noted these polymers possess the identify molecular formula of the conjugated backbones.
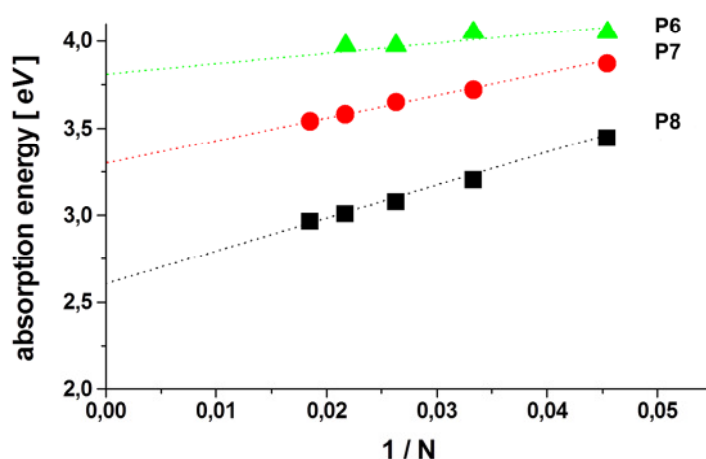
Figure 1.1 The optical bandgaps of oligomeric units of **P6-P8** vs reciprocal number of repeating units (This figure was provided by Prof. Martin Baumgarten, unpublished result).

Diketopyrrolopyrrole (DPP) monomer can be polymerized by 3,6 or 2,5-aryl substituents to produce the corresponding copolymers (Chart 1.2). The different linkage patterns of DPP-based polymers (**P12** and **P13**) were prepared using electropolymerization.[12] The one repeating unit of **P12** shows a bathochromic shift of 40 nm at the λ_{max} compared to monomeric **P13** in dichloromethane solutions. After electropolymerization, the λ_{max} of **P12** has a large red-shift of 138 nm compared to **P13** in the films. It implied that the π-conjugation of DPP–based polymers was disrupted when the lactam N-atoms of DPP were introduced into the conjugated backbone. That is why all of the high performing DPP-based polymers were always obtained by polymerization at 3,6-aryl positions.
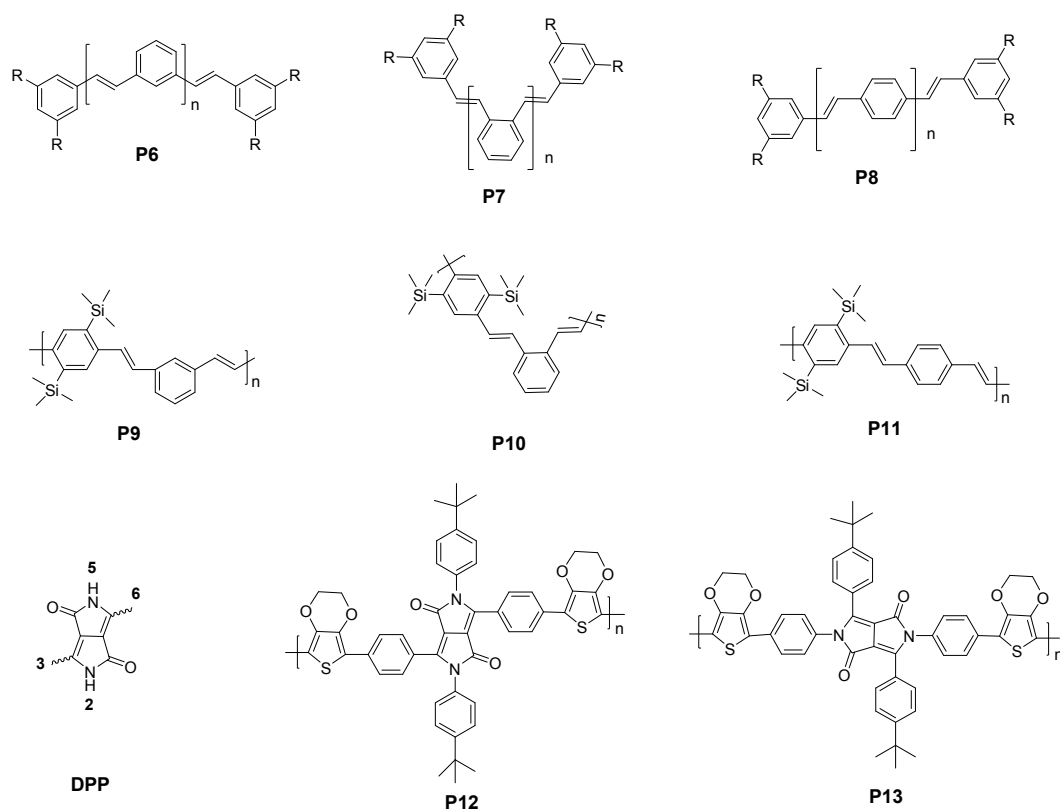
Chart 1.2 Extending conjugations in phenylenevinylene-based and DPP-based polymers by different linkages.

Tuning the polymer geometries is another important method to control the polymer bandgaps. The insolubility of unsubstituted **PT** made them unavailable for standard characterizations and applications, the first soluble substituted **PT** was reported by grafting an alkyl chain onto the 3-position of thiophene.[13] However, due to the asymmetrical 3-alkylthiophene, the dimerization can produce three different configurations as shown in Chart 1.3.[14] The 2-position and 5-position are noted as the "head" and "tail", respectively. For the dimerization, the dimer can be joined in head-to-head (HH), head-to-tail (HT), and tail-to-tail (TT).[15] Further, trimerization has four different combinations. It can be envisaged a more intricate arrangement for poly (3-alkylthiophene) (**P3AT**) without regiochemical control. The previous polymerization methods, electrochemical polymerization, Kumada coupling and FeCl$_3$-catalyzed reaction, were not regiocontrolled during the polymerization, thus producing the corresponding polymers within high degree of disorder. The UV-vis spectra in solution exhibited λ$_{max}$ at 428 and 436 nm for 50% and 70% HT coupling, respectively.[16,17] The HT

coupling of **P3ATs** can be determined by ^{1}H-NMR, there is only one signal at 6.98 nm, which belongs to the 4-position proton on the thiophene ring. Whereas the regioirregular **P3ATs** revealed four signals in the aromatic region that can be attributed to the protons on the 4-positions of the central thiophene ring in each trimer: HT-HT (δ = 6.98 nm), TT-HT (δ = 7.00 nm), HT-HH (δ = 7.03 nm), TT-HH (δ = 7.05 nm).[18,19] In order to develop new synthetic methods towards regioregular (rr) **P3ATs**, three methods (McCullough method,[20] Rieke method[16] and Grignard metathesis method[21,22]) were reported to afford more than 95% HT coupling in succession, their corresponding λ_{max} in solutions were achieved in a region of 440-460 nm. Notable, the λ_{max} of **P3ATs** not only depended on the regioregularity, but was affected by the degree of polymerization and the alkyl chain.
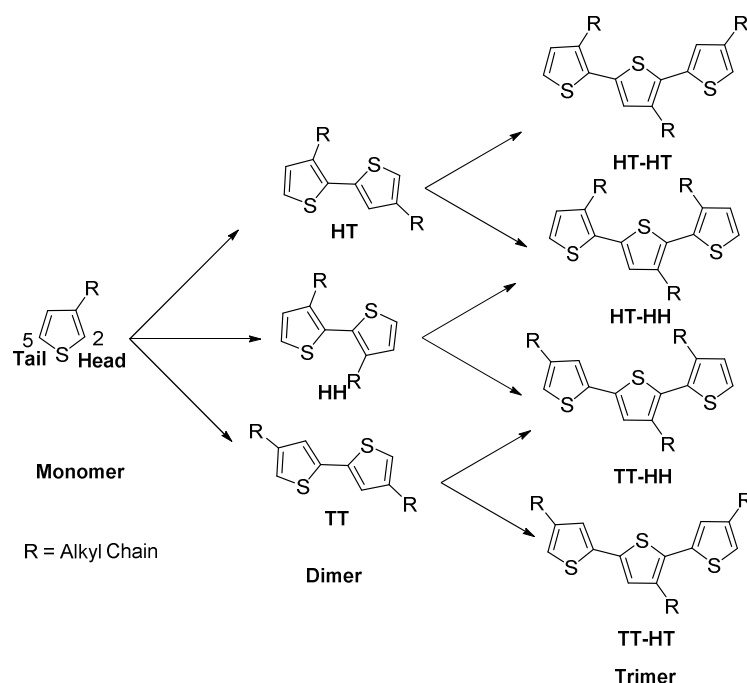
Chart 1.3 Description the regioisomers of 3-alkylthiophene.[23]

1.2.3 D-A alternating copolymers

In order to develop low bandgap semiconducting polymers, Havinga and coworkers designed a new approach using alternating donor and acceptor moieties to construct the conjugated chain.[24] They used squaric acid and croconic acid as strong acceptors to polymerize with few donors by polycondensation reaction. In spite of low molecular weights

of these polymers, extremely low bandgaps of such polymers were indeed achieved with $E_g <$ 0.5 eV. It was the first time to introduce the donor-acceptor (D-A) concept. Up to date the D-A approach has proved to be one of the most successful methods in developing low bandgap polymers. The LUMO and HOMO energy levels of the resulting polymers were determined by the LUMO of the acceptor moiety and the HOMO of the donor moiety, respectively (Figure 1.2). Their bandgaps can be further decreased with increasing the degree of polymerization. In comparison with homopolymers, more importantly, the bandgaps and energy levels of D-A alternating polymers can be tailored by varying donor or acceptor moieties. Additionally, the energy levels of D-A polymers can be further adjusted by modifying the substitution on donor and acceptor units with electron donating or withdrawing functional groups. Due to this unique feature of D-A copolymers, they have been widely used in organic electronics, especially in OFETs and OPVs.
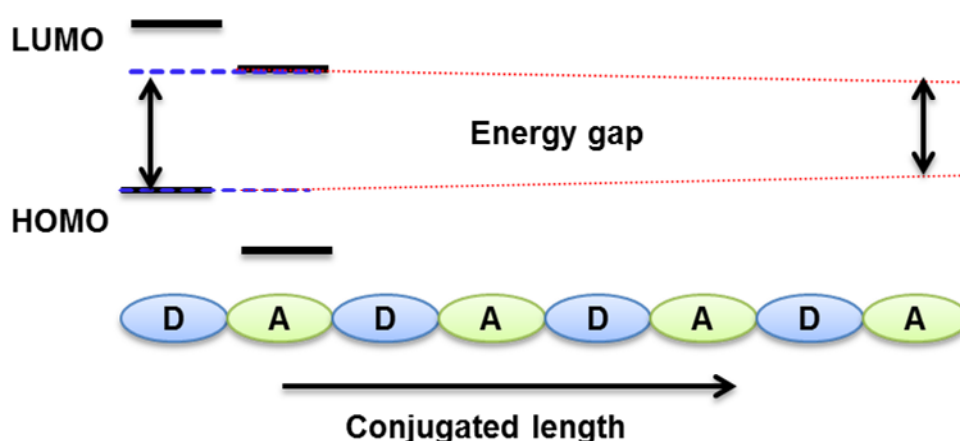
Figure 1.2 Schematic illustration of the bandgap engineering of D-A copolymer.
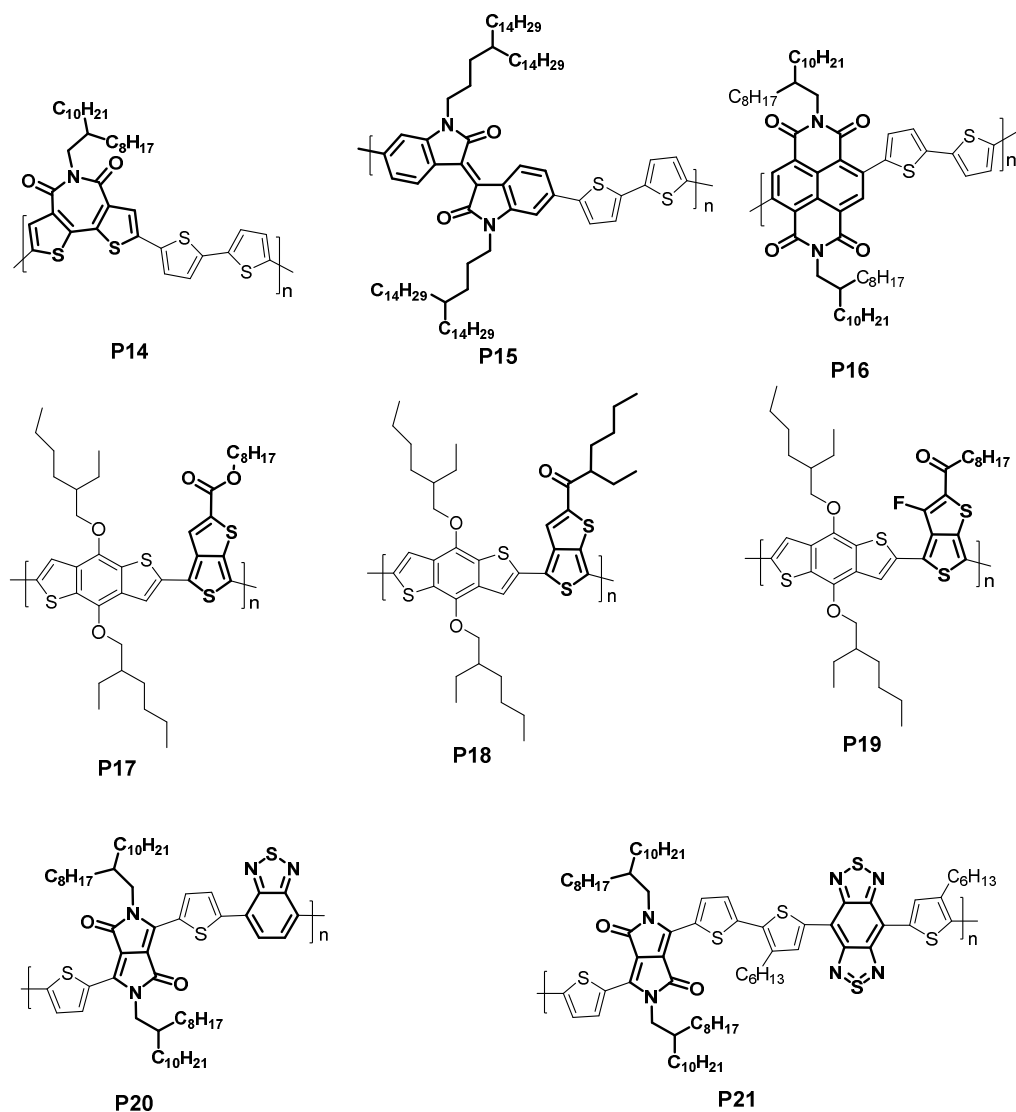
Chart 1.4 The bithiophene-based polymers containing different acceptors (**P14-P16**), the thieno[3, 4-b]thiophene-based polymers (**P17-P19**), and the dual-acceptor polymers (**P20-P21**).

It was proven that the charge transportation behaviors of D-A polymers depend on the affinity nature of acceptors in OFETs.[25] For example, three D-A copolymers **P14-P16** were synthesized using Stille coupling reaction, between bithiophene and different acceptor units (Chart 1.4).[26-28] The corresponding data are summarized in Table 1.1. The electron affinity (EA) of thiophene-acceptor-thiophene type of bithiophene-imide, isoindigo, and naphthalenediimide were -3.11,[26] -3.45,[29] and -3.73 eV,[30] respectively. Due to the varying electron withdrawing groups, these polymers have remarkable differences in the absorption

profile, bandgap, energy levels and charge carrier transport. Going from **P14**, **P15** to **P16**, the optical bandgap reduced from 1.9, 1.57 to 1.45 eV, especially the EA values were significantly decreased from -3.04, -3.74 to -3.91 eV, with increasing the electron withdrawing ability. At the same time, the charge transportation behaviors of these polymers were transformed from hole to ambipolar and electron transport. Therefore, it is very important to select suitable acceptors towards developing different types of OFETs.

In order to achieve high power conversion efficiency (PCE), it is extremely important to design well-matched energy levels between polymers and [6,6]-phenyl-C61-butyric acid methyl ester (PCBM).[2,5] Yang and coworkers reported three polymers (**P17-P19**) which were composed of the same conjugated backbone as shown in Chart 1.4. The electron withdrawing ability of thieno[3, 4-*b*]thiophene core was tuned by changing its substitutions.[31] The corresponding data are summarized in Table 1.1. Three polymers had the same values of λ_{max} and optical bandgap. When the (octyloxy)carbonyl group on the thieno[3,4-*b*]thiophene in **P17** was replaced by a branched alkyl carbonyl chain (**P18**), both the IP and EA values were decreased by 0.11 eV. When fluorine was introduced to the thieno[3,4-*b*]thiophene (**P19**), both of IP and EA were further reduced by 0.1 eV. It did not influence their optical and energy bandgaps. However, the difference is the low-lying IP (~0.1 eV), which can increase the open circuit voltage (V_{oc}) when these polymers were blended with PCBM as active layer for OPVs. The V_{oc} of these solar cell devices were 0.62, 0.70 and 0.76 V for **P17**, **P18** and **P19**, respectively. The increased V_{oc} of **P19** resulted in a high PCE of 7.4%. To date, the D-A copolymers have achieved higher performances with hole moibility of 52.7 $cm^2 V^{-1} s^{-1}$ in OFETs[32] and PCE of 10.8% in single junction OPVs.[33]

Most of low bandgap polymers containing one acceptor have higher hole than electron mobility in OFETs. In order to adjust the electron transporting ability of D-A polymers, a new concept of "dual-acceptor polymers" was proposed.[34] Due to the introduction of the other acceptor, such polymers usually show very low bandgaps with deep LUMO energy levels, thus leading to well-balanced or electron-dominant transporting ambipolar characteristics. Two dual-acceptor polymers are shown in Chart 1.4. Polymer **P20** afforded a relatively deep LUMO level of -4.00 eV, it is lower than those of single DPP and benzothiadiazole (BT) based polymers.[35] Such low LUMO level led to a well-balanced ambipolar transporting property of **P20** (Table 1.1). Polymer **P21** was constructed via combining two strong acceptors DPP and benzobisthiadiazole (BBT).[36] Obviously, the very narrow bandgap (0.65

eV) of **P21** was related to the stronger acceptor BBT in comparison with that of BT. The very low bandgap and deep LUMO level resulted in polymer **P21** also presenting ambipolar behavior, but electron-dominant transport characteristic.

Table 1.1 Optical absorption, electrochemical properties, and device performances of **P14**-**P19**.

Polymers	$\lambda_{max,film}$ (nm)	E_g^{opt} (eV)	IP (eV)	EA (eV)	μ_h ($cm^2 V^{-1} s^{-1}$)	μ_e ($cm^2 V^{-1} s^{-1}$)	PCE (%)	Ref.
P14	615	1.9	-5.88	-3.04	0.008	No	---	26
P15	620	1.57	-5.31	-3.74	0.66	0.06	---	27
P16	697	1.45	-5.36	-3.91	No	0.06	---	28
P17	675	1.61	-5.01	-3.24	---	---	4.8	31
P18	675	1.61	-5.12	-3.35	---	---	6.3	31
P19	675	1.61	-5.22	-3.45	---	---	7.4	31
P20	915	1.20	-5.20	-4.00	0.35	0.40	---	35
P21	---	0.65	-4.55	-3.90	0.81	1.2	---	36

---: The authors did not provide corresponding information in literatures.

1.3 Rational design of D-A conjugated copolymers in OFET

Conjugated polymers for OFETs have been tremendous successful. It was attributed to the good cooperation between physicists and organic chemists by unending optimization device performance and synthesis of conjugated materials, respectively. Some structure-morphology-charge carrier mobility relationships have been investigated and understood. With these relationships in mind, organic chemists have synthesized more and more high performance polymers by rational control of some factors, such as number-average molecular weight (M_n), polydispersity index (PDI), end capping, match donor and acceptor moieties, side chain groups and so on. Herein we only list those factors which are frequently investigated.

1.3.1 Molecular weight, **PDI, and end capping**

The molecular weight has proven to have significant influence on the charge carrier mobility. Usually, increasing the molecular weight is beneficial for improving device performance.[37,38] The polymer with a M_n above 20 kg mol^{-1} is important to obtain high-performing semiconductor material. However, it will decrease when the molecular weights are as high as 150 kg mol^{-1}, because such high molecular weight polymers have higher viscosity, which is not beneficial for formation of uniform thin films.[39] It is, therefore, very important to synthesize new polymers with proper molecular weights via optimized synthetic approaches.
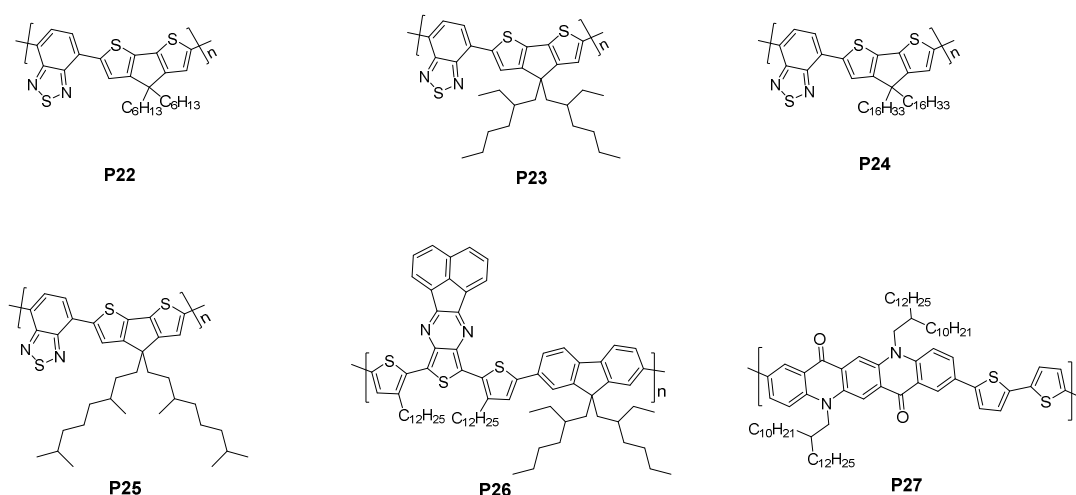
Chart 1.5 Chemical structures of CDT-BTZ based polymers, **P26**, and **P27**.

Two polymers cyclopentadithiophene-benzothiadiazole (CDT-BTZ), **P22** and **P23**, were first synthesized via a Stille coupling between distannyl-CDT and dibromo-BTZ.[40,41] Due to the poor solubility of **P22**, it wasn't further characterized. The polymer side chains were modified by replacing two hexyl linear chains in **P22** with a couple of 2-ethylhexyl chains to obtain **P23**, which exhibited good solubility and a high M_n of 20 kg mol^{-1}, the hole mobility was achieved to 0.015 cm^2 V^{-1} s^{-1}. However, the purification of the toxicity of distannyl-CDT is a major concern, because this liquid compound cannot be purified by recrystallization. Müllen and his coworkers optimized carefully this kind of polymer by employing side chains

engineering and Suzuki coupling polymerization.[38,42-45] Both polymers **P24** and P**25** with different side chains are shown in Chart 1.5. Controlled purification and concentration in solution of monomers enabled synthesis of varying molecular weights for **P24**. For example, the highest molecular weight of **P24** was accomplished by multiple recrystallizations of the diboronyl ester-BTZ, purifying dibromo-CDT through a recycling high performance liquid chromatography (HPLC) system, and decreased the concentration in solvent of monomers before polymerization.[45] The different molecular weights of **P25** were obtained by the adjustment ratio of both monomers. The results demonstrated that the molecular weights are very critical to achieve high mobilities as shown in Figure 1.3a, because molecular crystallinity were improved with increasing the molecular weights of the polymers. It is worth to mention that the charge carrier mobilities of some polymers, such as **P26** or **P27**, (Figure 1.3b) are insensitive or decreased with increasing their molecular weights.[46,47] It is related to the relationship between polymers film ordering and molecular weights.
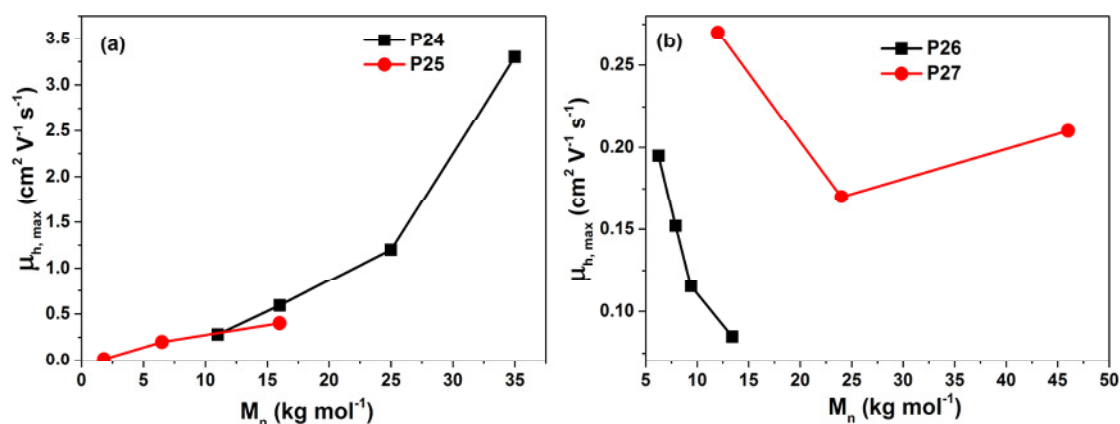
Figure 1.3 Graphical illustration of correlation between molecular weights and hole mobilities of **P24**, **P25** (a) and **P26**, **P27** (b).

Additionally, a large PDI has also a distinct negative effect on charge carrier mobility, due to the broad molecular weight leading to poor crystallization. However, some polymers still exhibited charge mobilities above 1 cm^2 V^{-1} s^{-1}, even though their PDI were reported higher than 4, it was attributed to their strong aggregation in solution.[48-51] Bao and her coworkers reported a DPP-based polymer **P28** (Chart 1.6).[48] This polymer exhibited a hole

mobility of 2.1 cm^2 V^{-1} s^{-1} when the annealing temperature of the active layer was increased to 190 °C. However, GPC result provided a M_n of 21.9 kg mol^{-1} with a large PDI of 6.75 at 140 °C, due to strong aggregation. When the measurement temperature was raised to 190 °C, the PDI was decreased to 3.25 with M_n of 20.5 kg mol^{-1}. The temperature was further increased to 200 °C, the influence of aggregation of **P28** was completely eliminated to show a M_n of 22.8 kg mol^{-1} and a PDI of 1.94. Therefore, it is important to measure molecular weights of polymers using high temperature by GPC to obtain a real M_n and PDI. End-capping of a D-A polymer is quite popular using mono-functionalized benzene or thiophene, because it can reduce the defects and increase the thermal stability of polymers. Two polymers, **P29** and **P30** (without and with end-capped thiophene unit), were investigated by Bazan and his coworkers as shown in Chart 1.6.[52] It was discovered that both polymers had negligible differences in optical and morphological characteristics of the active layer. But the end-capped polymer exhibited better thermal stability, fewer defects, and slightly higher PCE in OPVs. Similar studies, however, were rarely reported for OFETs.
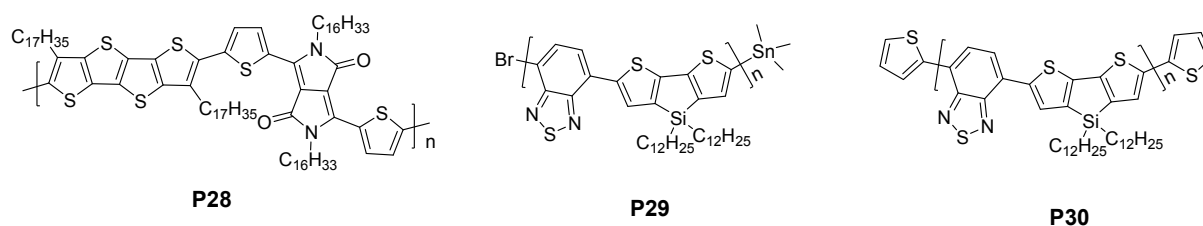
Chart 1.6 Chemical structures of **P28**-**P30**.

1.3.2 The match of donor and acceptor in D-A copolymer

The HOMO energy levels of polymer semiconductors are controlled between -5.0 and -5.5 eV by matching donors and acceptors, which are very important to develop stability and high performance OFETs. A high HOMO level (> -5.0 eV) of material usually yields low charge carrier mobility even in a glove box. Because the glove box conditions are composed of an oxygen concentration from 0.5 to 1 ppm and moisture concentration of around 0.2 ppm. The moderate doping of organic semiconductors by "dilute air" (O$_2$ ~1 ppm and H$_2$O ~1 ppm) dramatically decreased the field-effect performance.[53] When HOMO level of material is lower

than -5.5 eV, large current on/off ratio and good mobility can still be obtained, but such devices typically have an unacceptably large threshold voltages.[54] **P24** (Chart 1.7) is the most successful example achieving excellent charge carrier mobility among BTZ-based D-A copolymers in OFETs. After the optimization of the molecular weight of polymer and the fabricating conditions of devices, the hole mobility of **P24** was continuously improved from 0.17, 1.4, 3.3 5.5 to 6.5 cm^2 V^{-1} s^{-1}.[38,42-45] Dithienopyrole (DTP) is a stronger donor than CDT, due to the introduction of an electron-rich nitrogen atom at the bridge position. Therefore, the polymer **P31**, which used DTP as a donor, exhibited a lower E_{opt} (1.2 eV), and higher HOMO energy level (-4.65 eV) compared to **P24** (E_{opt}= 1.4 eV, HOMO= -5.3 eV). The M_n of **P31** was achieved as high as 44.8 kg mol^{-1} with a PDI of 1.8, but FET characteristic was not observed in devices.[55] Dithienosilole (DTS) is another donor. The σ*-orbital of the C-Si bone is more effectively interacting with the π*-orbital of the butadiene fragment, and thereby allow stronger π-stacking interactions to occur.[56] The polymer **32**, which used DTS as a donor, exhibited a low E_{opt} (1.4 eV), and HOMO energy level (-5.0 eV), and the device showed a hole mobility of 0.01 cm^2 V^{-1} s^{-1}.[37] Obviously, the CDT is the best donor with excellent charge carrier mobility in OFETs among these three BTZ-based D-A copolymers.

P24   **P31**   **P32**
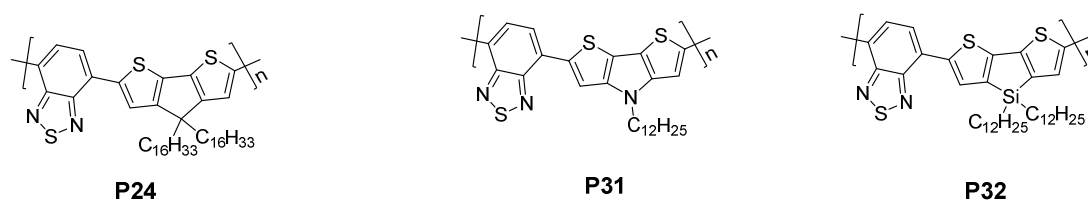
Chart 1.7 Chemical structures of **P24**, **P31**, and **P30**.

1.3.3 The side chains engineering in polymers

Solution-processed conjugated polymers include two parts: polymer main chains (conjugated backbones) and polymer side chains (flexible solubilizing chains). In polymeric semiconductors, although the conjugation backbones determine the optoelectronic properties of polymers, the flexible solubilizing chains also significantly improve the device performance by affecting molecular arrangement in the film.[57,58] It is, therefore, very

important to match side chains and conjugated backbones when designing polymers. Some representative works are summarized for discussion.
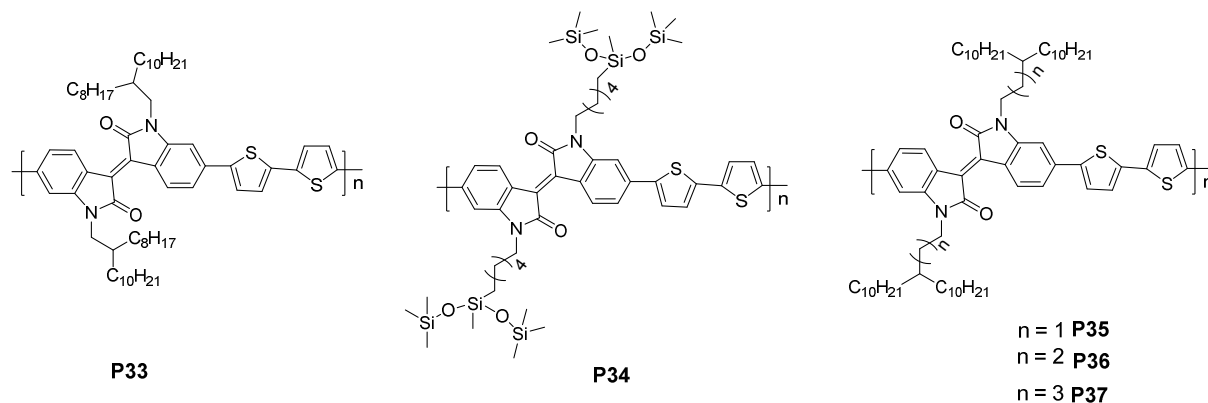
Chart 1.8 Chemical structures of **P33-P37**.

Chart 1.8 shows the structures of D-A copolymers **P33-P37**, which have the same conjugated backbones of isoindigo and bithiophene. Obviously, the linear alkyl chains cannot provide enough solubility for yielding the high molecular weight and solution processed polymers. A promising isoindigo-based polymer with a pair of 2-octyldodecyl groups **P33** was reported by Pei's group. This polymer exhibited an air stable hole mobility up to 0.79 cm^2 V^{-1} s^{-1}.[59] Bao and her coworkers reported the same conjugated backbone polymer **P34** with an unconventional siloxane-terminated hexyl solubilizing side chains, at the same time, the **P33** was also studied as a reference polymer. In their work, **P34** had a higher hole mobility of 2.48 cm^2 V^{-1} s^{-1} than **P33** (0.57 cm^2 V^{-1} s^{-1}). It was attributed to the smaller π-π distance of 3.58 Å in polymer **P34** compared to **P33** (3.75 Å).[60] Pei and his coworkers subsequently moved the branching point from 2-position (**P33**) to the 3-, 4-, 5-positions (**P35-P37**) to investigate the influence of moving the branching point away from the polymer main chains. The results demonstrated that **P36** gave a highest mobility up to 3.6 cm^2 V^{-1} s^{-1} with a shortest π-π distance of 3.57 Å among of them.[61] Currently, the siloxane-terminated side chains and the tuning of the distance of the branching of alkyl chains away from the conjugated backbone have been successfully applied to other acceptors and achieved high mobility in OFETs.[62-64]

1.4 Silylethynyl-substituents in acenes and heteroacenes

Like polymer semiconductors, the organic small molecules have also obtained great success in the past few years. Pentacene (**M1**) analogues are among the most important families of organic semiconductors because of their high charge carrier transport in OFETs. However, the solubility and stability of these molecules significantly impede their applications and development in organic semiconductors.[65,66] For example, their high-lying HOMOs make them sensitive to photooxidation, resulting in low device performance under ambient conditions.[67,68]
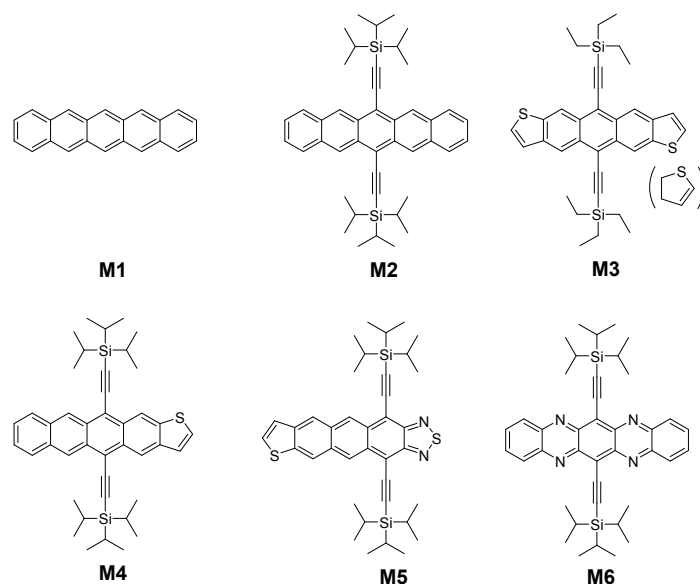
Chart 1.9 Chemical structures of **M1-M6**.

Anthony and his coworkers grafted the first example of the triisopropylsilylethynyl group onto pentacene and successfully improved the solubility and stability of pentacene. This molecule (**M2**) exhibited good solubility, strong π-π stacking and significant conductivity enhancements.[69] Since then, the functionalized pentacene analogues were widely synthesized.[70-72] At the same time, the hole mobility of **M2** was achieved up to 4.6 cm^2 V^{-1} s^{-1} by solution processed OFET.[73] Furthermore, introduction of heteroatoms (like sulfur and nitrogen) in conjugated backbone system (namely heteroacenes) was also proven to be one of effective approaches to improve molecular electronic properties or stabilize the HOMO

energy levels. As shown in chart 1.9, anthradithiophene (**M3**),[74] tetracenothiophene (**M4**)[75] and acenothiadiazole (**M5**)[76] were synthesized, providing lower lying HOMOs than that of pentacene, thereby exhibiting higher oxidation stability. These heteroacene molecules form good π-π interaction in the solid states and show relatively high hole mobilities (1.0 cm^2 V^{-1} s^{-1} for **M3**; 1.28 cm^2 V^{-1} s^{-1} for **M4**; 0.4 cm^2 V^{-1} s^{-1} for **M5**). On the other hand, nitrogen-rich heteroacenes have been computed as promising candidates for transporting negative charge carrier by Winkler and Houk.[77] Indeed, tetraazapentacene **M6**[78] molecule was reported to exhibit excellent electron mobility as high as 3.3 cm^2 V^{-1} s^{-1} by solution processing.[79] These properties indicate heteroacene molecules are promising candidates for n-type OFET materials.

1.4.1 Introduction of silylethynyl-substituted in acenes and heteroacenes
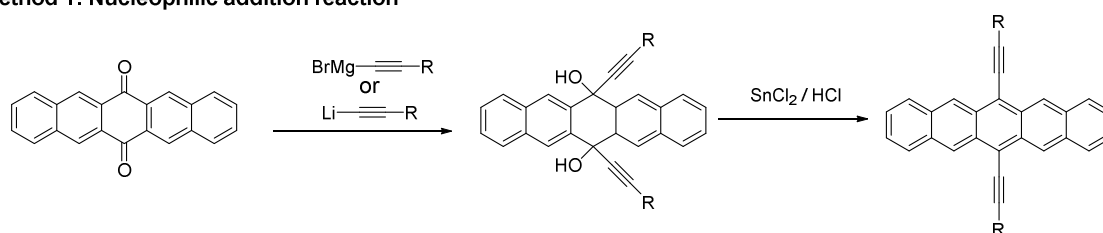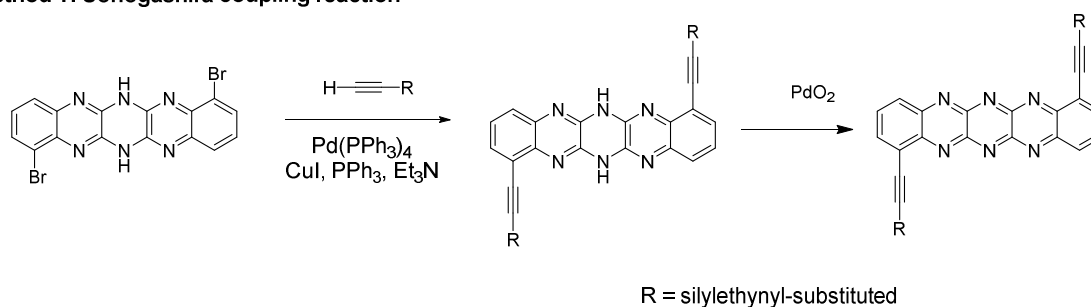
Scheme 1.1 The approaches for introduction of silylethynyl-substituted.

Introducing silylethynyl groups has proven to be successful not only in improving solubility and stability of acenes and heteroacenes, but also in enhancing their capability for π-stacked arrays. However, currently, only two familiar methods were used to introduce

siylethynyl groups into acenes and heteroacenes as shown in Scheme 1.1. The first is the nucleophilic addition of siylethynyl anion, which proceeds via the corresponding dione precursors, and then the reduction of the respective diols are performed.[69] The second method is the Sonogashira coupling reaction which is carried out between the silylacetylene and corresponding dibromo precusors.[80] Thus, the facile and diverse synthetic approaches are necessary for the rapid improvement of heteroacene-based OFET materials.

1.4.2 Crystal packing for silylethynyl-substituted acenes and heteroacenes

Silylethynyl substitution was proposed to improve the solubility of acenes and azacenes. More importantly, this functionalization strategy can tune their solid state order. Even though small differences were modified in the substitution of the silicon, they significantly changed molecular crystal packing, therefore leading to different device performances. Taking pentacene and its functionalization derivatives for example, the crystal packing of them are shown in Figure 1.4. Unsubstituted pentacene exhibited an edge-to-face herringbone arrangement (1.4a),[81-83] which may limit its electron transport properties.[84] The introduction of bulky substitutents disrupts the edge-to-face arrangement of the pentacene cores, and encourages face-to-face interaction between pentacene cores. The trimethylsilyl group of **M7** led to a 1D slipped packing arrangement (Firgure 1.4b),[85] while **M2** with the triisopropylsilyl group formed a 2D brick π-stacking arrangement (Figure 1.4c),[69] which is a desirable packing for more efficient charge transport in OFET. The ratio of diameter of bulky substituents to the long-axis dimension of aromatic ring strongly influences molecular packing styles. If the substituted diameters are significantly greater or smaller than half the length of the aromatic backbone, the molecular packing is beneficial for 1D arrangement. While the diameter of side group is close to half the length of the aromatic ring, the molecule commonly forms the 2D brickwall motif.[85] It could be the same reason that triethylsilylethynyl anthradithiophene (**M3**) adopt a 2D brickwall packing, while triisopropylsilylethynyl anthradithiophene displayed a 1D slipped packing arrangement.[74]
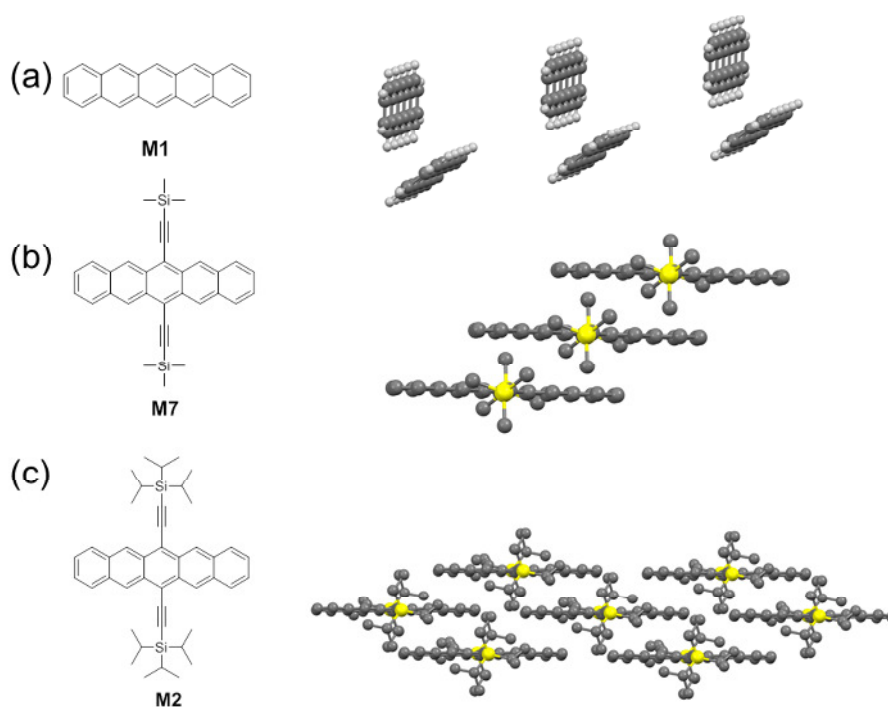
Figure 1.4 Crystal packing for unsubstituted pentacene (a)[83], trimethylsilylethynylpentacene (b)[85], and triisopropylsilylethynylpentacene (c)[69].

1.5 Motivation and objective

Currently, the strong acceptors received more and more attention, because they are promising in developing low band gap copolymers with deep LUMO levels, which impart characteristics of transporting negative charge through the polymers and improves the stability. In comparison with other strong acceptors, thiadiazoloquinoxalines (TQs) have some unique properties such as quinoid characters, diversity of the chemical structures, and rich electronic properties, which make them the most important building blocks in developing low band gap copolymers. However, some drawbacks of TQ small molecules and polymers limited their applications. Therefore, TQs were chosen as the research object in this thesis, the new TQ-containing polymers and small molecules will be designed, synthesized, and characterized as organic semiconductors. Herein the molecular structural design pursued was guided to address the following problems.

➢ TQs are strong electron acceptors with EA in a region of -3.43 to -3.83 eV,[86,87] but most of TQ-based polymers were reported as p-type materials in OFETs. It still has some problems in developing ambipolar polymer semiconductors.

In order to enable electron charge transport in the TQ-based polymers, our group's previous strategy was to introduce acetylenic π-spacers into the main chains of TQ-based polymers for reducing the twist within the polymer backbones and electron-donating part. Therefore, the first example of TQ-based ambipolar polymers was reported. However, it needs more steps to introduce diethynyl groups onto the donor part in synthesis, and also some diethynyl donors are quite unstable under air and catalyst. In order to more easily achieve electron charge transport in the TQ-based polymers, recently our group developed a higher electron affinity benzodithiophene condensed TQ acceptor with EA of -3.84 eV (**M8**, Figure 1.5), by condensing fused aromatic rings. This strong acceptor can be easily applied to construct copolymers by Stille coupling, which exhibits negative charge transport. Interestingly, the **M8** possesses two couples of active positions for polymerization, which should be first studied in this thesis.
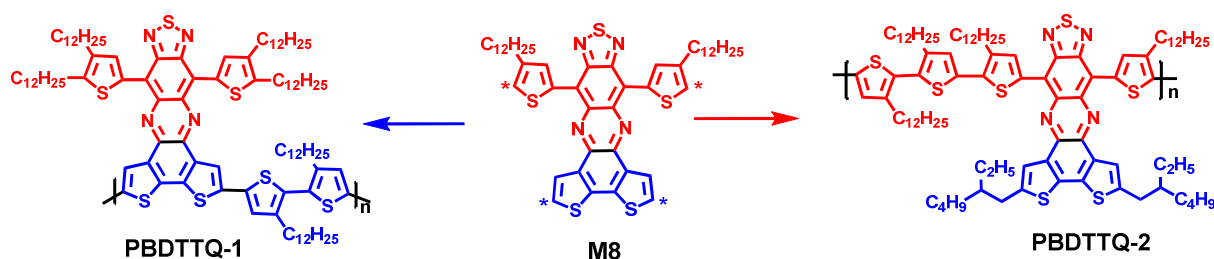
Figure 1.5 Two different linkage polymers based on **M8**.

➢ Usually, TQ-based polymers have poor solubility, low molecular weights and low charge carrier mobilities. However, an excellent candidate of polymer semiconductor needs a high molecular weight and good solubility.

Taking the rigid structure of TQ into account, it is normal that TQ small molecules, especially TQ-based polymers have poor solubility in organic solvents, such as chloroform,

THF, toluene, and chlorobenzene. The poor solubility directly led to low molecular weights of the resulting polymers, which further influenced the charge carrier transport in OFETs. In order to improve the device performance of TQ polymers, **M9** was employed as an acceptor to exploit a series of polymers (Figure 1.6), firstly in combination with the unsubstituted donors and then with side chain engineering in conjugated backbone of **PTQ4**. The structures and charge carrier mobility relationships of TQ polymers should be investigated and understood. Finally, based on these structure-property relationships, a new polymer **PBDTTQ-3** was constructed with higher molecular weight, good solubility, and high performance as ambipolar semiconductor.
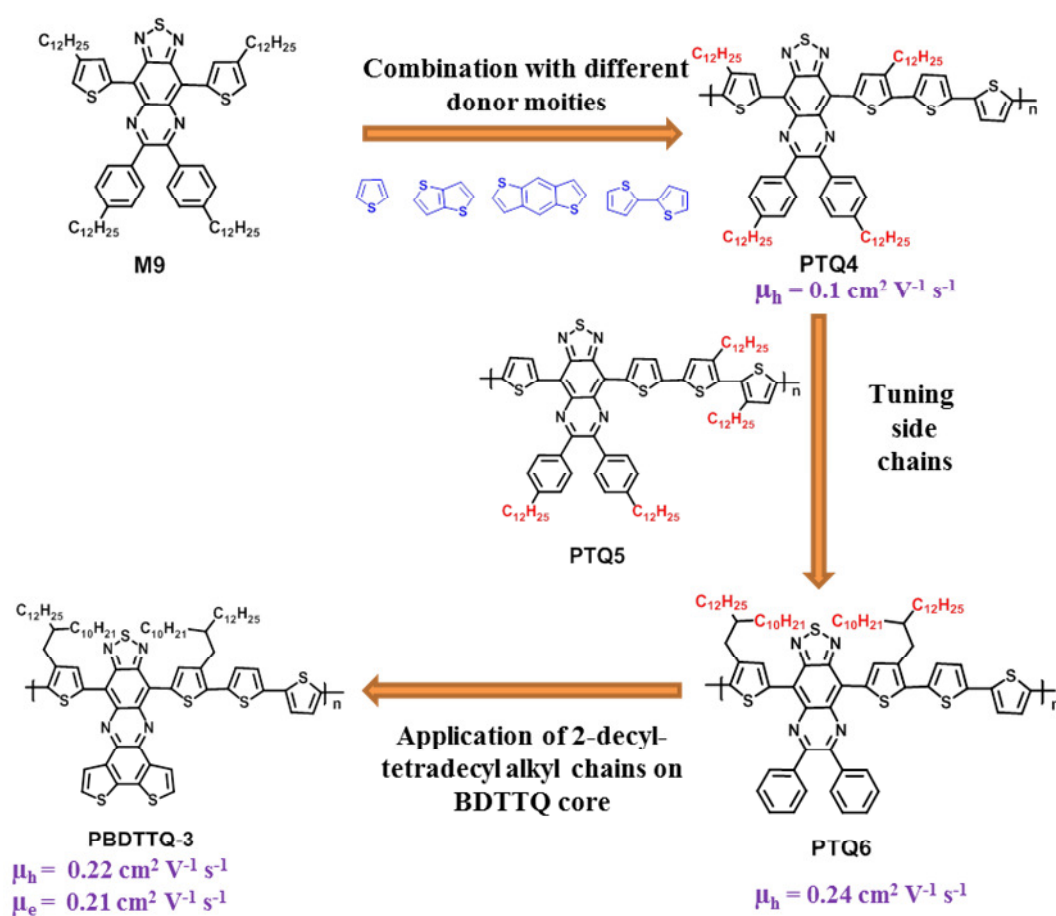
Figure 1.6 The map of design high performance TQ polymers in OFETs.

➢ The rich chemical structures of TQ molecules make it easy to manipulate their electronic properties. Therefore, they have potential applications in many electronic fields. How to design new TQ structures for new applications.

Indeed, the diversity of TQ electronic properties has yielded many polymers which can be applied in several fields, such as OPVs,[88,89] OFETs,[90,91] LEFETs,[92] polymer light emitting diodes (PLEDs),[93] near-infrared electroluminescence[94] and photoacoustic vascular imaging.[95] In our case, to enhance the practical applications of such polymers in organic electronics, a photosensitizer group, phenanthrene,[96,97] was attached onto the TQ moiety in **PBDTTQ-3** to develop a polymer **PPhTQ** (Figure 1.7). As expected, this polymer was found to act as an effective active layer for organic phototransistor devices.
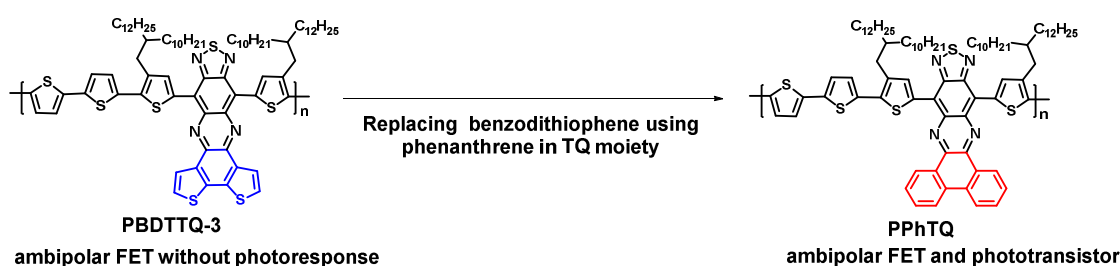
Figure 1.7 Multifunctional TQ-containing polymer.

➢ TQ has a quinoid character like strong acceptor benzobisthiadiazole (BBT),[98] But the TQ polymers usually show relatively large bandgaps ((E_{opt} > 1 eV)[99] compared to BBT containing polymers (E_{opt} < 0.7 eV).[100,101] What kind of strategies can be used to develop new TQ polymers with very low bandgaps.

In order to obtain very low bandgap polymers, a dual-acceptor design strategy was performed[34] to construct D-A1-D-A2 polymers.[102-106] In our studies, a strong acceptor TQ and a relatively weak DPP were successfully combined by Suzuki coupling reaction and achieved an optical bandgap as low as 0.60 eV (Figure 1.8).
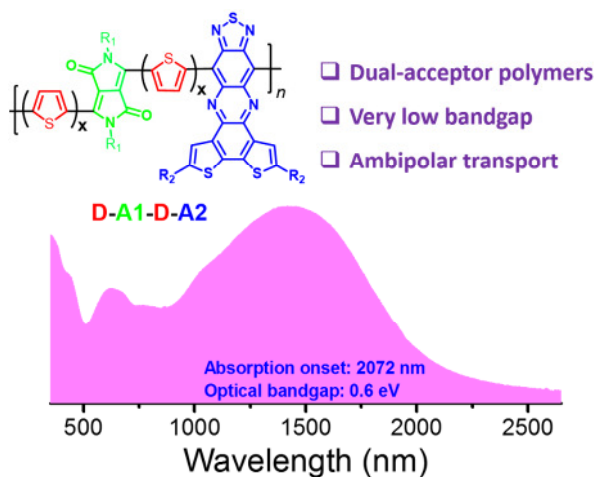
Figure 1.8 Dual-acceptor polymers with very low bandgap.

➢ TQ small molecules have been widely expanded by the condensation reaction in the past few years,[86,98,107,108] but their crystal structures were rarely reported and studied. One question, is it possible to synthesize new TQ small molecules with single crystals. Another question, is it possible to reduce the intermediates of dintro-benzothiadiazole derivatives to corresponding benzotetraamines, further preparing heteroacenes via condensation reaction.
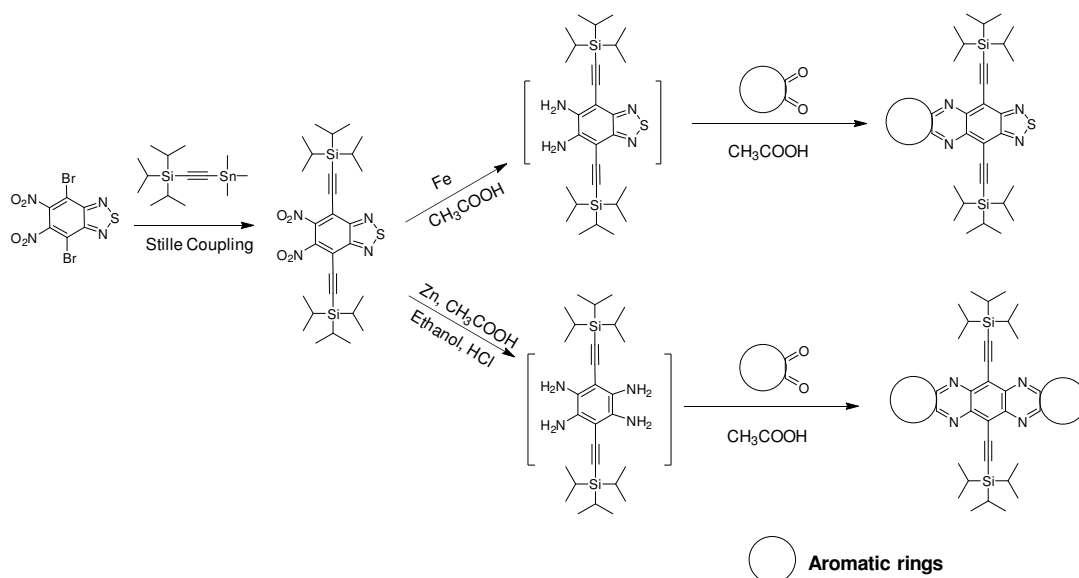
Scheme 1.2 New approaches for developing TQ small molecules and heteroacenes.

Silylethynyl groups are the best candidates for optimizing the molecular ordering, due to their enhancement of molecular crystallization ability. In order to introduce the silylethynyl groups onto conjugated backbone, we developed a new approach using Stille coupling between monostannyl silylethynyl and dibromo-dinitro-benzothiadiazole. Afterwards, the reduction and condensation reactions were carried out to obtain final expanded TQ small molecules (Scheme 1.2). As expected, all of them exhibited good crystallization ability. The reduction was further optimized and successfully obtained a very important intermediate benzotetraamine, which exhibited excellent solubility, and yielded a desired heteroacene by condensation reaction. It provides a chance to synthesize more centrosymmetric extended heteroacenes.

1.6 References

(1) Grimsdale, A. C.; Leok Chan, K.; Martin, R. E.; Jokisz, P. G.; Holmes, A. B. *Chem. Rev.,* **2009**, *109*, 897-1091.

(2) Günes, S.; Neugebauer, H.; Sariciftci, N. S. *Chem. Rev.,* **2007**, *107*, 1324-1338.

(3) Arias, A. C.; MacKenzie, J. D.; McCulloch, I.; Rivnay, J.; Salleo, A. *Chem. Rev.,* **2010**, *110*, 3-24.

(4) Burroughes, J. H.; Bradley, D. D. C.; Brown, A. R.; Marks, R. N.; Mackay, K.; Friend, R. H.; Burns, P. L.; Holmes, A. B. *Nature,* **1990**, *347*, 539-541.

(5) Cheng, Y.-J.; Yang, S.-H.; Hsu, C.-S. *Chem. Rev.,* **2009**, *109*, 5868-5923.

(6) Li, Z.; Meng, H. *Organic light-emitting materials and devices*; CRC press, 2006; Vol. 111.

(7) Kobayashi, M.; Chen, J.; Chung, T. C.; Moraes, F.; Heeger, A. J.; Wudl, F. *Synth. Met.,* **1984**, *9*, 77-86.

(8) Wudl, F.; Kobayashi, M.; Heeger, A. J. *J. Org. Chem.,* **1984**, *49*, 3382-3384.

(9) Pomerantz, M.; Chaloner-Gill, B.; Harding, L. O.; Tseng, J. J.; Pomerantz, W. J. *Synth. Met.,* **1993**, *55*, 960-965.

(10) Karabunarliev, S.; Baumgarten, M.; Tyutyulkov, N.; Müllen, K. *J. Phys. Chem.,* **1994**, *98*, 11892-11901.

(11) Ahn, T.; Jang, M. S.; Shim, H.-K.; Hwang, D.-H.; Zyung, T. *Macromolecules,* **1999**, *32*, 3279-3285.

(12) Zhang, K.; Tieke, B.; Forgie, J. C.; Skabara, P. J. *Macromol. Rapid Commun.,* **2009**, *30*, 1834-1840.

(13) Elsenbaumer, R. L.; Jen, K. Y.; Oboodi, R. *Synth. Met.,* **1986**, *15*, 169-174.

(14) McCullough, R. D. *Adv. Mater.,* **1998**, *10*, 93-116.

(15) Sato, M.; Morii, H. *Macromolecules,* **1991**, *24*, 1196-1200.

(16) Chen, T.-A.; Wu, X.; Rieke, R. D. *J. Am. Chem. Soc.,* **1995**, *117*, 233-244.

(17) McCullough, R. D.; Lowe, R. D.; Jayaraman, M.; Anderson, D. L. *J. Org. Chem.,* **1993**, *58*, 904-912.

(18) Barbarella, G.; Bongini, A.; Zambianchi, M. *Macromolecules,* **1994**, *27*, 3039-3045.

(19) Mao, H.; Xu, B.; Holdcroft, S. *Macromolecules,* **1993**, *26*, 1163-1169.

(20) McCullough, R. D.; Lowe, R. D. *J. Chem. Soc., Chem. Commun.,* **1992**, 70-72.

(21) Loewe, R. S.; Khersonsky, S. M.; McCullough, R. D. *Adv. Mater.,* **1999**, *11*, 250-253.

(22) Loewe, R. S.; Ewbank, P. C.; Liu, J.; Zhai, L.; McCullough, R. D. *Macromolecules,* **2001**, *34*, 4324-4333.

(23) Fichou, D. *Handbook of oligo-and polythiophenes*; John Wiley & Sons, 2008.

(24) Havinga, E. E.; ten Hoeve, W.; Wynberg, H. *Synth. Met.,* **1993**, *55*, 299-306.

(25) Yuen, J. D.; Wudl, F. *Energ. Environ. Sci.,* **2013**, *6*, 392-406.

(26) Letizia, J. A.; Salata, M. R.; Tribout, C. M.; Facchetti, A.; Ratner, M. A.; Marks, T. J. *J. Am. Chem. Soc.,* **2008**, *130*, 9679-9694.

(27) Lei, T.; Dou, J.-H.; Ma, Z.-J.; Yao, C.-H.; Liu, C.-J.; Wang, J.-Y.; Pei, J. *J. Am. Chem. Soc.,* **2012**, *134*, 20025-20028.

(28) Chen, Z.; Zheng, Y.; Yan, H.; Facchetti, A. *J. Am. Chem. Soc.,* **2009**, *131*, 8-9.

(29) He, X.; Borau-Garcia, J.; Woo, A. Y. Y.; Trudel, S.; Baumgartner, T. *J. Am. Chem. Soc.,* **2013**, *135*, 1137-1147.

(30) Matsidik, R.; Martin, J.; Schmidt, S.; Obermayer, J.; Lombeck, F.; Nübling, F.; Komber, H.; Fazzi, D.; Sommer, M. *J. Org. Chem.,* **2015**, *80*, 980-987.

(31) Chen, H.-Y.; Hou, J.; Zhang, S.; Liang, Y.; Yang, G.; Yang, Y.; Yu, L.; Wu, Y.; Li, G. *Nat. Photon.,* **2009**, *3*, 649-653.

(32) Luo, C.; Kyaw, A. K. K.; Perez, L. A.; Patel, S.; Wang, M.; Grimm, B.; Bazan, G. C.; Kramer, E. J.; Heeger, A. J. *Nano Lett.,* **2014**, *14*, 2764-2771.

(33) Liu, Y.; Zhao, J.; Li, Z.; Mu, C.; Ma, W.; Hu, H.; Jiang, K.; Lin, H.; Ade, H.; Yan, H. *Nat. Commun.,* **2014**, *5*, 5293.

(34) Guo, X.; Baumgarten, M.; Müllen, K. *Prog. Polym. Sci.,* **2013**, *38*, 1832-1908.

(35) Sonar, P.; Singh, S. P.; Li, Y.; Soh, M. S.; Dodabalapur, A. *Adv. Mater.,* **2010**, *22*, 5409-5413.

(36) Yuen, J. D.; Fan, J.; Seifter, J.; Lim, B.; Hufschmid, R.; Heeger, A. J.; Wudl, F. *J. Am. Chem. Soc.,* **2011**, *133*, 20799-20807.

(37) Beaujuge, P. M.; Tsao, H. N.; Hansen, M. R.; Amb, C. M.; Risko, C.; Subbiah, J.; Choudhury, K. R.; Mavrinskiy, A.; Pisula, W.; Bredas, J. L.; So, F.; Müllen, K.; Reynods, J. R. *J. Am. Chem. Soc.,* **2012**, *134*, 8944-8957.

(38) Tsao, H. N.; Cho, D. M.; Park, I.; Hansen, M. R.; Mavrinskiy, A.; Yoon, D. Y.; Graf, R.; Pisula, W.; Spiess, H. W.; Müllen, K. *J. Am. Chem. Soc.,* **2011**, *133*, 2605-2612.

(39) Klauk, H. *Organic Electronics II: More Materials and Applications*; John Wiley & Sons, 2012.

(40) Zhu, Z.; Waller, D.; Gaudiana, R.; Morana, M.; Mühlbacher, D.; Scharber, M.; Brabec, C. *Macromolecules,* **2007**, *40*, 1981-1986.

(41) Mühlbacher, D.; Scharber, M.; Morana, M.; Zhu, Z.; Waller, D.; Gaudiana, R.; Brabec, C. *Adv. Mater.,* **2006**, *18*, 2884-2889.

(42) Zhang, M.; Tsao, H. N.; Pisula, W.; Yang, C.; Mishra, A. K.; Müllen, K. *J. Am. Chem. Soc.,* **2007**, *129*, 3472-3473.

(43) Yamashita, Y.; Tsurumi, J.; Hinkel, F.; Okada, Y.; Soeda, J.; Zajączkowski, W.; Baumgarten, M.; Pisula, W.; Matsui, H.; Müllen, K.; Takeya, J. *Adv. Mater.,* **2014**, *26*, 8169-8173.

(44) Wang, S.; Kappl, M.; Liebewirth, I.; Müller, M.; Kirchhoff, K.; Pisula, W.; Müllen, K. *Adv. Mater.,* **2012**, *24*, 417-420.

(45) Tsao, H. N.; Cho, D.; Andreasen, J. W.; Rouhanipour, A.; Breiby, D. W.; Pisula, W.; Müllen, K. *Adv. Mater.,* **2009**, *21*, 209-212.

(46) Becerril, H. A.; Miyaki, N.; Tang, M. L.; Mondal, R.; Sun, Y.-S.; Mayer, A. C.; Parmer, J. E.; McGehee, M. D.; Bao, Z. *J. Mater. Chem.,* **2009**, *19*, 591-593.

(47) Osaka, I.; Akita, M.; Koganezawa, T.; Takimiya, K. *Chem. Mater.,* **2012**, *24*, 1235-1243.

(48) Matthews, J. R.; Niu, W.; Tandia, A.; Wallace, A. L.; Hu, J.; Lee, W.-Y.; Giri, G.; Mannsfeld, S. C. B.; Xie, Y.; Cai, S.; Fong, H. H.; Bao, Z.; He, M. *Chem. Mater.,* **2013**, *25*, 782-789.

(49) Chen, Z. Y.; Lee, M. J.; Ashraf, R. S.; Gu, Y.; Albert-Seifried, S.; Nielsen, M. M.; Schroeder, B.; Anthopoulos, T. D.; Heeney, M.; McCulloch, I.; Sirringhaus, H. *Adv. Mater.,* **2012**, *24*, 647-652.

(50) Shin, J.; Hong, T. R.; Lee, T. W.; Kim, A.; Kim, Y. H.; Cho, M. J.; Choi, D. H. *Adv. Mater.,* **2014**, 6031-6035.

(51) Kim, K.-H.; Park, S.; Yu, H.; Kang, H.; Song, I.; Oh, J. H.; Kim, B. J. *Chem. Mater.,* **2014**, *26*, 6963-6970.

(52) Park, J. K.; Jo, J.; Seo, J. H.; Moon, J. S.; Park, Y. D.; Lee, K.; Heeger, A. J.; Bazan, G. C. *Adv. Mater.,* **2011**, *23*, 2430-2435.

(53) Lu, G.; Blakesley, J.; Himmelberger, S.; Pingel, P.; Frisch, J.; Lieberwirth, I.; Salzmann, I.; Oehzelt, M.; Di Pietro, R.; Salleo, A.; Koch, N.; Neher, D. *Nat. Commun.,* **2013**, *4*, 1588.

(54) Facchetti, A. *Chem. Mater.,* **2011**, *23*, 733-758.

(55) Zhang, S.; Guo, Y.; Fan, H.; Liu, Y.; Chen, H.-Y.; Yang, G.; Zhan, X.; Liu, Y.; Li, Y.; Yang, Y. *J. Polym. Sci., Part A: Polym. Chem.,* **2009**, *47*, 5498-5508.

(56) Usta, H.; Lu, G.; Facchetti, A.; Marks, T. J. *J. Am. Chem. Soc.,* **2006**, *128*, 9034-9035.

(57) Mei, J.; Bao, Z. *Chem. Mater.,* **2013**, *26*, 604–615.

(58) Lei, T.; Wang, J.-Y.; Pei, J. *Chem. Mater.,* **2013**, *26*, 594-603.

(59) Lei, T.; Cao, Y.; Fan, Y.; Liu, C.-J.; Yuan, S.-C.; Pei, J. *J. Am. Chem. Soc.,* **2011**, *133*, 6099-6101.

(60) Mei, J.; Kim, D. H.; Ayzner, A. L.; Toney, M. F.; Bao, Z. *J. Am. Chem. Soc.,* **2011**, *133*, 20130-20133.

(61) Lei, T.; Dou, J.-H.; Pei, J. *Adv. Mater.,* **2012**, *24*, 6457-6461.

(62) Lee, J.; Han, A. R.; Yu, H.; Shin, T. J.; Yang, C.; Oh, J. H. *J. Am. Chem. Soc.,* **2013**, *135*, 9540-9547.

(63) Kang, I.; Yun, H.-J.; Chung, D. S.; Kwon, S.-K.; Kim, Y.-H. *J. Am. Chem. Soc.,* **2013**, *135*, 14896-14899.

(64) Back, J. Y.; Yu, H.; Song, I.; Kang, I.; Ahn, H.; Shin, T. J.; Kwon, S.-K.; Oh, J. H.; Kim, Y.-H. *Chem. Mater.,* **2015**, *27*, 1732-1739.

(65) Anthony, J. E. *Chem. Rev.,* **2006**, *106*, 5028-5048.

(66) Anthony, J. E. *Angew. Chem. Int. Ed.,* **2008**, *47*, 452-483.

(67) Duong, H. M.; Bendikov, M.; Steiger, D.; Zhang, Q.; Sonmez, G.; Yamada, J.; Wudl, F. *Org. Lett.,* **2003**, *5*, 4433-4436.

(68) Maliakal, A.; Raghavachari, K.; Katz, H.; Chandross, E.; Siegrist, T. *Chem. Mater.,* **2004**, *16*, 4980-4986.

(69) Anthony, J. E.; Brooks, J. S.; Eaton, D. L.; Parkin, S. R. *J. Am. Chem. Soc.,* **2001**, *123*, 9482-9483.

(70) Payne, M. M.; Parkin, S. R.; Anthony, J. E. *J. Am. Chem. Soc.,* **2005**, *127*, 8028-8029.

(71) Swartz, C. R.; Parkin, S. R.; Bullock, J. E.; Anthony, J. E.; Mayer, A. C.; Malliaras, G. G. *Org. Lett.,* **2005**, *7*, 3163-3166.

(72) Purushothaman, B.; Parkin, S. R.; Anthony, J. E. *Org. Lett.,* **2010**, *12*, 2060-2063.

(73) Giri, G.; Verploegen, E.; Mannsfeld, S. C. B.; Atahan-Evrenk, S.; Kim, D. H.; Lee, S. Y.; Becerril, H. A.; Aspuru-Guzik, A.; Toney, M. F.; Bao, Z. *Nature,* **2011**, *480*, 504-508.

(74) Payne, M. M.; Parkin, S. R.; Anthony, J. E.; Kuo, C.-C.; Jackson, T. N. *J. Am. Chem. Soc.,* **2005**, *127*, 4986-4987.

(75) Tang, M. L.; Reichardt, A. D.; Siegrist, T.; Mannsfeld, S. C. B.; Bao, Z. *Chem. Mater.,* **2008**, *20*, 4669-4676.

(76) Lei, T.; Zhou, Y.; Cheng, C.-Y.; Cao, Y.; Peng, Y.; Bian, J.; Pei, J. *Org. Lett.,* **2011**, *13*, 2642-2645.

(77) Winkler, M.; Houk, K. N. *J. Am. Chem. Soc.,* **2007**, *129*, 1805-1815.

(78) Miao, S.; Appleton, A. L.; Berger, N.; Barlow, S.; Marder, S. R.; Hardcastle, K. I.; Bunz, U. H. F. *Chem. Eur. J.,* **2009**, *15*, 4990-4993.

(79) Liang, Z.; Tang, Q.; Xu, J.; Miao, Q. *Adv. Mater.,* **2011**, *23*, 1535-1539.

(80) He, Z.; Mao, R.; Liu, D.; Miao, Q. *Org. Lett.,* **2012**, *14*, 4190-4193.

(81) Campbell, R. B.; Robertson, J. M.; Trotter, J. *Acta Cryst.,* **1961**, *14*, 705-711.

(82) Mattheus, C. C.; Dros, A. B.; Baas, J.; Meetsma, A.; Boer, J. L. d.; Palstra, T. T. M. *Acta Cryst.,* **2001**, *C57*, 939-941.

(83) Holmes, D.; Kumaraswamy, S.; Matzger, A. J.; Vollhardt, K. P. C. *Chem. Eur. J.,* **1999**, *5*, 3399-3412.

(84) Cornil, J.; Calbert, J. P.; Brédas, J. L. *J. Am. Chem. Soc.,* **2001**, *123*, 1250-1251.

(85) Anthony, J. E.; Eaton, D. L.; Parkin, S. R. *Org. Lett.,* **2002**, *4*, 15-18.

(86) Li, H.; Tam, T. L.; Lam, Y. M.; Mhaisalkar, S. G.; Grimsdale, A. C. *Org. Lett.* **2011**, *13*, 46-49.

(87) Dallos, T.; Hamburger, M.; Baumgarten, M. *Org. Lett.,* **2011**, *13*, 1936-1939.

(88) Inganäs, O.; Zhang, F.; Tvingstedt, K.; Andersson, L. M.; Hellström, S.; Andersson, M. R. *Adv. Mater.,* **2010**, *22*, E100-E116.

(89) Keshtov, M. L.; Marochkin, D. V.; Kochurov, V. S.; Khokhlov, A. R.; Koukaras, E. N.; Sharma, G. D. *Poly. Chem.,* **2013**, *4*, 4033-4044.

(90) Zhang, X.; Steckler, T. T.; Dasari, R. R.; Ohira, S.; Potscavage, W. J.; Tiwari, S. P.; Coppee, S.; Ellinger, S.; Barlow, S.; Bredas, J.-L.; Kippelen, B.; Reynolds, J. R.; Marder, S. R. *J. Mater. Chem.,* **2010**, *20*, 123-134.

(91) Dallos, T.; Beckmann, D.; Brunklaus, G.; Baumgarten, M. *J. Am. Chem. Soc.,* **2011**, *133*, 13898-13901.

(92) Steckler, T. T.; Lee, M. J.; Chen, Z.; Fenwick, O.; Andersson, M. R.; Cacialli, F.; Sirringhaus, H. *J. Mater. Chem. C,* **2014**, *2*, 5133-5141.

(93) Steckler, T. T.; Fenwick, O.; Lockwood, T.; Andersson, M. R.; Cacialli, F. *Macromol. Rapid Commun.,* **2013**, *34*, 990-996.

(94) Steckler, T. T.; Henriksson, P.; Mollinger, S.; Lundin, A.; Salleo, A.; Andersson, M. R. *J. Am. Chem. Soc.,* **2014**, *136*, 1190-1193.

(95) Liu, J.; Geng, J.; Liao, L.-D.; Thakor, N.; Gao, X.; Liu, B. *Poly. Chem.,* **2014**, *5*, 2854-2862.

(96) Matsui, J.; Mitsuishi, M.; Aoki, A.; Miyashita, T. *Angew. Chem. Int. Ed.,* **2003**, *42*, 2272-2275.

(97) Matsui, J.; Mitsuishi, M.; Aoki, A.; Miyashita, T. *J. Am. Chem. Soc.,* **2004**, *126*, 3708-3709.

(98) Li, H.; Zhou, F.; Tam, T. L. D.; Lam, Y. M.; Mhaisalkar, S. G.; Su, H.; Grimsdale, A. C. *J. Mater. Chem. C,* **2013**, *1*, 1745-1752.

(99) Inganäs, O.; Zhang, F. L.; Andersson, M. R. *Acc. Chem. Res.,* **2009**, *42*, 1731-1739.

(100) Fan, J.; Yuen, J. D.; Cui, W. B.; Seifter, J.; Mohebbi, A. R.; Wang, M. F.; Zhou, H. Q.; Heeger, A.; Wudl, F. *Adv. Mater.,* **2012**, *24*, 6164-6168.

(101) Steckler, T. T.; Zhang, X.; Hwang, J.; Honeyager, R.; Ohira, S.; Zhang, X.-H.; Grant, A.; Ellinger, S.; Odom, S. A.; Sweat, D.; Tanner, D. B.; Rinzler, A. G.; Barlow, S.; Brédas, J.-L.; Kippelen, B.; Marder, S. R.; Reynolds, J. R. *J. Am. Chem. Soc.,* **2009**, *131*, 2824-2826.

(102) Sonar, P.; Singh, S. P.; Li, Y.; Soh, M. S.; Dodabalapur, A. *Adv. Mater.,* **2010**, *22*, 5409-5413.

(103) Cho, S.; Lee, J.; Tong, M.; Seo, J. H.; Yang, C. *Adv. Funct. Mater.,* **2011**, *21*, 1910-1916.

(104) Ashraf, R. S.; Kronemeijer, A. J.; James, D. I.; Sirringhaus, H.; McCulloch, I. *Chem. Commun.,* **2012**, *48*, 3939-3941.

(105) Kronemeijer, A. J.; Gili, E.; Shahid, M.; Rivnay, J.; Salleo, A.; Heeney, M.; Sirringhaus, H. *Adv. Mater.,* **2012**, *24*, 1558-1565.

(106) Sonar, P.; Foong, T. R. B.; Singh, S. P.; Li, Y. N.; Dodabalapur, A. *Chem. Commun.,* **2012**, *48*, 8383-8385.

(107) Luo, M.; Shadnia, H.; Qian, G.; Du, X.; Yu, D.; Ma, D.; Wright, J. S.; Wang, Z. Y. *Chem. Eur. J.,* **2009**, *15*, 8902-8908.

(108) Tam, T. L.; Li, H.; Lam, Y. M.; Mhaisalkar, S. G.; Grimsdale, A. C. *Org. Lett.,* **2011**, *13*, 4612-4615.

Chapter 2. Benzodithiophene-Thiadiazoloquinoxaline Based Polymers with Distinct Linkage Patterns
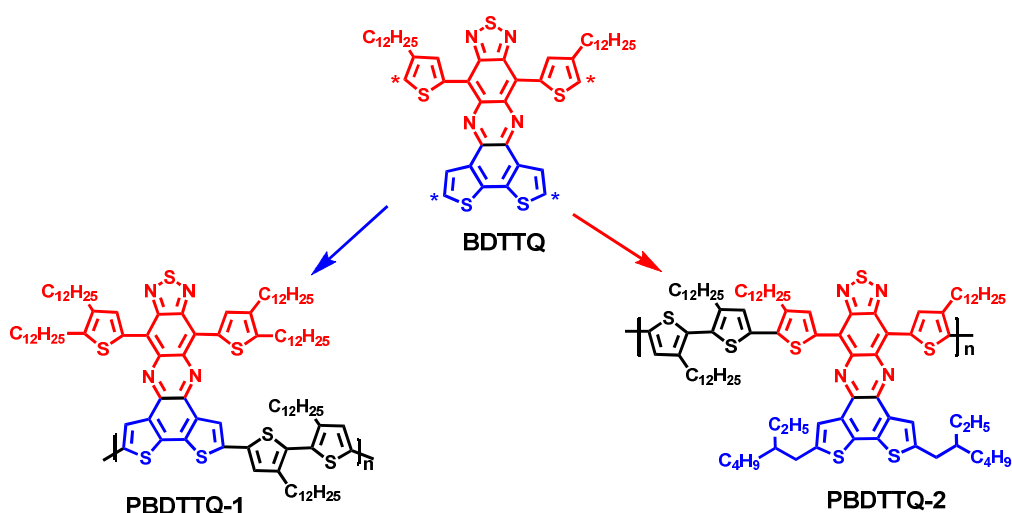
A highly conjugated benzodithiophene-thiadiazoloquinoxaline (**BDTTQ**) was synthesized. Two new conjugated copolymers, **PBDTTQ-1** and **PBDTTQ-2**, were constructed with distinct linkage patterns between **BDTTQ** and alkylated bithiophene. The difference in the linkage between donor and acceptor exerts great influence on their optoelectronic properties. Surprisingly, density functional theory calculations demonstrate that the electron density is mainly confined on the acceptor unit in both HOMO and LUMO of **PBDTTQ-1**, while the electronic density almost delocalizes along the entire backbone of **PBDTTQ-2**. In contrast to **PBDTTQ-1** not providing a field-effect transistor response, **PBDTTQ-2** exhibits ambipolar charge transporting behavior. **PBDTTQ-2** was fabricated for all-polymeric solar cells with P3HT as donor part. The power conversion efficiency, however, was very low.

Note: Large part of this chapter has been published in *Macromolecules,* **2014**, *47*, 979-986.

2.1 Introduction

Low bandgap π-conjugated copolymers composed of alternating donor (D) and acceptor (A) moieties have proven to be successful in improving device properties in organic light-emitting diodes (OLEDs), organic photovoltaics (OPVs) and organic field-effect transistors (OFETs).[1-5] The strong acceptor can be beneficial for developing low bandgap copolymers with deep LUMO levels, which imparts characteristics of transporting negative charge through the polymers and improves the stability. Currently, some strong acceptors (Figure 2.1) have been applied to make promising D-A copolymers, such as diketopyrrolopyrrole (DPP),[6,7] perylene bisimide (PBI),[8,9] naphthalene diimide (NDI),[10,11] and benzobisthiadiazole (BBT).[12,13] The development of new strong acceptors that can be used for constructing D-A polymers with deep LUMO levels and ambipolar charge carrier transport remains still challenging.
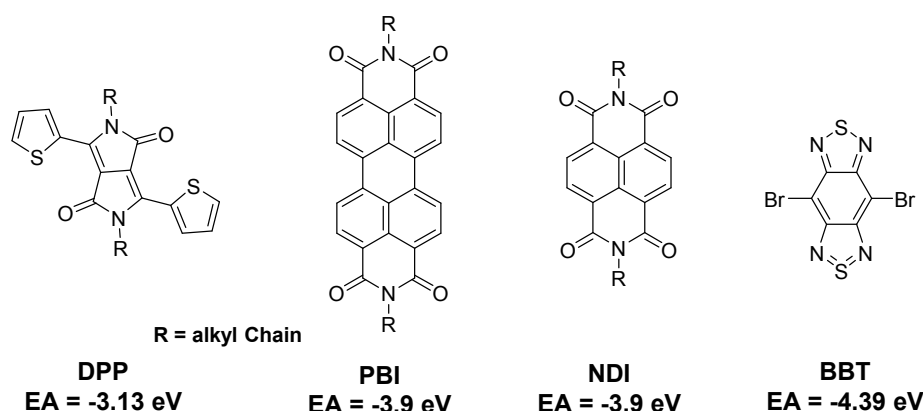
Figure 2.1 The structures of DPP[14], PBI[15], NDI[16] and BBT[17]. Their electron affinities (EA) were investigated by cyclic voltammetry.

As previous redox potential investigations, thiadiazoloquinoxalines (TQs) are much stronger electron acceptors (EA~ -3.43 to -3.83 eV)[18,19] than DPP (EA~ -3.13 eV).[14] Additionally, TQs can be modified via functionalization at the 6 and 7 positions (Figure 2.2, I) to increase the solubility or improve device performance.[20-24] Copolymers made from TQs have been reported as promising p-type semiconductors. In these polymers, TQs which were usually flanked with two thiophene units at the 4 and 9 positions were copolymerized with donors such as fluorene,[25] thiophene[26] and dithieno[3,2-*b*:2',3'-*d*]pyrrole[27] and only a few

copolymers showed decent hole transporting properties, but no ambipolar behavior was observed. Introducing acetylenic π-spacers into the main chains of TQ-based polymers can reduce the twist within the polymer backbones (Figure 2.2, II),[19] leading to ambipolar polymer semiconductors. The extension of π-conjugation length in the TQ core has also been proven to effectively lower the LUMO level and strengthen the electron-withdrawing ability.[28] However, these extended fused TQ derivatives have not been used as acceptors to construct D-A copolymers applied in OFETs until now.
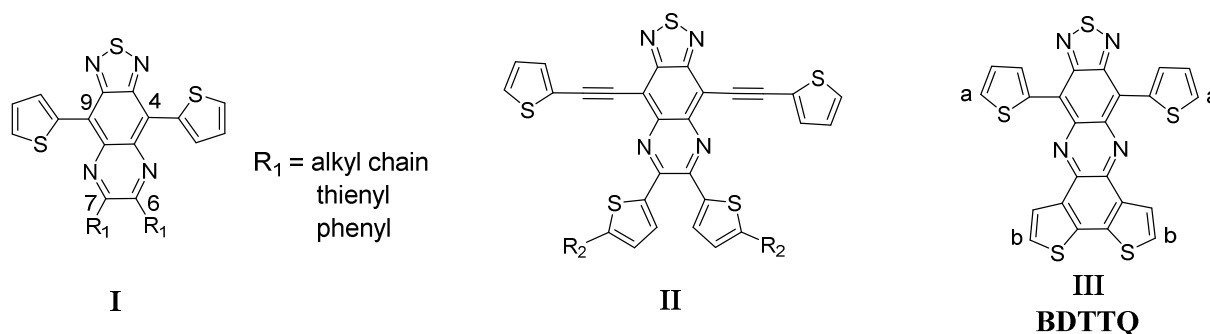

Figure 2.2 TQ-based acceptors from the literature and a new TQ condensed core acceptor III presented in this chapter.

Benzodithiophene-thiadiazoloquinoxaline (**BDTTQ**) was thus designed by fusing the thiophene rings to form a larger π-conjugated system (Figure 2.2, III). The two thiophenes at both sides provide more alkylated positions to improve its solubility. This new acceptor can be expected to provide lower LUMO level and electron transporting property when being incorporated into the polymer backbone. More interestingly, the **BDTTQ** unit possesses two couples of active sites (a and b Figure 2.2, III) for polymerization, which offers an opportunity to make D-A polymers with distinct linkage pattern between **BDTTQ** core and donors. In view of the different electron density distribution on the **BDTTQ** core (electron-donating BDT part and electron-accepting TQ part), we can tune the optical behavior, energy levels, as well as the transport behavior of the copolymers by changing the linking pathway.

In this chapter, we report two new D-A copolymers (**PBDTTQ-1** and **PBDTTQ-2**, Scheme 2.4) containing **BDTTQ** as acceptor. To increase the solubility of both copolymers, substituents as n-dodecyl and 2-ethylhexyl were introduced for **PBDTTQ-1** and **PBDTTQ-2**, respectively. In spite of having same donor and acceptor units in the polymers, both polymers

present remarkably different electron distributions and D-A interactions in the polymer chains. For **PBDTTQ-1**, the **BDT** part of **BDTTQ** is located in the conjugated backbone, whereas the **TQ** moiety is suspended around the periphery of the polymer main chains, which implies that the electron density will be mostly confined on the **TQ** moiety, thereby weakening the charge transfer between donor and acceptor units. In comparison, the **TQ** moiety of **BDTTQ** in **PBDTTQ-2** fully participates in the conjugation along the polymer main chain facilitating the D-A interaction. Comparative investigations on both polymers revealed that the linkage pattern in **PBDTTQ-2** is far better for extension of the conjugation thereby narrowing the bandgap, deepening the LUMO level, and improving the charge carrier transport.

2.2 Synthesis and characterization

Although both monomers have the same skeleton, they were prepared using completely different routes, taking the introduction of solubilizing side chains and bromines at different positions into account. The synthesis of **Br$_2$-BDTTQ-1** is depicted in Scheme 2.1. The starting material 2-bromo-3-dodecylthiophene (**1**) was prepared from commercial 3-bromothiophene after Kumada coupling followed by bromination,[29,30] which was converted to 1,2-didodecylthiophene (**2**) by Kumada coupling again with Grignard regent in 79% yield.
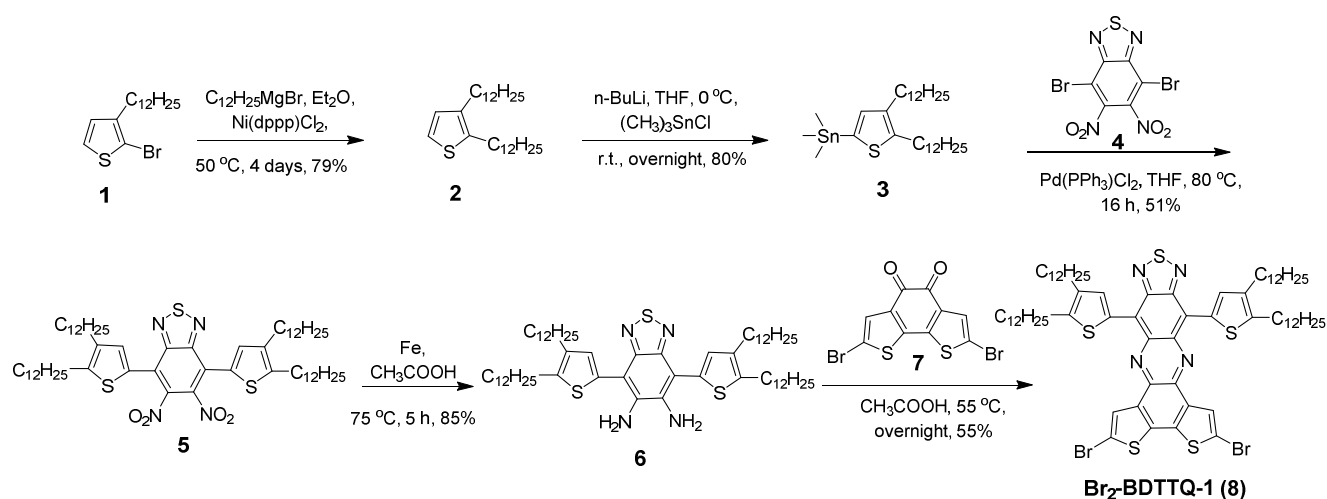
Scheme 2.1 Synthetic routes for monomer **Br$_2$-BDTTQ-1**.

Afterwards, the dialkylated thiophene **2** was used in a stanylation reaction to provide 2-

trimethylstannyl-4,5-didodecylthiophene (**3**). Stille coupling reaction between **3** and 4,7-dibromo-5,6-dinitrobenzothiadizole (**4**) produced dinitro compound **5**, which was reduced by iron in acetic acid to obtain diamine **6**. Subsequently, condensation between **6** and dibromo-diketone **7** gave the monomer **Br$_2$-BDTTQ-1**.
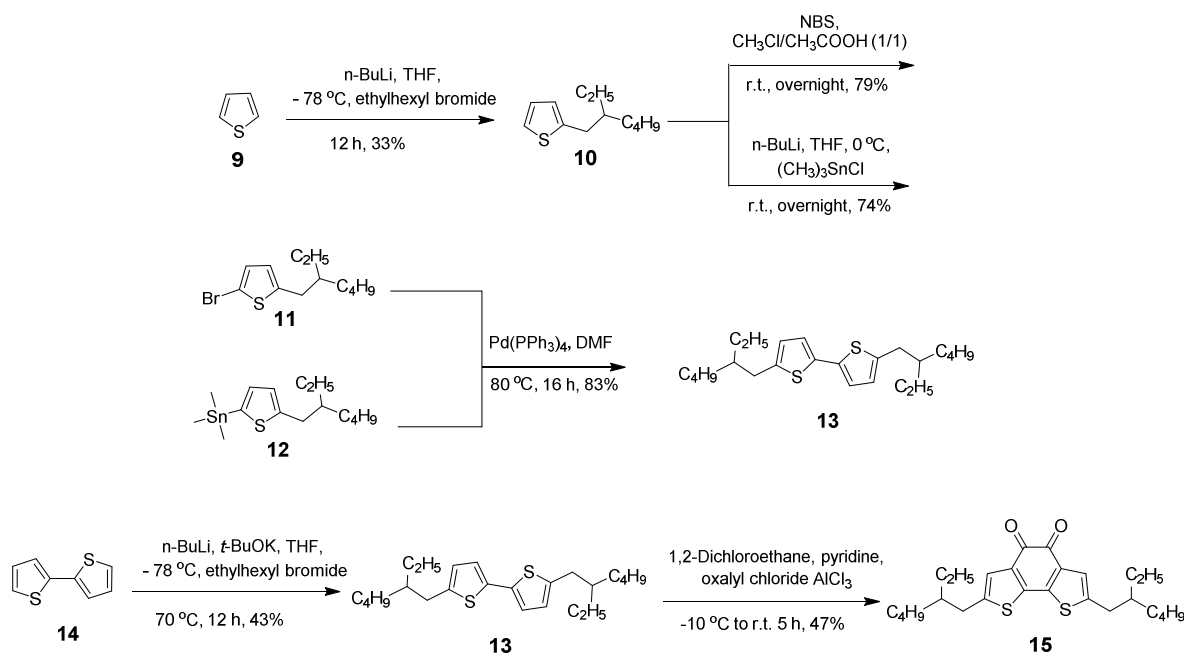
**Scheme 2.2** The optimized synthetic route for compound **15**.

In order to obtain a more soluble monomer **Br$_2$-BDTTQ-2,** the key intermediate 2,7-bis(2-ethylhexyl)benzo[2,1-b:3,4-b']dithiophene-4,5-dione (**15**) was synthesized and optimized as shown in Scheme 2.2. Initially, compound **13** was synthesized from commercial thiophene by a well-known procedure. This synthetic procedure is time-consuming for workup due to a four-step reaction. Another issue is a low yield in the first step. To improve working efficiency, we designed and achieved one step reaction to obtain compound **13** from bithiophene in yield of 43%. It is noteworthy that use of *t*-BuOK to enhance the reactivity of lithiated bithiophene[31] and heating to reflux were crucially important. Afterwards, inspired by our previous synthesis for alkylated phenyl-diketones,[19] compound **15** was obtained in just one step through Friedel-Crafts acylation in yield of 47%.

Monomer **Br$_2$-BDTTQ-2** was synthesized using another path as shown in Scheme 2.3. (4-Dodecylthiophen-2-yl)trimethylstannane (**16**) was prepared from commercial 3-

bromothiophene by first introducing n-dodecyl via Kumada coupling then performing stanylation.[29,32] The corresponding dinitro compound **17** was obtained using Stille coupling between **16** and **4**. Afterwards, it was reduced by iron and acetic acid to give diamine **18.** Considering the acidity of silica column gel could cause to alkaline substance loss even though the eluent was added to 5% triethylamine, compound **18** could be directly used without purification to condense with diketone **15** to yield compound **BDTTQ-2**. However, special attention needs to be paid to remove residual iron. Otherwise, the traces of iron could significantly decrease the yield in the following condensation. **BDTTQ-2** was then treated with NBS to produce **Br₂-BDTTQ-2**.
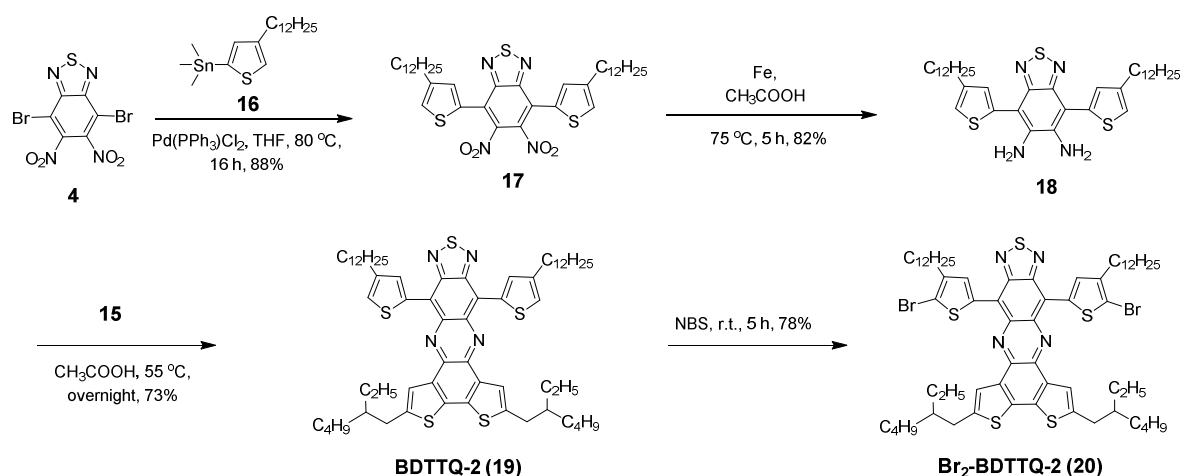
Scheme 2.3 Synthetic routes for monomer **Br₂-BDTTQ**

Before polymerization, both precursors, **Br₂-BDTTQ-1** and **Br₂-BDTTQ-2**, were dried more than 12 hours at 50 $^{\circ}$C under vacuum to remove residual solvents and water. Due to different solubility of both precursors, their ^{1}H-NMR spectra were measured in CDCl$_3$ for **Br₂-BDTTQ-1** and CD$_2$Cl$_2$ for **Br₂-BDTTQ-2**, respectively. Figure 2.3 displays two very clear ^{1}H-NMR spectra except the signal of water, which could stem from deuterated solvents. **Br₂-BDTTQ-1** and **Br₂-BDTTQ-2** have two aromatic peaks. However, the significant different peaks were observed in the NMR spectra. In the region between 2 and 3 ppm, the double triplet peaks of **Br₂-BDTTQ-1** are from its different dodecyl groups, while one doublet peak and one triplet peak of **Br₂-BDTTQ-2** are attributed to its 2-ethylhexyl and dodecyl side chains.
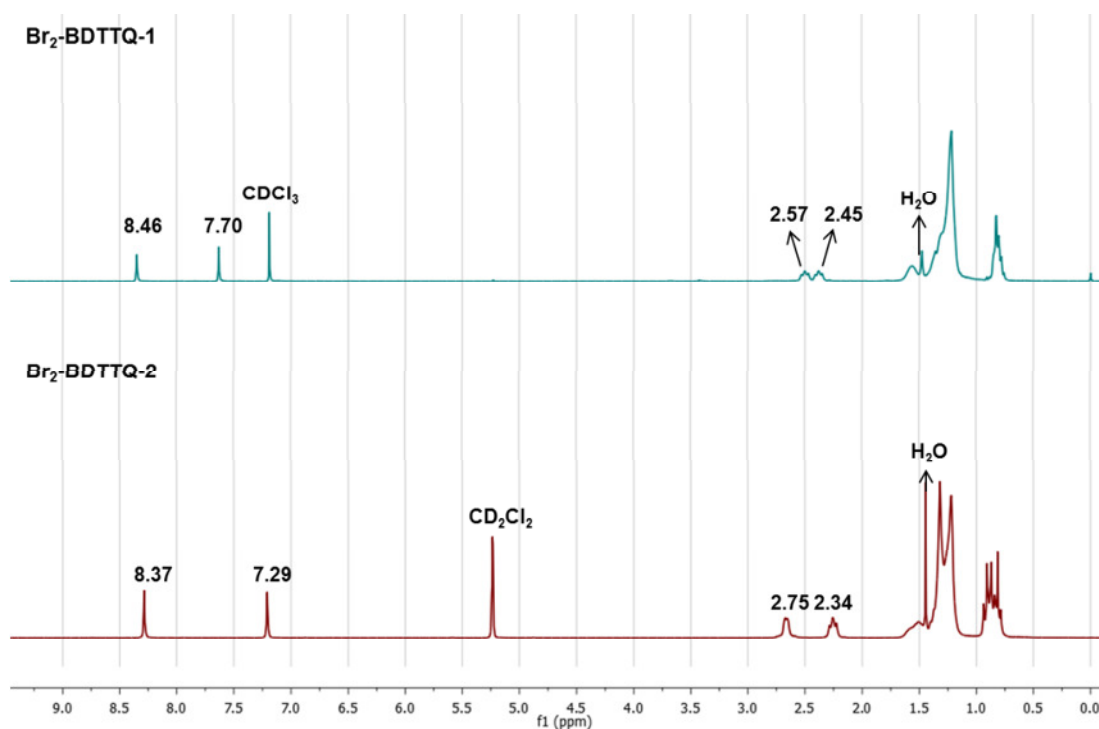
Figure 2.3 The ^{1}H-NMR spectra of **Br$_2$-BDTTQ-1** and **Br$_2$-BDTTQ-2**.
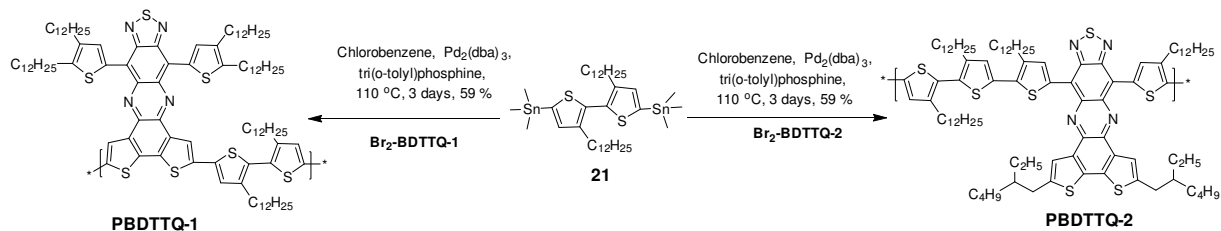
Scheme 2.4 Synthetic routes for two **BDTTQ**-based polymers.

The polymerizations were carried out through Stille coupling reaction between **Br$_2$-BDTTQ-1** or **Br$_2$-BDTTQ-2** and the same donor alkylated bithiophene (**21**, Scheme 2.4). Both polymers have excellent solubility in chloroform, tetrahydrofuran, toluene and chlorobenzene. The number-average molecular weights (M$_n$) of the polymers **PBDTTQ-1** and **PBDTTQ-2** were determined as 37.3 kg mol^{-1} and 11.8 kg mol^{-1} with polydispersity index (PDI) of 2.43 and 1.66, respectively (Figure 2.4, Table 2.1). The polymerization was tried several times to enhance the M$_n$ of **PBDTTQ-2**, including microwave reaction (M$_n$ 9.6 K, PDI 1.27, Figure 2.4), but the results were similar to those mentioned above. It may arise from the steric hindrance induced by the n-dodecyl chain at β position of the thiophene in monomer **Br$_2$-BDTTQ-2** preventing to produce higher molecular weight during polymerization.
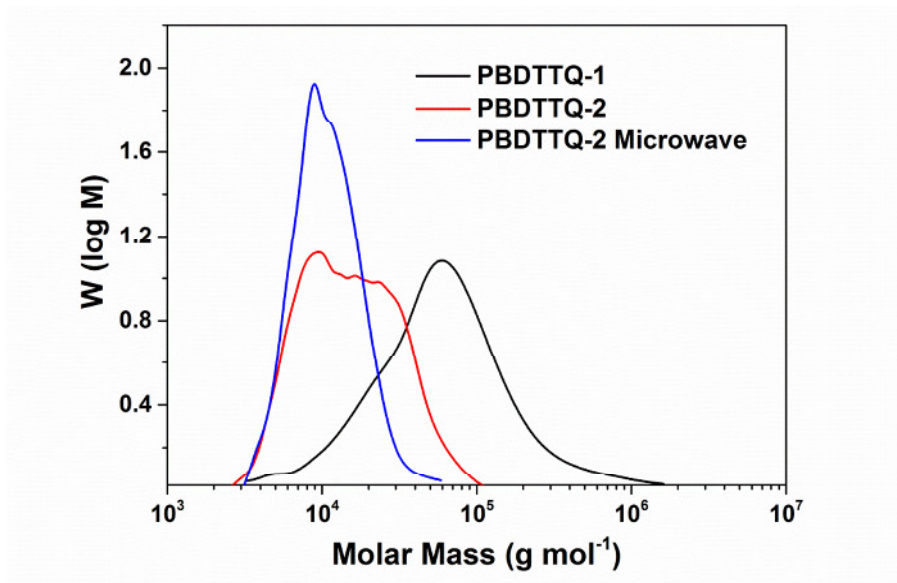
Figure 2.4 GPC curves for **PBDTTQ-1** and **PBDTTQ-2**. Polystyrene was used as standard and THF as eluent at 30 °C.
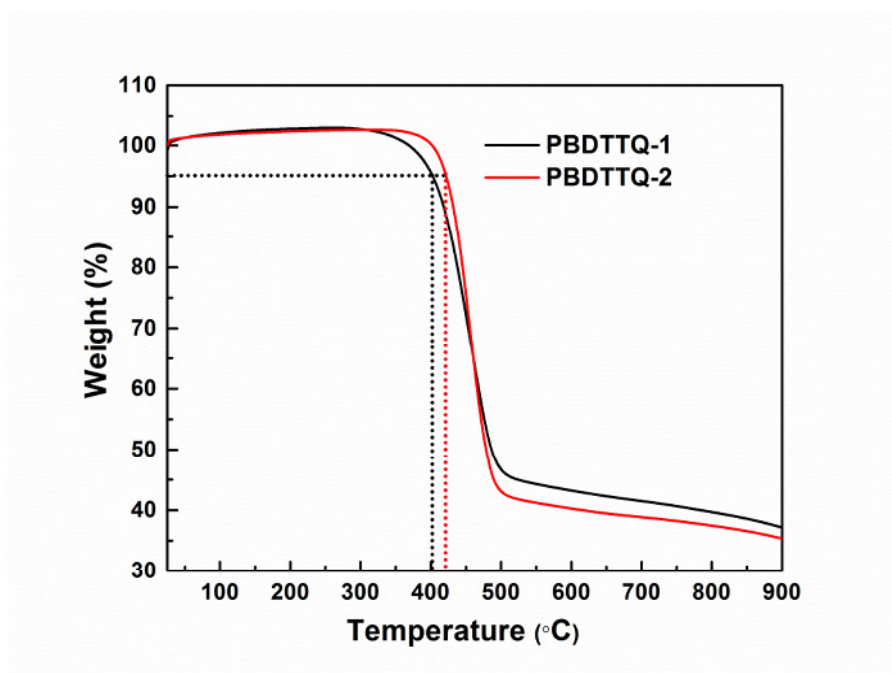
Figure 2.5 TGA curves for **PBDTTQ-1** and **PBDTTQ-2** measured under a nitrogen atmosphere at a heating rate of 10 °C/min.

The thermal properties of the copolymers were investigated by thermogravimetric analysis (TGA) as shown in Figure 2.5. Both copolymers exhibited excellent thermal stability, with 5% weight loss upon heating at 403 and 422 °C for **PBDTTQ-1** and **PBDTTQ-2**,

respectively. The weight of both polymers are lost around 54% and 57% when the temperature was raised to 500 °C, these values are very close to the weight ratio of the side chains (57% and 60%) in **PBDTTQ-1** and **PBDTTQ-2,** respectively. It suggests that first side chains of both polymers are decomposed with increasing temperature.

2.3 Optical properties

The optical properties of both polymers were investigated in chloroform solutions (c = 10^{-5} M) and in films prepared by drop-casting onto glass slides from 10 mg/mL chloroform solutions. The data are summarized in Table 1. In dilute chloroform solutions, **PBDTTQ-1** and **PBDTTQ-2** exhibit two main absorption bands as shown in Figure 2.6a. The first intense band covers from 300 to 550 nm and the second ranges from 600 to 1200 nm. The higher energy absorption band corresponds to the π-π* transition of the conjugated backbone, whereas the lower one should be attributed to intramolecular charge transfer (ICT) between donor and acceptor in the conjugated backbone.[33] To investigate the influence of the different pattern of linkage on the optical properties of the two polymers, the absorptions of two monomers **Br$_2$-BDTTQ-1** and **Br$_2$-BDTTQ-2** were also recorded in Figure 2.6a. Two monomers present π-π* transitions at higher energy region and broad absorption band between 600 and 1000 nm similar to those of the corresponding polymers. The latter can be assigned to the ICT between thiophene and fused aromatic ring condensed **TQ** moiety. The difference in maximum absorption of both monomers may originate from the different electron-donating contribution of alkyl chains. Interestingly, compared to the absorption maxima of the monomers, **PBDTTQ-2** exhibits a red shift around 130 nm, while polymer **PBDTTQ-1** shows a smaller red shift of only 40 nm, implying the stronger ICT process in **PBDTTQ-2** than that in **PBDTTQ-1**. This result suggest that electrons are mainly limited on the **TQ** moiety in **PBDTTQ-1**, leading to ineffective charge transfer along the polymer chains, whereas in **PBDTTQ-2**, the electrons can better delocalize along the whole polymer backbone.
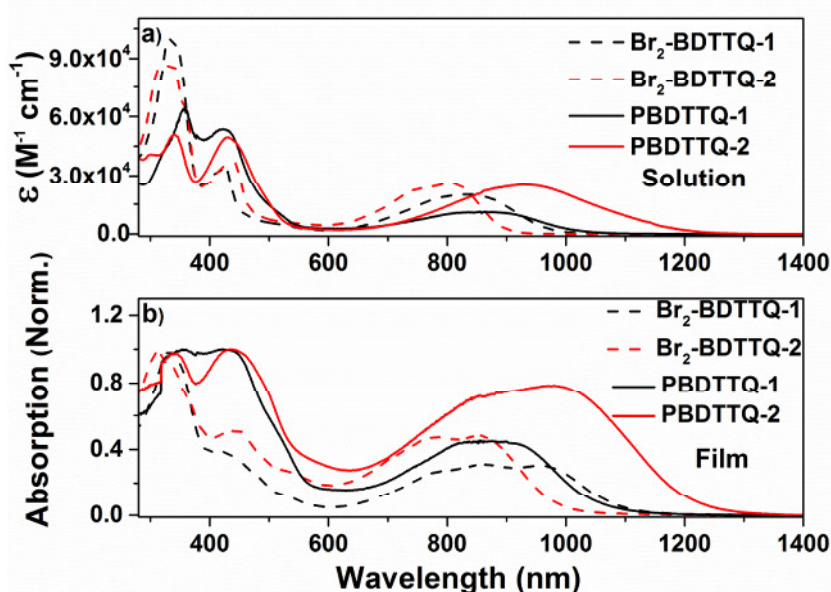
Figure 2.6 UV-visible-NIR absorption spectra of two monomers and copolymers in a) chloroform solutions (c = 10^{-5} M) and b**)** films.

In the films (Figure 2.6b), the two polymers display slightly broader spectra which are even further bathochromically shifted compared with those in solutions. **PBDTTQ-2** shifts to red around 50 nm contrasted with around 15 nm for **PBDTTQ-1**, indicating that **PBDTTQ-2** possesses stronger interaction between the polymer chains than **PBDTTQ-1** in the solid state. In comparison with **Br$_2$-BDTTQ-1**, surprisingly, the optical band edge of **PBDTTQ-1** has a slight blue-shift, it is related to two aspects: (1) **PBDTTQ-1** has an ineffective charge transfer along the polymer main chains as confirmed by absorption spectra in solution. (2) The head-to-head alkylated bithiophene in **PBDTTQ-1** led to its twisted conjugated backbone, it thereby decreased interaction between the polymer main chains, while more planar **Br$_2$-BDTTQ-1** was beneficial for intermolecular interactions.

On the other hand, the intensity of long wavelength of these polymers is weaker than the low ones in solution and solid state. The intensity of long wavelength to low wavelength ratio (OD$_2$/OD$_1$) represented the molecular charge transfer ability. The OD$_2$/OD$_1$ values of both polymers are 0.17 and 0.49 in solutions, 0.45 and 0.78 in films for **PBDTTQ-1** and **PBDTTQ-2**, respectively. These results are related to the fact that **PBDTTQ-2** has stronger charge carrier transfer ability than **PBDTTQ-1** in solutions and films. Additionally, optical band gaps are 1.18 eV and 1.03 eV, calculated according to the absorption onset of the thin

films for **PBDTTQ-1** and **PBDTTQ-2**, respectively. These results demonstrate that the strong acceptor **BDTTQ** is favorable to develop narrow bandgap copolymers, and the different combination between donor and **BDTTQ** core allow efficient tuning of the optical properties.
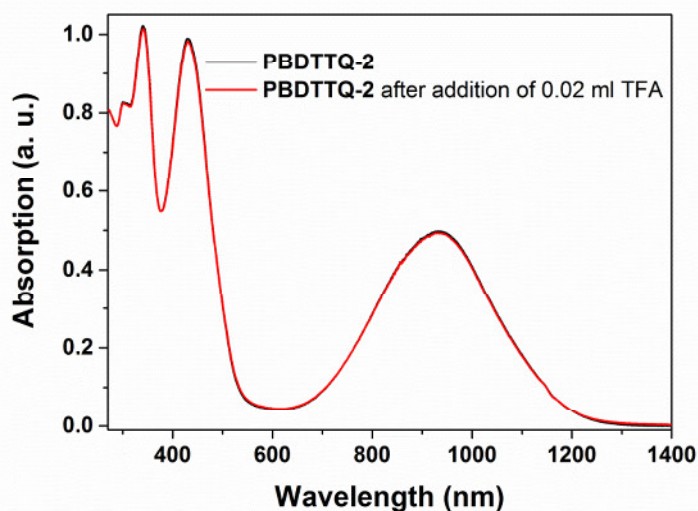
Figure 2.7 UV-visible-NIR absorption spectra of **PBDTTQ-2** in chloroform solution
(c = 2×10^{-5} M) with and without TFA.

To investigate protonation of the nitrogens in **PBDTTQ-2**, we measured the UV-vis-NIR spectrum of **PBDTTQ-2** in chloroform solution (Figure 2.7). Then 0.02 mL of trifloroacetic acid (TFA) was added into the sample cell, and shaken it for ten seconds. After 2 minutes, the solution was measured again (red line) and found that the two spectra overlapped very well, implying TFA did not protonate the nitrogens in **PBDTTQ-2**. It might originate from that the pair of electrons in nitrogens were delocalized over the whole π-conjugated system.

2.4 Electrochemical properties

The electron affinity (EA) and ionization potential (IP) of both copolymers were evaluated by cyclic volatammetry (CV) of the thin films.[34] The reduction and oxidation curves of copolymers are shown in Figure 2.8 and the corresponding electrochemical data are summarized in Table 2.1. Both copolymers exhibit irreversible oxidation waves and reversible reduction waves, implying their potential in transporting negative charge. According to the

first onset potentials, the EA and IP were estimated to be -5.50 and -3.86 eV for **PBDTTQ-1**, -5.48 and -4.01 eV for **PBDTTQ-2**, respectively. This result shows that the extension of π-conjugation of TQ is a viable strategy to obtain stronger acceptors with lower band gap of the polymers thus possessing deep EA. Moreover, the linkage pattern in **PBDTTQ-2** can obviously lower the EA more than that in **PBDTTQ-1**. The electrochemical band gaps are 1.64 eV and 1.47 eV for **PBDTTQ-1** and **PBDTTQ-2**, respectively. The difference between the optically and electrochemically measured energy gaps can be explained by the exciton binding energy of the copolymers.[35]
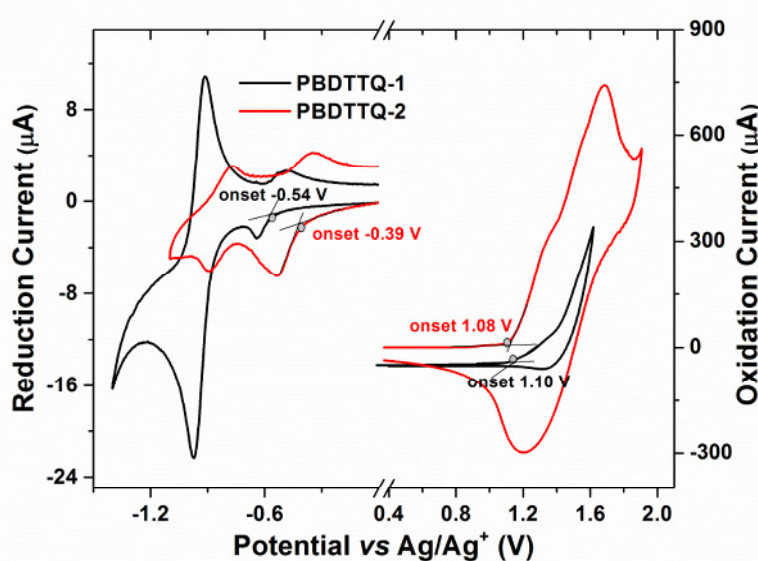
Figure 2.8 Reduction (left) and oxidation (right) of two polymer films deposited from chloroform.

Table 2.1 Optical and electrochemical data of the polymers.

Polymers	M_w/M_n[a] (kg/mol)	λ_{abs} (nm) soln.[b]	λ_{abs} (nm) film[c]	E_g^{opt} (eV)[c]	IP (eV)[d]	EA (eV)[d]	E_g^{ec} (eV)
PBDTTQ-1	90.7/37.3	358, 422, 860	357, 421, 875	1.18	-5.50	-3.86	1.64
PBDTTQ-2	19.6/11.8	340, 430, 928	340, 438, 978	1.03	-5.48	-4.01	1.47

[a]Determined by GPC in THF using polystyrene standards. [b]Dissolved in choloform (c = 10^{-5} M). [c]Drop-casted from choloform solution (10 mg/mL). [d]HOMO and LUMO levels were estimated from the onsets of the first oxidation and reduction peak, respectively, while the potentials were determined using ferrocene (Fc) as standard by empirical formulas E_{EA} = - (E_{Red}^{onset} - $E_{Fc/Fc+}^{1/2}$ + 4.8) eV and E_{IP} = - (E_{Ox}^{onset} - $E_{Fc/Fc+}^{1/2}$ + 4.8) eV , wherein $E_{Fc/Fc+}^{1/2}$ = 0.40 eV.

2.5 OFET and self-organization properties

Figure 2.9 Transfer (a) and output (b) curves of **PBDTTQ-2**.

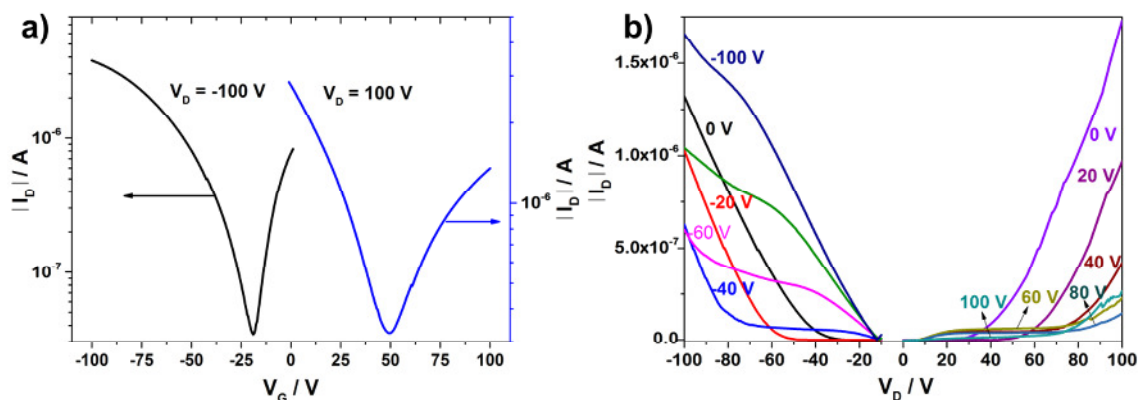The charge carrier transport of both polymers was studied in collaboration with ███ ██████████████████████████ (Max Planck Institute for Polymer Research, Mainz). The field-effect transistors were fabricated based on a bottom-gate, bottom-contact architecture. The 200 nm thick SiO_2 dielectric was functionalized with hexamethyldisilazane (HMDS) to minimize interfacial trapping sites. The copolymer thin films were deposited by spin-coating (1200 rpm, 60 s) of a 10 mg/mL $CHCl_3$ solution under nitrogen atmosphere, followed by annealing at 150 °C for 1 h. **PBDTTQ-1** and **PBDTTQ-2** exhibited significant differences in device performance. **PBDTTQ-1** did not show any field-effect response, While **PBDTTQ-2** led to an ambipolar transport with mobilities of 1.2×10^{-3} cm^2 V^{-1} s^{-1} for holes and 6.0×10^{-4} cm^2 V^{-1} s^{-1} for electrons with the I_{on}/I_{off} around 100 and 10, respectively (Figure 2.9a). The low I_{on}/I_{off} values of **PBDTTQ-2** are very common in TQ based polymers as semiconductors. In the negative drain mode for $V_D < 0$ V (Figure 2.9a), the crossover point is located at round $V_G = -18$ V, implying a current conversion from electron- to hole-dominated transport. Below this gate voltage the transistor exhibit p-type behavior. Additionally, the output characteristic (Figure 2.9b) shows a nonlinear behavior of the current at low V_D. It is related to the device contact resistance.

To gain an understanding of the device performance, the organization of both copolymers in the bulk and thin film were investigated in collaboration with ████████████████
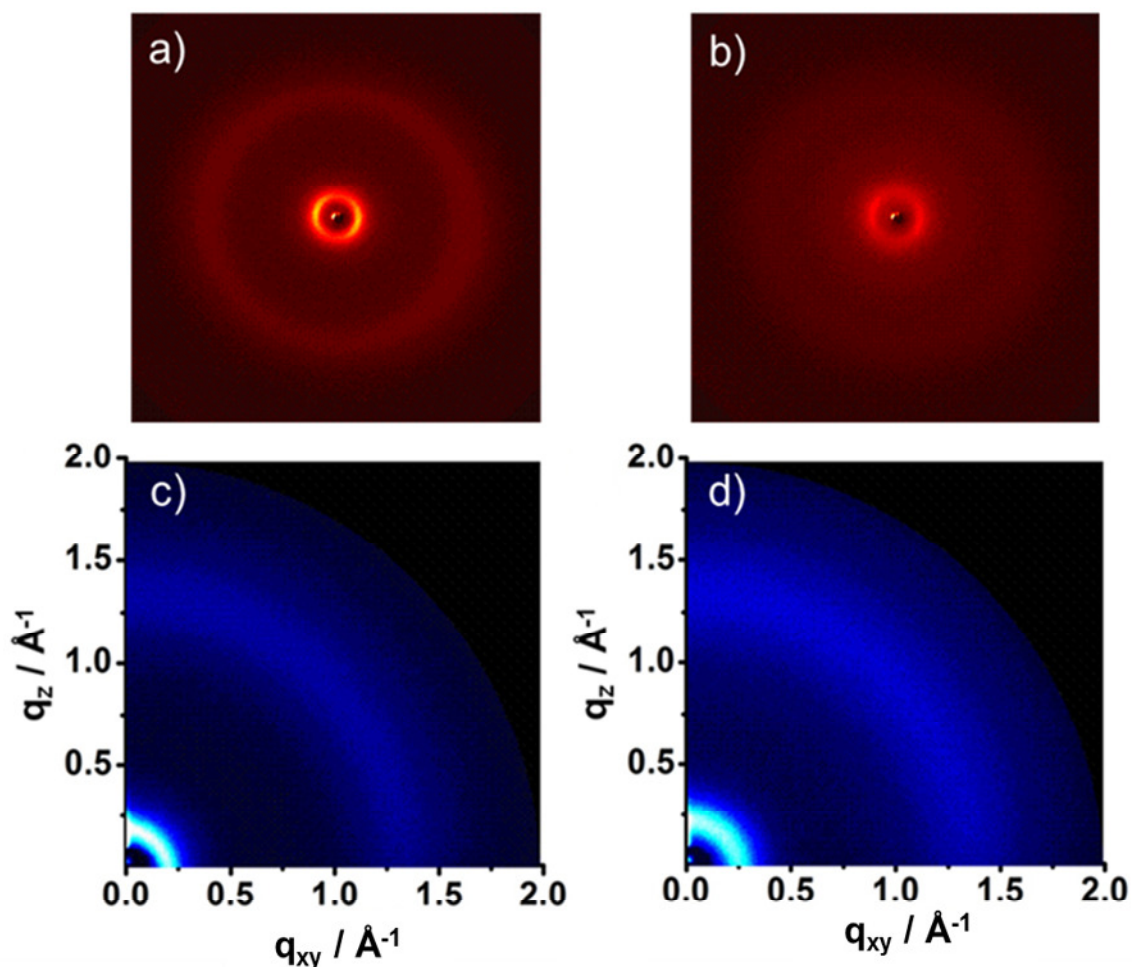
Figure 2.10 2DWAXS of a) **PBDTTQ-1** and b) **PBDTTQ-2**. The fiber sample was mounted vertical towards the 2D detector. GIWAXS of c) **PBDTTQ-1** and d) **PBDTTQ-2**.

For the bulk organization, two-dimensional wide-angle X-ray scattering measurements (2DWAXS) of extruded, macroscopically aligned fibers were performed. For both cases, only equatorial reflections in the small-angle region appeared which were related to the chain-to-chain distance between lamellar stacks aligned along the extrusion direction of the fiber (Figure 2.10a and 2.10b). A distance of 2.50 nm for **PBDTTQ-1** and 2.20 nm for **PBDTTQ-2** was determined. However, no scattering intensities for the π-stacking were found indicating pronounced disorder of the conjugated polymers in the lamellar structures. The disordered assembly may be due to the high steric hindrance between the alkyl chains as well as the large size of **BDTTQ** unit at the lateral direction not allowing a close and defined packing of the

backbones on top of each other. This was further confirmed by the strong amorphous halo of the alkyl side chains. Grazing incidence WAXS (GIWAXS) confirmed the low order also in thin films (Figure 2.10c and 2.10d). The GIWAXS patterns revealed only one isotropic reflection which was correlated to the chain-to-chain spacing of randomly arranged lamellar structures towards the surface. Therefore, the amorphous morphology should be responsible for the relative low charge mobility. However, no obvious difference was observed for both polymers from the X-ray characterizations which could provide an explanation for the discrepancy between both polymers in device performance. Therefore, density functional theory (DFT) calculations were carried out.

2.6 Density functional theory calculations
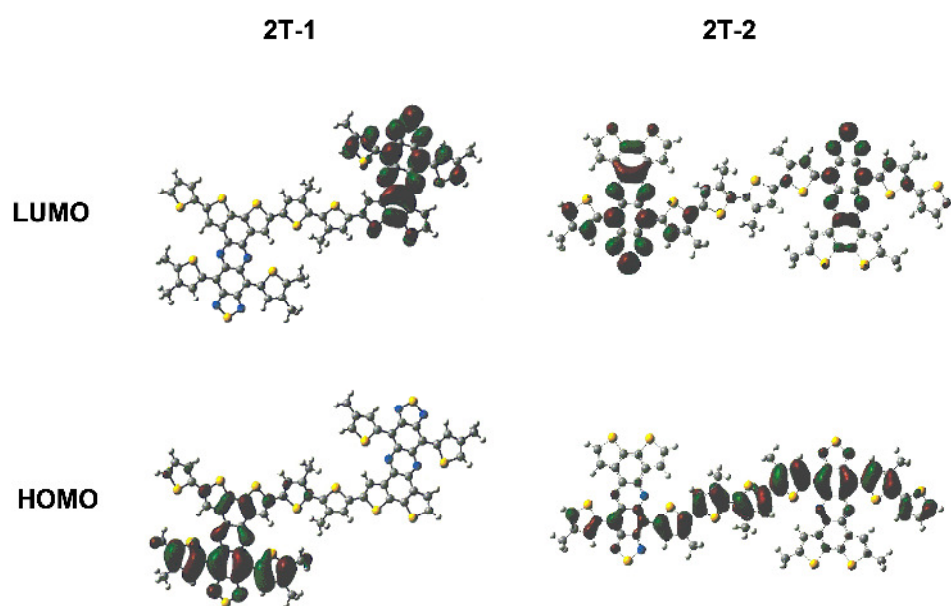
Figure 2.11 LUMO (top) and HOMO (bottom) distributions for the minimum energy conformations of methyl substituted models of **2T-2BDTTQ-1 (2T-1)** and **2T-2BDTTQ-2 (2T-2)** optimized with Gaussian at the B3LYP/6-31G* level.

DFT calculations were carried out on two models of acceptor-donor-acceptor arrangement carrying methyl substituents, named **2T-1** and **2T-2** for **2T-2BDTTQ-1** and **2T-2BDTTQ-2**, respectively. The electron density distributions of the LUMO and HOMO of geometry optimized structures are shown in Figure 2.11. For both LUMO and HOMO levels

of **2T-1**, the electrons are only localized upon one of both electron accepting **BDTTQ** cores, which could prevent the efficient electron transport along the conjugated backbone. This in combination with its disorder assembly prevents interchain charge transfer that leads to absent of charge carrier transporting in **PBDTTQ-1**. In contrast, electrons of the HOMO and LUMO levels of **2T-2** are both well delocalized over the conjugated repeat unit. This may partly explain the observed ambipolar behavior of **PBDTTQ-2**.[36] In addition, the results from DFT calculations are well consistent with the observations from absorption spectra, demonstrating the stronger ICT process between donor and acceptor in **PBDTTQ-2** than that in **PBDTTQ-1**. It can hence be concluded that the way of linking cannot tune the organization behavior in bulk and in film as verified by the structural analysis but can strongly influence the electron distributions along the polymers main chains and therefore the change of carrier mobility.

2.7 All-polymeric solar cells for PBDTTQ-2
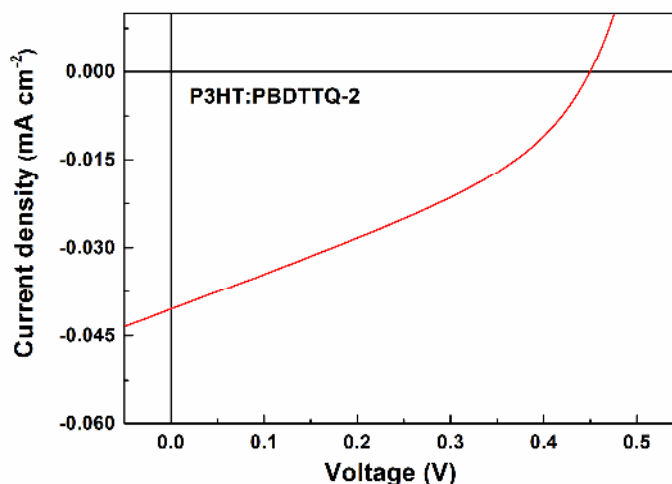
Figure 2.12 The J-V curve of all-polymer solar cells based on **P3HT**:**PBDTTQ-2** (5:4, w/w) under the illumination of AM 1.5 G 100 mW cm^{-2}.

PBDTTQ-2 exhibits a suitable LUMO energy levels (-4.01 eV) as acceptor in application for all-polymeric solar cells. It needs to be mentioned that the EA and IP were replaced by LUMO and HOMO energy levels in this section, in order to facilitate discussion based on the concepts of OPVs. Poly(3-hexylthiophene) (**P3HT**) was chosen as donor

material based on two reasons. Firstly, **P3HT** has match energy levels with LUMO of -3.20 eV and HOMO of -5.10 eV[37] for **PBDTTQ-2** (LUMO, -4.01 eV; HOMO, -5.48 eV). Secondly, **P3HT** is one of most studied donor material in OPVs.

The all-polymer solar cell devices were fabricated in collaboration with ██████ ████ (Max Planck Institute for Polymer Research, Mainz). The active layer was deposited by spin-coating (800 rpm, 30 s) from a chlorobenzene solution of the **P3HT:PBDTTQ-2** (5:4 weight ratio) onto indium tin oxide (ITO) glass substrates, which were precoated with PEDOT:PSS, followed by annealing at 150 °C for 30 min. Afterwards, 100 nm thick Al layer was vapor deposited onto the active layer. The device reached a very low power conversion efficiency (PCE, η) of 0.01%, with an open circuit voltage (V_{oc}) of 0.45 V, a fill factor (*FF*) of 0.36 and a short circuit current (J_{sc}) of 0.04 mA cm^{-2} (Figure 2.12). In our system, the low J_{sc} is a major reason to cause the low PCE as our group previously studied. Several reasons cause a low J_{sc},[38] such as an inefficient photoinduced electron transfer, short-lived free charges in the active layer and bad morphology for charge separation or transport. The device performance could not be further optimized and characterized, due to extremely low PCE. Previously, a TQ polymer **PPTQP** was also attempted in all–polymer solar cells with **P3HT** in our group, the PCE was only achieved up to 0.04%, with a low J_{sc} of 0.18 mA cm^{-2}. The investigation of morphology and mobility implied the unfavorable morphology of the active layer and low limited mobility of the acceptor could be the major factor for low PCE.[39]

2.8 Summary

In this chapter, we presented two copolymers **PBDTTQ-1** and **PBDTTQ-2** with different linkage between acceptor **BDTTQ** and donor alkylated bithiophene. With the **TQ** moiety of **BDTTQ** located in the main chains, **PBDTTQ-2** shows narrow optical bandgap of 1.03 eV and relatively strong EA of -4.01 eV, approximately 0.15 eV deeper than that for **PBDTTQ-1**, while maintaining IP at -5.50 eV. DFT calculations demonstrate that the electronic densities are only localized upon one of both electron accepting **BDTTQ** cores for **2T-1**, whereas the electron density of the LUMO and HOMO are both well delocalized over the conjugated repeat unit for **2T-2**. This is the reason for the pronounced differences of **PBDTTQ-1** and **PBDTTQ-2** in device performance. While **PBDTTQ-1** does not show any field-effect response, **PBDTTQ-2** exhibits an ambipolar transport with mobilities of 1.2×10^{-3}

cm^2 V^{-1} s^{-1} for holes and 6.0×10^{-4} cm^2 V^{-1} s^{-1} for electrons. Although **PBDTTQ-2** as acceptor match as the energy levels with **P3HT** as donor very well, the all polymeric solar cell exhibits a very low PCE of 0.01%, due to the extremely low J_{sc} (0.04 mA cm^{-2}).

The relatively low mobilities in OFET devices are mainly related to the lack of good π-stacking induced by the alkyl chains, as confirmed by 2DWAXS. It is believed that the charge carrier mobility can be further improved by deliberately reducing the number of alkyl chains in the polymer, on premise of ensuring solubility, to optimize assembled structure of the polymer. In order to understand this issue, it is necessary to investigate the structure-property relationships of TQ polymers. The charge carrier mobility and TQ polymer structure correlations are presented in Chapter 3.

2.9 Synthetic details

Intermediates 2-bromo-3-dodecylthiophene (**1**),[29,30] 4,7-dibromo-5,6-dinitro-2,1,3-benzothiadiazole (**4**),[40,41] 2,5-dibromo-benzo[2,1-b:3,4-b']dithiophene-7,8-quinone (**7**),[42,43] 2-trimethyl-4-dodecylthiophene (**16**)[32] and 5,5'-bis(trimethylstannyl)-3,3'-didodecyl-2,2'-bithiophene (**21**)[44] were prepared according to the literature procedures as shown in the schemes 2.5-2.9 below.
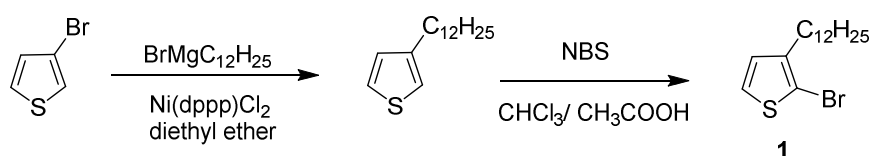
Scheme 2.5 Synthetic route for compound **1**.[29,30]
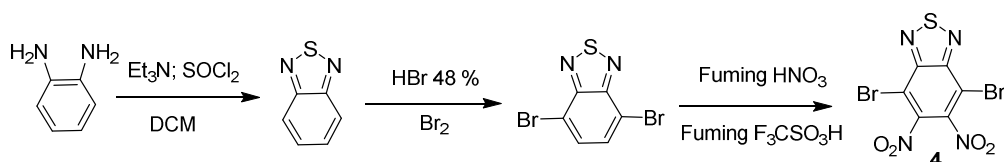
Scheme 2.6 Synthetic route for compound **4**.[40]
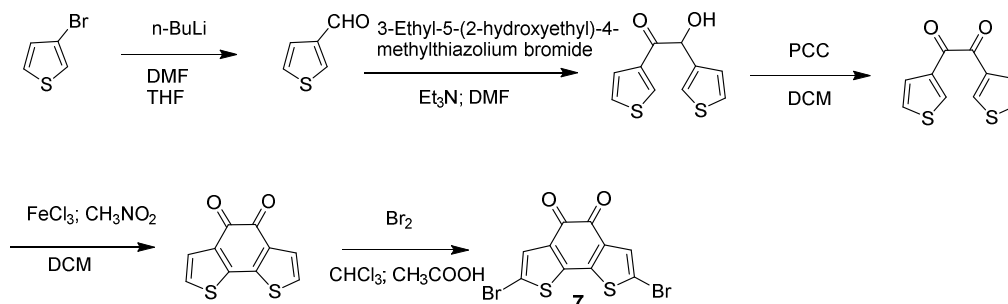
Scheme 2.7 Synthetic route for compound **7**.[41,42]
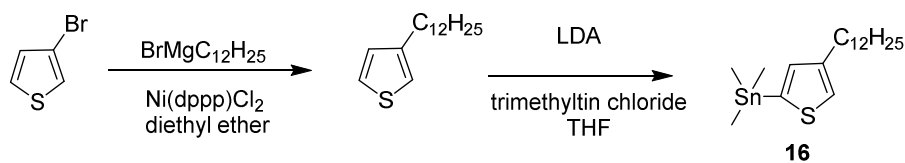
Scheme 2.8 Synthetic route for compound **16**.[29,32]
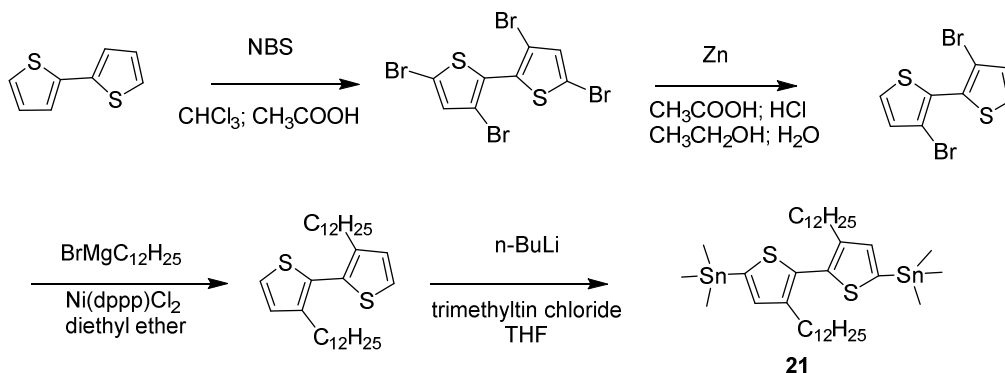
Scheme 2.9 Synthetic route for compound **21**.[43]

2,3-Didodecylthiophene (2)
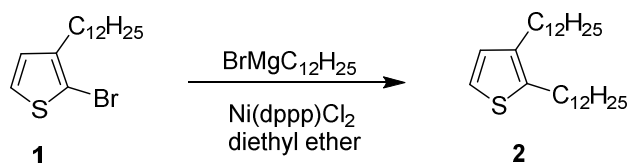
2-Bromo-3-dodecylthiophene (**1**, 2.5 g, 7.54 mmol) and Ni(dppp)Cl$_2$ (48.78 mg, 0.09

mmol) were dissolved in dry diethyl ether (20 mL) using a 100 mL flask. The mixture was cooled to 0 °C, and then *n*-dodecylmagnesium bromide (9.05 mL, 9.05 mmol, 1 M in diethyl ether) was added dropwise within 10 min. The resulting mixture was refluxed for 4 days. After cooling to room temperature, the mixture was poured into 100 mL of ice water and hydrolyzed with 1 N HCl. The mixture was extracted with diethyl ether (3×20 mL). The combined organic phases were dried with $MgSO_4$, and the solvent was removed under reduced pressure to afford a dark-red oil, which was purified by reduced pressure distillation (0.75 mbar; 180 °C) to give 2.49 g (colorless oil, 79%) of compound **2**. ^{1}H NMR (250 MHz, CD_2Cl_2) δ 7.01 (d, *J* = 5.00 Hz 1H), 6.80 (d, *J* = 5.25 Hz 1H), 2.71 (t, *J* = 7.50 Hz, 2H), 2.50 (t, *J* = 7.25 Hz, 2H), 1.64-1.52 (m, 4H), 1.27 (br, 36H), 0.88 (m, 6H); ^{13}C NMR (62.5 MHz, CD_2Cl_2) δ 139.28, 138.31, 129.13, 121.24, 32.53, 32.42, 31.39, 30.17, 30.14, 30.12, 30.08, 30.00, 29.98, 29.90, 29.85, 28.61, 28.17, 23.18, 14.35.

2-Trimethylstannyl-4,5-didodecylthiophene (3)
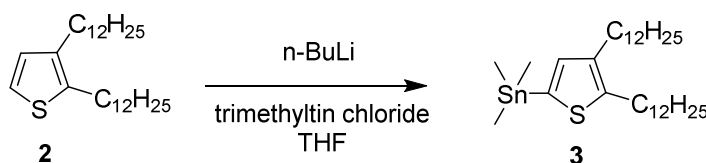
2,3-Didodecylthiophene (**2**, 1.80 g, 4.28 mmol) was dissolved in 36 mL of anhydrous THF. The n-BuLi (4.0 mL, 6.40 mmol, 1.6 M in hexane) was added slowly into this mixture whithin 15 min under 0 °C. The resulting solution was stirred for 20 min at 0 °C and warmed to room temperature over 30 min. The mixture was cooled to 0 °C again, and trimethyltin chloride (6.40 mL, 6.40 mmol, 1 M in hexane) was added dropwise. The mixture was stirred overnight, then poured into water and extracted with ether. The combined organic phases were washed with brine, dried by $MgSO_4$, and filtered. The filtrate was concentrated under reduced pressure to obtain compound **3** (yellow oil, 80%). This crude product was used for next step without further purification. ^{1}H NMR (250 MHz, CD_2Cl_2) δ 6.89 (s, 1H), 2.72 (t, *J* = 7.75 Hz, 2H), 2.50 (t, *J* = 7.50 Hz, 2H), 1.66-1.52 (m, 4H), 1.27 (br, 36H), 0.88 (m, 6H), 0.31 (m, 9H). ^{13}C NMR (62.5 MHz, CD_2Cl_2) δ 145.22, 139.77, 137.72, 132.73, 32.57, 32.42, 31.58, 30.17, 30.14, 30.11, 29.85, 28.59, 28.39, 23.17, 14.35, -8.27.

4,7-Bis(4,5-didodecylthiophen-2-yl)-5,6-dinitrobenzo[c][1,2,5]thiadiazole (5)
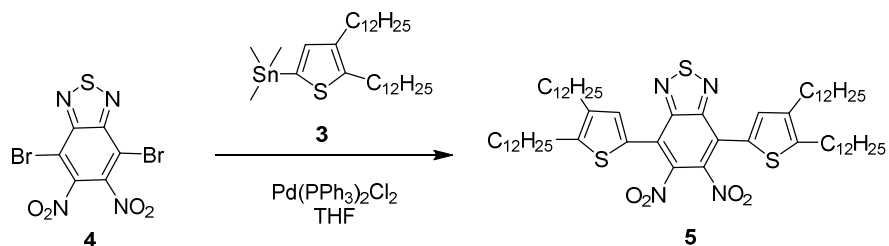
4,7-Dibromo-5,6-dinitrobenzothiadiazole (**4**, 441.6 mg, 1.15 mmol), compound **3** (1.88 g, 3.22 mmol), and Pd(PPh$_3$)$_2$Cl$_2$ (81.4 mg, 0.12 mmol) were dissolved in 25 mL of anhydrous THF under argon. The resulting solution was stirred for 16 h at 80 °C. The solvent was removed under reduced pressure to afford a dark-red oil, which was purified by column chromatography using hexane/dichloromethane (4:1) as eluent to give 0.62 g (deep red solid, 51%) of compound **5**. ^{1}H NMR (250 MHz, CD$_2$Cl$_2$) δ 7.25 (s, 2H), 2.83 (t, *J* = 7.50 Hz, 4H), 2.57 (t, *J* = 7.50 Hz, 4H), 1.73-1.68 (m, 4H), 1.58-1.52 (m, 4H), 1.27 (br, 72H), 0.90-0.85 (m, 12H). ^{13}C NMR (62.5 MHz, CD$_2$Cl$_2$) δ 152.67, 147.43, 141.61, 140.04, 133.40, 125.65, 121.35, 32.39, 32.11, 31.09, 30.15, 30.11, 30.07, 30.00, 29.93, 29.88, 29.82, 28.60, 28.49, 23.15, 14.32. HRMS (ESI+Na): m/z calcd 1085.6961, found 1085.6970.

4,7-Bis(4,5-didodecylthiophen-2-yl)benzo[c][1,2,5]thiadiazole-5,6-diamine (6)
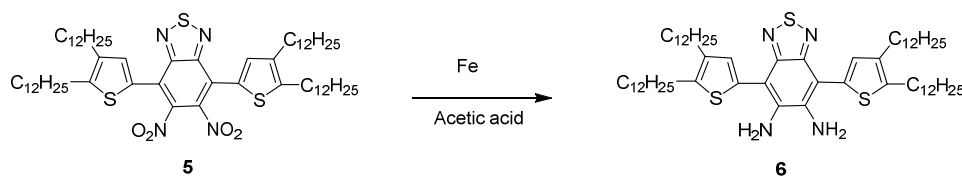
Compound **5** (0.3 g, 0.28 mmol) and fine iron powder (186 mg, 3.32 mmol) in acetic acid (8 mL) were stirred for 5 h at 75 °C. The reaction mixture was cooled to room temperature, precipitated in 5% aqueous NaOH and extracted with diethyl ether. The combined organic layers were washed with brine, dried with MgSO$_4$ and the solvent was removed under reduced pressure. The crude product was purified by column chromatography using hexane/dichloromethane (3:1) with 5% triethylamine as eluent to give 238 mg (yellow solid, 85%) of compound **6**. ^{1}H NMR (250 MHz, CD$_2$Cl$_2$) δ 7.06 (s, 2H), 4.46 (s, 4H), 2.80 (t,

J = 7.50 Hz, 4H), 2.58 (t, J = 7.50 Hz, 4H), 1.72-1.53 (m, 8H), 1.27 (br, 72H), 0.90-0.85 (m, 12H). ^{13}C NMR (62.5 MHz, CD$_2$Cl$_2$) δ 151.41, 141.18, 139.60, 138.64, 131.27, 130.75, 107.62, 32.44, 32.40, 31.40, 30.16, 30.13, 30.07, 29.99, 29.96, 29.89, 29.83, 28.73, 28.39, 23.15, 14.33. HRMS (ESI+): m/z calcd 1003.7658, found 1003.7648.

2,5-Dibromo-8,12-bis(4,5-didodecylthiophen-2-yl)-[1,2,5]thiadiazolo[3,4-i]dithieno[3,2-a:2',3'-c]phenazine (Br$_2$-BDTTQ-1) (8)
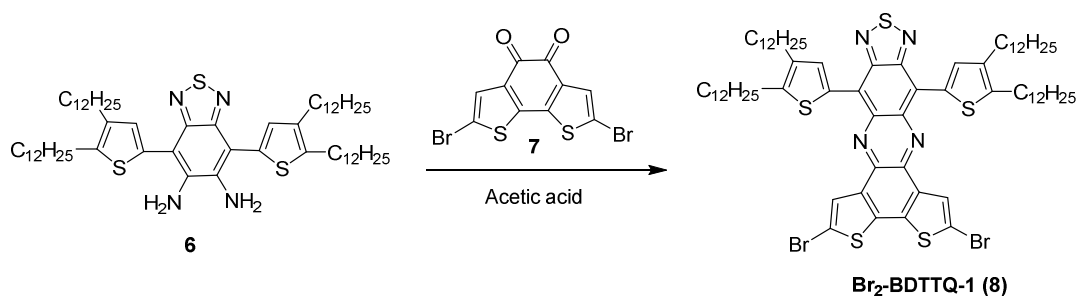
A suspension of **6** (0.2 mmol), 2,5-dibromo-benzo[2,1-b:3,4-b']dithiophene-7,8-quinone (**7**, 0.2 mmol) and 15 mL acetic acid were added into a 50 mL Schlenk tube. The mixture was heated to 55 °C overnight. After cooling to room temperature, the reaction mixture was filtered, washed with methanol and collected solid, then purified by column using hexane as eluent to get 165 mg of **Br$_2$-BDTTQ-1** (green solid, 55%). ^{1}H NMR (250 MHz, CDCl$_3$) δ 8.42 (s, 2H), 7.70 (s, 2H), 2.57 (t, J = 7.50 Hz, 4H), 2.46 (t, J = 7.75 Hz, 4H), 1.55 (br, 8H), 1.27 (br, 72H), 0.88 (br, 12H). ^{13}C NMR (62.5 MHz, CDCl$_3$) δ 150.56, 146.71, 137.50, 136.68, 135.84, 134.42, 134.34, 132.28, 129.33, 119.29, 113.11, 32.15, 31.19, 31.00, 30.43, 30.19, 30.04, 29.95, 29.62, 28.59, 22.89, 14.30. HRMS (ESI+): m/z calcd 1342.5231, found 1342.5231.

5, 5'-Bis(2-ethylhexyl)-2,2'-bithiophene (13)
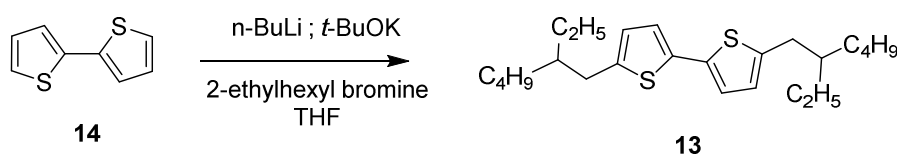
2,2'-Bithiophene (**14**, 1.5 g, 9.02 mmol) was dissolved in 40 mL of anhydrous THF.

The mixture was cooled to -78 °C and a solution of n-BuLi (15.75 mL, 25.2 mmol, 1.6 M in hexane) was added. The reaction mixture was stirred for 10 min at this temperature, then a solution of *t*-BuOK (3.83 g, 34.2 mmol in 30 mL THF) was added and kept at -78 °C another 15 min. Afterwards, 2-ethylhexyl bromine (3.45 mL, 18.0 mmol) was added in one portion and the mixture was refluxed overnight. The mixture was poured into 100 mL of ice water and hydrolyzed with 1 N HCl, then extracted with diethyl ether (3×30 mL). The combined organic phase were dried using MgSO$_4$, and the solvent was removed under reduced pressure to afford a dark-red oil, which was purified by column chromatography using hexane as eluent to give 1.51 g (colorless oil, 43%) of compound **13**. ^{1}H NMR (25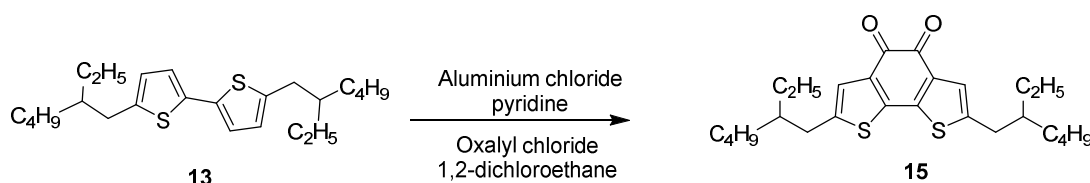0 MHz, CD$_2$Cl$_2$) δ 6.91 (d, *J* = 3.50 Hz, 2H), 6.65 (d, *J* = 3.25 Hz, 2H), 2.73 (d, *J* = 6.50 Hz, 4H), 1.58-1.52 (m, 2H), 1.35 (br, 16H), 0.93-0.87 (br, 12H). ^{13}C NMR (62.5 MHz, CD$_2$Cl$_2$) δ 143.79, 135.90, 126.17, 122.87, 41.90, 34.46, 32.80, 29.31, 25.96, 23.46, 14.32, 11.05. HRMS (ESI+): m/z calcd 391.2493, found 391.2482.

2,7-Bis(2-ethylhexyl)benzo[1,2-b:6,5-b']dithiophene-4,5-dione (15)

To a solution of aluminium chloride (768 mg, 5.76mmol) in 1,2-dichloroethane (25 mL) cooled to -10 °C was added dropwise a solution of **13** (500 mg, 1.28 mmol), pyridine (200 mg, 0.21 mmol) in 1,2-dichloroethane (5 mL) and a solution of oxalyl chloride (0.11 mL, 1.28 mmol) in 1, 2-dichloroethane (10 mL). Afterwards the mixture was raised to room temperature and stirred overnight. The mixture was poured over ice and extracted with methylene chloride. The extract was washed with water for neutralization and dried over MgSO$_4$. After removing the solvent under reduced pressure, the residue was purified by column chromatography using hexane/dichloromethane (1:1) as eluent to give 263 mg (purple viscous oil, 47%) of compound **15** . ^{1}H NMR (250 MHz, CD$_2$Cl$_2$) δ 7.08 (s, 2H), 2.73 (dd, *J* = 0.75 Hz, *J* = 6.00 Hz, 4H), 1.64-1.53 (m, 2H), 1.35 (br, 16H), 0.93-0.87 (br, 12H). ^{13}C NMR (62.5 MHz, CD$_2$Cl$_2$) δ 175.12, 145.98, 143.14, 135.09, 125.21, 41.70, 34.25, 32.72, 29.23, 25.90, 23.37, 14.27, 10.98. HRMS (ESI+): m/z calcd 445.2235, found 445.2246.

4,7-Bis(4-dodecylthiophen-2-yl)benzo[c][1,2,5]thiadiazole-5,6-dinitro (17)
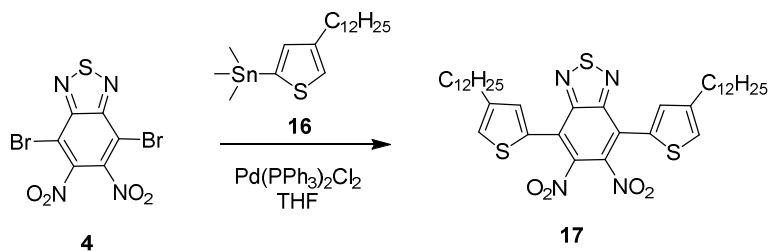
4,7-Dibromo-5,6-dinitrobenzothiadiazole (**4**, 384.0 mg, 1.0 mmol), 2-trimethyltin-4-dodecylthiophene (**16**, 1.04 g, 2.5 mmol), and Pd(PPh$_3$)$_2$Cl$_2$ (70.1 mg, 0.1 mmol) were dissolved in 25 mL of anhydrous THF under argon. The resulting solution was stirred for 16 h at 80 °C. The solvent was removed under reduced pressure to afford a dark-red solid, which was purified by column chromatography using hexane/dichloromethane (4:1) as eluent to give 0.64 g (light yellow solid, 88%) of compound **17**. ^{1}H NMR (250 MHz, CD$_2$Cl$_2$) δ 7.36 (d, J = 1.25 Hz, 2H), 7.34 (d, J = 1.25 Hz, 2H), 2.68 (t, J = 7.25 Hz, 4H), 1.68-1.63 (m, 4H), 1.33-1.27 (m, 36H), 0.90-0.85 (m, 6H). ^{13}C NMR (62.5 MHz, CD$_2$Cl$_2$) δ 152.77, 145.11, 142.11, 132.79, 129.76, 126.92, 122.12, 32.49, 30.24, 30.21, 30.15, 29.98, 29.92, 23.25, 14.44. HRMS (ESI+): m/z calcd 727.3385, found 727.3362.

4,7-Bis(4-dodecylthiophen-2-yl)benzo[c][1,2,5]thiadiazole-5,6-diamine (18)
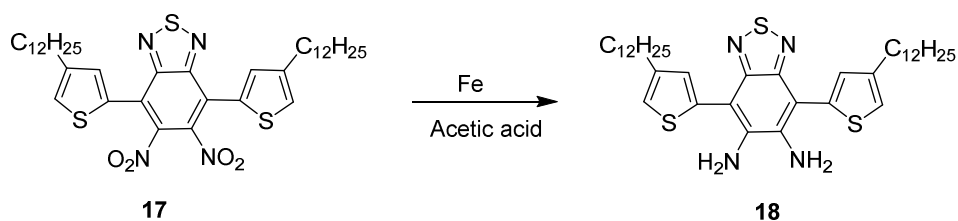
Compound **17** (0.364 g, 0.5 mmol) and fine iron powder (333 mg, 5.95 mmol) in acetic acid (10 mL) were stirred for 5 h at 75 °C. The reaction mixture was cooled to room temperature, precipitated in 5% aqueous NaOH and extracted with diethyl ether. The combined organic layers were washed with brine, dried with MgSO$_4$ and the solvent was removed under reduced pressure. The crude product was purified by column chromatography using hexane/dichloromethane (3:1) with 5% triethylamine as eluent to give 273 mg (yellow

solid, 82%) of compound **18**. ^{1}H NMR (250 MHz, CD_2Cl_2) δ 7.19 (d, *J* = 1.25 Hz, 2H), 7.15 (d, *J* = 1.25 Hz, 2H), 4.46 (s, 4H), 2.70 (t, *J* = 7.25 Hz, 4H), 1.73-1.64 (m, 4H), 1.43-1.28 (m, 36H), 0.91-0.85 (m, 6H). ^{13}C NMR (62.5 MHz, CD_2Cl_2) δ 151.45, 144.30, 139.90, 135.60, 130.44, 122.02, 107.62, 32.50, 30.26, 30.22, 30.06, 30.03, 29.93, 23.26, 14.45. HRMS (ESI+): m/z calcd 667.3902, found 667.3879.

8,12-Bis(4-dodecylthiophen-2-yl)-2,5-bis(2-ethylhexyl)-[1,2,5]thiadiazolo[3,4-i]dithieno[3,2-a:2',3'-c]phenazine (BDTTQ-2) (19)
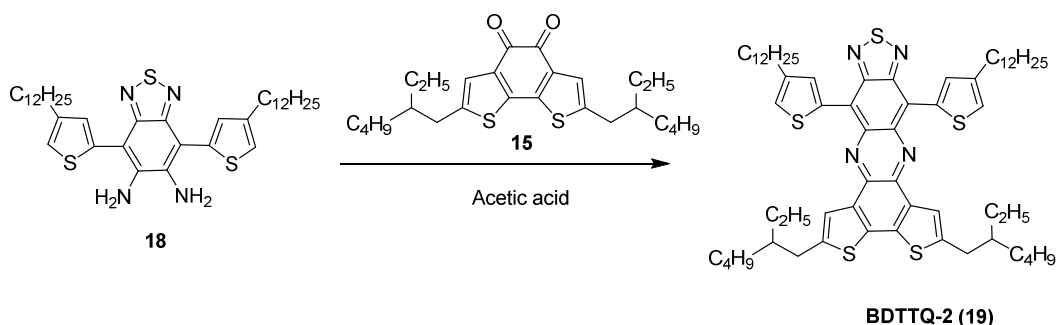
A suspension of 2,7-bis(2-ethylhexyl)benzo[1,2-b:6,5-b']dithiophene-4,5-dione (**15**, 0.1 g, 0.23 mmol), **18** (0.17 g, 0.25 mmol) and 15 mL acetic acid were placed into a 50 mL Schlenk tube. The mixture was heated to 55 °C and stirred overnight. After cooling to room temperature, the product was filtered and washed with methanol, then purified by column using hexane as eluent to give 0.18 g of compound **BDTTQ-2** (dark green solid, 73%). ^{1}H NMR (250 MHz, CD_2Cl_2) δ 8.86 (s, 2H), 7.90 (s, 2H), 7.16 (s, 2H), 2.93 (d, *J* = 6.50 Hz, 4H), 2.73 (t, *J* = 7.50 Hz, 4H), 1.48 (br, 4H), 1.27 (br, 54H), 1.03-0.88 (br, 18H). ^{13}C NMR (62.5 MHz, CD_2Cl_2) δ 149.92, 143.87, 141.03, 138.38, 136.38, 136.06, 134.02, 133.54, 124.90, 118.56, 118.33, 41.71, 34.58, 33.03, 32.40, 30.27, 30.18, 30.09, 29.97, 29.86, 29.49, 25.95, 23.55, 23.15, 14.49, 14.33, 11.23. HRMS (ESI+): m/z calcd 1075.5847, found 1075.5852.

8,12-Bis(5-bromo-4-dodecylthiophen-2-yl)-2,5-bis(2-ethylhexyl)-[1,2,5]thiadiazolo[3,4-i]dithieno[3,2-a:2',3'-c]phenazine (Br₂-BDTTQ-2) (20)

BDTTQ-2 (19) → Br₂-BDTTQ-2 (20)
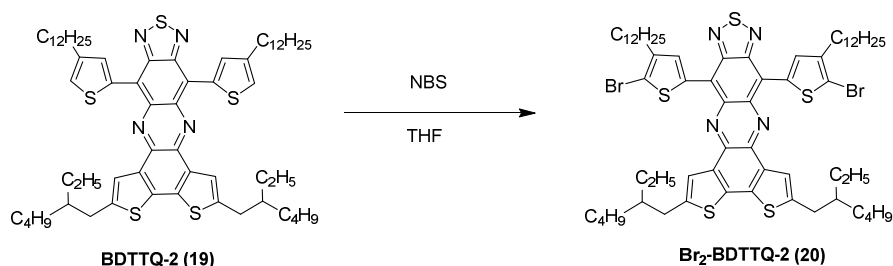
Compound **BDTTQ-2** (150 mg, 0.14 mmol) was dissolved in 15 mL THF at the room temperature. NBS (56.6 mg, 0.32 mmol) was carefully added into the solution in small batches under dark. The mixture was stirred for 5 h. After removing the solvent under reduced pressure, the residue was purified by column chromatography using hexane as eluent to give **Br₂-BDTTQ-2** as a dark green solid (146 mg, 78%). ^{1}H NMR (250 MHz, CD$_2$Cl$_2$) δ 8.34 (s, 2H), 7.29 (s, 2H), 2.75 (d, J = 6.50 Hz, 4H), 2.35 (t, J = 7.50 Hz, 4H), 1.67-1.59 (br, 4H), 1.48-1.30 (br, 54H), 1.02-0.87 (br, 18H). ^{13}C NMR (62.5 MHz, CD$_2$Cl$_2$) δ 149.94, 143.88, 141.04, 138.41, 136.40, 136.10, 134.06, 133.60, 124.95, 118.59, 118.35, 41.76, 34.65, 33.10, 32.44, 30.32, 30.30, 30.28, 30.21, 30.19, 30.00, 29.89, 29.54, 26.01, 23.58, 23.18, 14.51, 14.35, 11.26. HRMS (ESI+): m/z calcd 1230.3979, found 1230.4012.

PBDTTQ-1

Br₂-BDTTQ-1 (8) + 21 → PBDTTQ-1

Pd₂(dba)₃
P(o-tolyl)₃
chlorobenzene
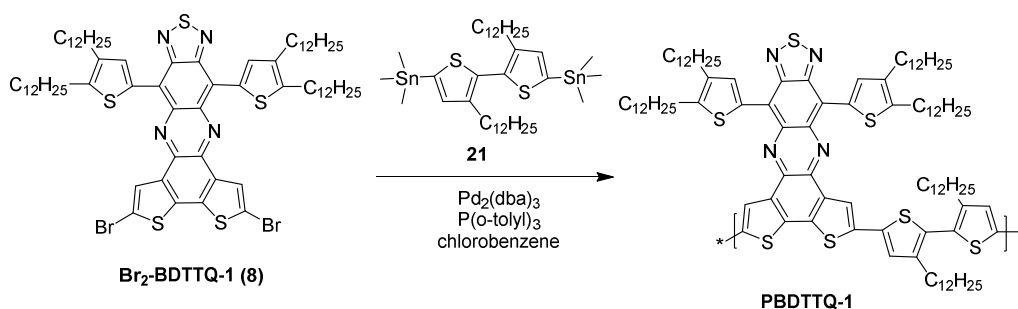
Br₂-BDTTQ-1 (0.1 mmol), 5,5'-bis(trimethylstannyl)-3,3'-didodecyl-2,2'-bithiophene (**21**, 0.1 mmol), chlorobenzene (8 mL) were placed in a 50 mL two-neck flask. The mixture was purged with argon for 5 min, and then 5.5 mg of tris(dibenzylideneacetone)dipalladium(0) (Pd₂(dba)₃) and 7.3 mg of tri(o-tolyl)phosphine (P(o-tolyl)₃) were added. Then the mixture

was heated up to 110 °C under argon. After 3 days, the reaction mixture was poured into methanol. The target polymer was precipitated as olive brown solid and filtered through a Soxhlet thimble, which was then subjected to Soxhlet extraction with methanol, acetone, hexane and chloroform. The polymer was collected from the chloroform fraction and dried in vacuum to afford an olive brown solid 99.6 mg (59%).

Molecular weight by GPC (30 °C): M_n = 37.3 kg mol^{-1}, PDI = 2.43.

^{1}H NMR (250 MHz, CDCl$_3$) δ 8.96-8.51 (br, 6H), 2.46 (br, 12H), 1.18-0.78 (br, 138H).

PBDTTQ-2
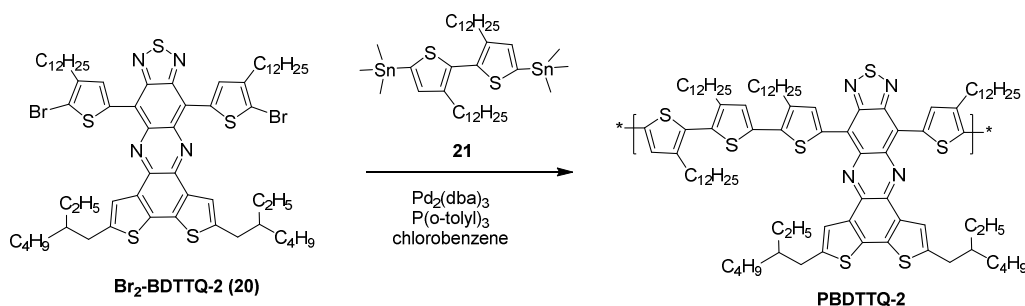
This polymer was prepared from **Br$_2$-BDTTQ-2** and **21** in similar procedure to **PBDTTQ-1** as an olive brown solid 99 mg (63%).

Molecular weight by GPC (30 °C): M_n = 11.8 kg mol^{-1}, PDI = 1.66.

^{1}H NMR (250 MHz, CDCl$_3$) δ 9.16-8.10 (br, 6H), 3.0-2.71 (br, 12H), 1.18-0.78 (br, 122H).

Microwave reaction for PBDTTQ-2
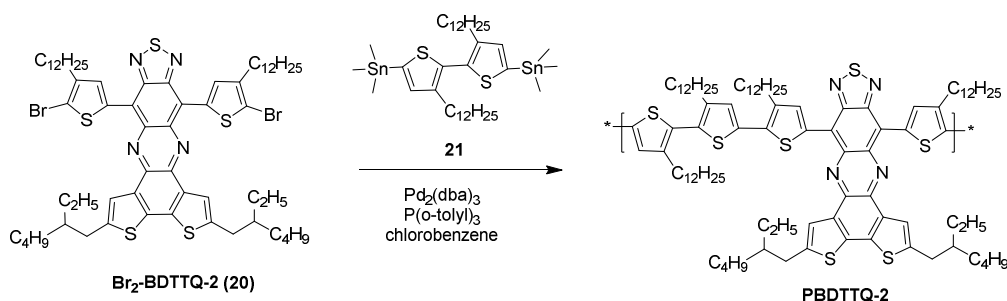
Br$_2$-BDTTQ-2 (0.089 mmol), 5,5'-bis(trimethylstannyl)-3,3'-didodecyl-2,2'-bithiophene (**21**, 0.089 mmol), chlorobenzene (4 mL) were placed in a 10 mL microwave

reactor. The mixture was purged with argon for 20 min, and then 0.00445 mmol of tris(dibenzylideneacetone)dipalladium(0) (Pd$_2$(dba)$_3$) and 0.0178 mmol of tri(*o*-tolyl)phosphine (P(*o*-tolyl)$_3$) were added. Then the mixture was heated up to 150 °C for 2 h. The workup is same to oil bath reaction as above mention. An olive brown solid was obtained 79 mg (50%).

Molecular weight by GPC (30 °C): M$_n$ = 9.6 kg mol^{-1}, PDI = 1.27.

2.10 References

(1) Grimsdale, A. C.; Leok Chan, K.; Martin, R. E.; Jokisz, P. G.; Holmes, A. B. *Chem. Rev.,* **2009**, *109*, 897-1091.

(2) Günes, S.; Neugebauer, H.; Sariciftci, N. S. *Chem. Rev.,* **2007**, *107*, 1324-1338.

(3) Guo, X.; Baumgarten, M.; Müllen, K. *Prog. Polym. Sci.,* **2013**, *38*, 1832-1908.

(4) Arias, A. C.; MacKenzie, J. D.; McCulloch, I.; Rivnay, J.; Salleo, A. *Chem. Rev.,* **2010**, *110*, 3-24.

(5) Li, C.; Liu, M.; Pschirer, N. G.; Baumgarten, M.; Müllen, K. *Chem. Rev.,* **2010**, *110*, 6817-6855.

(6) Bürgi, L.; Turbiez, M.; Pfeiffer, R.; Bienewald, F.; Kirner, H.-J.; Winnewisser, C. *Adv. Mater.,* **2008**, *20*, 2217-2224.

(7) Li, Y. N.; Singh, S. P.; Sonar, P. *Adv. Mater.,* **2010**, *22*, 4862-4866.

(8) Zhan, X.; Tan, Z. a.; Domercq, B.; An, Z.; Zhang, X.; Barlow, S.; Li, Y.; Zhu, D.; Kippelen, B.; Marder, S. R. *J. Am. Chem. Soc.,* **2007**, *129*, 7246-7247.

(9) Zhou, E.; Cong, J.; Wei, Q.; Tajima, K.; Yang, C.; Hashimoto, K. *Angew. Chem. Int. Ed.,* **2011**, *50*, 2799-2803.

(10) Yan, H.; Chen, Z.; Zheng, Y.; Newman, C.; Quinn, J. R.; Dotz, F.; Kastler, M.; Facchetti, A. *Nature,* **2009**, *457*, 679-686.

(11) Durban, M. M.; Kazarinoff, P. D.; Luscombe, C. K. *Macromolecules,* **2010**, *43*, 6348-6352.

(12) Steckler, T. T.; Zhang, X.; Hwang, J.; Honeyager, R.; Ohira, S.; Zhang, X.-H.; Grant, A.; Ellinger, S.; Odom, S. A.; Sweat, D.; Tanner, D. B.; Rinzler, A. G.; Barlow, S.; Brédas, J.-L.; Kippelen, B.; Marder, S. R.; Reynolds, J. R. *J. Am. Chem. Soc.,* **2009**, *131*, 2824-2826.

(13) Yuen, J. D.; Fan, J.; Seifter, J.; Lim, B.; Hufschmid, R.; Heeger, A. J.; Wudl, F. *J. Am. Chem. Soc.,* **2011**, *133*, 20799-20807.

(14) Qian, G.; Qi, J.; Davey, J. A.; Wright, J. S.; Wang, Z. Y. *Chem. Mater.,* **2012**, *24*, 2364-2372.

(15) Jones, B. A.; Facchetti, A.; Wasielewski, M. R.; Marks, T. J. *J. Am. Chem. Soc.,* **2007**, *129*, 15259-15278.

(16) Fukutomi, Y.; Nakano, M.; Hu, J.-Y.; Osaka, I.; Takimiya, K. *J. Am. Chem. Soc.,* **2013**, *135*, 11445-11448.

(17) Ono, K.; Tanaka, S.; Yamashita, Y. *Angew. Chem. Int. Ed.,* **1994**, *33*, 1977-1979.

(18) Li, H.; Tam, T. L.; Lam, Y. M.; Mhaisalkar, S. G.; Grimsdale, A. C. *Org. Lett.,* **2011**, *13*, 46-49.

(19) Dallos, T.; Hamburger, M.; Baumgarten, M. *Org. Lett.,* **2011**, *13*, 1936-1939.

(20) Kitamura, C.; Tanaka, S.; Yamashita, Y. *Chem. Mater.,* **1996**, *8*, 570-578.

(21) Tam, T. L.; Li, H.; Lam, Y. M.; Mhaisalkar, S. G.; Grimsdale, A. C. *Org. Lett.,* **2011**, *13*, 4612-4615.

(22) Perzon, E.; Zhang, F. L.; Andersson, M.; Mammo, W.; Inganas, O.; Andersson, M. R. *Adv. Mater.,* **2007**, *19*, 3308-3311.

(23) Lee, Y.; Jo, W. H. *J. Phys. Chem. C,* **2012**, *116*, 8379-8386.

(24) Dexter Tam, T. L.; Salim, T.; Li, H.; Zhou, F.; Mhaisalkar, S. G.; Su, H.; Lam, Y. M.; Grimsdale, A. C. *J. Mater. Chem.,* **2012**, *22*, 18528-18534.

(25) Chen, M. X.; Crispin, X.; Perzon, E.; Andersson, M. R.; Pullerits, T.; Andersson, M.; Inganas, O.; Berggren, M. *Appl. Phys. Lett.,* **2005**, *87*, 252105.

(26) Cheng, K.-F.; Chueh, C.-C.; Lin, C.-H.; Chen, W.-C. *J. Polym. Sci., Part A: Polym. Chem.,* **2008**, *46*, 6305-6316.

(27) Zhang, X.; Steckler, T. T.; Dasari, R. R.; Ohira, S.; Potscavage, W. J.; Tiwari, S. P.; Coppee, S.; Ellinger, S.; Barlow, S.; Bredas, J.-L.; Kippelen, B.; Reynolds, J. R.; Marder, S. R. *J. Mater. Chem.,* **2010**, *20*, 123-134.

(28) Qian, G.; Zhong, Z.; Luo, M.; Yu, D.; Zhang, Z.; Ma, D.; Wang, Z. Y. *J. Phys. Chem. C,* **2009**, *113*, 1589-1595.

(29) Delgado, P. A.; Liu, D. Y.; Kean, Z.; Wagener, K. B. *Macromolecules,* **2011**, *44*, 9529-9532.

(30) Usta, H.; Risko, C.; Wang, Z.; Huang, H.; Deliomeroglu, M. K.; Zhukhovitskiy, A.; Facchetti, A.; Marks, T. J. *J. Am. Chem. Soc.,* **2009**, *131*, 5586-5608.

(31) Leroy, J.; Levin, J.; Sergeyev, S.; Geerts, Y. *Chem. Lett.,* **2006**, *35*, 166-167.

(32) Biniek, L.; Fall, S.; Chochos, C. L.; Anokhin, D. V.; Ivanov, D. A.; Leclerc, N.; Lévêque, P.; Heiser, T. *Macromolecules,* **2010**, *43*, 9779-9786.

(33) Kim, B.; Yeom, H. R.; Yun, M. H.; Kim, J. Y.; Yang, C. *Macromolecules,* **2012**, *45*, 8658-8664.

(34) Bredas, J.-L. *Mater. Horiz.,* **2014**, *1*, 17-19.

(35) Sariciftci, N. S. *Primary Photoexcitations in Conjugated Polymers:Molecular Excitons vs Semiconductor Band Model; World Scientific: Singapore, 1997.*

(36) Ashraf, R. S.; Kronemeijer, A. J.; James, D. I.; Sirringhaus, H.; McCulloch, I. *Chem. Commun.,* **2012**, *48*, 3939-3941.

(37) Veldman, D.; Meskers, S. C. J.; Janssen, R. A. J. *Adv. Funct. Mater.,* **2009**, *19*, 1939-1948.

(38) Falzon, M.-F.; Wienk, M. M.; Janssen, R. A. J. *J. Phys. Chem., C* **2011**, *115*, 3178-3187.

(39) STELZIG, T. Donor-Acceptor System in the Quest for Organic Semiconductors. Ph. D. Dissertation, Johannes Gutenberg-University Mainz, 2012.

(40) Wang, E.; Hou, L.; Wang, Z.; Hellström, S.; Mammo, W.; Zhang, F.; Inganäs, O.; Andersson, M. R. *Org. Lett.,* **2010**, *12*, 4470-4473.

(41) Meyer, A.; Sigmund, E.; Luppertz, F.; Schnakenburg, G.; Gadaczek, I.; Bredow, T.; Jester, S.-S.; Höger, S. *Beilstein J. Org. Chem.,* **2010**, *6*, 1180-1187.

(42) Fragnelli, M. C.; Hoyos, P.; Romano, D.; Gandolfi, R.; Alcántara, A. R.; Molinari, F. *Tetrahedron,* **2012**, *68*, 523-528.

(43) Yue, W.; Zhao, Y.; Tian, H.; Song, D.; Xie, Z.; Yan, D.; Geng, Y.; Wang, F. *Macromolecules,* **2009**, *42*, 6510-6518.

Chapter 3. Optimized Property of Thiadiazoloquinoxaline Based Copolymers in Semiconductors via Molecular Engineering
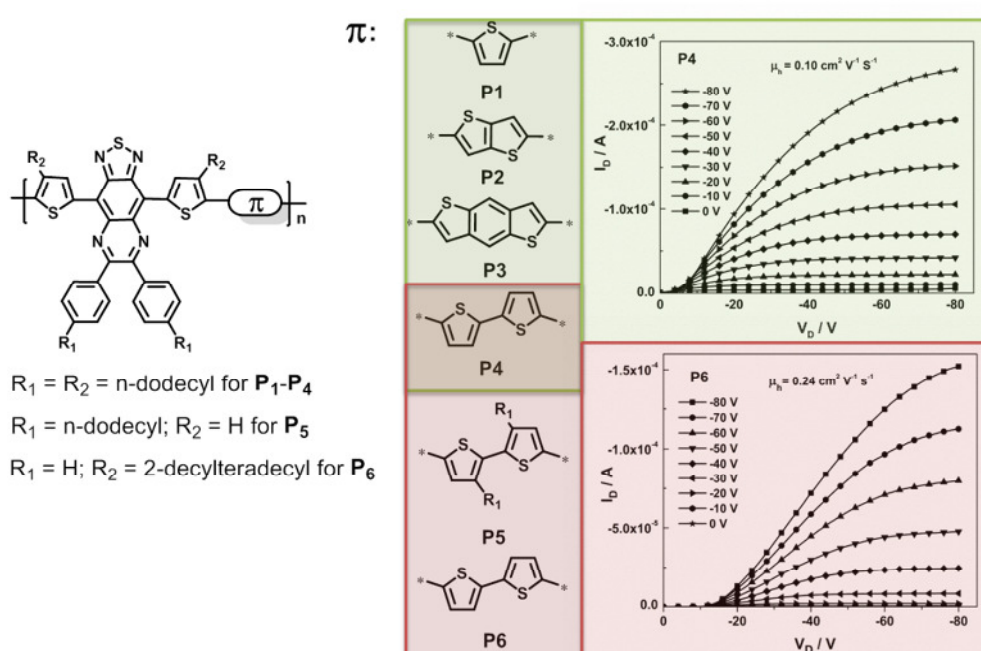
In this chapter, we synthesized six thiadiazoloquinoxaline (TQ) containing copolymers and studied structure-property relationships in organic field-effect transistor via two steps, namely, optimization of the donor moieties (**P1**-**P4**) and substitution positions and architectures of polymer side chains (**P4**-**P6**). Compared to **P1**-**P4**, The unsubstituted bithiophene as donor made TQ copolymer (**P4**) exhibit a best field effect hole mobility of 0.1 cm^2 V^{-1} s^{-1}. Afterwards, the polymers **P4**-**P6,** which had identical molecular formulas of side chains and main chains, were investigated in device performance. However, a pair of 2-decyl-tetradecyl alkyl chains was grafted onto thiophene units adjacent to the TQ core in **P6**, further improving the hole mobility up to 0.24 cm^2 V^{-1} s^{-1} in this series of polymers.

Note: Large part of this chapter has been published in *J. Mater. Chem. C*, **2015**, *3*, 3876-3881.

3.1 Introduction

Thiadiazoloquinoxalines (TQs) possess outstanding electron affinity and variable chemical structures,[1-5] therefore becoming a class of important building blocks for polymer semiconductors. However, TQ polymers usually exhibit relatively low FET performances due to their disorder arrangement in thin films.[6-8] In Chapter 2, we reported a strong acceptor, benzodithiophene condensed TQ derivative (**BDTTQ**, Figure 3.1). Such acceptor containing copolymer exhibited ambipolar behaviour by regulating the linkage pattern between **BDTTQ** and alkylated bithiophene. But the relatively low mobility of **PBDTTQ-2** (1.2×10^{-3} cm^2 V^{-1} s^{-1} for hole and 0.6×10^{-3} cm^2 V^{-1} s^{-1} for electron) was also related to its disorder morphology because of grafting many side chains onto the repeat unit of conjugated backbone. Investigation of the structure-property relationships of copolymers is an important strategy to understand and design high-performance optoelectronic materials.[9,10] Some strong acceptors have been reported to achieve high charge carrier mobilities, like diketopyrrolopyrrole (DPP),[11-13] naphthalene diimide (NDI),[14-16] benzobisthiadiazole (BBT)[17] and isoindigo (IID).[18,19] It is therefore necessary to systematically study the structure and charge transport relationships of TQ polymers in order to identify the essential parameters for highly ordered microstructures which could further improve their charge carrier mobility.
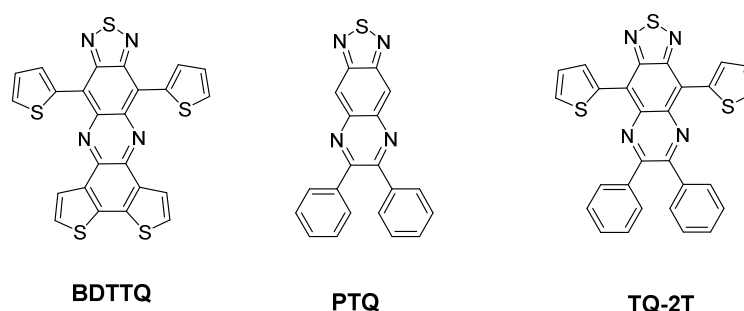
Figure 3.1 Chemical structures of **BDTTQ**, **PTQ** and **TQ-2T**.

A TQ derivative, 6,7-diphenyl-[1,2,5]thiadiazolo[3,4-g]quinoxaline (**PTQ**, Figure 3.1), has been widely investigated as an acceptor for creating polymer semiconductors, because of its ease of synthesis and good charge carrier mobilities compared to other TQ derivatives.[20-22] A D-A-D combination fashion of **PTQ**, 6,7-diphenyl-4,9-di(thiophen-2-yl)-[1,2,5]thiadiazolo[3,4-g]quinoxaline (**TQ-2T**, Figure 3.1) was also reported by modifying the

PTQ core with two flanking thiophenes, which can offer more alkylation positions to improve their solubility.[8,23-26] In view of the lack of study on the structure-property relationships of TQ polymers, we herein investigate this topic based on **TQ-2T** polymers from two crucial aspects. Firstly, introduction of unsubstituted donor units with different electron-donating abilities, which enhances backbone coplanarity of the **TQ-2T** polymers and potentially leads to ordered arrangement in the polymer films. Secondly, tuning the substitution positions and architectures of polymer side chains improves the polymer solubility, the molecular weights as well as the device performance.
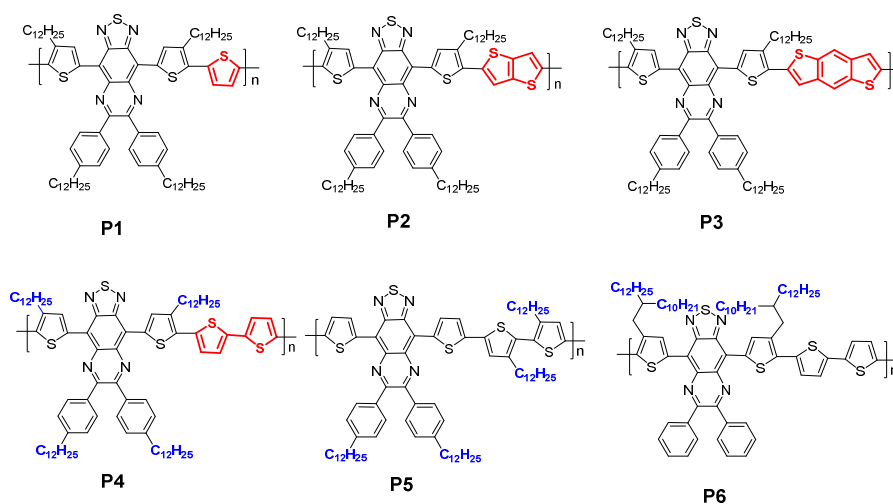
Figure 3.2 Structures of **P1-P6** synthesized and studied in this work.

In this chapter, we report six new **TQ-2T** based copolymers **P1**-**P6** as shown in Figure 3.2. Firstly, different unsubstituted donors, namely, thiophene (**T**), thieno[3, 2-b]thiophene (**TT**), benzo[1,2-b:4,5-b']dithiophene (**BDT**) and 2,2'-bithiophene (**BT**) were introduced alternatingly with **TQ-2T** proving the corresponding polymers **P1**-**P4**. These donor units were expected to decrease the torsion angles along the conjugated backbone. Secondly, the best donor containing polymer (**P4**) was further optimized by side chain engineering. The polymers **P4**-**P6** had identical molecular formulas of side chains and conjugated skeleton. In comparison with **P4**, **P5** was designed and synthesized by varying the substitution positions of the alkyl chains. This polymer design aims to improve the solubility and molecular weight but at the cost of sacrificing coplanarity of the polymer main chain. In order to possess better solubility, higher molecular weight and similar backbone coplanarity in comparison with **P4**, the substitution architectures and the bulkiness of the alkyl chains were modified by replacing

four dodecyl linear chains in **P4** with a pair of 2-decyl-tetradecyl alkyl chains to obtain **P6**. The optical, electrochemical, charge carrier transport and self-organization properties of these copolymers were comparatively characterized and studied in details.

3.2 Synthesis and characterization
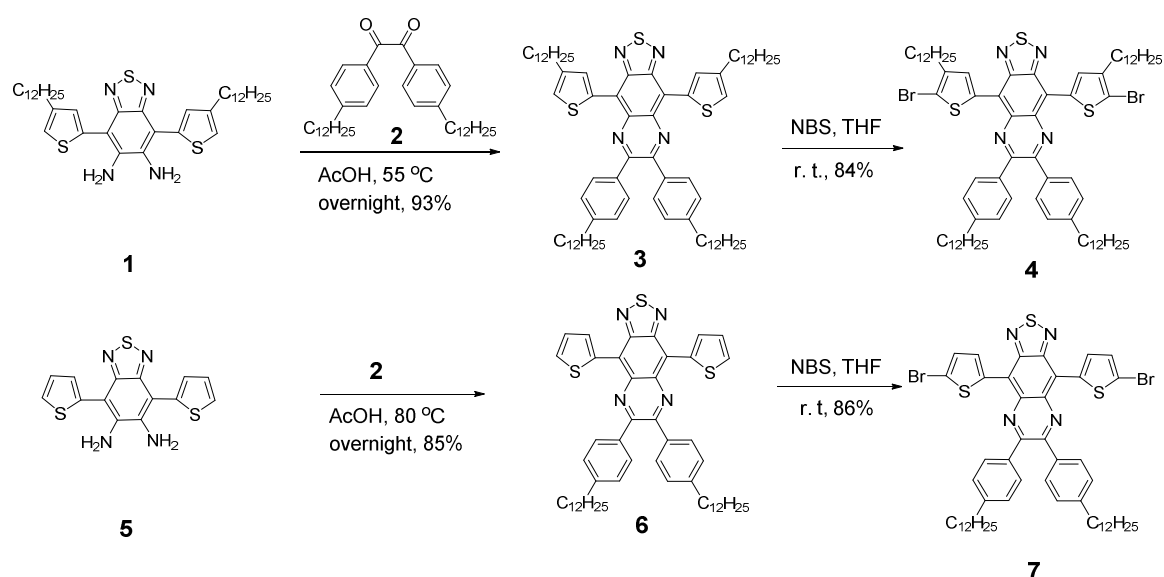
Scheme 3.1 Synthetic route for precursors **4** and **7**.

The synthesis of precursors **4** and **7** is outlined in Scheme 3. 1. Monomer **3** was obtained via a condensation reaction between 4,7-bis(4-dodecylthiophen-2-yl)benzo[c][1,2,5]thiadiazole-5,6-diamine (**1**) and 1,2-bis(4-dodecylphenyl)ethane-1,2-dione (**2**), and then it was dibrominated to produce precursor **4**. Polymerization of precursor **7** was obtained following the similar procedure to that for precursor **4** from the 4,7-di(thiophen-2-yl)benzo[c][1,2,5]thiadiazole-5,6-diamine (**5**).

The synthetic route of precursor **17** is shown in Scheme 3.2. Fresh Grignard reagent **9** was prepared from 2-decyl-tetradecylbromide (**8**), which was directly reaction with 3-bromothiophene by a Kumada coupling to produce 3-(2-decyl-tetradecyl)thiophene (**10**). The corresponding stanylated thiophene **11** was obtained from **10** via a stanylation reaction. The Stille coupling reaction was carried out between **11** and 4,7-dibromo-5,6-dinitrobenzo[c][1,2,5]thiadiazole (**12**) to give the 4,7-bis(4-(2-decyltetradecyl)thiophen-2-yl)-

5,6-dinitrobenzo[c][1,2,5]thiadiazole (**13**). The corresponding diamine **14** was synthesized by reduction of compound **13**. The diamine **14** was directly used without purification and converted to the corresponding monomer **16** via a condensation coupling with benzil (**15**). Finally, precursor **17** was then obtained by dibromination of **16**.
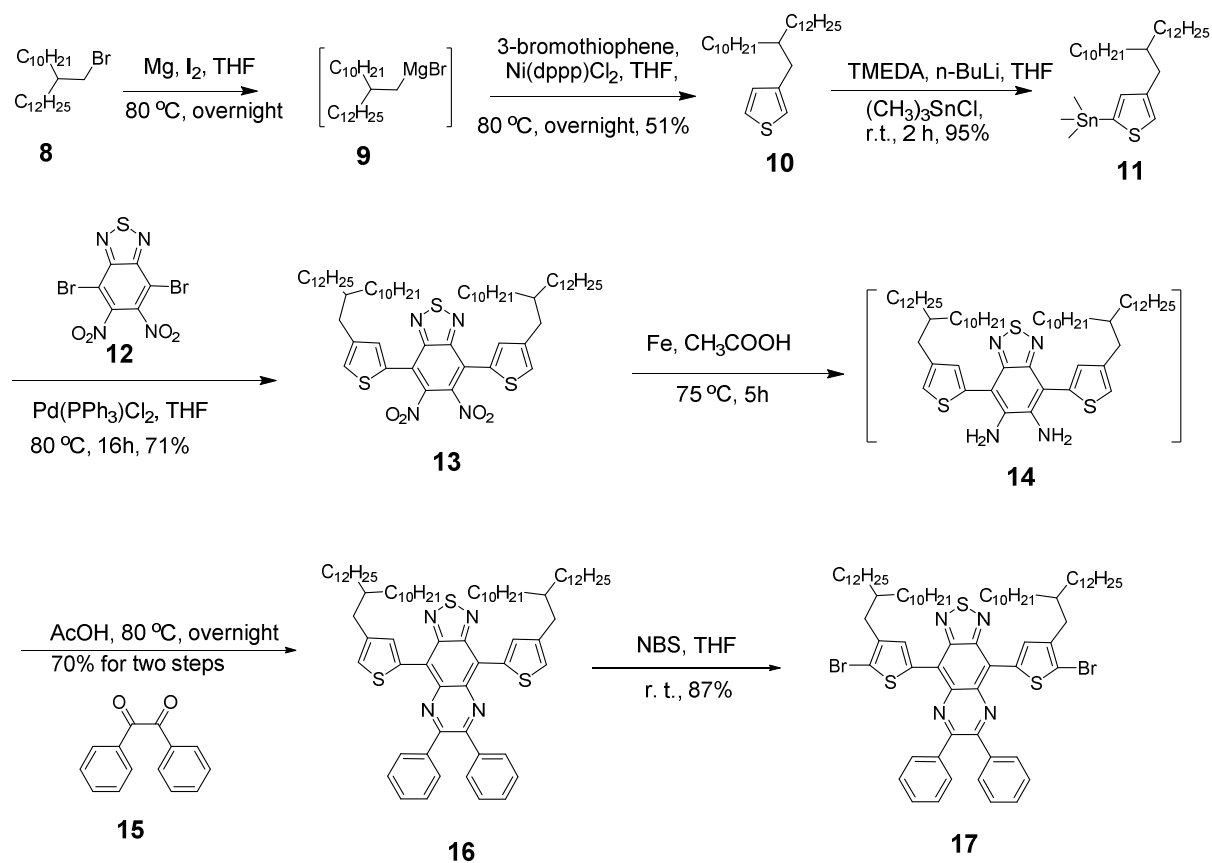
Scheme 3.2 Synthetic route for precursors **16** and **17**.

The substitution number and architectures of alkyl chains onto conjugated backbone led to their significant difference in solubility. Precursors **4** and **17** have excellent solubility in dichloromethane, while **7** has a poor solubility in dichloromethane and chloroform. Therefore the ^{1}H- or ^{13}C- NMR spectra of **7** were characterized in THF-d_8. Before polymerization was carried out, the three compounds were dried more than 12 hours at 50 °C under vacuum to remove residual solvents and water. The three precursors show very high purity indicated by their ^{1}H-NMR spectra (Figure 3.3) except the signals of water, which were believed to originate from the deuterated solvents. In the aromatic region, compounds **4** and **17** exhibit a clear single peak at 8.8 ppm, it was assigned to the proton of thiophene (β_1), while compound **7** has two double peaks at 8.8 and 7.1 ppm, it was attributed to the protons of thiophene (β_1

and β_2). It is also very easily to distinguish the three precursors through their aliphatic region signals in ^{1}H-NMR spectra. The two triplet peaks at 2.5 ppm belong to two different methylene of dodecyl groups linked to the aromatic ring of compound **4**. The precursor **7** has a pair of the same dodecyl groups, therefore displaying a triplet peak at 2.6 ppm. With a couple of 2-decyl-tetradecyl groups of compound **17** exhibits a double peak at 2.6 ppm.
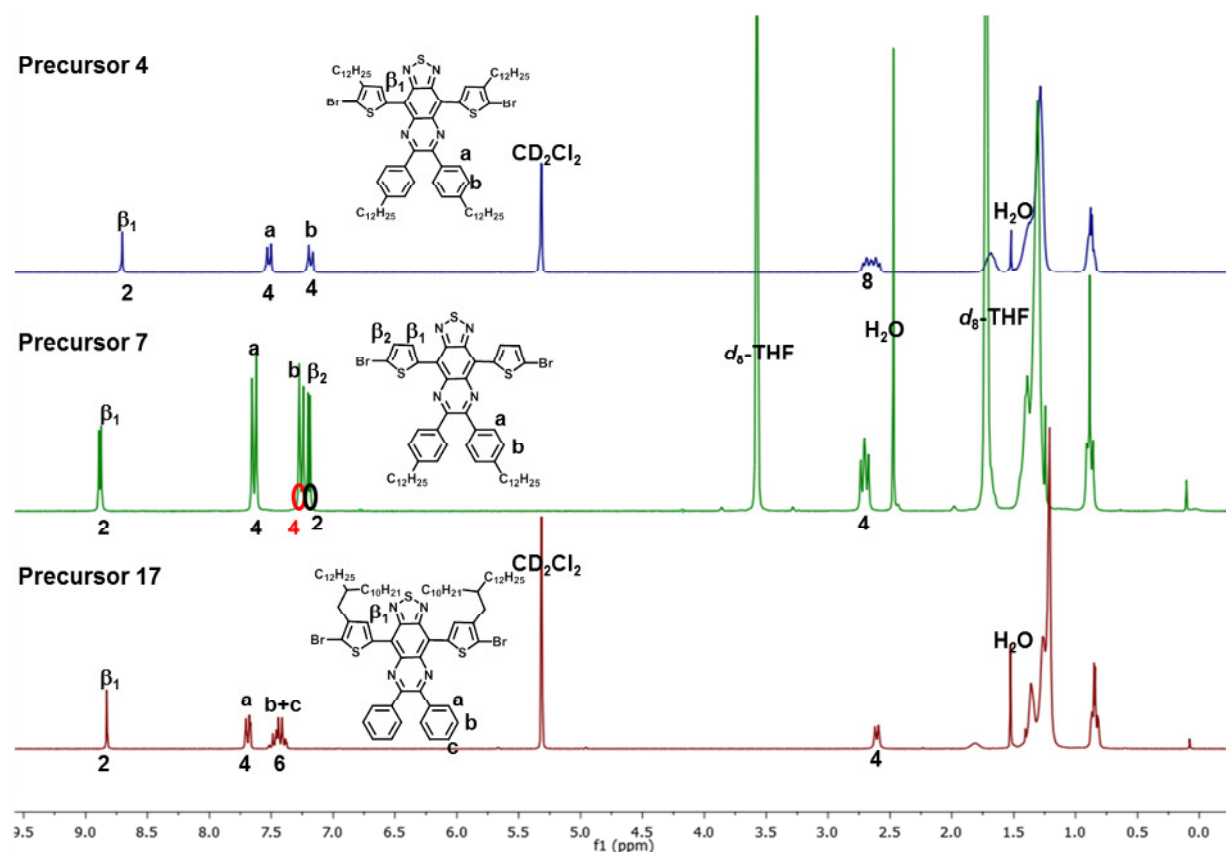
Figure 3.3 The ^{1}H-NMR spectra of three precursors **4**, **7** and **17**.

The Stille coupling reaction was performed to synthesize **P1-P6** between the three precursors (**4**, **7** and **17**) and corresponding donors (**18**-**22**) as shown in Scheme 3.2. The crude polymers were purified using Soxhlet extraction. Polymers **P1**-**P4** were obtained from chlorobenzene fraction, while **P5** and **P6** were collected from chloroform. Among these polymers, **P4** has the poorest solubility, for example, the chlorobenzene solution (2 mg/ml) of **P4** was not completely soluble until the solution was heated up to 80 °C.
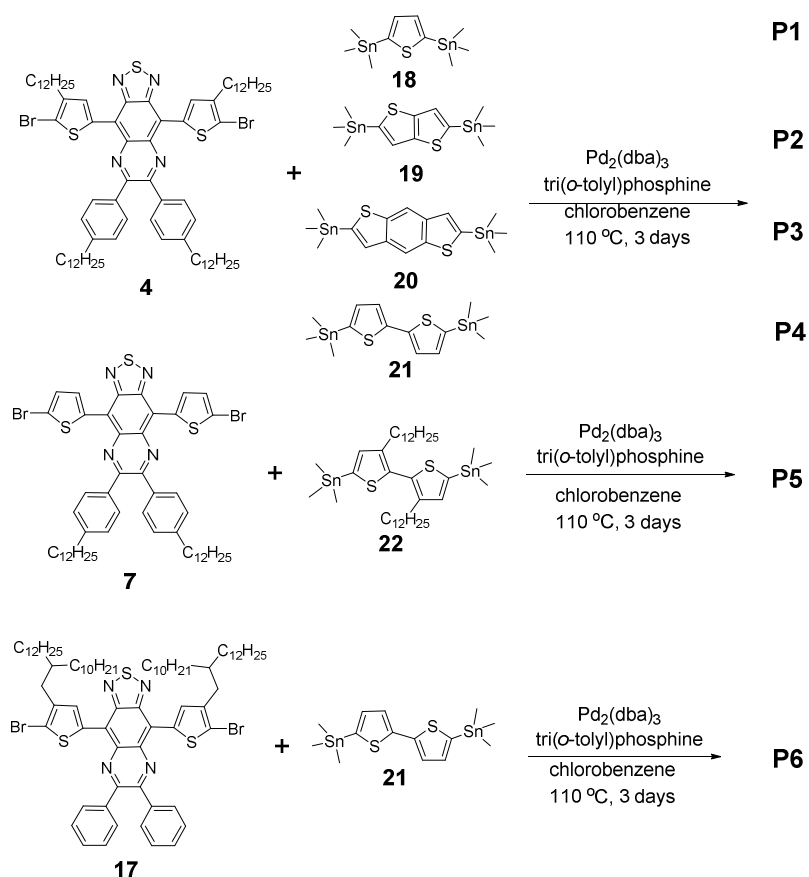
Scheme 3.3 Synthetic routes for **TQ-2T**-based polymers.

The number-average molecular weight (M_n) and polydispersity index (PDI) of these polymers were determined by GPC as shown in Figure 3.4. The data are listed in Table 3.3. The low M_n of **P1**-**P4** could be attributed to their poor solubility. Similar results were also observed in other TQ polymers.[27,28] After tuning the substitution positions and architectures of the side chains, **P5** and **P6** exhibited relatively high M_n, due to excellent solubility in common solvents such as chloroform and tetrahydrofuran at room temperature. The thermal properties of the copolymers were measured under nitrogen atmosphere at a heating rate of 10 ºC/min by thermogravimetric analysis (TGA) (Figure 3.5). All copolymers exhibited excellent thermal stability, with the similar decomposed temperature of 415 °C at 5% weight loss. However, when the temperature was raised to 500 °C, the polymer side chains were firstly decomposed. The weight loss up to 500 °C for **P1**-**P6** were around 54%, 49%, 46%, 49%, 46% and 50%, which is fully in agreement with the side chains weight ratio 54%, 51%, 49%, 50%, 50% and 50% in the corresponding polymers. The differential scanning calorimetry (DSC) curves of these copolymers didn't show any phase transition in the range from -50 °C to 300 °C.
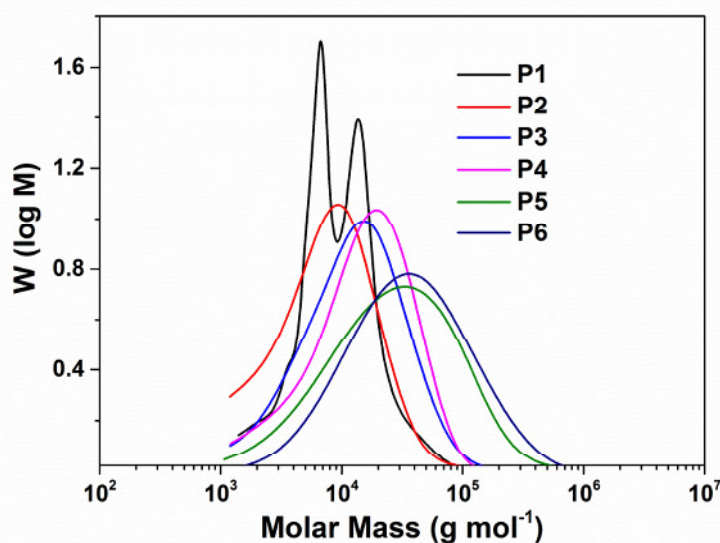
Figure 3.4 GPC curves for **PBDTTQ-1** and **PBDTTQ-2**. Polystyrene was used as standard and 1,2,4-trichlorobenzene as eluent at 135 °C.
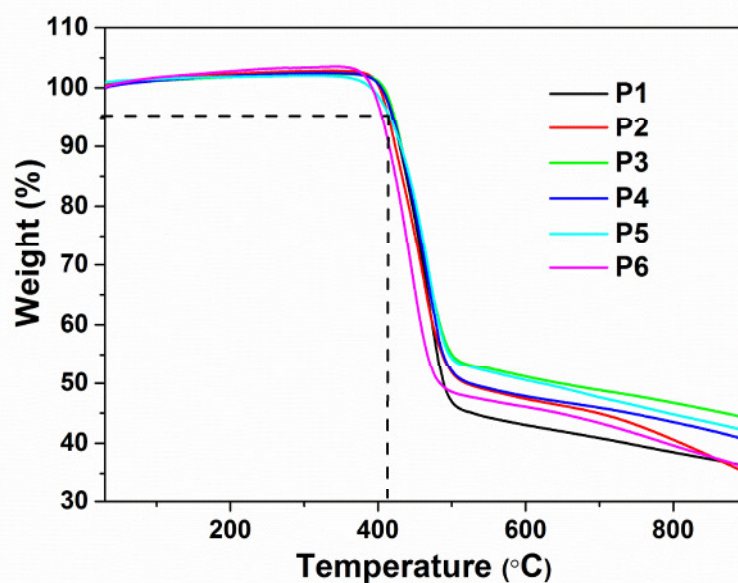
Figure 3.5 TGA curves for **P1-P6** measured under nitrogen atmosphere.

3.3 Optical properties

UV-vis-NIR absorption spectra of the polymers were recorded in toluene solutions as well as in thin films (Figure 3.6). The relevant data are summarized in Table 3.3. In dilute toluene solutions, all polymers exhibit typical dual-band absorption profile as other TQ polymers. The first one covers the range from 300 to 600 nm and the second one starts from

650 to 1650 nm. The former band corresponds to the π-π* transition of the conjugated backbone, whereas the latter could be attributed to intramolecular charge transfer (ICT) between donor and acceptor within the polymer backbone.[29] It is worthy to mention that the intensity of the second absorption bands of these polymers (OD_2) is close to or beyond the first ones (OD_1), the data are collected in Table 3.1), these values are higher than those of **PBDTTQ-1** and **PBDTTQ-2** in solution (Chapter 2), implying that these polymers could have stronger ICT than previous both **BDTTQ**-polymers.
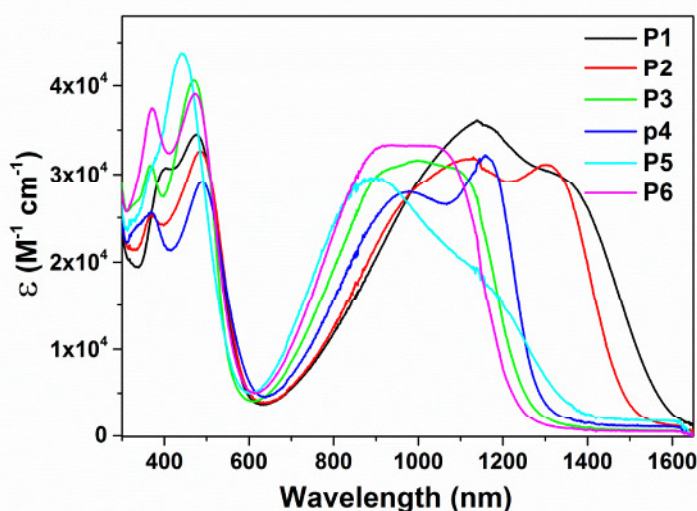
Figure 3.6 UV-visible-NIR absorption spectra of **P1**-**P6** investigated in toluene solutions.

Table 3.1 The ratio of high wavelength and low wavelength bands (OD_2 /OD_1) for **P1-P6** and **BDTTQ-**polymers.

OD_2/OD_1	P1	P2	P3	P4	P5	P6	PBDTTQ-1	PBDTTQ-2
Solution	1.04	0.95	0.77	1.10	0.67	0.85	0.17	0.49
Film	1.10	1.09	0.86	1.14	0.81	1.03	0.45	0.78

Polymers **P1**-**P4** exhibit significantly different red-shifts between 1200 and 1600 nm. The electron-donating ability of the donor moieties were estimated from their HOMO levels (Table 3.2), which were calculated using the density functional theory (DFT) with the B3LYP functional and 6-31 G* basis set. The HOMO levels follow order of **T** (-6.34 eV) < **TT** (-6.03 eV) < **BT** (-5.54 eV) < **BDT** (-5.47 eV). The HOMO energy of the **TQ-2T** (methyl groups replaced dodecyl group in monomer **3**) moiety itself, however, is already higher lying with -4.90 eV, due to the two thiophenes acting as donor strongly raising the HOMO of methyl

groups substituted **PTQ** (HOMO = -5.98 eV) by more than 1 eV. Therefore the introduction of additional donor bridges and their donor strength not influence the absorption band edges as often assumed.[30] More important, therefore is the extend of conjugation in the combined molecules and that can already nicely be predicted by considering the HOMO and LUMO values of monomeric subunits **M1-M4** of **P1-P4**. These values implied that additional donor strength do not determine the energy bandgaps of **TQ-2T** based polymers. This can then explain why **P1** and **P2** show the longest wavelength absorption followed by **P4** and **P3**. Compared to **P4**, **P5** shows a blue-shift around 10 nm of the maximum wavelength (λ_{max}) and significant lower molar extinction coefficient. The λ_{max} value of **P6** reveals a blue shift of 100 nm in comparison with that of **P4**. These results were related to different substitution positions and architectures of alkyl chains affect intramolecular interaction in polymer backbone, thereby changing the optical behavior of **TQ-2T** polymers. On the other hand, **P5** exhibits a long tail extending to 1500 nm, suggesting a high tendency to aggregate even in diluted solution.[31] This is in agreement with the high PDI of **P5**.

Table 3.2 The HOMO and LUMO levels of **PTQ**, **TQ-2T**, **T**, **TT**, **BDT**, **BT** and **M1-M4**. Calculations were carried out at the DFT//B3LYP/6-31G* level.[32]

Energy Levels	PTQ	TQ-2T	T	TT	BDT	BT	M1	M2	M3	M4
HOMO (eV)	-5.98	-4.90	-6.34	-6.04	-5.47	-5.54	-4.71	-4.71	-4.77	-4.65
LUMO (eV)	-2.96	-3.03	-0.21	-0.99	-1.08	-1.18	-3.05	-3.10	-3.14	-3.09

The films of these polymers were prepared by drop-casting toluene solutions of these polymers onto glass slides. In order to clear the UV-visible-NIR spectra of **P1**-**P6** in solutions and films, their spectra are shown in Figure 3.7 one by one. **P1**-**P6** display slightly broadened spectra but with only small red-shifts from 8 to 35 nm at λ_{max} compared with those in solution indicating aggregation in thin film. The values of OD_2/OD_1 of these polymers were further increased in solid state (shown in Table 3.1). **P5** has a smallest OD_2/OD_1 value of 0.81, because the head-to-head alkylated chain onto bithiophene caused this polymer a significant twist in the conjugated backbone. The former mentioned low mobility of **PBDTTQ-2** (Chapter 2) had also a low with OD_2/OD_1 value of 0.78. The unsubstituted donor **BT** of **P4** and **P6** have the OD_2/OD_1 value up to 1.14 and 1.03, respectively, suggesting that both polymers could have better charge transport ability. The optical band gaps are calculated according to the absorption onset of the solid films and listed in Table 3.3. These results

demonstrated that changing donors can be effective for tuning the optical behavior of the polymers.
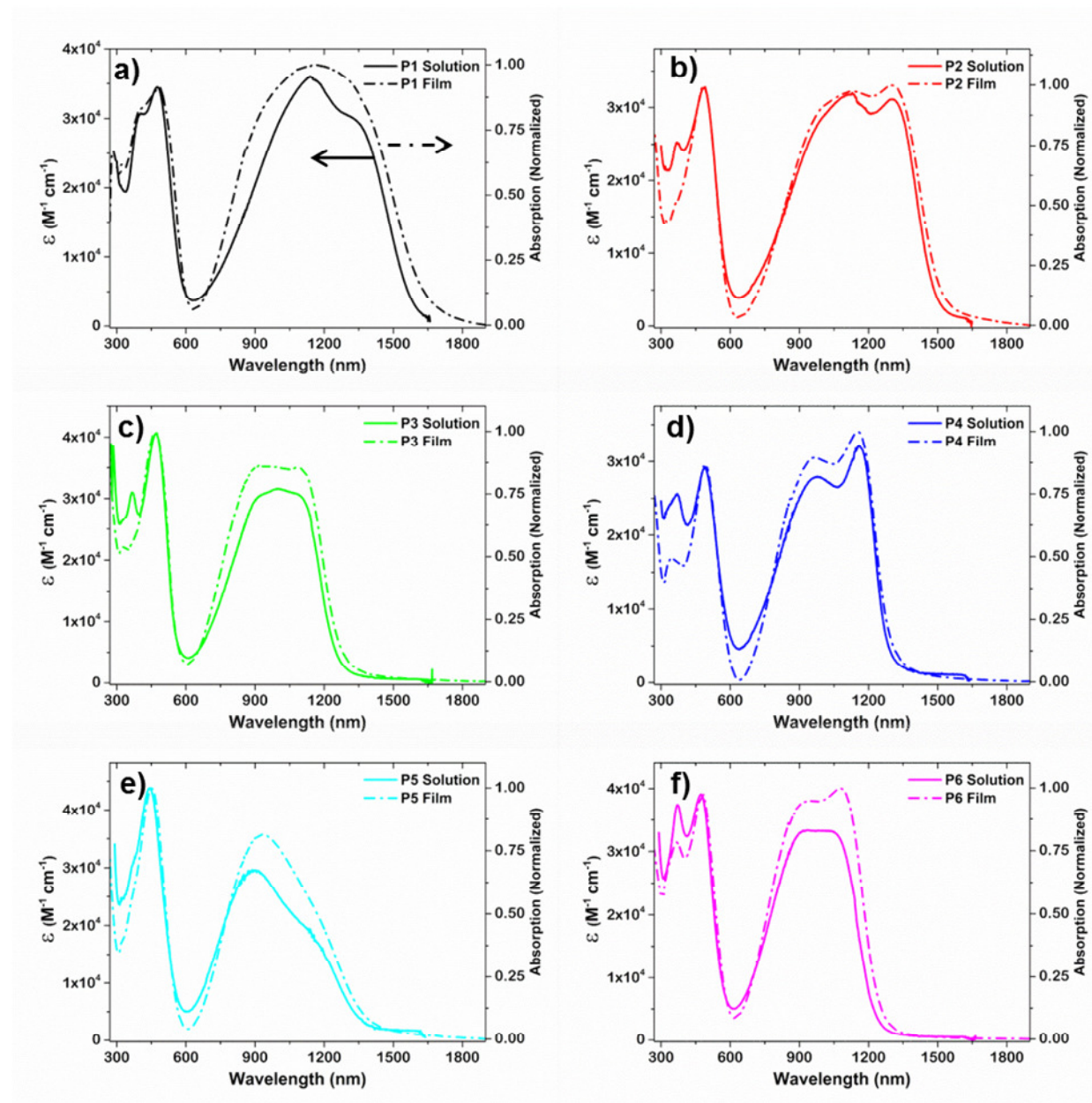

Figure 3.7 UV-visible-NIR absorption spectra of **P1**-**P6** (a-f) investigated in toluene solutions and thin films.

Table 3.3 Molecular weights, optical absorption and electrochemical properties of **P1-P6**.

Polymers	Mn [a] (kg/mol)	PDI [a]	λ_{max} (nm) soln. [b]	λ_{max} (nm) film [c]	E_g^{opt} (eV)[c]	IP (eV)[d]	EA (eV)[d]
P1	7.0	2.68	1140,1330	1165	0.75	-4.95	-3.92
P2	5.4	2.15	1130, 1305	1135, 1313	0.81	-5.04	-3.99
P3	8.0	2.34	910-1090	916-1100	0.96	-5.28	-3.93
P4	9.1	2.33	975, 1160	962, 1169	0.94	-5.19	-3.94
P5	12.7	4.05	890, 1150	930, 1184	0.91	-5.21	-3.98
P6	18.8	3.48	900-1060	926, 1095	0.95	-5.23	-3.99

[a]Determined by GPC in 1,2,4-trichlorobenzene using polystyrene standards at 135 °C; [b]Dissolved in toluene. [c]Drop-cast from toluene solution (2 mg/mL), E_{opt} = 1240 nm/λ_{onset}. [d]IP and EA were estimated from the onsets of the first oxidation and reduction peaks, while the potentials were determined using ferrocene (Fc) as standard by empirical formulas $E_{IP/EA}$ = - ($E_{Ox/Red}^{onset}$ - $E_{Fc/Fc+}^{(1/2)}$ + 4.8) eV , wherein $E_{Fc/Fc}^{+1/2}$ = 0.40 eV.

3.4 Electrochemical properties

The cyclic voltammetry was carried out to investigate the ionization potentials (IP) and electron affinities (EA) of the polymers.[33] The EA of three monomers **3**, **6** and **16** were also studied to clarify the influence of the side chains, which were attached on the **TQ-2T** core. The reduction curves of monomers are shown in Figure 3.8. The corresponding values of EA were calculated to be -3.77 -3.78 and -3.77 eV, according to the onset of the first reduction peak. These results implied that the substituent number and architecture of the side chains grafted onto the **TQ-2T** core induce a very weak change their electron withdrawing ability.

The reduction and oxidation curves of all **TQ-2T** polymers are shown in Figure 3.9. The corresponding data are calculated based on the onset potentials and listed in Table 3.3. For **P1**-**P4**, we found that the IP values decreased gradually with increasing donor ability of the bridge and this is different with other acceptors.[30,34,35] Therefore, the significant difference in IP of **P1**-**P4** originated not only from different donors, but also from the conformation of the polymer backbone. Compared to IP, the slightly different EA of **P1**-**P4** was attributed to a dominant contribution of the same TQ core. The variation of the IP and EA values for **P4**-**P6** was small. These results suggested that the adjustment of the substitution positions and architectures has a weak influence on IP and EA of the polymers, while variation of the donors in **P1**-**P4** bear a strong effect on the IP of the polymers.
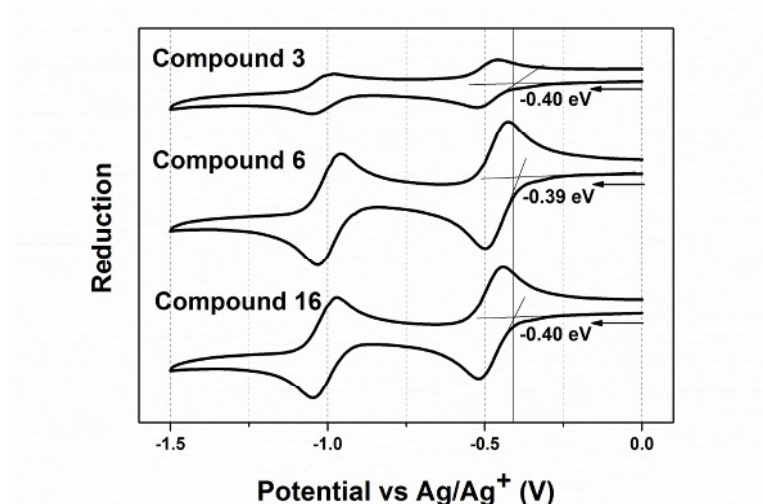
Figure 3.8 Reduction curves of three compounds (**3**, **6**, and **16**) in dichloromethane solutions.
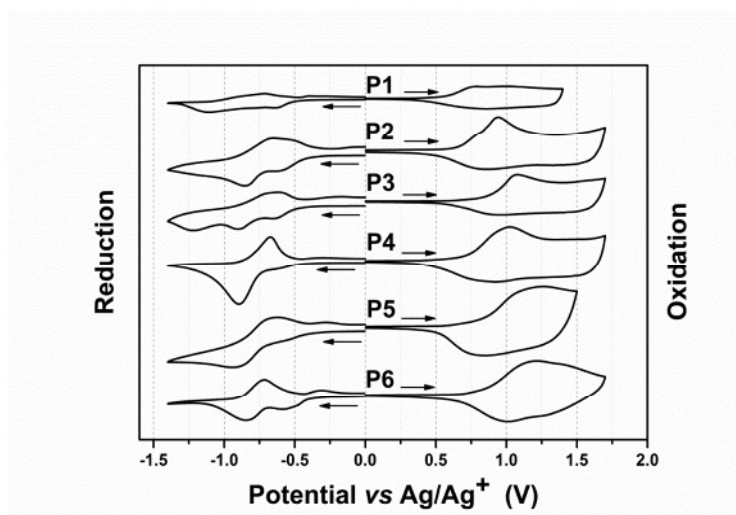
Figure 3.9 Reduction and oxidation curves of **P1**-**P6**.

3.5 OFET properties

The charge transport properties of polymers were studied in collaboration with ██████████ (Max Planck Institute for Polymer Research, Mainz). OFET devices with bottom-gate bottom-contact architecture were fabricated onto the heavily doped silicon wafers with 300 nm thick thermally grown SiO_2 as the dielectric. The dielectric was functionalized by hexamethyldisilazane (HMDS) to minimize interfacial trapping sites. Au electrodes with

60 nm in thickness were evaporated, which acts as source and drain. All polymers were drop-casted from 2 mg/mL chlorobenzene solutions and subsequently annealed at 180 °C for 30 min to remove the residual solvent. The field-effect measurement was carried out under nitrogen atmosphere, and corresponding data including charge carrier mobilities (μ), current on/off ratios (I_{on}/I_{off}) and threshold voltages (V_T) are summarized in Table 3.4.

Table 3.4 Field-effect transistor characteristics of **P1-P6**.

Polymers	$\mu_{h, max.}$ (cm^2 V^{-1} s^{-1})	$\mu_{h, ave.}$ (cm^2 V^{-1} s^{-1})	I_{on}/I_{off}	V_T (V)
P1	0.063	0.046	~10	0
P2	0.081	0.066	50-100	-2
P3	0.042	0.033	100-150	-6
P4	0.10	0.097	100-150	-1
P5	0.012	0.007	100-150	-20
P6	0.24	0.19	~10^4	-15

The transistors of all polymers, **P1**-**P6,** only exhibit p-type field-effect behavior due to the many thiophenes into conjugated backbone. Indeed, some ambipolar D-A polymer semiconductors based **PTQ** were reported by combining alternating weak donors, like alkylated 2,5-diethynylthiophene[20] and unsubstituted thiophene.[21] The transfer and output characteristics of **P1** -**P6** are presented in Figure 3.10. Among **P1**-**P4**, **P4** showed the highest mobility of 0.1 cm^2 V^{-1} s^{-1} with an extremely low threshold voltage of -1 V (Figure 3.10g and h). Due to the incorporation of **BDT** unit, the transistor performance of **P3** is significantly reduced with the mobility of 0.033 cm^2 V^{-1} s^{-1} and the threshold voltage of -6 V. In comparison to **P3**, **P1** and **P2** exhibited a minor improvement in hole transport with mobilities of 0.046 and 0.066 cm^2 V^{-1} s^{-1}. Meanwhile their on/off ratio is lowered to <10^2. This behavior suggested that the donor segments play a crucial role on the charge carrier transport of **TQ-2T** polymers. Since the charge carrier transport in **P4** was limited due to poor solubility and low molecular weight of the polymer, **P5** and **P6** were designed and synthesized bearing higher molecular weight and increased solubility. Unfortunately, **P5** shows a hole mobility approximately one order of magnitude lower than **P4**, most probably because of the increased torsion between the head-to-head alkylated bithiophene unit. Replacing four linear side chains on the **TQ-2T** core (**P4**) by a pair of branched ones (**P6**) led to a dramatic improvement of the transistor performance with maximum hole mobility of 0.24 cm^2 V^{-1} s^{-1} and on/off ratio of 10^4,

although the threshold voltage is slightly increased to -15 V. To the best of our knowledge, this value is the highest, meanwhile, one of best on/off ratio was achieved among TQ-containing semiconductors. These results proved that the substitution positions and architectures of the side chains critically affect the charge carrier transport in **TQ-2T**-based polymers. The nonlinear behavior of the drain current (I_D) at low source-drain voltage (V_D) in the output characteristics of **P4** and **P6** was attributed to the contact resistance and charge injection limitation.[36]
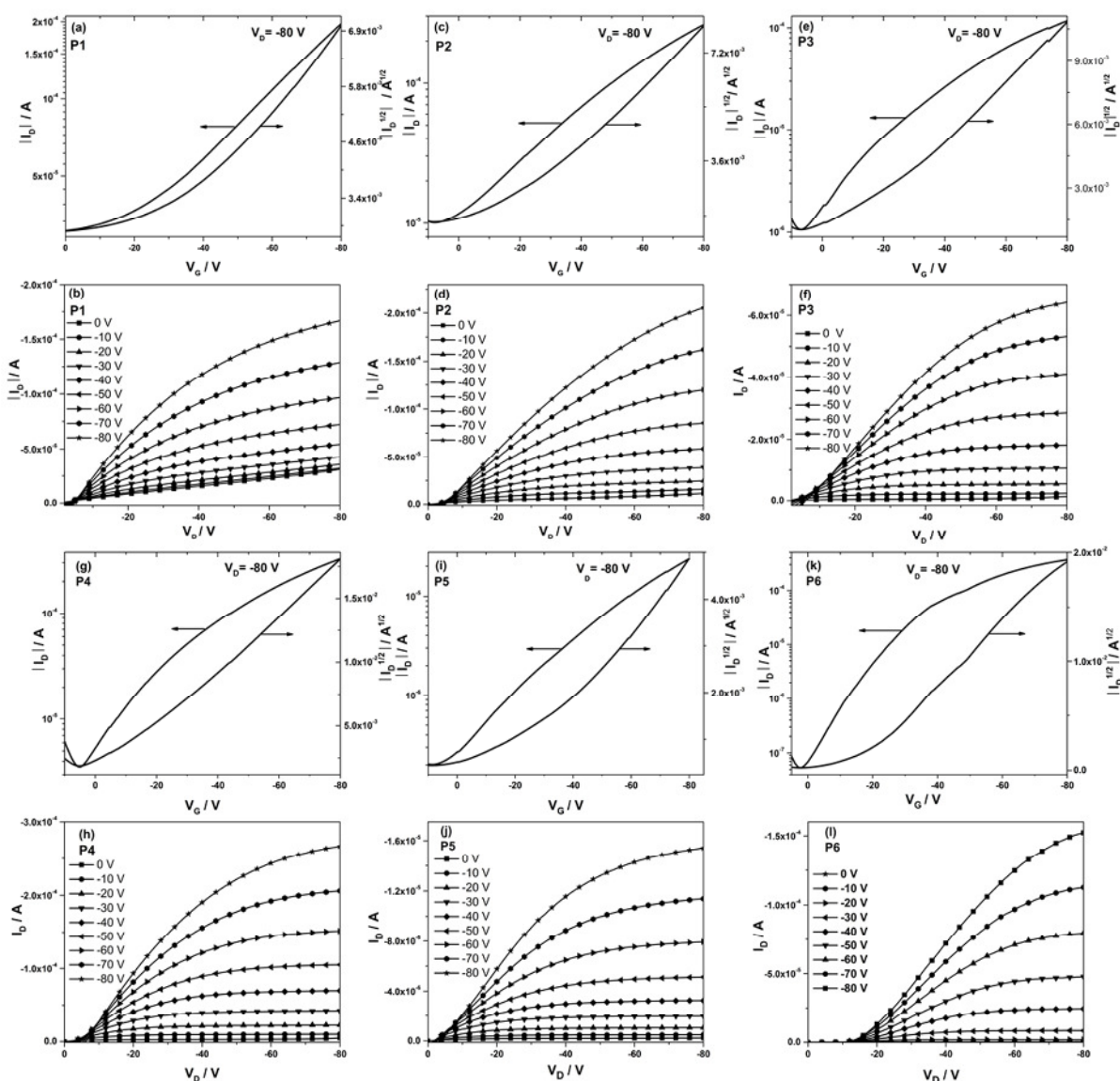

Figure 3.10 Transfer (a), (c), (e), (g), (i), (k) and output (b), (d), (f), (h), (j), (l) curves of **P1**- **P6,** respectively.

Additionally, the relatively low on/off ratio of **P1**-**P6** might be related to adventitious doping, due to the high-lying IP of these polymers.[37,38] In spite of low on/off ratios for these polymers, it has to be emphasized that the reproducibility of OFET performances is relatively good. As shown in Table 3.4, the difference between maximum mobility and average value is only ranging from 3% to 27% for **P1-P4** and **P6**, For **P5**, this difference is slightly increased to 41%.

3.6 Self-organization in the bulk

To understand the variation in device performance, the molecular organization in bulk was investigated using two-dimensional wide-angle X-ray scattering (2DWAXS) which was done by ███████████████ (Max Planck Institute for Polymer Research, Mainz). The 2DWAXS measurements were performed on mechanical extruded fibers which were subsequently thermally annealed at 180 °C for 30 min. For the measurements, the fibers were mounted vertically towards the 2D detector and the scattering was recorded at 30 °C. The 2D patterns confirm slight variations between **P1**, **P2, P5** and **P3**. Significant differences were observed for **P4** and **P6**.

In the equatorial plane of the patterns reflections at small-angles are ascribed to the layer structure of conjugated polymer backbones oriented along the alignment direction of the fiber (Figure 3.11). The interlayer distance between lamellar structures of 3.06 nm for **P1,** 3.02 nm for **P2** and 2.87 nm for **P5** were determined from the main peak position. The scattering intensities on the meridional plane with d-spacing of 1.45 nm for **P1**, 1.65 nm for **P2** and 1.85 nm for **P5** are related to the length of a single repeat unit. These values are in agreement with the theoretical lengths of 1.46 nm for **P1**, 1.62 nm for **P2** and 1.80 nm for **P5** as calculated by Cerius^2 simulations.[39] More crucially, wide-angle equatorial scattering intensities are assigned to π-stacking distances of 0.38 nm for **P1**, 0.36 nm for **P2** and 0.37 nm for **P5**. Additionally, the π-stacking reflection for **P2** showed a slightly smaller full width at half maximum (FWHM)[40] than for **P1** and **P5,** indicating a larger coherence length along the stacking direction for **P2**. Table 3.5 summarized the FWHM value and coherent length for the π-stacking direction for all investigated polymers. Interestingly, due to an improved overall crystallinity, the alkyl side chains of **P2** exhibit a preferential ordered direction as evident from off-meridional reflections in the middle-angle region (dashed circles in Figure 3.111b).

In contrast, the patterns for **P1** and **P5** display only a broad amorphous halo characteristic for disordered alkyl chains.
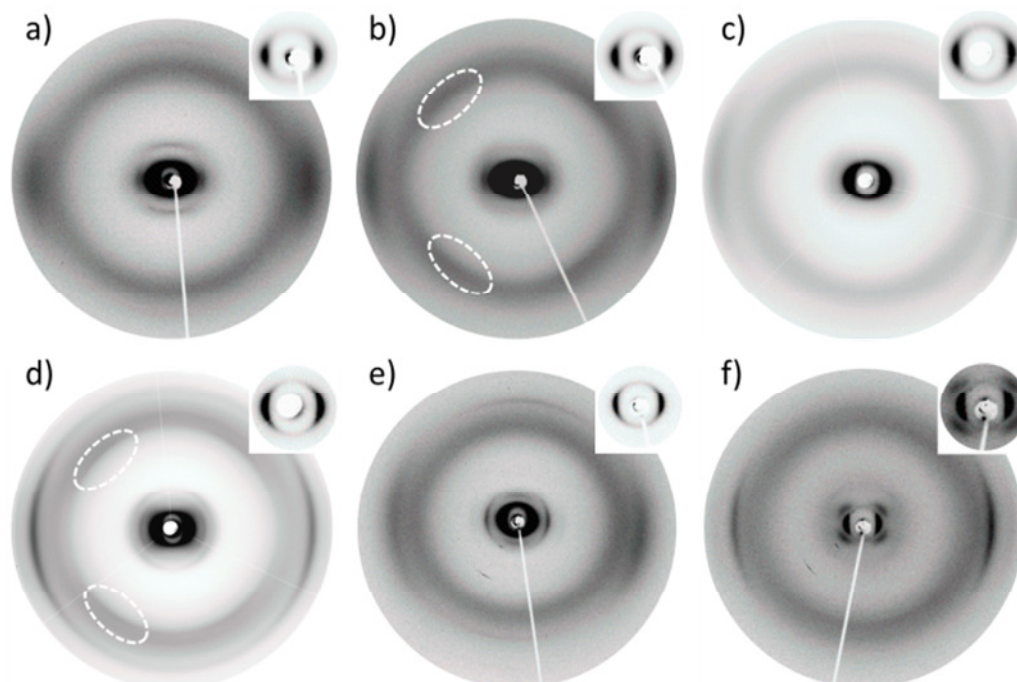

Figure 3.11 2DWAXS patterns of a) **P1**, b) **P2**, c) **P3**, d) **P4**, e) **P5** and f) **P6** (insets show the small-angle scattering range). Off-meridional reflections related to a preferential organization of the alkyl chains are indicated in b) and d) by dashed circles.

In comparison to **P1** and **P2**, the interlayer distance of **P3** decreases to 2.80 nm, due to a slightly smaller backbone curvature, while a π-stacking distance of 0.36 nm is found. The amorphous halo related to a d-spacing of 0.45 nm is correlated also to the isotropic arrangement of alkyl chains. The interlayer distance observed for **P4** and **P6** is 3.03 nm and 2.94 nm, respectively. In comparison to the other polymers within this series, both compounds show more distinct π-stacking reflections corresponding to distances of 0.37 for **P4** and 0.38 for **P6**. The variations in the interlayer and π-stacking distance within this polymer series are due to the modifications in backbone composition and substitution position. A less planar donor unit in **P4** and **P6** in comparison to **P2** and **P3** increases the π-stacking distance. Avoiding alkyl chains at the acceptor and replacing the linear to branched alkyl chains for **P6,** on the other hand, slightly reduce the interlayer distance and increase the π-stacking distance. Surprisingly, at the same time the degree of order in **P4** and **P6** increases as evident from a higher coherence length π-stacking for both polymers in comparison to the other polymers

(Table 3.5). Reflections in the off-meridional middle-angle region corresponding to the d-spacings of 1.23 nm for **P4** and 2.00 for **P6** suggest that the repeat units of the polymer chains in neighbouring layers are shifted in the extrusion direction with respect to each other. Cerius[2] simulations confirm this effect on the scattering pattern (Figure 3.12). In such organization **P6** with branched alkyl chains and with non-planar donor unit arranges in a more energetically favourable fashion. The shift is induced by the steric demand of the branched substituents allowing a more efficient space filling in the layer periphery. In this configuration, the donor units occupy positions adjacent to acceptor units in the neighboring layers. This packing of **P6** induces higher crystallinity than for **P1**, **P2**, **P3** and **P5**. Additional anisotropic off-meridional reflections for **P4** corresponding to a d-spacing of 0.45 nm are assigned to alkyl chain ordering and confirm higher overall order in comparison to **P1** and **P3**.

Table 3.5 Summary of the structural data of **P1-P6** from 2DWAXS. FWHM and coherence length have been calculated in the π-stacking direction.

Polymers	FWHM (°)	Coherence length (nm)	π-π spacing (nm)	Interlayer distance (nm)
P1	4.7	1.7	0.38	3.06
P2	3.1	2.6	0.36	3.02
P3	2.8	2.9	0.36	2.80
P4	1.4	5.8	0.37	3.03
P5	4.2	1.9	0.37	2.87
P6	1.2	6.6	0.38	2.94

For this polymer series, the charge carrier transport in field-effect transistors is insensitive on the interlayer and π-stacking distance. It has been found that the coherence length in the π-stacking direction is more crucial for the electrical properties. In other words, a more ordered packing of the polymers chains in the layer structures ensures a more unhindered migration of charges as observed in the case of **P4** and **P6**.
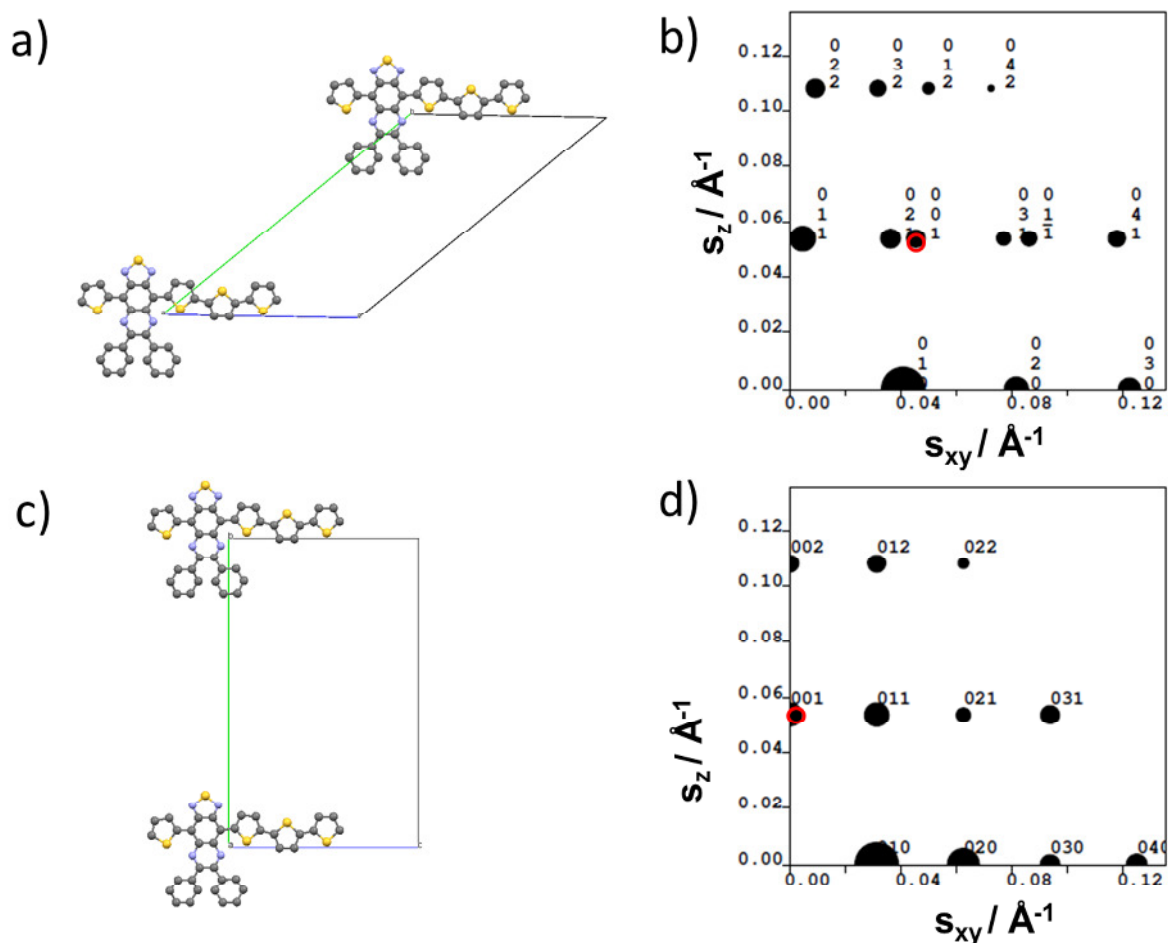
Figure 3.12 Schematic illustrations of the unit cells with (a) and without (c) polymer shift in neighbouring layers. This shift occurs along the fibre extrusion direction. (b) and (d) simulated 2DWAXS patterns with and without translation. The 001 reflection, which is observed in the experimental patterns and corresponding to the length of a monomeric unit, is indicated by red color. This reflection is shifted in the simulated pattern from meridional to off-meridional position with translation of the polymer backbones towards each other. Wherein $S_{xy} = q_{xy}/2\pi$, $S_z = q_z/2\pi$.

3.7 Self-organization in films

The significant different device performance of **P1-P6** should be also related to their different self-organization in thin films. In order to understand how to effect on morphologies of the films via varying donor moieties, substitution positions and architectures of alkyl chains on polymers. The out-of-plane X-ray measurements of thin films were performed. All samples were fabricated on 300 nm thick SiO_2 dielectric covering the highly doped Si. Such substrates were functionalized by hexamethyldisilazane (HMDS) to minimize interfacial

trapping sites. The semiconducting layer was drop-cast from a 2 mg/mL chlorobenzene solution onto the substrates. Afterwards, the substrates were heated 180 $^{\circ}$C for 30 min to remove residual chlorobenzene in a glove box. These samples were measured by ▮▮▮▮ ▮▮▮▮ (Max Planck Institute for Polymer Research, Mainz).
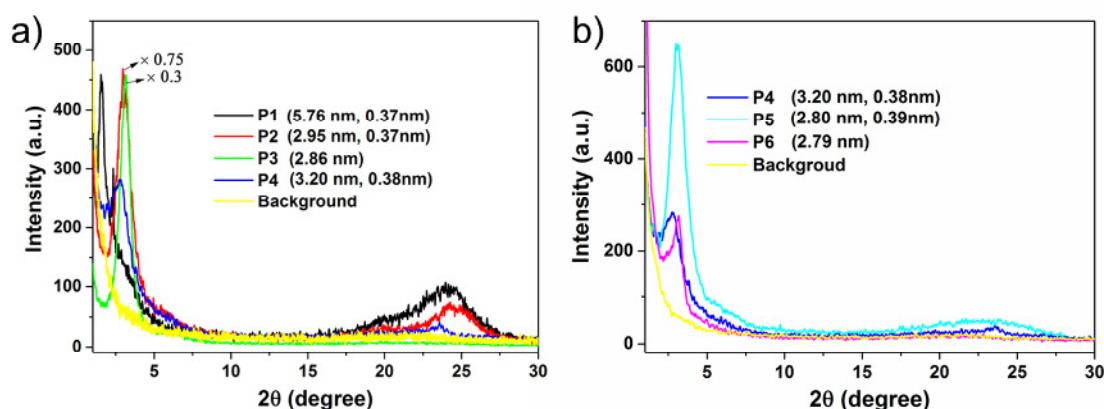

Figure 3.13 Out-of-plane films XRD of (a) **P1-P4** and (b) **P4-P6**.

Out-of-plane XRDs of the polymers films are shown in Figure 3.13. The polymers displayed chain-to-chain distances of 2.95, 2.86, 3.20, 2.80 and 2.79 nm for **P2**-**P6**, respectively. While the chain to chain distance of **P1** had a value of 5.76 nm, which is two times larger than those of other TQ polymers, implying that the real chain-to-chain distance of **P1** could be 2.88 nm. The axialsymmetric TQ units have three different patterns which lead to corresponding TQ polymers follow themselves: head-to-head, head-to-tail and tail-to-tail (Figure 3.14). Grimsdale and his coworkers reported two TQ-based polymers, which were determined two clear chain-to-chain distances in films using out-of-plane XRDs.[41] However, our TQ polymers have only one chain-to-chain distance. This result suggested that our TQ polymers have higher ordered arrangement in films. This could be one of the reasons that these polymers exhibited excellent charge carrier mobility. Different donor parts of polymers can siginificantly effect the molecular self-organization in films as shown in Figure 3.13a. **P1**, **P2** and **P4** showed a significant π-π stacking signal with π distance of 0.37, 0.37 and 0.38 nm, which might suggest face-on configuration. The sharp peak of **P4** was related to its high hole mobility of 0.1 cm^2 V^{-1} s^{-1}. An extending conjugated donor **BDT** was introduced into **TQ-2T** containing polymers, **P3** didn't show any π stacking signal, it is in agreement with its

relatively low hole mobility of 0.042 cm^2 V^{-1} s^{-1}. Figure 3.13b demonstrated the packing of **P4**-**P6**. A broad peak of **P5** implied that it has a very weak π-π stacking, due to the head-to-head alkylated bithiophene which led to strong twisting in the conjugated backbone of this polymer. The maximum hole mobility of **P5** had only 0.012 cm^2 V^{-1} s^{-1}. Surprising, **P6** didn't show π-π stacking, but the high crystallinity of this polymer is a key factor for highest hole mobility in this series of TQ polymers as discussed in 2DWAXS measurements. These result demonstrated varying donor moieties, alkyl chain substitution positions and architectures in **TQ-2T** polymers can affect the π-π stacking of the polymers.

head-to-head

head-to-tail

tail-to-tail
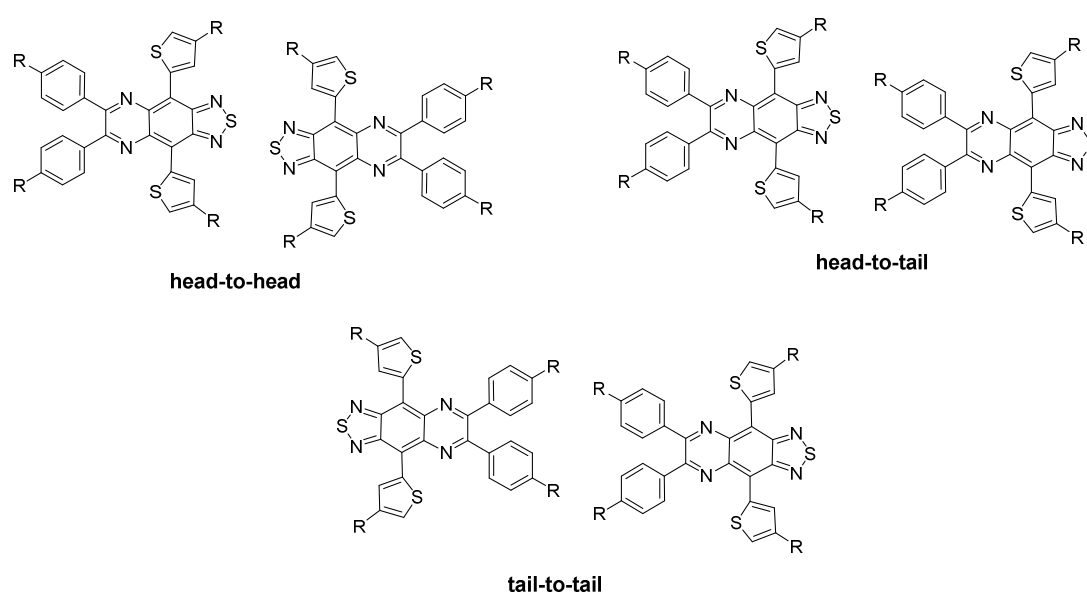
Figure 3.14 Schematic diagram for TQ molecule with three different arrangement patterns.

3.8. Summary

In this chapter, in order to develop new high performance TQ polymer semiconductors, six new **TQ-2T**-based polymers have been synthesized and characterized. Varying donor moieties, alkyl chain substitution positions and architectures in **TQ-2T** polymers can facilitate the tuning of the optoelectronic behaviors, self-organization in bulk and charge carrier transport.

Firstly, the different unsubstituted donors, **T**, **TT**, **BDT** and **BT** were introduced into **TQ-2T** copolymer and successfully improved the conjugated backbone. All of them achieved

high hole mobilities, these value are highest among reported TQ polymers. Especially, **P4** achieved charge carrier mobility as high as 0.1 cm^2 V^{-1} s^{-1}. The issue of these polymers is that the four dodecyl side chains cannot provide enough solubility for polymerization with unsubstituted donor groups. **P1**-**P4** have poor solubility, low molecular weight, thereby these factors still limited their charge carrier mobilities.

Secondly, in order to overcome above drawback, we regrouped the four dodecyl side chains in conjugated skeleton of **P4** to obtain other two polymers **P5** and **P6** by side chain substitution positions and architectures. These polymers had the identical molecular formulas of side chains and conjugated backbone. Although **P5** showed an enhanced solubility and molecular weight than **P4**, it produces a low crystallinity due to the conjugated backbone torsion and leads therefore a low mobility of 0.007 cm^2 V^{-1} s^{-1}. Interestingly, A pair of 2-decyl-tetradecyl alkyl chains is used to replace the linear side chains, it does not significantly change the planarity of the polymers, but improves its molecular weight and solubility. Due to a higher coherence length in the π-stacking direction, the charge carrier mobility of **P6** is increased up to 0.24 cm^2 V^{-1} s^{-1}.

High performance TQ polymers were successfully designed and synthesized by investigation in structure-property relationships of **TQ-2T**-polymers. It is beneficial to broaden the understanding of TQ-containing polymers and apply our strong acceptor **BDTTQ** towards to high performance ambipolar polymer semiconductors. This part is shown in Chapter 4.

3.9 Synthetic details

Intermediates 4,7-bis(4-dodecylthiophen-2-yl)benzo[c][1,2,5]thiadiazole-5,6-diamine (**1**), 4,7-dibromo-5,6-dintrobenzo[c][1,2,5]thiadiazole (**12**) and (3,3'-didodecyl-[2,2'-bithiophene]-5,5'-diyl)bis(trimethylstannane) (**22**) were prepared according to synthetic details of Chapter 2. 1,2-bis(4-dodecylphenyl)ethane-1,2-dione (**2**),[2] 4,7-di(thiophen-2-yl)benzo[c][1,2,5]thiadiazole-5,6-diamine (**5**),[42] 2-decyl-tetradecylbromide (**8**),[43] 2,5-bis(trimethylstannyl)thiophene (**18**),[44] 2,5-bis(trimethylstannyl)thieno[3,2-b]thiophene (**19**),[45] 2,6-bis(trimethylstannyl)benzo[1,2-b:4,5-b']dithiophene (**20**)[46] and 5,5'-bis(trimethylstannyl)-2,2'-bithiophene (**21**)[47] were prepared according to the literature procedures as shown in the schemes 3.4-3.7 below.
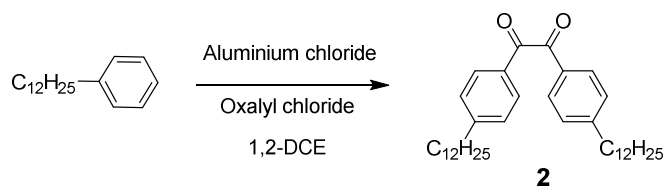
Scheme 3.4 Synthetic route for compound **2**.[2]
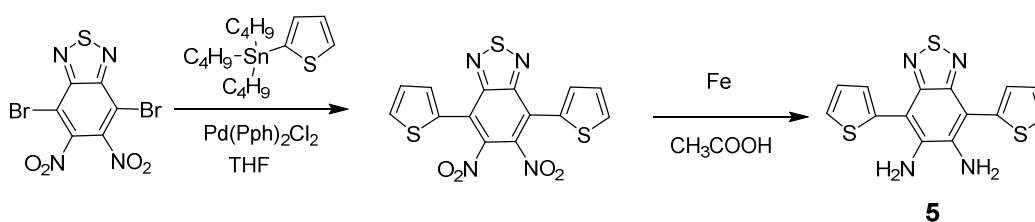
Scheme 3.5 Synthetic route for compound **5**.[42]
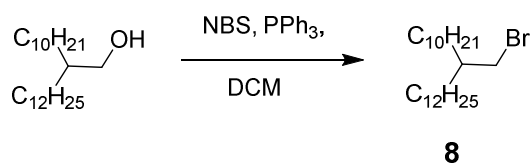
Scheme 3.6 Synthetic route for compound **8**.[43]

Scheme 3.7 Synthetic route for compounds **18-21**.[44-47]

6,7-Bis(4-dodecylphenyl)-4,9-bis(4-dodecylthiophen-2-yl)-[1,2,5]thiadiazolo[3,4-g]quinoxaline (3)
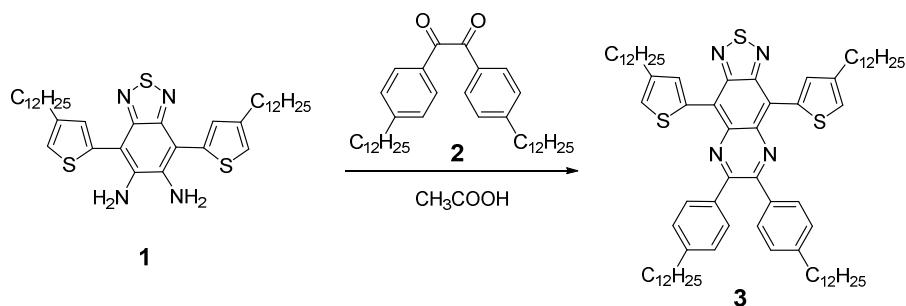
A suspension of **1** (0.2 g, 0.30 mmol) and 1,2-bis(4-dodecylphenyl)ethane-1,2-dione (**2**, 0.164 g, 0.30 mmol) in 20 mL of acetic acid was placed into a 50 mL Schlenk tube. The mixture was heated to 55 ºC and stirred overnight. After cooling to room temperature, the product was 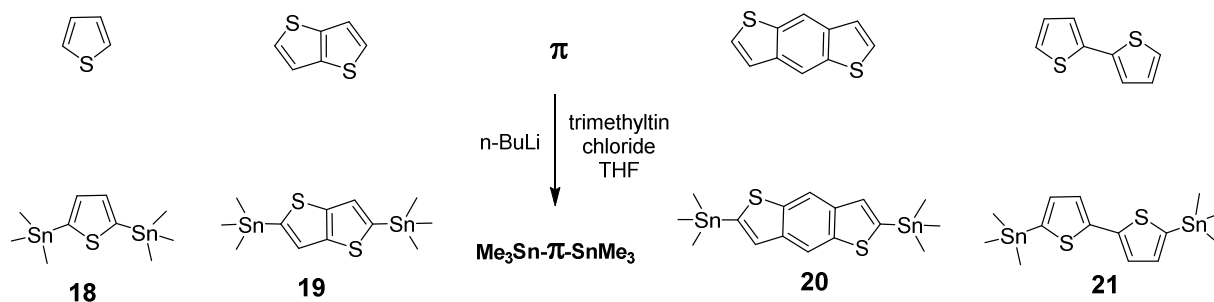filtered and washed with methanol. The crude product was purified by column using hexane/dichloromethane (3:1) as eluent to give 0.328 g of compound **3** (green solid, 93%). ^{1}H NMR (250 MHz, CD_2Cl_2) δ 8.83 (d, J = 2.50 Hz, 2H), 7.73 (s, J = 10.0 Hz, 4H), 7.9 (m, 6H), 2.80-2.64 (m, 8H), 1.78-1.63 (br, 8H), 1.28 (br, 72H), 0.90-0.85 (br, 12H). ^{13}C NMR (62.5 MHz, CD_2Cl_2) δ 153.63, 152.27, 145.38, 143.44, 136.09, 135.96, 135.24, 135.02, 130.88, 128.63, 126.86, 121.39, 36.21, 32.34, 31.67, 31.19, 30.99, 30.12, 30.08, 29.98, 29.93, 29.88, 29.78, 29.73, 23.10, 14.29. HRMS (ESI+): m/z calcd 1177.8127, found 1177.8116.

4,9-Bis(5-bromo-4-dodecylthiophen-2-yl)-6,7-bis(4-dodecylphenyl)-[1,2,5]thiadiazolo[3,4-g]quinoxaline (4)
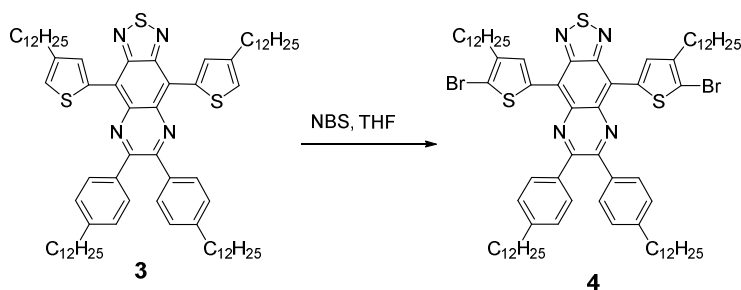
Compound **3** (236 mg, 0.2 mmol) was dissolved in 15 mL of THF at room temperature. NBS (39 mg, 0.22 mmol) was carefully added into the solution in small batches under dark.

The mixture was stirred for 5 h. After removing the solvent under reduced pressure, the residue was purified by column chromatography using hexane/dichloromethane (3:1) as eluent to give monomer **4** as a green solid (198 mg, 74%). ^{1}H NMR (250 MHz, CD$_2$Cl$_2$) δ 8.70 (s, 2H), 7.53 (d, J = 7.50 Hz, 4H), 7.20 (d, J = 10.0 Hz, 4H), 2.72-2.58 (m, 8H), 1.69 (br, 8H), 1.31-1.27 (br, 72H), 0.91-084 (br, 12H). ^{13}C NMR (62.5 MHz, CD$_2$Cl$_2$) δ 153.78, 151.18, 145.35, 142.03, 135.83, 135.48, 134.46, 134.46, 131.16, 128.46, 119.93, 118.15, 36.26, 32.37, 31.66, 30.26, 30.18, 30.16, 30.12, 30.04, 30.01, 29.99, 29.94, 29.85, 23.13, 14.31. HRMS (ESI+): m/z calcd 1333.6338, found 1333.6329.

6,7-Bis(4-dodecylphenyl)-4,9-di(thiophen-2-yl)-[1,2,5]thiadiazolo[3,4-g]quinoxaline (6)
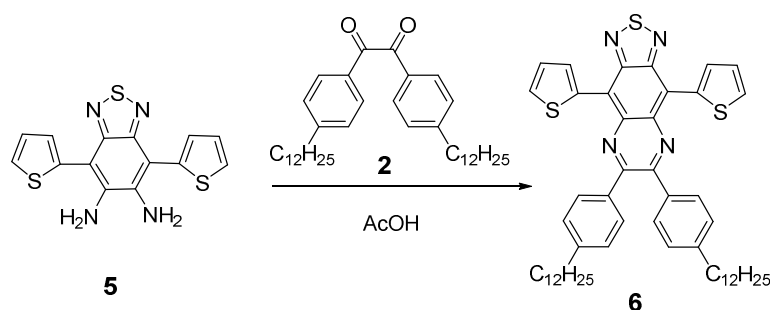
Following the same procedure for the preparation of compound **3**, 4,7-di(thiophen-2-yl)benzo[c][1,2,5]thiadiazole-5,6-diamine (**5**, 99 mg, 0.3 mmol) was used to replace 4,7-bis(4-dodecylthiophen-2-yl)benzo[c][1,2,5]thiadiazole-5,6-diamine (**1**). Compound **6** was obtained as a green solid (215 mg, 85%). ^{1}H NMR (250 MHz, THF-d_8) δ 9.11-9.09 (dd, J = 2.50 Hz, J = 5.0 Hz, 2H), 7.76-7.69 (m, 6H), 7.27-7.22 (m, 6H), 2.68 (t, J = 7.50 Hz, 4H), 1.71-1.63 (br, 4H), 1.38-1.29 (br, 36H), 0.89 (t, J = 7.50 Hz, 6H). ^{13}C NMR (62.5 MHz, THF-d_8) δ 154.51,151.57, 145.58, 138.24, 136.04, 134.68, 134.09, 131.63, 130.17, 128.70, 120.88, 120.51, 36.50, 32.72, 32.01, 30.52, 30.47, 30.36, 30.25, 30.17, (overlap with THF-d$_8$) , 23.40, 14.28. HRMS (ESI+): m/z calcd 841.4371, found 841.4370.

4,9-Bis(5-bromothiophen-2-yl)-6,7-bis(4-dodecylphenyl)-[1,2,5]thiadiazolo[3,4-g]quinoxaline(7)
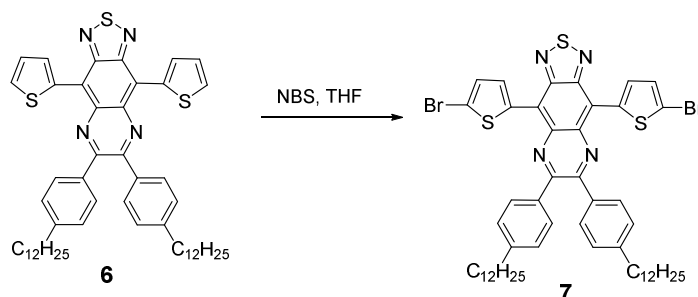
Following the same procedure for the preparation of compound **4**, 6,7-bis(4-dodecylphenyl)-4,9-di(thiophen-2-yl)-[1,2,5]thiadiazolo[3,4-g]quinoxaline (**6**, 168 mg, 0.2 mmol) was used to replace compound **3**. Compound **7** was obtained as a green solid (172 mg, 86%). ^{1}H NMR (250 MHz, THF-d_8) δ 8.90 (d, $J = 5.0$ Hz, 2H), 7.66-7.63 (dd, $J = 2.5$ Hz, $J = 5.0$ Hz, 4H), 7.28-7.25 (dd, $J = 2.5$ Hz, $J = 5.0$ Hz, 4H), 7.21(d, $J = 5.0$ Hz, 2H), 2.71 (t, $J = 7.50$ Hz, 4H), 1.71-1.65 (br, 4H), 1.41-1.25 (br, 36H), 0.89 (t, $J = 7.50$ Hz, 6H). ^{13}C NMR (62.5 MHz, THF-d_8) δ 154.01, 152.40, 145.24, 136.67, 136.64, 135.31, 133.79, 131.89, 131.45, 128.67, 126.90, 121.73, 36.49, 32.70, 32.02, 30.49, 30.45, 30.33, 30.20, 30.15, (overlap with THF-d_8) , 23.39, 14.26. HRMS (ESI+): m/z calc. 997.2582 found 997.2589.

3-(2-Decyltetradecyl)thiophene (10)
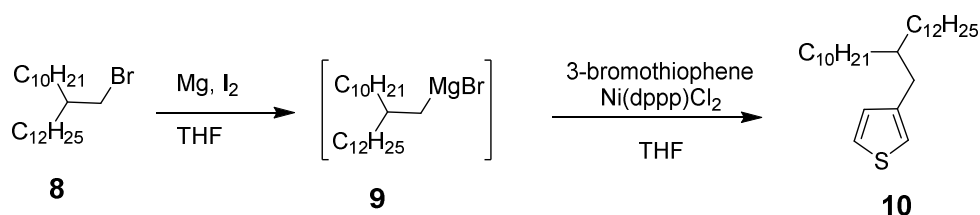
Magnesium turnings (0.7 g, 29 mmol), a catalytic amount of iodine and 30 mL of dry THF were mixed in a 100 mL flask and heated to 80 °C under argon. A solution of 2-decyl-tetradecylbromide (10 g, 24 mL) in 20 mL of dry THF was added dropwise into the flask within 30 min. The resulting mixture was refluxed overnight. After cooling to room temperature, the grey solution was transferred into a dry constant pressure funnel and added

dropwise into a dry THF (20 mL) solution of 3-bromothiophene (3.9 g, 24 mmol) and Ni(dppp)Cl$_2$ (316 mg, 0.58 mmol) at room temperature. The mixture was heated to reflux overnight under argon. The mixture was then cooled to room temperature and then 1 N HCl was added to quench excess Grignard reagent. The crude product was extracted with diethyl ether (3×20 mL). The combined organic phases were dried with MgSO4, and the solvent was removed under reduced pressure to afford dark oil, which was purified by column chromatography eluting with hexane to give 5.1 g (colorless oil, 51%) of compound **10**. ^{1}H NMR: (250 MHz, CD$_2$Cl$_2$, ppm) δ 7.25-7.22 (m, 1H), 6.93-6.90 (m, 2H), 2.58-2.55 (d, 2H, J = 7.5 Hz), 1.63-1.58 (m, 1H), 1.35-1.22 (br, 40H), 0.91-0.86 (t, 6H, J = 5.0 Hz, J = 7.5 Hz). ^{13}C NMR (62.5 MHz, CD$_2$Cl$_2$, ppm) δ 142.48, 129.24, 125.10, 121.02, 39.38, 35.04, 33.72, 32.38, 30.44, 30.17, 30.14, 30.11, 29.81, 28.99, 23.14, 14.34. HRMS (ESI+): m/z calc. 421.3868, found 421.3874.

2-Trimethylstannyl-4-(2-decyltetradecyl)thiophene (11)
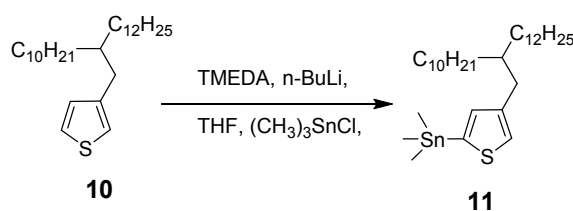
3-(2-Decyltetradecyl)thiophene (**10**, 3.63 g, 8.63 mmol) and N,N,N',N'-tetramethylethylenediamine (TMEDA, 1.42 mL, 9.49 mmol) were dissolved in 36 mL of anhydrous THF. After cooling to 0 °C, the n-BuLi (5.93 mL, 9.49 mmol, 1.6 M in hexane) was added slowly into this mixture solution over 10 min. The resulting solution was stirred for 5 min at 0 °C and warmed to room temperature over 30 min. The mixture was cooled to 0 °C again, and trimethyltin chloride (9.49 mL, 9.49 mmol, 1 M in hexane) was added dropwise. The mixture was stirred for 30 min at 0 °C and warmed to room temperature. After two hours, the resulting solution was poured into water and extracted with diethyl ether (3×20 mL). The combined organic phases were washed with brine, dried with MgSO$_4$, and filtered. The filtrate was concentrated under reduced pressure to obtain compound **11** (4.8 g, yellow oil, 95%). This crude product was used for next step without further purification. ^{1}H NMR: (250 MHz, CD$_2$Cl$_2$, ppm) δ 7.16 (s, 1H), 6.98 (s, 1H), 2.59 (d, 2H, J = 7.5 Hz), 1.63-1.58 (m, 1H),

1.34-1.22 (br, 40H), 0.91-0.85 (t, 6H, *J* = 7.5 Hz), 0.34(s, 9H). ^{13}C NMR (62.5 MHz, CD$_2$Cl$_2$, ppm) δ 143.71, 137.73, 137.27, 126.92, 39.56, 34.77, 33.90, 32.51, 30.59, 30.28, 30.25, 29.95, 27.13, 23.27, 14.48, -8.12.

4,7-Bis(4-(2-decyltetradecyl)thiophen-2-yl)-5,6 dinitrobenzo[c][1,2,5]thiadiazole (13)
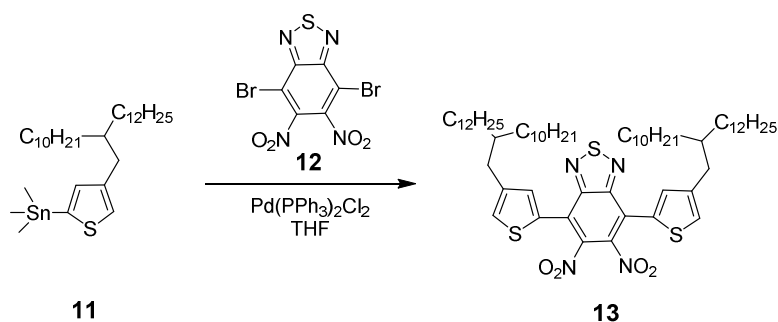
4,7-Dibromo-5,6-dinitrobenzothiadiazole (**12**) (1.23g, 3.2 mmol), compound **11** (4.30 g, 7.40 mmol) and Pd(PPh$_3$)$_2$Cl$_2$ (225 mg, 0.32 mmol) were dissolved in 40 mL of anhydrous THF under argon. The resulting solution was stirred for 16 h at 80 °C. The solvent was removed under reduced pressure to afford a dark-red oil, which was purified by column chromatography using hexane/dichloromethane (4:1) as eluent to give 2.42 g (red solid, 71%) of compound **13**. ^{1}H NMR (250 MHz, CD$_2$Cl$_2$, ppm) δ 7.34 (s, 2H), 7.32 (s, 2H), 2.65 (d, *J* = 7.50 Hz, 4H), 1.69-1.63 (m, 2H), 1.29-1.27 (m, 80H), 0.91-0.86 (t, *J* = 7.50 Hz, *J* = 5.0 Hz, 12H). ^{13}C NMR (62.5 MHz, CD$_2$Cl$_2$, ppm) δ 152.59, 143.57, 141.97, 133.16, 129.45, 127.69, 121.85, 39.40, 34.94, 33.66, 32.37, 30.41, 30.14, 30.10, 29.80, 27.04, 23.13, 14.33. HRMS (ESI+ Na): m/z calc. 1085.6961, found 1085.6981.

4,9-Bis(4-(2-decyltetradecyl)thiophen-2-yl)-6,7-diphenyl-[1,2,5]thiadiazolo[3,4-g]quinoxaline (16)
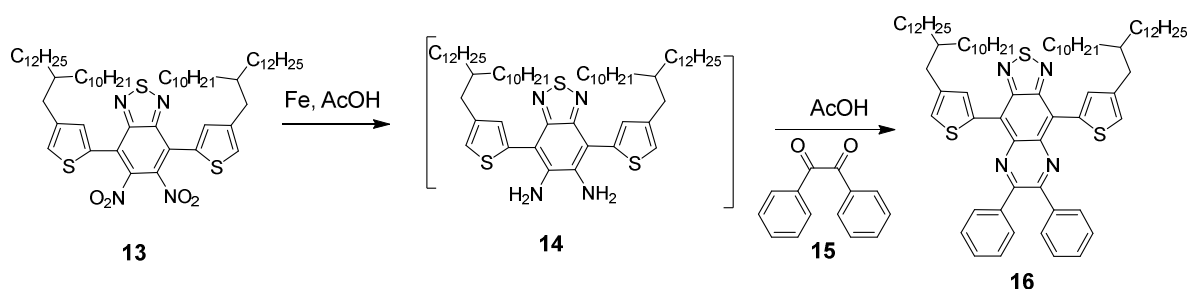
Compound **13** (0.5 g, 0.47 mmol) and fine iron powder (311 mg, 5.55 mmol) in acetic acid (15 mL) was stirred for 5 h at 75 °C under argon. The reaction mixture was cooled to room temperature, precipitated in 5% aqueous NaOH and extracted with diethyl ether (3×20 mL). The combined organic layers were washed with brine, dried with MgSO$_4$ and the solvent was removed under reduced pressure to give corresponding diamine (**14**) with deep red oil. This crude product was directly added into acetic acid (15 mL) solution of benzil (99 mg, 0.47 mmol). The mixture was heated to 80 °C overnight under argon. After cooling down to room temperature, the mixture was poured into 100 mL 5% aqueous NaOH and extracted with dichloromethane (3×20 mL). The combined organic phases were dried with MgSO$_4$ and filtered. The filtrate was concentrated and purified by column chromatography eluting with hexane dichloromethane (4:1) to give 0.387 g (green solid, two steps 70%) of compound **16**. ^{1}H NMR (250 MHz, CD$_2$Cl$_2$, ppm) δ 8.87 (d, *J* = 2.5 Hz, 2H), 7.82-7.78 (m, 4H), 7.47-7.38 (m, 6H), 7.27 (d, 2H), 2.72 (d, *J* = 5.0 Hz, 4H), 1.80-1.73 (m, 2H), 1.28-1.24 (br, 80H), 0.88-0.83 (m, 12H). ^{13}C NMR (62.5 MHz, CD$_2$Cl$_2$, ppm) δ 153.39, 152.32, 142.10, 138.64, 135.85, 135.73, 135.14, 130.98, 129.88, 128.58, 128.15, 121.59, 39.48, 35.29, 33.79, 32.33, 30.50, 30.13, 30.08, 30.07, 29.77, 27.07, 23.10, 14.29. HRMS (ESI+): m/z calc. 1177.8127 found 1177.8153.

**4,9-Bis(5-bromo-4-(2-decyltetradecyl)thiophen-2-yl)-6,7-diphenyl-[1,2,5]thiadiazolo[3,4-g]quinoxaline (17)**
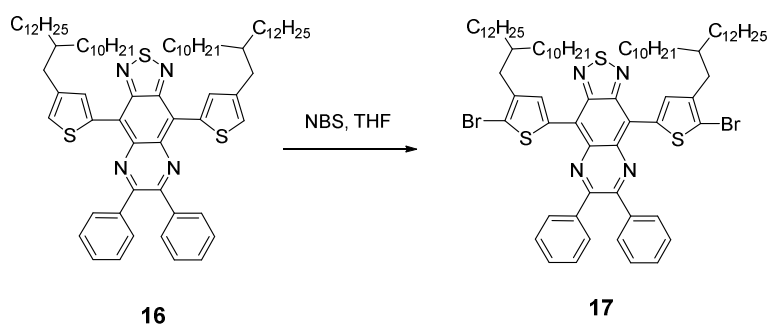
Compound **16** (235 mg, 0.2 mmol) was dissolved in 15 mL THF at the room temperature. NBS (39 mg, 0.22 mmol) was carefully added into the solution in small batches under dark. The mixture was stirred for 5 h. After removing the solvent under reduced pressure, the

residue was purified by column chromatography using hexane/dichloromethane (3:1) as eluent to give compound **17** as a green solid (232 mg, 87%). ^{1}H NMR (250 MHz, CD_2Cl_2, ppm) δ 8.83 (s, 2H), 7.72-7.67 (m, 4H), 7.75-7.38 (m, 6H), 2.62 (d, *J* = 7.5 Hz, 4H), 1.81 (br, 2H), 1.36-1.22 (br, 80H), 0.88-0.82 (m, 12H). ^{13}C NMR (62.5 MHz, CD_2Cl_2, ppm) δ 153.76, 151.60, 141.34, 138.07, 135.67, 135.40, 134.71, 131.14, 130.05, 128.56, 120.48, 119.14, 38.98, 34.54, 33.81, 32.34, 30.50, 30.15, 30.13, 30.08, 29.78, 26.97, 23.10, 14.30. HRMS (ESI+): m/z calc. 1333.6338 found 1333.6306.

Synthesis of P1
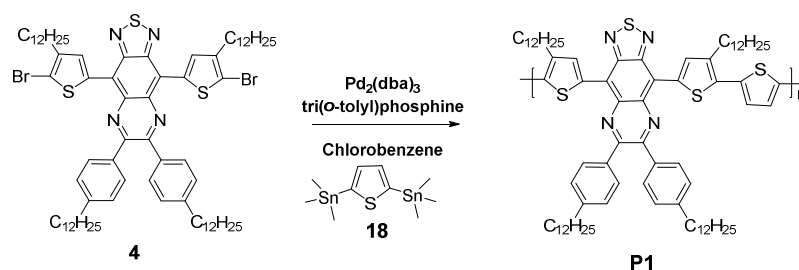
Compound **4** (0.1 mmol), 2,5-bis(trimethylstannyl)thiophene (**18**, 0.1 mmol) and chlorobenzene (8 mL) were placed in a 50 mL two-neck flask. The mixture was purged with argon for 5 min, and then 5.5 mg of tris(dibenzylideneacetone)dipalladium(0) ($Pd_2(dba)_3$) and 7.3 mg of tri(*o*-tolyl)phosphine (P(*o*-tolyl)$_3$) were added. Then the mixture was heated up to 110 °C under argon. After 3 days, the polymer was end-capped with tributylphenylstannane and bromobenzene in sequence. After cooling to room temperature, the reaction mixture was poured into methanol. The polymer was filtered and subjected to Soxhlet extraction with methanol, acetone, hexane, chloroform and chlorobenzene. The chlorobenzene fraction was collected and added 30 mL of sodium diethyldithiocarbamate aqueous solution (1 g/100 mL), the mixture was heated to 60 °C with vigorous stirring for 2 h. The mixture was separated and organic phase was washed with water for 3 times. The polymer was collected from the chlorobenzene fraction and dried in vacuum to afford **P1**.

P1 (black solid, 103 mg, 81%).

Molecular weight by GPC (135 °C): M_n = 7.0 kg mol^{-1}, PDI = 2.68.

Elemental analysis: Calcd. For $C_{80}H_{112}N_4S_4$: C, 76.40; H, 8.97; N, 4.45; S, 10.17. Found: C, 75.44; H, 10.17; N, 4.27; S, 10.13.

Synthesis of P2

Following the same procedure for the preparation of **P1**, 2,5-bis(trimethylstannyl)thieno [3,2-b]thiophene (**19**, 0.1 mmol) was used to replace donor **18**.
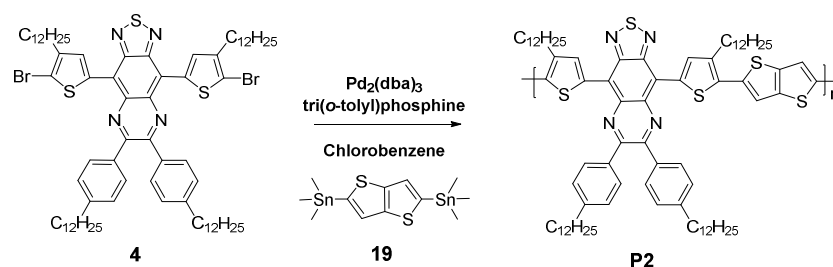
P2 (black solid, 88 mg, 67%).

Molecular weight by GPC (135 °C): M_n = 5.4 kg mol^{-1}, PDI = 2.15.

Elemental analysis: Calcd. For $C_{82}H_{112}N_4S_5$: C, 74.97; H, 8.59; N, 4.26; S, 12.17. Found: C, 74.08; H, 9.42; N, 4.13; S, 11.79.

Synthesis of P3

Following the same procedure for the preparation of **P1**, 2,6-bis(trimethylstannyl)benzo [1,2-b:4,5-b']dithiophene (**20**, 0.1 mmol) was used to replace donor **18**.

P3 (black solid, 118 mg, 86%).

Molecular weight by GPC (135 °C): M_n = 8.0 kg mol^{-1}, PDI = 2.34.

Elemental analysis: Calcd. For $C_{86}H_{114}N_4S_5$: C, 75.75; H, 8.42; N, 4.11; S, 11.72. Found: C, 74.41; H, 10.02; N, 3.88; S, 11.41.

Synthesis of P4

Following the same procedure for the preparation of **P1**, 5,5'-bis(trimethylstannyl)-2,2'-bithiophene (**21**, 0.1 mmol) was used to replace donor **18**.


P4 (black solid, 77 mg, 57%).

Molecular weight by GPC (135 °C): M_n = 9.1 kg mol^{-1}, PDI = 2.33.

Elemental analysis: Calcd. For $C_{84}H_{112}N_4S_5$: C, 75.31; H, 8.58; N, 4.18; S, 11.93. Found: C, 74.18; H, 8.94; N, 3.98; S, 11.73.

Synthesis of P5

Following the same procedure for the preparation of **P1**, the polymerization precursors were changed into acceptor 4,9-bis(5-bromothiophen-2-yl)-6,7-bis(4-dodecylphenyl)-[1,2,5]thiadiazolo[3,4-g]quinoxaline (**7**, 0.1 mmol) and donor (3,3'-didodecyl-[2,2'-bithiophene]-5,5'-diyl)bis(trimethylstannane) (**22**, 0.1 mmol). But **P5** was collected from chloroform fraction during the Soxhlet extraction process, due to its good solubility.

P5 (black solid, 115 mg, 85%).

Molecular weight by GPC (30 °C): M_n = 16.1 kg mol^{-1}, PDI = 5.49.

Molecular weight by GPC (135 °C): M_n = 12.7 kg mol^{-1}, PDI = 4.05.

Elemental analysis: Calcd. For $C_{84}H_{114}N_4S_5$: C, 75.31; H, 8.58; N, 4.18; S, 11.93. Found: C, 74.08; H, 10.00; N, 4.02; S, 11.87.

Synthesis of P6

Following the same procedure for the preparation of **P5**, the polymerization precursors were changed into acceptor (**17**, 0.1 mmol) and 5,5'-bis(trimethylstannyl)-2,2'-bithiophene (**21**, 0.1 mmol).
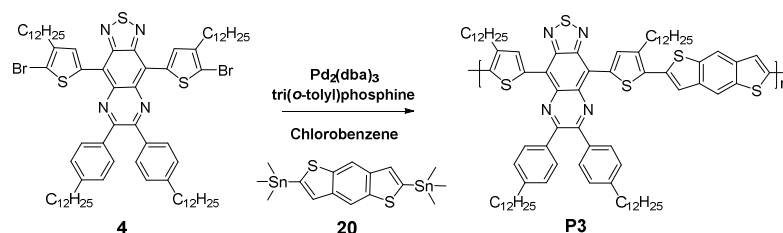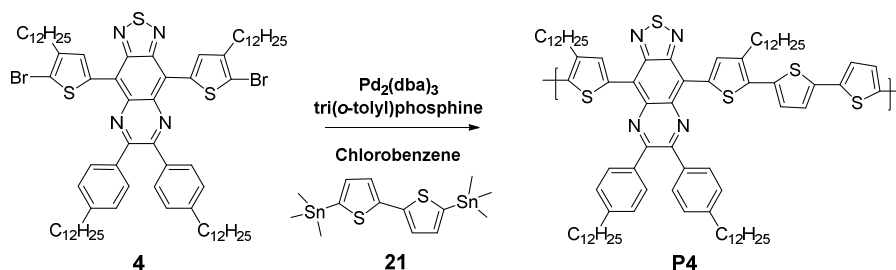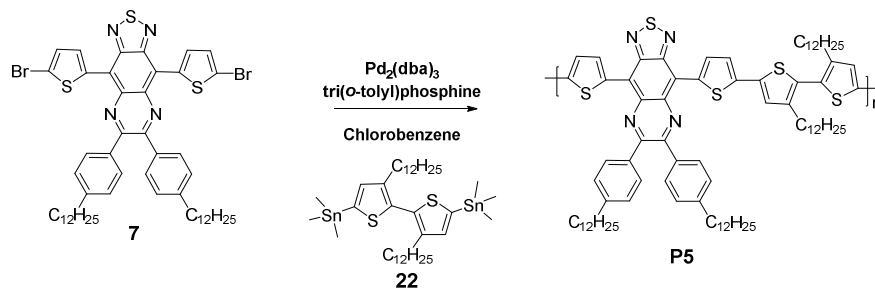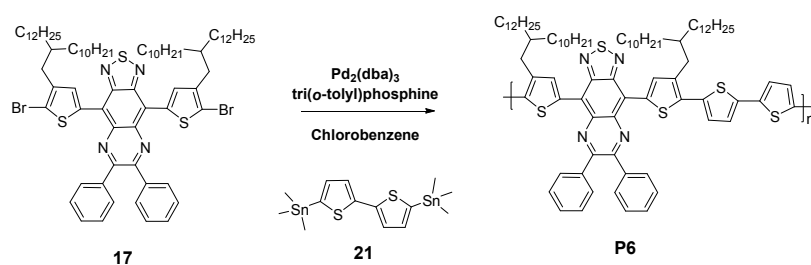

P6 (black solid, 96 mg, 71%).

Molecular weight by GPC (135 °C): M_n= 18.8 kg mol^{-1}, PDI = 3.48.

Elemental analysis: Calcd. For $C_{84}H_{114}N_4S_5$: C, 75.31; H, 8.58; N, 4.18; S, 11.93. Found: C, 74.67; H, 10.29; N, 4.11; S, 11.06.

3.10 References

(1) Li, H.; Tam, T. L.; Lam, Y. M.; Mhaisalkar, S. G.; Grimsdale, A. C. *Org. Lett.,* **2011**, *13*, 46-49.

(2) Dallos, T.; Hamburger, M.; Baumgarten, M. *Org. Lett.,* **2011**, *13*, 1936-1939.

(3) Ellinger, S.; Graham, K. R.; Shi, P.; Farley, R. T.; Steckler, T. T.; Brookins, R. N.; Taranekar, P.; Mei, J.; Padilha, L. A.; Ensley, T. R.; Hu, H.; Webster, S.; Hagan, D. J.; Van Stryland, E. W.; Schanze, K. S.; Reynolds, J. R. *Chem. Mater.,* **2011**, *23*, 3805-3817.

(4) Li, H.; Zhou, F.; Tam, T. L. D.; Lam, Y. M.; Mhaisalkar, S. G.; Su, H.; Grimsdale, A. C. *J. Mater. Chem. C,* **2013**, *1*, 1745-1752.

(5) Tam, T. L.; Li, H.; Lam, Y. M.; Mhaisalkar, S. G.; Grimsdale, A. C. *Org. Lett.,* **2011**, *13*, 4612-4615.

(6) Chen, M. X.; Perzon, E.; Robisson, N.; Jönsson, S. K. M.; Andersson, M. R.; Fahlman, M.; Berggren, M. *Synth. Met.,* **2004**, *146*, 233-236.

(7) Yu, C.-Y.; Chen, C.-P.; Chan, S.-H.; Hwang, G.-W.; Ting, C. *Chem. Mater.,* **2009**, *21*, 3262-3269.

(8) Zoombelt, A. P.; Fonrodona, M.; Wienk, M. M.; Sieval, A. B.; Hummelen, J. C.; Janssen, R. A. J. *Org. Lett.,* **2009**, *11*, 903-906.

(9) Lei, T.; Wang, J.-Y.; Pei, J. *Chem. Mater.,* **2013**, *26*, 594-603.

(10) Mei, J.; Bao, Z. *Chem. Mater.,* **2013**, *26*, 604–615.

(11) Yiu, A. T.; Beaujuge, P. M.; Lee, O. P.; Woo, C. H.; Toney, M. F.; Fréchet, J. M. J. *J. Am. Chem. Soc.,* **2011**, *134*, 2180-2185.

(12) Meager, I.; Ashraf, R. S.; Mollinger, S.; Schroeder, B. C.; Bronstein, H.; Beatrup, D.; Vezie, M. S.; Kirchartz, T.; Salleo, A.; Nelson, J.; McCulloch, I. *J. Am. Chem. Soc.,* **2013**, *135*, 11537-11540.

(13) Li, W.; Hendriks, K. H.; Furlan, A.; Roelofs, W. S. C.; Wienk, M. M.; Janssen, R. A. J. *J. Am. Chem. Soc.,* **2013**, *135*, 18942-18948.

(14) Guo, X.; Kim, F. S.; Seger, M. J.; Jenekhe, S. A.; Watson, M. D. *Chem. Mater.,* **2012**, *24*, 1434-1442.

(15) Kim, Y.; Hong, J.; Oh, J. H.; Yang, C. *Chem. Mater.,* **2013**, *25*, 3251-3259.

(16) Earmme, T.; Hwang, Y.-J.; Murari, N. M.; Subramaniyan, S.; Jenekhe, S. A. *J. Am. Chem. Soc.,* **2013**, *135*, 14960-14963.

(17) Yuen, J. D.; Kumar, R.; Zakhidov, D.; Seifter, J.; Lim, B.; Heeger, A. J.; Wudl, F. *Adv. Mater.,* **2011**, *23*, 3780-3785.

(18) Lei, T.; Cao, Y.; Zhou, X.; Peng, Y.; Bian, J.; Pei, J. *Chem. Mater.,* **2012**, *24*, 1762-1770.

(19) Zhuang, W.; Bolognesi, M.; Seri, M.; Henriksson, P.; Gedefaw, D.; Kroon, R.; Jarvid, M.; Lundin, A.; Wang, E.; Muccini, M.; Andersson, M. R. *Macromolecules,* **2013**, *46*, 8488-8499.

(20) Dallos, T.; Beckmann, D.; Brunklaus, G.; Baumgarten, M. *J. Am. Chem. Soc.,* **2011**, *133*, 13898-13901.

(21) Steckler, T. T.; Henriksson, P.; Mollinger, S.; Lundin, A.; Salleo, A.; Andersson, M. R. *J. Am. Chem. Soc.,* **2014**, *136*, 1190-1193.

(22) Foster, M. E.; Zhang, B. A.; Murtagh, D.; Liu, Y.; Sfeir, M. Y.; Wong, B. M.; Azoulay, J. D. *Macromol. Rapid Commun.,* **2014**, *35*, 1516-1521.

(23) Chen, M. X.; Crispin, X.; Perzon, E.; Andersson, M. R.; Pullerits, T.; Andersson, M.; Inganas, O.; Berggren, M. *Appl. Phys. Lett.,* **2005**, *87*, 252105.

(24) Steckler, T. T.; Fenwick, O.; Lockwood, T.; Andersson, M. R.; Cacialli, F. *Macromol. Rapid Commun.,* **2013**, *34*, 990-996.

(25) Steckler, T. T.; Lee, M. J.; Chen, Z.; Fenwick, O.; Andersson, M. R.; Cacialli, F.; Sirringhaus, H. *J. Mater. Chem. C,* **2014**, *2*, 5133-5141.

(26) Lee, Y.; Russell, T. P.; Jo, W. H. *Org. Electron.,* **2010**, *11*, 846-853.

(27) Yi, H.; Johnson, R. G.; Iraqi, A.; Mohamad, D.; Royce, R.; Lidzey, D. G. *Macromol. Rapid Commun.,* **2008**, *29*, 1804-1809.

(28) Cheng, K.-F.; Chueh, C.-C.; Lin, C.-H.; Chen, W.-C. *J. Polym. Sci., Part A: Polym. Chem.,* **2008**, *46*, 6305-6316.

(29) An, C.; Puniredd, S. R.; Guo, X.; Stelzig, T.; Zhao, Y.; Pisula, W.; Baumgarten, M. *Macromolecules,* **2014**, *47*, 979-986.

(30) Durban, M. M.; Kazarinoff, P. D.; Luscombe, C. K. *Macromolecules,* **2010**, *43*, 6348-6352.

(31) Guo, X.; Puniredd, S. R.; Baumgarten, M.; Pisula, W.; Müllen, K. *Adv. Mater.,* **2013**, *25*, 5467-5472.

(32) Becke, A. D. *J. Chem. Phys.,* **1993**, *98*, 5648-5652.

(33) Bredas, J.-L. *Mater. Horiz.,* **2014**, *1*, 17-19.

(34) Li, H.; Kim, F. S.; Ren, G.; Jenekhe, S. A. *J. Am. Chem. Soc.,* **2013**, *135*, 14920-14923.

(35) Zhou, W.; Zhang, Z.-G.; Ma, L.; Li, Y.; Zhan, X. *Sol. Energy Mater. Sol. Cells,* **2013**, *112*, 13-19.

(36) Wang, S.; Kiersnowski, A.; Pisula, W.; Müllen, K. *J. Am. Chem. Soc.,* **2012**, *134*, 4015-4018.

(37) Zhang, X.; Steckler, T. T.; Dasari, R. R.; Ohira, S.; Potscavage, W. J.; Tiwari, S. P.; Coppee, S.; Ellinger, S.; Barlow, S.; Bredas, J.-L.; Kippelen, B.; Reynolds, J. R.; Marder, S. R. *J. Mater. Chem.,* **2010**, *20*, 123-134.

(38) Liu, J.; Zhang, R.; Sauvé, G. v.; Kowalewski, T.; McCullough, R. D. *J. Am. Chem. Soc.,* **2008**, *130*, 13167-13176.

(39) Cerius[2] calculation (Accelrys, S. D., CA, USA).

(40) Balzar, D.; Audebrand, N.; Daymond, M. R.; Fitch, A.; Hewat, A.; Langford, J. I.; Le Bail, A.; Louer, D.; Masson, O.; McCowan, C. N.; Popa, N. C.; Stephens, P. W.; Toby, B. H. *J. Appl. Cryst.,* **2004**, *37*, 911-924.

(41) Dexter Tam, T. L.; Salim, T.; Li, H.; Zhou, F.; Mhaisalkar, S. G.; Su, H.; Lam, Y. M.; Grimsdale, A. C. *J. Mater. Chem.,* **2012**, *22*, 18528-18534.

(42) Kitamura, C.; Tanaka, S.; Yamashita, Y. *Chem. Mater.,* **1996**, *8*, 570-578.

(43) Pisula, W.; Kastler, M.; Wasserfallen, D.; Pakula, T.; Müllen, K. *J. Am. Chem. Soc.,* **2004**, *126*, 8074-8075.

(44) Burkhart, B.; Khlyabich, P. P.; Cakir Canak, T.; LaJoie, T. W.; Thompson, B. C. *Macromolecules,* **2011**, *44*, 1242-1246.

(45) Rieger, R.; Beckmann, D.; Pisula, W.; Kastler, M.; Müllen, K. *Macromolecules,* **2010**, *43*, 6264-6267.

(46) Rieger, R.; Beckmann, D.; Mavrinskiy, A.; Kastler, M.; Müllen, K. *Chem. Mater.,* **2010**, *22*, 5314-5318.

(47) Ha, J. S.; Kim, K. H.; Choi, D. H. *J. Am. Chem. Soc.,* **2011**, *133*, 10364-10367.

Chapter 4. The Condensed Thiadiazoloquinoxaline derivatives-Based Polymers as High Performance Ambipolar Semiconductors
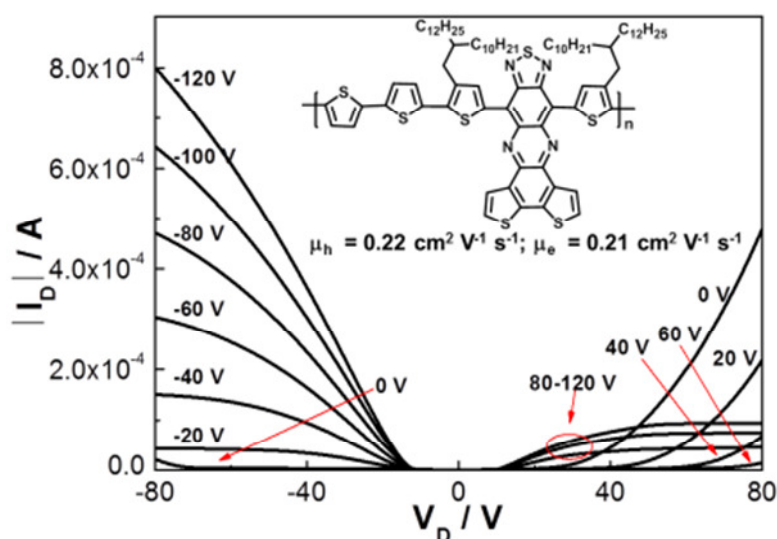
In this chapter, two novel conjugated polymers with high molecular weights, **PBDTTQ-3** and **PAPhTQ**, were synthesized based on previously investigated structure-properties relationship of **TQ-2T** polymers. Both polymers have excellent solubility in common organic solvents. UV-vis-NIR absorption and cyclic voltammetry indicate a bandgap of (0.76 eV) and high electron affinity level (-4.08 eV) for **PBDTTQ-3**. **PBDTTQ-3** exhibits good ambipolar transport, with a maximum hole mobility of 0.22 cm^2 V^{-1} s^{-1} and comparable electron mobility of 0.21 cm^2 V^{-1} s^{-1}.

Note: Large part of this chapter has been published in *Chem. Mater*, **2014**, *26*, 5923-5929.

4.1 Introduction

Ambipolar organic field-effect transistors (OFETs) that transport simultaneously holes and electrons have attracted attention in recent years, owing to their application in complementary metal-oxide semiconductors logic circuits and organic light-emitting transistors.[1-4] Strong acceptors were widely used to create high performance alternating donor (D) - acceptor (A) ambipolar semiconductors because of their electron-deficient nature. Due to the trapping of electrons at the semiconductor/dielectric interface and the scarcity of high-electron-affinity building blocks,[5] only few acceptors have been used to design ambipolar polymers with hole and electron mobilities both above 0.1 cm^2 V^{-1} s^{-1} such as benzobisthiadiazole (BBT),[6-8] naphthalene diimide (NDI),[9] diketopyrrolopyrrole (DPP), [10-12] isoindigo (IID)[13] and benzodifurandione-based oligo(p-phenylene vinylene) (BDOPV).[14]
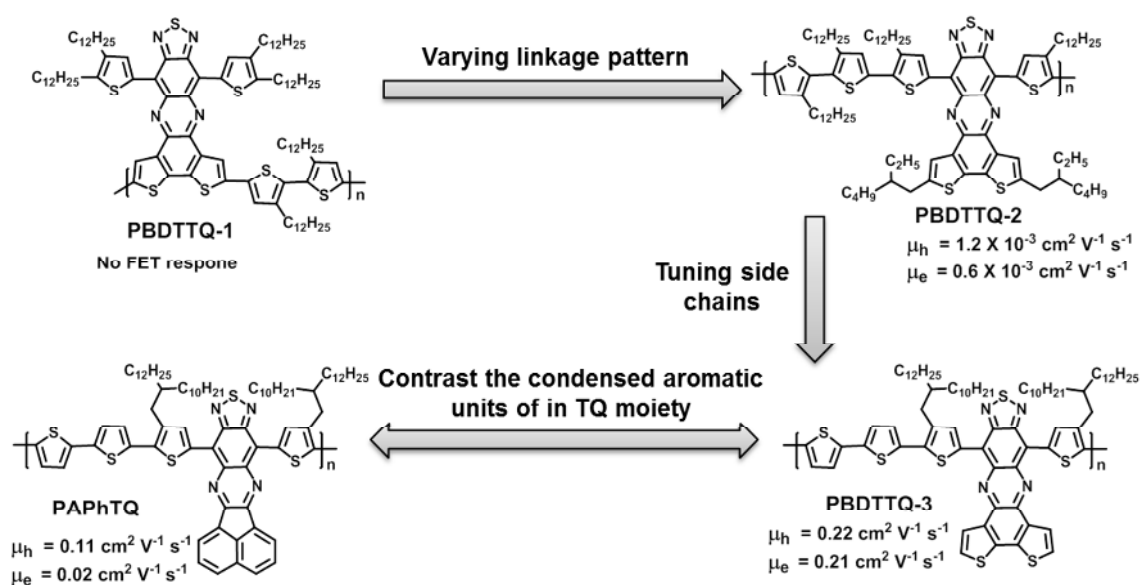
Figure 4.1 Rational design changes for improving the device perfor-mance of TQ-containing polymers.

Long branched alkyl chains with one methylene group past the branching point have been proven to play a key role not only in increasing the molecular weight and the solubility of the polymers but also in influencing the microstructural morphology and charge carrier transport.[7-9] To develop high performance of ambipolar **BDTTQ**-based polymer

semiconductors, we optimized previous **BDTTQ** core and modified a new benzodithiophene condensed TQ unit (**BDTTQ-3**) with excellent solubility in common organic solvents, by removing all the alkyl chains from the TQ unit and replacing linear alkyl chains using a pair of 2-decyl-tetradecyl alkyl chains in the neighboring thiophene units (Figure 4.1). Additionally, another new acenaphthylene condensed TQ core (**APhTQ**) was also developed for comparison with **BDTTQ-3** (Scheme 4.1).

In this chapter, we report the design and synthesis of two D-A polymers **PBDTTQ-3** and **PAPhTQ** (Figure 4.1) and their significantly enhanced device performance compared to **PBDTTQ-2**. For both polymers, 2-decyl-tetradecyl alkyl chains with branching positions one carbon away from the polymer main chain on thiophenes adjacent to the acceptors are crucial for tuning the attractive forces and improving the solubility of the macromolecules. More importantly, this approach minimizes steric interactions and promotes the polymer backbone coplanarity, which facilitates charge carrier transport. **PBDTTQ-3** shows significantly improved and balanced holes and electrons mobilities as high as 0.22 and 0.21 cm^2 V^{-1} s^{-1}, respectively. **PAPhTQ** exhibits also ambipolarity with slightly lower maximum mobilities of 0.11 cm^2 V^{-1} s^{-1} for holes and 0.02 cm^2 V^{-1} s^{-1} for electrons. Additionally, the influence of the fused aromatic system in the TQ moiety on the device performance was studied.

4.2 Synthesis and characterization

The synthesis of the both polymers is illustrated in Scheme 4.1. 4,7-Bis(4-(2-decyltetradecyl)thiophen-2-yl)-5,6-dinitrobenzo[c][1,2,5]thiadiazole (**1**) was prepared according to Chapter 3. The compound **1** was reduced using iron and acetic acid to give corresponding diamine **2**, which was directly used without purification and converted to the monomers **BDTTQ-3** and **APhTQ** via a condensation coupling with benzo[2,1-b:3,4-b']dithiophene-4,5-dione (**3**) and acenaphthylene-1,2-dione (**6**), respectively. Consequently, precursors **Br₂-BDTTQ-3** and **Br₂-APhTQ** were then obtained by dibromination of **BDTTQ-3** and **APhTQ**. Both polymers were prepared via Stille coupling between **Br₂-BDTTQ-3** or **Br₂-APhTQ** and distannylbithiophene **9**.
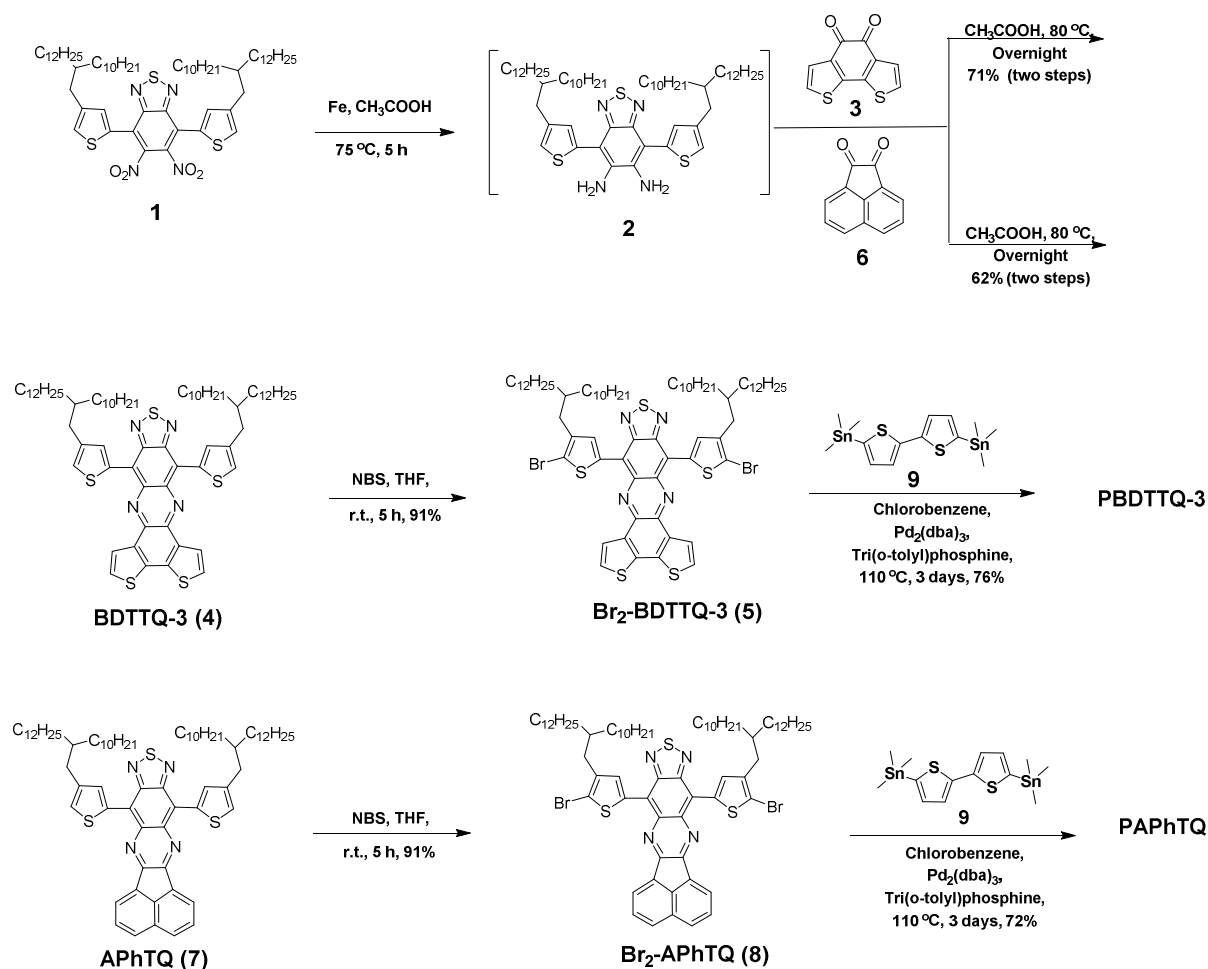
Scheme 4.1 Synthetic route to polymers **PBDTTQ-3** and **PAPhTQ**.

Polymers **PBDTTQ-3** and **PAPhTQ** possess good solubility in chloroform, tetrahydrofuran and chlorobenzene. The number-average molecular weights (M_n) of the polymers were 76.3 kg mol^{-1} and 100.9 kg mol^{-1}, with a polydispersity index (PDI) of 3.64 and 6.48 for **PBDTTQ-3** and **PAPhTQ**, respectively, determined by GPC method using polystyrene as standard and tetrahydrofuran as eluent at 30 °C (Table 4.1). The relatively large polydispersity index (PDI) of both polymers could originate from the aggregation in solution (see 4.3 section). The same issue was also reported for other polymers.[9,10] Additionally, both polymers demonstrated excellent thermal stability, with 5% weight loss upon heating at 415 °C (Figure 4.2). In the next region from 415 to 500 °C, the polymer side chains were firstly decomposed as previously discussed (Chapter 2 and 3).
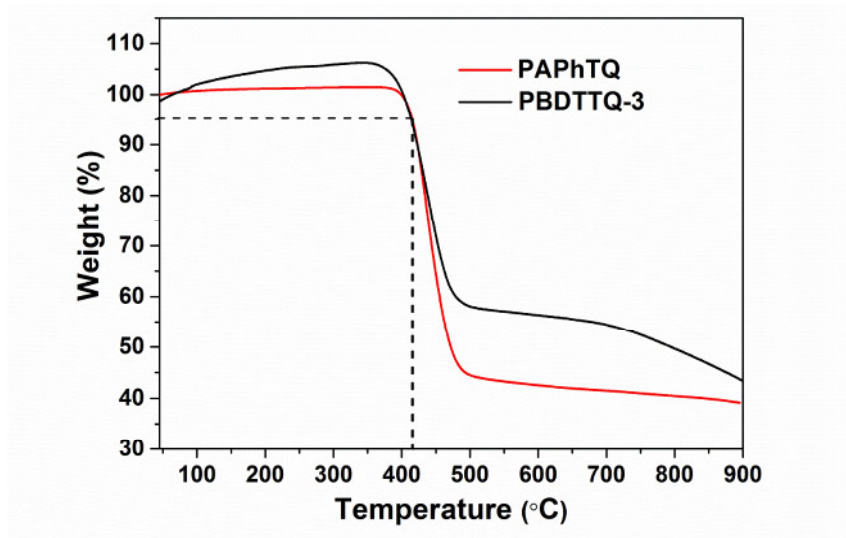
Figure 4.2 TGA curves for **PBDTTQ-3** and **PAPhTQ** measured under a nitrogen atmosphere at a heating rate of 10 ºC/min.
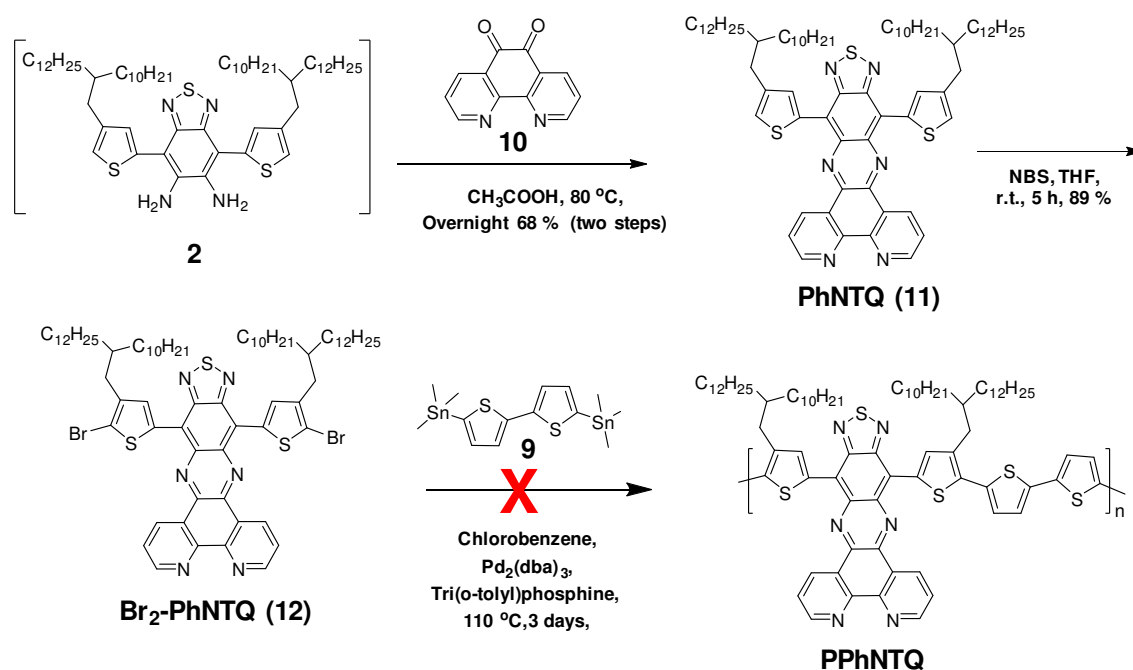
Scheme 4.2 Synthetic route to polymer **PPhNTQ**.

PhNTQ core is stronger acceptor than **BDTTQ** core as confirmed by cyclic voltammetry.[15] In order to pursue higher electron affinity condensed TQ acceptor containing polymer, the **PhNTQ** was prepared according to the similar synthetic apporach of **BDTTQ-3** and **APhTQ** as shown in Scheme 4.2. The bromination was performed for **PhNTQ** to make higher electron affinity polymer **PPhNTQ**, which was expected as n-type semiconductor.

Unfortunately, the **PPhNTQ** wasn't obtained through Stille coupling after 3 days at 110 °C. In order to clearity the reason of failure in this coupling, one unknown compound was recycled after polymerization. The FD-MS and ^{1}H-NMR were carried out to analyze the structure of unknown compound. FD-MS displayed that this compound had the same signal with **Br₂-PhNTQ**. ^{1}H-NMR spectra of both compounds are presented in Figure 4.3. In comparison to **Br₂-PhNTQ**, the aromatic proton chemical shift of unknown compound went down field, implying that the phenanthroline part of **Br₂-PhNTQ** could be coordinated with palladium from the catalyst (Pd₂(dba)₃), leading to the catalyst deactivation in this system. However, the palladium will be removed from **Br₂-PhNTQ** in a high-potential electric field. That is why both compounds exhibit the same peak values by FD-MS measurements.
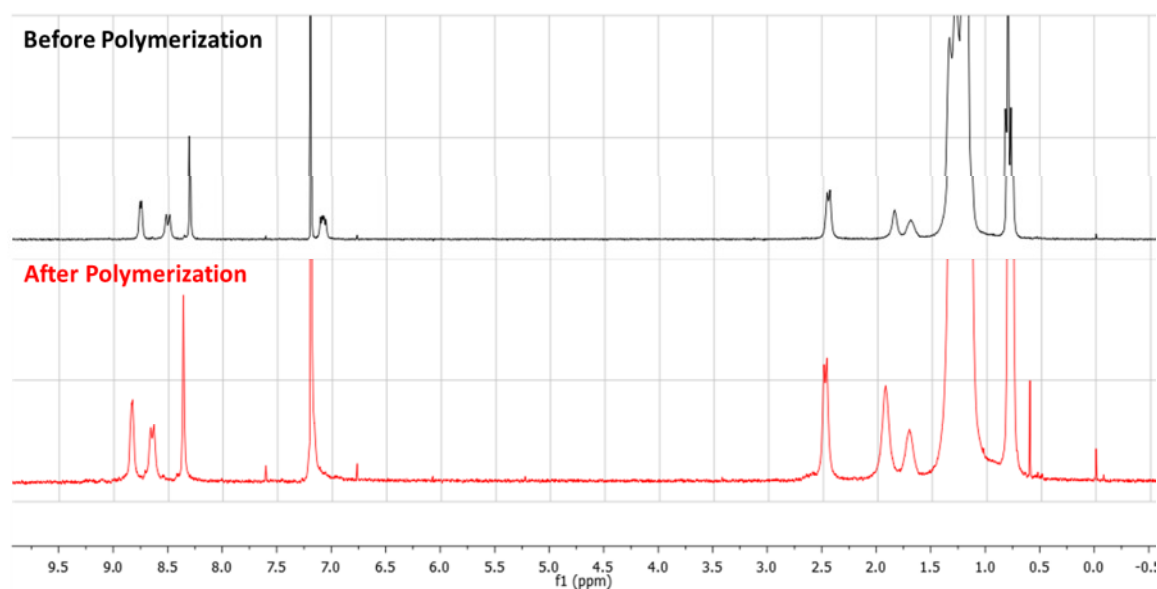
Figure 4.3 The ^{1}H-NMR spectra before (black) and after (red) polymerization of **Br₂-PhNTQ**.

4.3 Optical properties

To figure out aggregation behaviour of both polymers in dilute chloroform solutions (10^{-5} M), UV-vis-NIR absorption spectra of both polymers were recorded in chloroform solution at the two different temperatures (room temperature and 45 °C). The absorption profiles are shown in Figure 4.4. Both polymers showed absorption maximum (λ_{max}) at 1206 nm and 1005 nm at room temperature for **PBDTTQ-3** and **PAPhTQ**, respectively. When the

temperature was raised to 45 °C, the λ_{max} of both polymers shifted to 1163 nm for **PBDTTQ-3** and 982 nm for **PAPhTQ**. This suggests both polymers have aggregation even in dilute solution. This result is in good agreement with their large PDI.
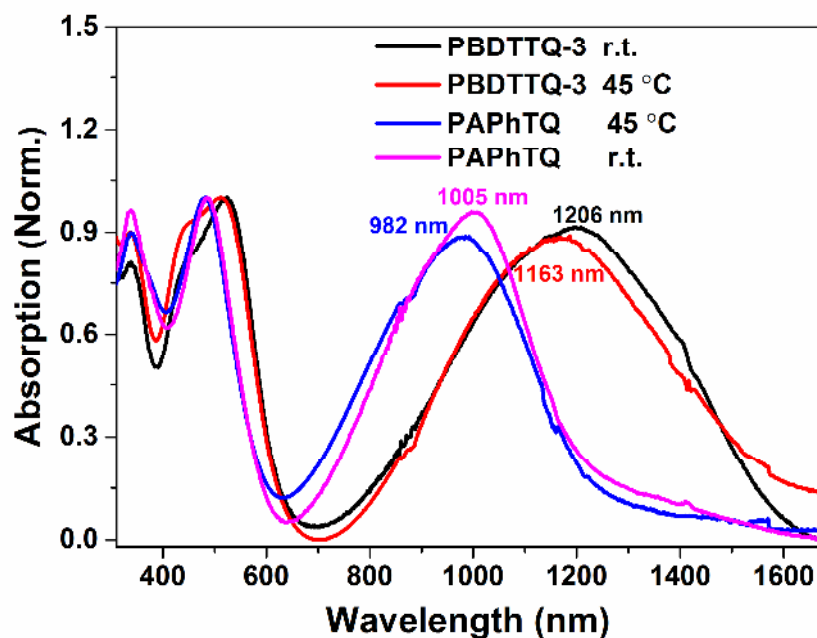
Figure 4.4 UV-visible-NIR absorption spectra of the polymers in chloroform solutions.

UV-vis-NIR absorption spectra of the polymers in solutions and in films are shown in Figure 4.5. The relevant data are summarized in Table 4.1. **PBDTTQ-3** exhibits an absorption maximum (λ_{max}) at 1206 nm in solution corresponding to a large red-shift of 278 nm as compared to that of **PBDTTQ-2**. This was related to different alkyl chain substitution positions and architectures which affect intramolecular interactions in the polymer backbone, thereby changing their optical behavior. Compared to **PBDTTQ-3**, the λ_{max} of **PAPhTQ** reveals a blue shift of 201 nm indicating that the condensed acenaphthylene, **APhTQ**, has a larger HOMO-LUMO gap than the benzo[2,1-b:3,4-b']dithiophene condensed TQ in **BDTTQ-3**. This leads to the larger bandgap of **PAPhTQ** compared to **PBDTTQ-3**.

Thin films were prepared by drop-casting onto glass slides from chloroform solutions. Both polymers displayed red-shifts of 64 and 67 nm at λ_{max} compared with those in solutions suggesting aggregation in solid state. The optical bandgaps are 0.76 and 0.99 eV, calculated according to the absorption onset of the solid films for **PBDTTQ-3** and **PAPhTQ**, respectively. These results demonstrate that changing the aromatic rings condensed TQ core

are effective tools in tuning the bandgaps of the polymers. On the other hand, **PBDTTQ-3** (0.97) has is higher OD_2/OD_1 value (see in Chapter 2) than previous **PBDTTQ-2** (0.78), suggesting that **PBDTTQ-3** has stronger charge carrier transfer ability than previous **PBDTTQ-2**. As discussed in Chapter 3, this value of **PBDTTQ-3** could have excellent charge carrier mobility in OFETs.
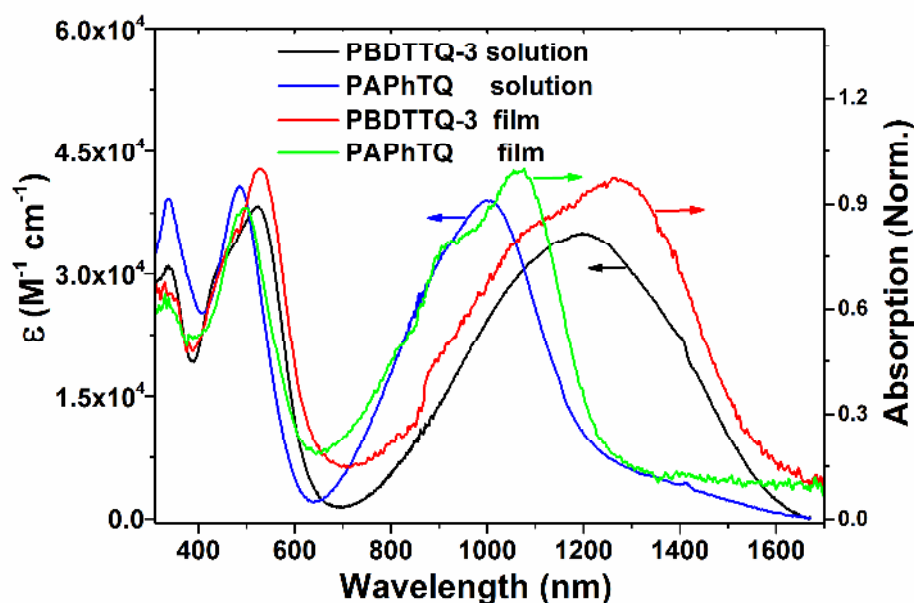
Figure 4.5 UV-visible-NIR absorption spectra of the polymers in chloroform solutions and in films

4.4 Electrochemical properties

The electrochemical behaviour of both monomers was determined from cyclic voltammetry (CV) as shown in Figure 4.6. The corresponding data are collected in Table 4.1. To avoid the electron withdrawing effects of bromine, CV of the acceptors **BDTTQ-3** and **APhTQ** were carried out. The electron affinity (EA) of **BDTTQ-3** estimated from the reduction onset potential is -3.92 eV, which is lower lying than that of **APhTQ** (-3.73 eV). This proved that **BDTTQ-3** is a stronger electron acceptor than **APhTQ**.
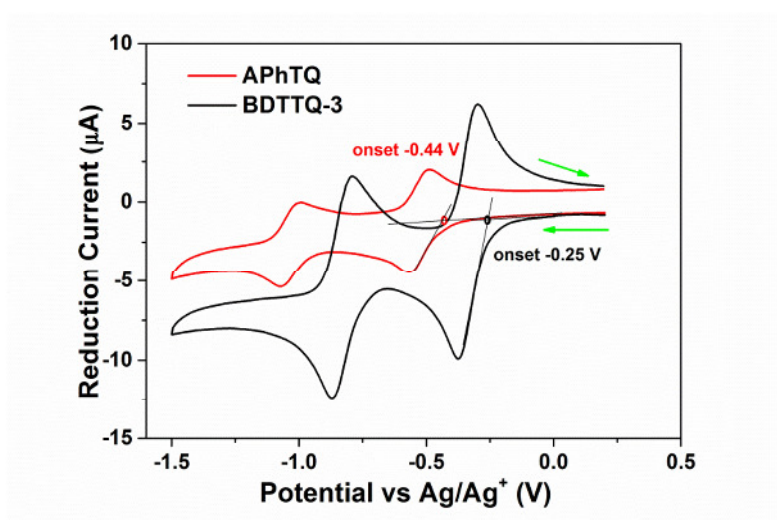
Figure 4.6 Reduction curves of **BDTTQ-3** and **APhTQ** in dichloromethane solutions.
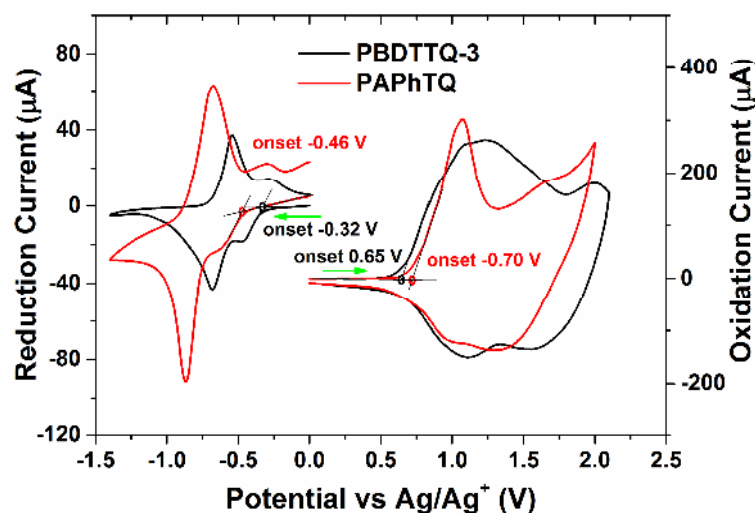
Figure 4.7 Reduction (left) and oxidation (right) of two polymers films deposited from chloroform solutions.

Polymers thin film CV provided the EA values of -4.08 and -3.94 eV for **PBDTTQ-3** and **PAPhTQ**, respectively, whereas the ionization potential (IP) values of -5.05 eV for **PBDTTQ-3** and -5.10 eV for **PAPhTQ** (Figure 4.7). These results proved that the benzodithiophene condensed TQ derivative is a stronger electron acceptor than acenaphthylene on the TQ segment, resulting in the lower EA of **PBDTTQ-3** compared to **PAPhTQ**. The EA of **PBDTTQ-3** was found around 0.14 eV lower than that of **PAPhTQ**, while the IP of the two polymers were nearly equivalent due to a dominant contribution of the tetrathiophene units to the IP for each polymer. Both polymers exhibit two reversible

reductions and low EA, indicating their potential for electron charge carrier transport. The electrochemical band gaps of the polymers are larger than the optical band gaps, which is attributed to the exciton binding energy of conjugated polymers.

Table 4.1 Molecular weights, optical absorption, electrochemical properties and field-effect mobilities of **PBDTTQ-3** and **PAPhTQ**.

Polymer	M_n/M_w (kg/mol) [a]	λ_{abs} (nm) soln. [b]	λ_{abs} (nm) film [b]	E_g^{opt} (eV) [b]	IP (eV) [d]	EA (eV) [d]	$\mu_{h\ max,\ ave}$ (cm^2 V^{-1} s^{-1})	$\mu_{e,\ max,\ ave}$ (cm^2 V^{-1} s^{-1})
PBDTTQ-3	76.3/277.3	1206	1270	0.76	-5.05	-4.08	0.22, 0.19($\pm$ 0.03)	0.21, 0.10($\pm$ 0.07)
PAPhTQ	100.9/654.5	1005	1072	0.99	-5.10	-3.94	0.11, 0.10($\pm$ 0.02)	0.02, 0.02($\pm$ 0.01)

[a]Determined by GPC in THF using polystyrene standards; [b]Dissolved in choloform (c = 10^{-5} M); [c]Drop-cast from choloform solution (2 mg/mL); [d]IP and EA were estimated from the onsets of the first oxidation and reduction peak, while the potentials were determined using ferrocene (Fc) as standard by empirical formulas $E_{IP/EA} = - (E_{Ox/Red}^{onset} - E_{Fc/Fc+}^{1/2} + 4.8)$ eV wherein $E_{Fc/Fc+}^{1/2} = 0.40$ eV.

4.5 Density functional theory calculations
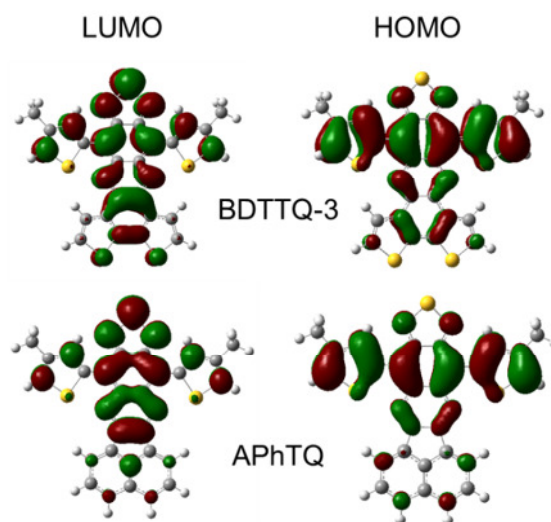
Figure 4.8 LUMO and HOMO of **BDTTQ-3** (-3.70, -5.07 eV) and **APhTQ** (-3.38, -5.05 eV). DFT (B3LYP, 6-31G).

To further understand the electronic structures and optical properties of the polymers, density functional theory (DFT) calculations were carried out. In agreement with the CV

results similar HOMO levels were found for the two monomers **APhTQ** and **BDTTQ-3**, but striking differences in the LUMO values (Figure 4.8) with lower LUMO for **BDTTQ-3**.
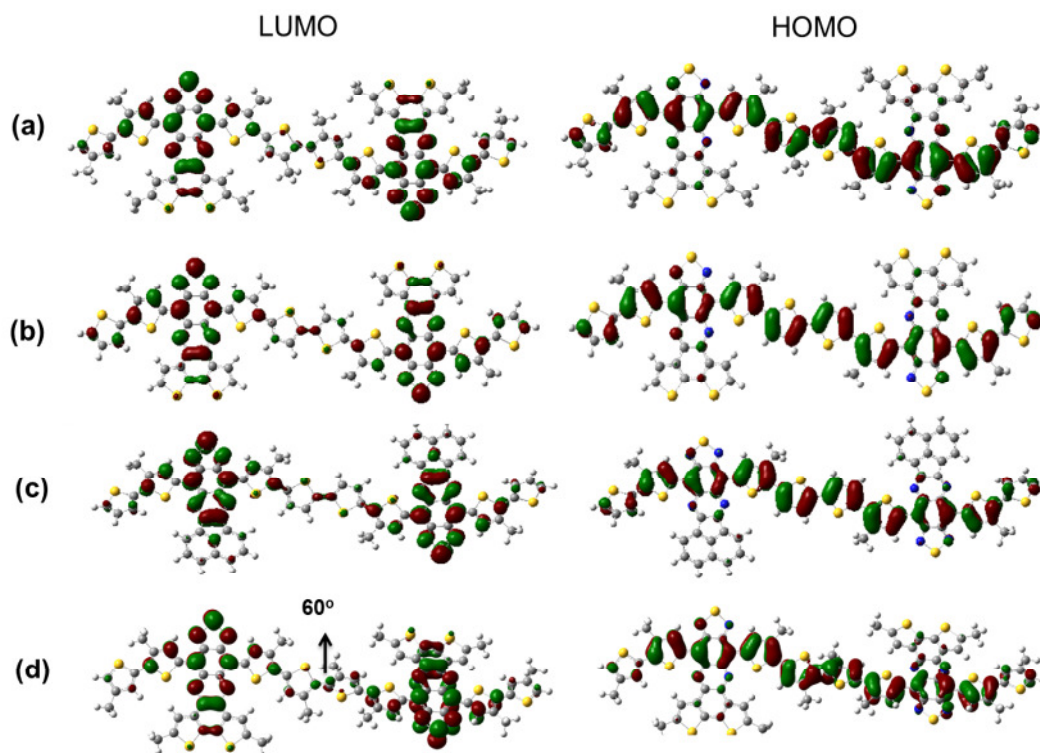
Figure 4.9 LUMO (left) and HOMO (right) distributions for the dimers of (a) **BDTTQ-2**, (b) **BDTTQ-3**, (c) **APhTQ** and (d) **BDTTQ-2** with strong twist. DFT (B3LYP, 6-31G∗).

The electronic density distributions of the LUMO and HOMO of the dimers of **BDTTQ-2**, **BDTTQ-3** and **APhTQ** were derived from DFT analysis as shown in Figure 4.9. The dihedral angle for the 3, 3'-dimethyl-2, 2'-bithiophene in the dimer of **BDTTQ-2** is slightly larger, while it is computed to be only ~7° for 2,2'-bithiophene in **BDTTQ-3**. The more effective extension of the π-conjugation in the latter case is due to the reduced number of alkyl chain interactions and therefore affording the smaller band gap as also confirmed by UV-vis-NIR. The HOMO and LUMO levels of three polymers, on the other hand, show very similar degrees of delocalization. In order to make clear whether the electron density was affected by a large dihedral angle between the central two alkylated bithiophene or not, we calculated the the dimer **BDTTQ-2** with the 60 degree of 3, 3'-dimethyl-2, 2'-bithiophene as shown in Figure 4.9d. The result demonstrate electron density of dimer **BDTTQ-2** with a

large dihedral angle between 3, 3'-dimethyl-2, 2'-bithiophene are still nearly equivalent to **BDTTQ-3**, but difference were found in the HOMO and LUMO values. It should be mentioned that the twisting angle of these polymers will be smaller in the solid state than determined by DFT calculations.

4.6 OFET properties

Bottom contact, bottom gate transistors were fabricated to investigate the charge carrier transport for both polymers. This was in collaboration with ▬▬▬▬▬▬ (Max Planck Institute for Polymer Research, Mainz). The transfer and output characteristics of both polymers are presented in Figure 4.10. The ambipolar behavior of **PBDTTQ-3** was clearly evident from the transfer curves in both p- and n-type operation modes for negative and positive gate voltages, with average mobilities of 0.19 ± 0.03 cm^2 V^{-1} s^{-1} for holes and 0.10 ± 0.07 cm^2 V^{-1} s^{-1} for electrons (Table 4.1). In the negative drain mode for $V_D < 0$ V (Figure 4.10a) the crossover point was located at around $V_G = -20$ V, indicating a change from electron- to hole-dominated current. Below this gate voltage the transistor exhibited a typical hole transport behavior in the accumulation mode. In the positive regime at $V_D > 0$ V (Figure 4.10a) the electrons dominate the device operation up from approximately $V_G = 70$ V. The high crossover voltage can be attributed to two parallel existing effects: charge trapping at semiconductor/dielectric interface and contact resistance. The proposed mechanism for the trapping of electrons in the conductive channel is the formation of immobile Si–O$^-$ ions at the dielectric surface. Self-assembled monolayers (SAMs) lead to a reduced number of hydroxy groups and thus to an increase of the electron current.[5] The hexamethyldisilazane (HMDS) surface modification can reduce the trapping effect but not hinder it completely. Moreover, the contact resistance is evident on the output characteristic (Figure 4.10b) from the nonlinear behavior of the current at low V_D. In spite of this negative effect, the an ambipolar device behavior was observed due to the low band gap and LUMO level, reaching highest values of 0.22 cm^2 V^{-1} s^{-1} and 0.21 cm^2 V^{-1} s^{-1} for holes and electrons, respectively. A well-balanced transport of holes and electrons for **PBDTTQ-3** was observed, whereas significant differences in threshold voltage were attributed to the deep traps existing in the semiconducting layer.[11] Polymer **PAPhTQ** revealed also ambipolarity but with slightly lower average mobilities for holes of 0.10 ± 0.02 cm^2 V^{-1} s^{-1} and with significant difference for electrons of 0.02 ± 0.01

cm^2 V^{-1} s^{-1} (Figure 4.10c and 4.10d).
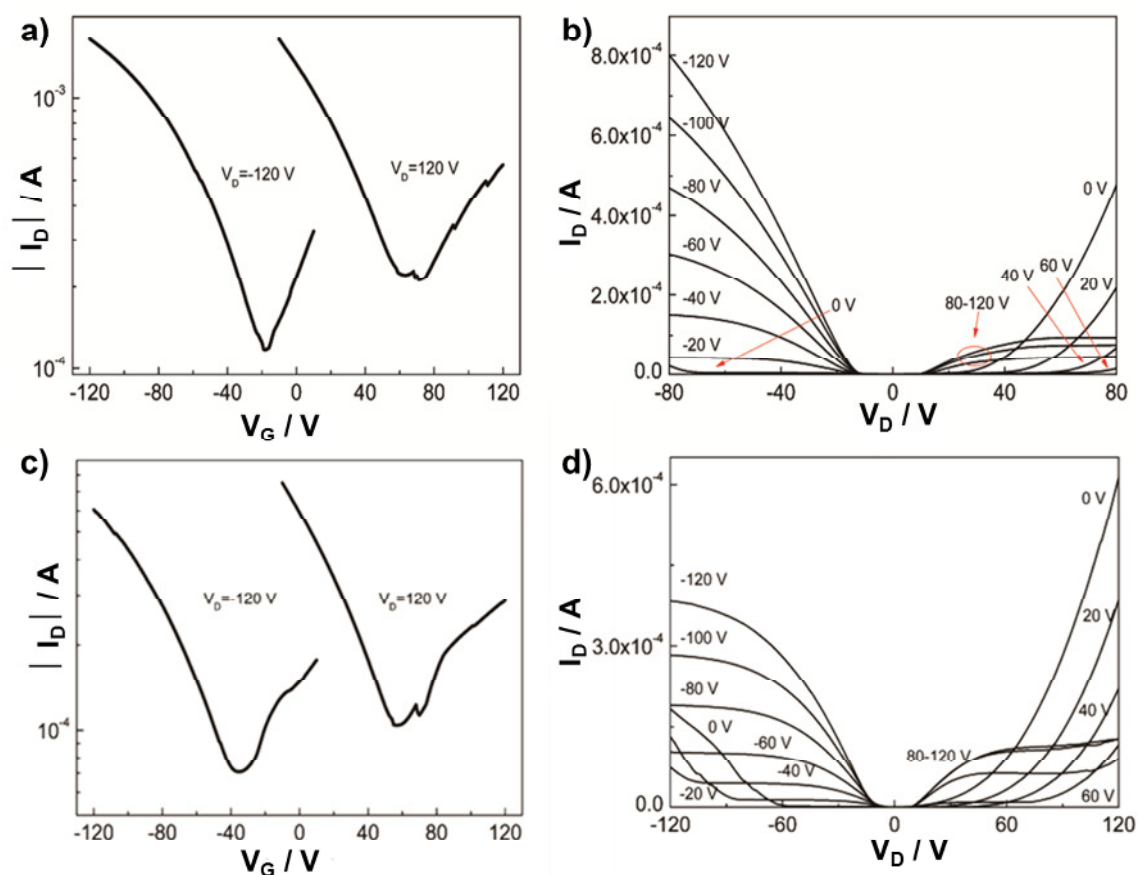
Figure 4.10 The transfer and output curves of (a and b) **PBDTTQ-3** and (c and d) **PAPhTQ**.

The air stability of both polymers was also investigated. The devices were moved from glove box to air ambience and exposed 1 hour. The mobilities were measured under air. Only a hole transport was observed with highest mobilities of 0.11 and 0.09 cm^2 V^{-1} s^{-1} for **PBDTTQ-3** and **PAPhTQ**, respectively (Figure 4.11). The air unstable behaviors of both polymers were related to their high lying EA , which are not in air stable region below around -4.3 eV of materials.[12]
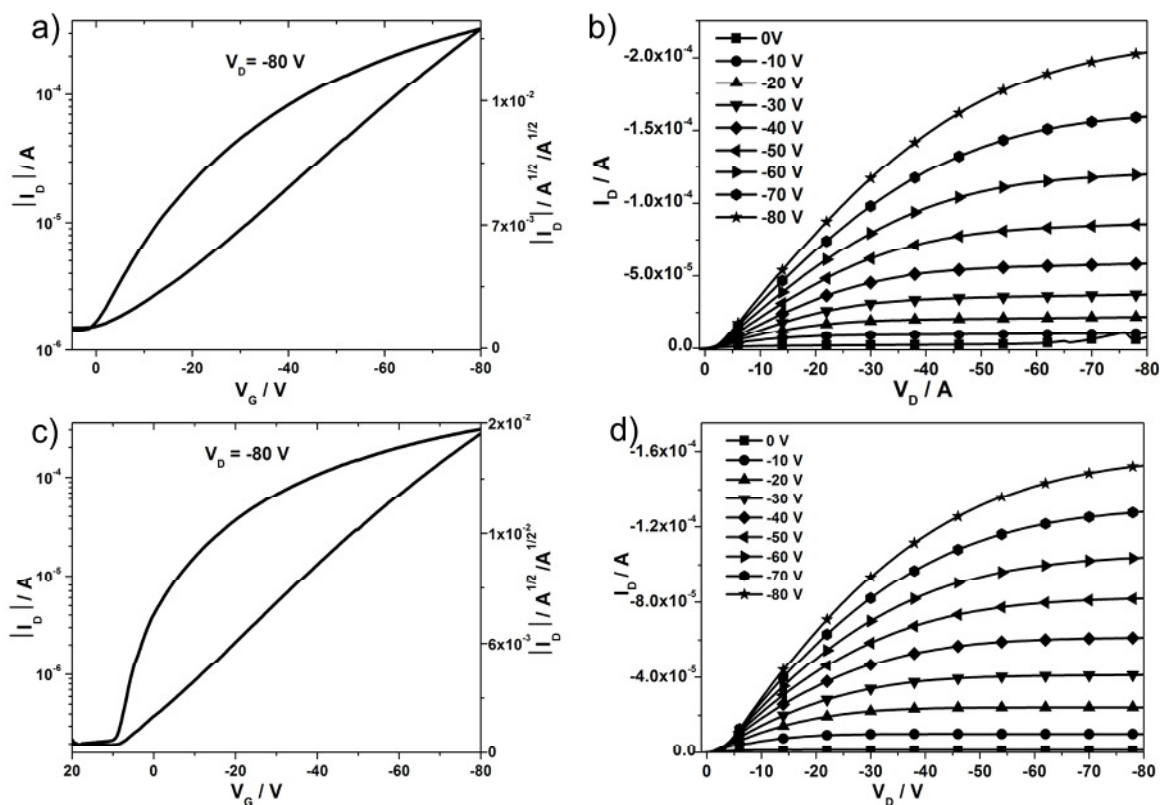
Figure 4.11 Transfer and output curves of (a, b) **PBDTTQ-3** and (c, d) **PAPhTQ** under air.

4.7 Self-organization

To gain an insight into the organization of both polymers in the bulk, 2DWAXS (Figure 4.12a and 4.12b) was carried out in collaboration with ████████████████ (Max Planck Institute for Polymer Research, Mainz). The 2DWAXS measurements were performed on extruded fibres which were subsequently thermally annealed at 180 °C. The 2D patterns are quite identical for both compounds where reflections at small-angles on the equatorial plane of the pattern are ascribed to polymer chains oriented along the alignment direction of the fiber. The chain-to-chain distance between lamellas of 2.73 nm for **PBDTTQ-3** and 2.5 nm for **PAPhTQ** were determined from the main peak positions. Meridional reflections corresponding to a d-spacing of 1.80 nm are equal for both systems and are attributed to the length of a single repeat unit. More crucially, wide-angle, equatorial scattering intensities are assigned to a relatively small π-stacking distance of 0.36 nm for both polymers which might be one factor responsible for the good charge carrier transport. However, this reflection is

significantly weaker for **PAPhTQ** than for **PBDTTQ-3** (Figure 4.12a and 4.12b), which indicates slightly less ordering. This might be one of the reasons for the lower mobility of **PAPhTQ**.
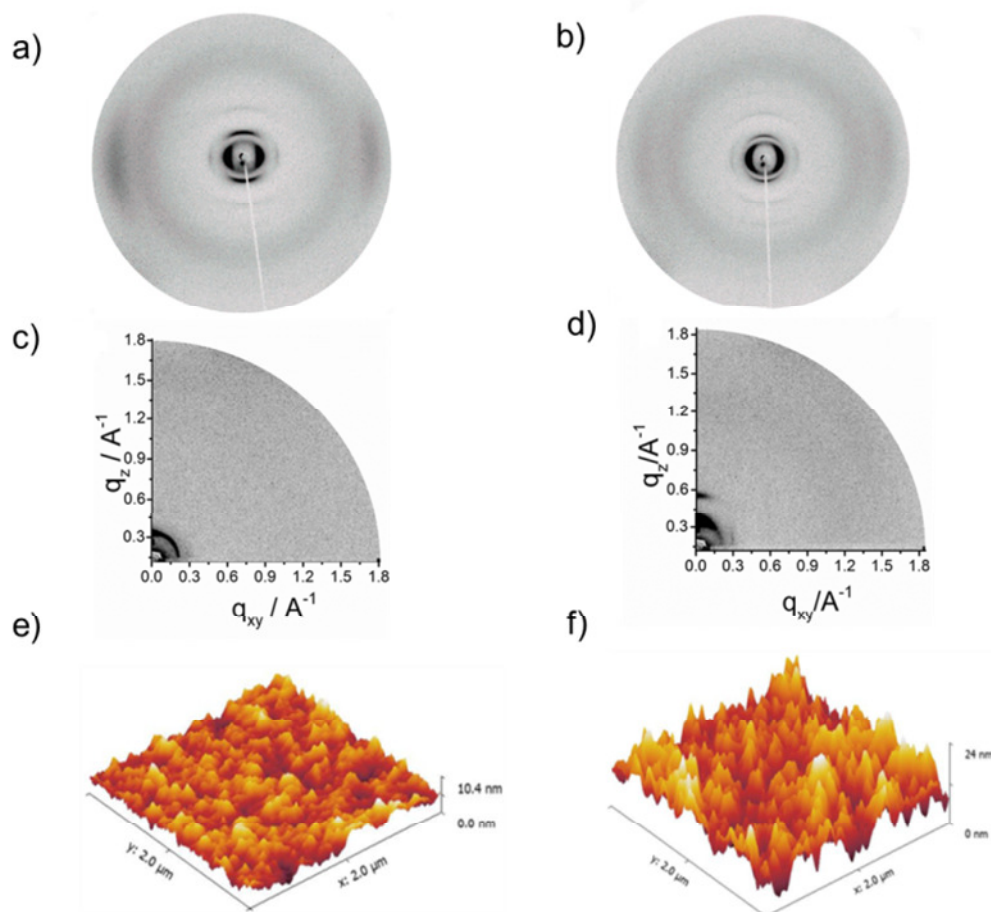
Figure 4.12 2DWAXS patterns for extruded fibers of a) **PBDTTQ-3** and b) **PAPhTQ**. The fiber sample was mounted vertically towards the detector. GIWAXS patterns for c) **PBDTTQ-3** and d) **PAPhTQ** thin films. SFM topography images of **PBDTTQ-3** (e) and **PAPhTQ** (f) thin film in the transistor channel. The RMS roughness values are 1.3 nm for **PBDTTQ-3** film and 3.3 nm for **PAPhTQ** film, respectively.

To understand the surface organization in thin film, GIWAXS was additionally performed in collaboration with ████████████████ (Max Planck Institute for Polymer Research, Mainz) (Figure 4.12c and 4.12d). For these measurements the same procedure for the film preparation was used as for the transistor devices. The GIWAXS pattern for **PBDTTQ-3** revealed only one isotropic reflection which correlates well with the chain-to-chain spacing of 2.73 nm of randomly arranged lamellas towards the surface. The thin film of

PAPhTQ displayed a slightly higher order and enhanced orientation of the polymer chains. The meridional scattering intensity at $q_{xy} = 0$ Å^{-1} and $q_z = 0.27$ Å^{-1} was attributed to the chain-to-chain spacing of 2.33 nm of edge-on arranged polymer backbones. The reflection at q_{xy} =0.31 Å^{-1} and $q_z = 0$ Å^{-1} corresponded to the length of a single repeat unit. In both cases, the HMDS modified silicon dioxide surface slightly decreased the chain-to-chain distance, however, the lack of a π-stacking reflection was an evidence for poor packing of the polymers on the surface in comparison to the bulk. This indicated that strong π-π stacking might not be always necessary for reaching high charge carrier mobilities. Some high performing semiconducting polymers also were reported with less ordered or disordered morphology.[13] In order to investigate the film structure in the nanometer scale, the scanning force microscopy (SFM) measurements were performed in collaboration with ▮▮▮▮ (Max Planck Institute for Polymer Research, Mainz). The transistors were directly used for active layer morphology investigation (Figure 4.12e and 4.12f). The root-mean-square (RMS) surface roughness of the **PAPhTQ** film was determined to be 3.3 nm being significantly higher than that one of a **PBDTTQ-3** film (RMS = 1.3 nm). This difference indicates that **PBDTTQ-3** shows better order at the air interface. As reported in the literature,[14] a high surface roughness indicates that large domains form an only non-uniform transport layer is limiting the conduction. On the other hand, smoother polymer films provide a higher uniformity due to smaller grain microstructures and finally higher charge carrier mobilities. This may be one reason why **PBDTTQ-3** has a higher mobility than **PAPhTQ**.

4.8 Summary

In this chapter, we have presented two new D-A copolymers based on extended TQ derivatives with a high molecular weight and good solubility in common solvents. Changing the electron-donor of the fused aromatic system from acenaphthylene to benzodithiophene in the TQ moiety played a significant role on the optoelectronic properties and the device performance. **PBDTTQ-3** exhibited a very low bandgap of 0.76 eV with high EA of -4.08 eV.

Although both polymers had quite disordered thin films as evident from GIWAXS measurement, their device performances are far higher than other TQ-based polymers. **PBDTTQ-3** exhibited balanced ambipolar charge carrier transport with transistor mobilities up to 0.22 cm^2 V^{-1} s^{-1} for holes and 0.21 cm^2 V^{-1} s^{-1} for electrons. **PAPhTQ** revealed also

ambipolarity with slightly lower average mobilities for holes of 0.10 ± 0.02 cm^2 V^{-1} s^{-1} and with significant difference for electrons of 0.02 ± 0.01 cm^2 V^{-1} s^{-1}. However, the mobilities of both polymer were significantly decreased when the transistors was moved to air 1 hour.

4.9 Synthetic details

The intermediate compounds benzo[2,1-b:3,4-b']dithiophene-4,5-dione (**3**) was prepared as description in Chapter 2. 4,7-bis(4-(2-decyltetradecyl)thiophen-2-yl)-5,6-dinitrobenzo[c][1,2,5]thiadiazole (**1**) and 5,5'-bis(trimethylstannyl)-2,2'-bithiophene (**9**) were synthesized following Chapter 3.

8,12-Bis(4-(2-decyltetradecyl)thiophen-2-yl)-[1,2,5]thiadiazolo[3,4-i]dithieno[3,2-a:2',3'-c]phenazine (**BDTTQ-3**) (**4**)
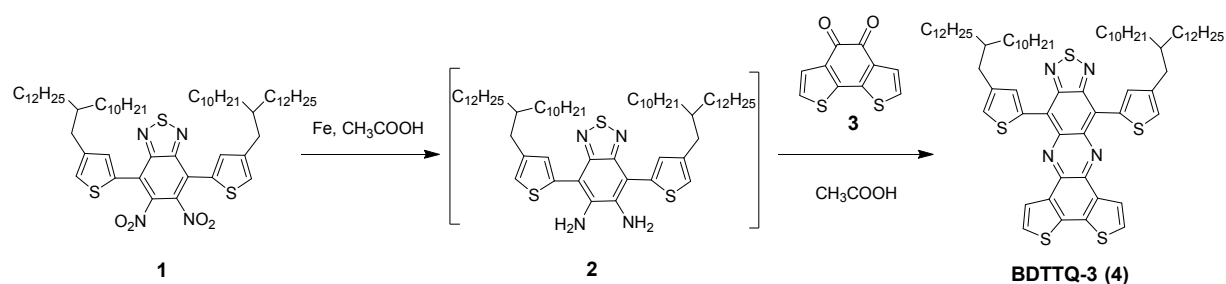
A mixture of compound **1** (0.5 g, 0.47 mmol) and fine iron powder (311 mg, 5.55 mmol) in acetic acid (15 mL) was stirred for 5 h at 75 °C under argon. The reaction mixture was cooled to room temperature, precipitated in 5% aqueous NaOH and extracted with diethyl ether (3×20 mL). The combined organic layers were washed with brine, dried with MgSO$_4$. After removal the solvent, this crude product diamine **2** was added into acetic acid (15 mL) solution of benzo[2,1-b:3,4-b']dithiophene-4,5-dione (**3**, 103 mg, 0.47 mmol). The mixture was heated to 80 °C overnight under argon. After cooling to room temperature, the mixture was poured into 100 mL 5% aqueous NaOH and extracted with dichloromethane (3×50 mL). The combined organic phases were dried with MgSO$_4$ and filtered. The filtrate was concentrated and purified by column chromatography eluting with hexane dichloromethane (3:1) to give 0.4 g (green solid, two steps 71%) of **BDTTQ-3**. ^{1}H NMR (250 MHz, CD$_2$Cl$_2$,

ppm) δ 8.86 (d, *J* = 1.25 Hz, 2H), 8.22 (d, *J* = 5.0 Hz, 2H), 7.40 (d, *J* = 5.0 Hz, 2H), 7.13 (d, *J* = 2.5 Hz, 2H), 2.65 (d, *J* = 7.50 Hz, 4H),1.82-1.75 (m, 2H), 1.41-1.23 (m, 80H), 0.88-0.82 (t, *J* = 7.50 Hz, 12H). ^{13}C NMR (62.5 MHz, CDCl₃, ppm) δ 151.00, 141.44, 139.73, 137.38, 136.09, 135.58, 135.15, 134.76, 128.13, 127.15, 124.56, 120.42, 39.21, 35.18, 33.60, 32.09, 30.38, 29.96, 29.92, 29.90, 29.87, 29.84, 29.56, 29.53, 26.94, 22.85, 14.28. HRMS (ESI+): m/z calc. 1187.7099, found 1187.7086.

8,12-Bis(5-bromo-4-(2-decyltetradecyl)thiophen-2-yl)-[1,2,5]thiadiazolo[3,4-i]dithieno[3,2-a:2',3'-c]phenazine (Br₂-BDTTQ-3) (5)

BDTTQ-3 (4)   Br₂-BDTTQ-3 (5)
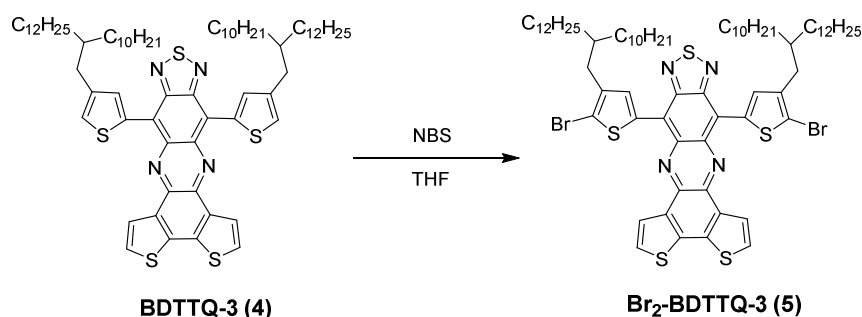
BDTTQ-3 (**4**, 150 mg, 0.126 mmol) was dissolved in THF (15 mL) at room temperature. NBS (51.7 mg, 0.29 mmol) was carefully added into the solution in small batches. The mixture was stirred for 5 h. After removal the solvent under reduced pressure, the residue was purified by column chromatography using hexane dichloromethane (3:1) as eluent to give **Br₂-BDTTQ-3** as a green solid (154 mg, 91%). ^{1}H NMR (250 MHz, CDCl₃, ppm) δ 8.56 (s, 2H), 7.62 (d, *J* = 5.0 Hz, 2H), 7.10 (d, *J* = 5.0 Hz, 2H), 2.50 (d, *J* = 7.50 Hz, 4H),1.82-1.74 (m, 2H), 1.25-1.23 (br, 80H), 0.88-0.83 (t, *J* = 7.50 Hz, 12H). ^{13}C NMR (62.5 MHz, CDCl₃, ppm) δ 149.98, 140.17, 138.66, 137.20, 135.56, 134.60, 133.78, 133.71, 126.66, 124.29, 119.34, 118.72, 38.78, 34.30, 33.59, 32.13, 32.11, 30.49, 30.08, 30.03, 29.98, 29.94, 29.88, 29.60, 29.57, 26.86, 22.87, 14.30. HRMS (ESI+): m/z calc. 1343.5310, found 1343.5322.

8,12-Bis(4-(2-decyltetradecyl)thiophen-2-yl)acenaphtho[1,2-b][1,2,5]thiadiazolo[3,4-g]quinoxaline (APhTQ) (7)
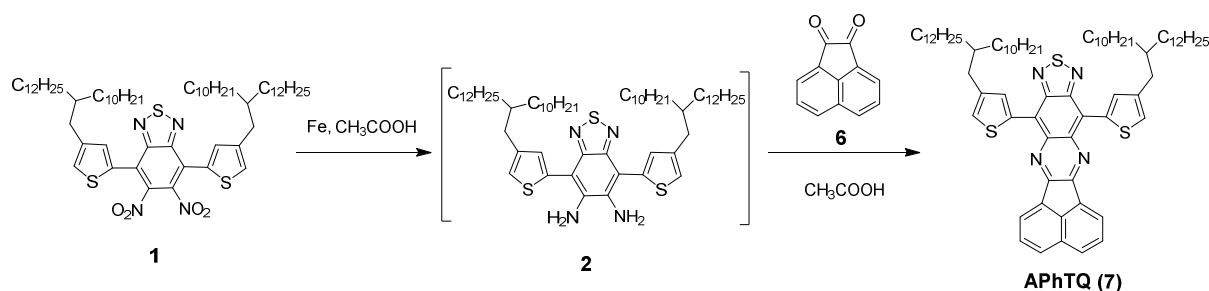
Following the procedure for the preparation of **BDTTQ-3, APhTQ** was obtain as a green solid (0.34 g, two steps 62%). ^{1}H NMR (250 MHz, CD_2Cl_2, ppm) δ 8.86 (s, 2H), 8.32 (d, J=5.0 Hz, 2H), 8.09 (d, J = 7.5 Hz, 2H), 7.81 (t, J = 7.5 Hz, 2H), 7.23 (s, 2H), 2.71 (d, J = 7.50 Hz, 4H), 1.82-1.77 (m, 2H), 1.26-1.23 (br, 80H), 0.87-0.82 (t, J = 7.50 Hz, 12H). ^{13}C NMR (62.5 MHz, $CDCl_3$, ppm) δ 153.19, 151.91, 141.41, 139.34, 135.78, 135.54, 135.50, 131.56, 130.27, 129.64, 128.84, 127.82, 122.64, 122.27, 39.19, 35.16, 33.57, 32.08, 30.33, 29.96, 29.92, 29.89, 29.85, 29.83, 29.54, 29.52, 26.91, 22.84, 14.28. HRMS (ESI+): m/z calc. 1149.7814 found 1149.7826.

8,12-Bis(5-bromo-4-(2-decyltetradecyl)thiophen-2-yl)acenaphtho[1,2-b][1,2,5]thiadiazolo[3,4-g]quinoxaline (Br$_2$-APhTQ) (8)
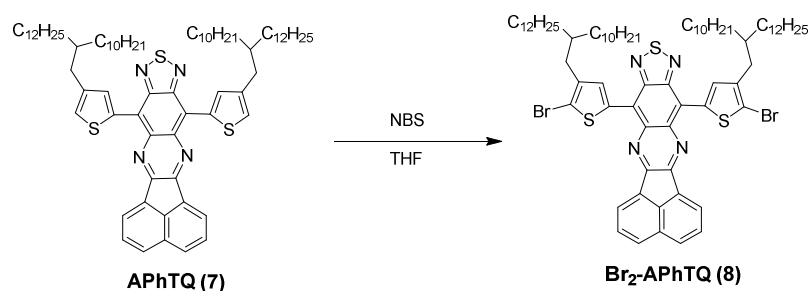
Following the procedure for the preparation of **Br$_2$-BDTTQ-3, Br$_2$-APhTQ** was obtain as a green solid (200 mg, 91%). ^{1}H NMR (250 MHz, CD_2Cl_2, ppm) δ 8.43 (s, 2H), 7.71 (d, J = 10.0 Hz, 2H), 7.42 (d, J = 5.0 Hz, 2H), 7.32 (t, J = 7.5 Hz, 2H), 2.36 (d, J = 5.0 Hz, 4H), 1.75-1.67 (m, 2H), 1.35-1.24 (br, 80H), 0.89-0.80 (t, J = 7.50 Hz, 12H). ^{13}C NMR (62.5 MHz, $CDCl_3$, ppm) δ 152.34, 150.98, 140.17, 138.95, 135.65, 134.67, 134.26, 130.75, 129.98, 129.53, 128.71, 122.73, 120.72, 119.20, 38.73, 34.28, 33.60, 32.11, 32.09, 30.40,

30.01, 29.98, 29.94, 29.91, 29.89, 29.85, 29.57, 29.54, 26.83, 22.85, 14.28. HRMS (ESI+): m/z calc. 1305.6025, found 1305.6067.

10,14-Bis(4-(2-decyltetradecyl)thiophen-2-yl)dipyrido[3,2-a:2',3'-c][1,2,5]thiadiazolo[3,4-i]phenazine (PhNTQ)

Following the procedure for the preparation of **BDTTQ-3, PhNTQ** was obtained as a green solid (0.36 g, two steps 65%).
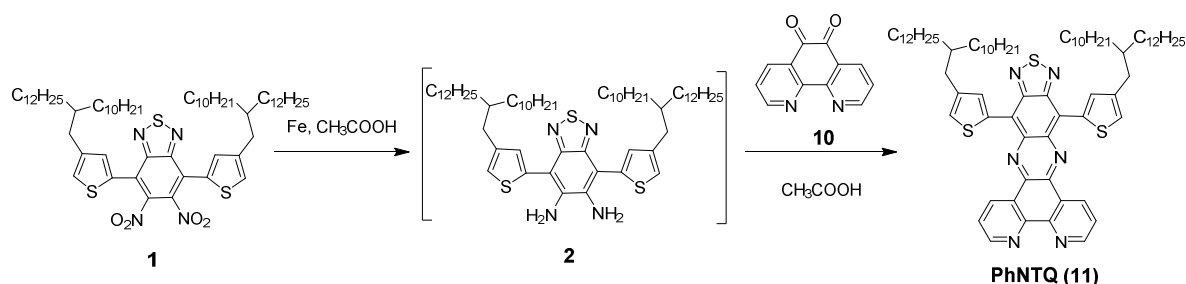
PhNTQ: ^{1}H NMR (250 MHz, CD$_2$Cl$_2$, ppm) δ 9.20 (d, J = 7.5 Hz, 2H), 9.00 (d, J = 2.5 Hz, 2H), 8.67 (s, 2H), 7.49 (dd, J = 7.5 Hz, J = 50 Hz, 2H), 7.11 (s, 2H), 2.65 (d, J = 7.50 Hz, 4H), 1.77 (br, 2H), 1.42-1.23 (br, 80H), 0.87-0.82 (m, 12H). ^{13}C NMR (62.5 MHz, CDCl$_3$, ppm) δ 152.73, 151.55, 149.60, 143.38, 141.90, 135.82, 135.75, 135.70, 127.92, 127.24, 124.35, 121.40, 120.62, 39.29, 35.16, 32.34, 30.59, 30.21, 30.19, 30.16, 30.14, 30.12, 30.08, 29.81, 29.78, 27.12, 23.10, 14.29. FD-MS: m/z calc. 1177.90 found 1177.86.

10,14-Bis(5-bromo-4-(2-decyltetradecyl)thiophen-2-yl)dipyrido[3,2-a:2',3'-c][1,2,5]thiadiazolo[3,4-i]phenazine (Br$_2$-PhNTQ)

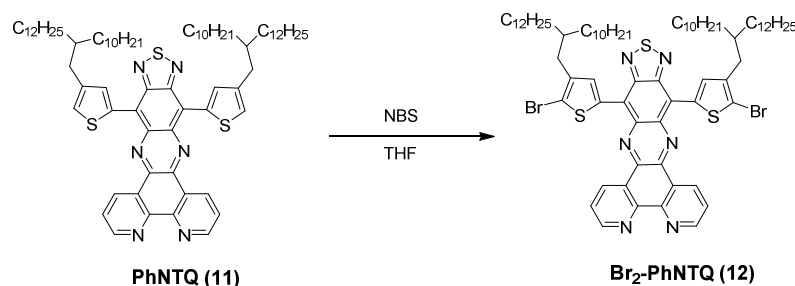Following the procedure for the preparation of **Br$_2$-BDTTQ-3, Br$_2$-PhNTQ** was obtained as a green solid (340 mg, 85%). ^{1}H NMR (250 MHz, CD$_2$Cl$_2$, ppm) δ 8.70 (dd, J =

2.5 Hz, J = 5.0 Hz, 2H), 8.45 (dd, J = 2.5 Hz, J = 5.0 Hz, 2H), 8.27 (s, , 2H), 7.09 (dd, J = 2.5 Hz, J = 5.0 Hz, 2H), 2.45 (d, J = 7.5 Hz, 4H), 1.73 (m, 2H), 1.36-1.24 (br, 80H), 0.88-0.83 (m, 12H). ^{13}C NMR (62.5 MHz, CDCl$_3$, ppm) δ 151.73, 151.62, 149.81, 141.06, 140.12, 135.85, 134.02, 133.74, 129.91, 126.12, 124.13, 119.70, 119.13, 38.86, 33.48, 32.13, 32.10, 30.52, 30.07, 30.02, 29.99, 29.94, 29.88, 29.59, 29.56, 26.78, 22.86 , 14.29. FD-MS: m/z calc. 1335.69, found 1335.60.

PBDTTQ-3

Br$_2$-BDTTQ-3 (5)   9   PBDTTQ-3
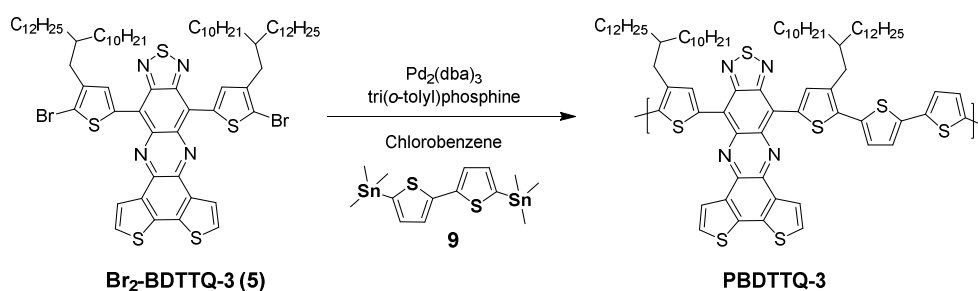
Br$_2$-BDTTQ-3 (**5**, 0.1 mmol), 5,5'-bis(trimethylstannyl)-2,2'-bithiophene (**9**, 0.1 mmol) and chlorobenzene (8 mL) were placed in a 50 mL Schlenk tube. The mixture was purged with argon for 5 min, and then 5.5 mg of tris(dibenzylideneacetone)dipalladium(0) (Pd$_2$(dba)$_3$) and 7.3 mg of tri(o-tolyl)phosphine (P(o-tolyl)$_3$) were added. Then the mixture was heated up to 110 °C under argon for 3 days. The polymer was end-capped with tributylphenylstannane and bromobenzene in sequence. After cooling to room temperature, the reaction mixture was poured into methanol. The polymer was filtered and subjected to Soxhlet extraction with methanol, acetone, hexane, dichloromethane and chloroform. The chloroform fraction was collected and added 30 mL of sodium diethyldithiocarbamate aqueous solution (1 g/100 mL) to remove residual palladium catalyst, the mixture was heated to 60 °C with vigorous stirring for 2 h. The mixture was separated and organic phase was washed with water for 3 times. The chloroform solution was concentrated and precipitated in methanol. The target polymer was collected by filtration and dried in vacuum to afford a black solid 102.7 mg (76%). Molecular weight by GPC (30 °C): M_n = 76.3 kg mol^{-1}, PDI = 3.64.

Elemental analysis: Calcd. For C$_{80}$H$_{108}$N$_4$S$_7$: C, 71.20; H, 8.07; N, 4.15; S, 16.58. Found: C, 70.66; H, 8.38; N, 3.98; S, 16.04.

PAPhTQ
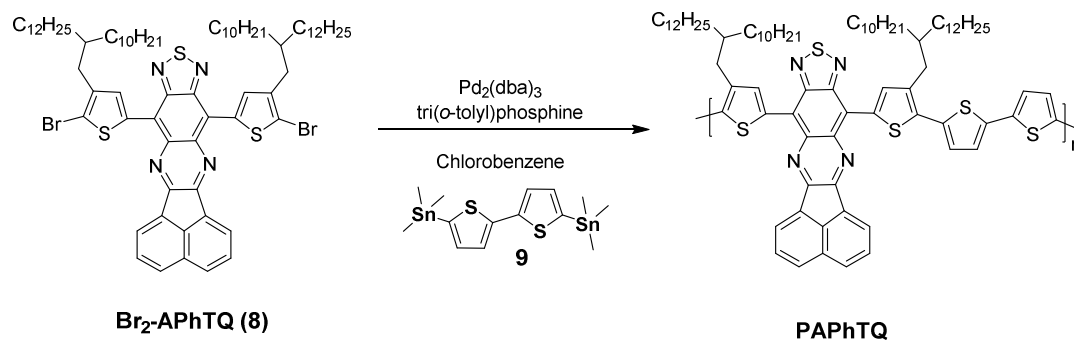
This polymer was prepared from **Br$_2$-APhTQ** (**8**, 0.1mmol) and 5,5'-bis(trimethylstannyl)-2,2'-bithiophene (**9**, 0.1 mmol) in similar procedure to **PBDTTQ-3** as a black solid 94.6 mg (72%).

Molecular weight by GPC (30 °C): M_n = 100.9 kg mol^{-1}, PDI = 6.48.

Elemental analysis: Calcd. For $C_{82}H_{110}N_4S_5$: C, 75.09; H, 8.45; N, 4.27; S, 12.19. Found: C, 74.73; H, 8.91; N, 4.01; S, 11.61.

4.10 References

(1) Kelley, T. W.; Baude, P. F.; Gerlach, C.; Ender, D. E.; Muyres, D.; Haase, M. A.; Vogel, D. E.; Theiss, S. D. *Chem. Mater.,* **2004**, *16*, 4413-4422.

(2) Forrest, S. R. *Nature* **2004**,, *428*, 911-918.

(3) Tsao, H. N.; Cho, D. M.; Park, I.; Hansen, M. R.; Mavrinskiy, A.; Yoon, D. Y.; Graf, R.; Pisula, W.; Spiess, H. W.; Müllen, K. *J. Am. Chem. Soc.,* **2011**, *133*, 2605-2612.

(4) Capelli, R.; Toffanin, S.; Generali, G.; Usta, H.; Facchetti, A.; Muccini, M. *Nat. Mater.,* **2010**, *9*, 496-503.

(5) Chua, L.-L.; Zaumseil, J.; Chang, J.-F.; Ou, E. C. W.; Ho, P. K. H.; Sirringhaus, H.; Friend, R. H. *Nature,* **2005**, *434*, 194-199.

(6) Yuen, J. D.; Kumar, R.; Zakhidov, D.; Seifter, J.; Lim, B.; Heeger, A. J.; Wudl, F. *Adv. Mater.,* **2011**, *23*, 3780-3785.

(7) Fan, J.; Yuen, J. D.; Wang, M. F.; Seifter, J.; Seo, J. H.; Mohebbi, A. R.; Zakhidov, D.; Heeger, A.; Wudl, F. *Adv. Mater.,* **2012**, *24*, 2186-2190.

(8) Yuen, J. D.; Fan, J.; Seifter, J.; Lim, B.; Hufschmid, R.; Heeger, A. J.; Wudl, F. *J. Am. Chem. Soc.,* **2011**, *133*, 20799-20807.

(9) Matthews, J. R.; Niu, W.; Tandia, A.; Wallace, A. L.; Hu, J.; Lee, W.-Y.; Giri, G.; Mannsfeld, S. C. B.; Xie, Y.; Cai, S.; Fong, H. H.; Bao, Z.; He, M. *Chem. Mater.,* **2013**, *25*, 782-789.

(10) Osaka, I.; Shimawaki, M.; Mori, H.; Doi, I.; Miyazaki, E.; Koganezawa, T.; Takimiya, K. *J. Am. Chem. Soc.,* **2012**, *134*, 3498-3507.

(11) Braga, D.; Horowitz, G. *Adv. Mater.,* **2009**, *21*, 1473-1486.

(12) Jones, B. A.; Facchetti, A.; Wasielewski, M. R.; Marks, T. J. *J. Am. Chem. Soc.,* **2007**, *129*, 15259-15278.

(13) Osaka, I.; Zhang, R.; Sauvé, G. v.; Smilgies, D.-M.; Kowalewski, T.; McCullough, R. D. *J. Am. Chem. Soc.,* **2009**, *131*, 2521-2529.

(14) Liu, J.; Zhang, R.; Osaka, I.; Mishra, S.; Javier, A. E.; Smilgies, D.-M.; Kowalewski, T.; McCullough, R. D. *Adv. Funct. Mater.,* **2009**, *19*, 3427-3434.

(15) Zhou, S.; An, C.; Stelzig, T.; Puniredd, S. R.; Guo, X.; Pisula, W.; Baumgarten, M. *New J. Chem.,* **2015**, DOI: 10.1039/c5nj00517e

Chapter 5. Phenanthrene Condensed Thiadiazoloquinoxaline Polymer as Phototransistor
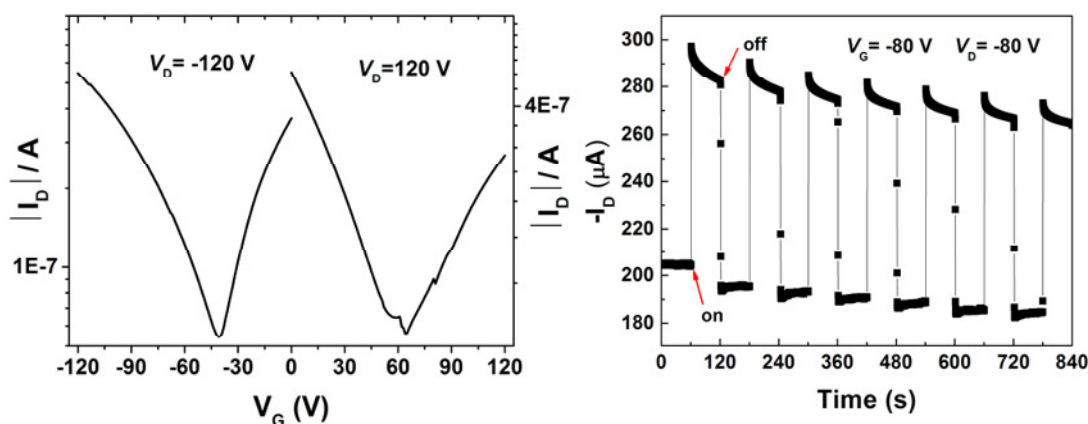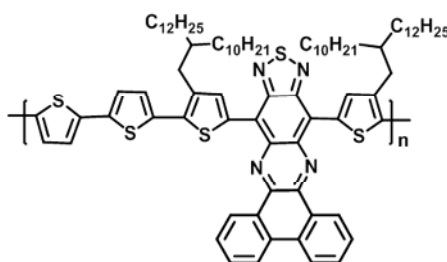
A new acceptor (**PhTQ**) was designed by attachment a photosensitizer group, phenanthrene, onto thiadiazoloquinoxaline moiety. Subsequently, the corresponding polymer (**PPhTQ**) was synthesized via Stille coupling between dibromo-**PhTQ** and distannyl-bithiophene. This polymer exhibits a balanced ambipolar behavior in field-effect transistor, with mobilities of 0.09 $cm^2 V^{-1} s^{-1}$ for holes and 0.06 $cm^2 V^{-1} s^{-1}$ for electrons. More interesting is the new application as a phototransistor of **PPhTQ** with a maximum photoresponsivity of 400 A/W.

5.1 Introduction

Organic phototransistors (OPTs) are a type of photosensitive transistors that use the incident light intensity to modulate the charge-carrier density in the transistor channel.[1] The first OPT was traced back to 2011, regioregular poly(3-octylthiophene-2,5-diyl) as active layer with photoresponsivity (P_R) of 100 A/W.[2] Up to now, the P_R of small molecules have been improved up to 10^3 A/W,[3,4] one order of magnitude higher than that of their single-crystal silicon counterpart (~300 A/W).[5] In particular, single-crystal OPTs, the P_R value is as high as 10^4 A/W.[6,7] However, donor-acceptor (D-A) conjugated polymers as the semiconductors for OPTs were rarely reported, especially D-A ambipolarity polymers. Several key issues limited polymers application in OPTs, such as light induced carriers generation, carriers transport and collection.[8] Although the highest P_R values have been achieved to 1000 A/W in D-A copolymers,[9,10] they only exhibited hole mobilities in OFETs. However, the ambipolar polymers as OPTs should be more interesting, due to their potential applications in complementary metal-oxide semiconductors logic circuits.

PBDTTQ-3
Ambipolar FET without photoresponse

p(tPA/Phen)
Photoswitching

PPhTQ
Ambipolar FET and Phototransistor
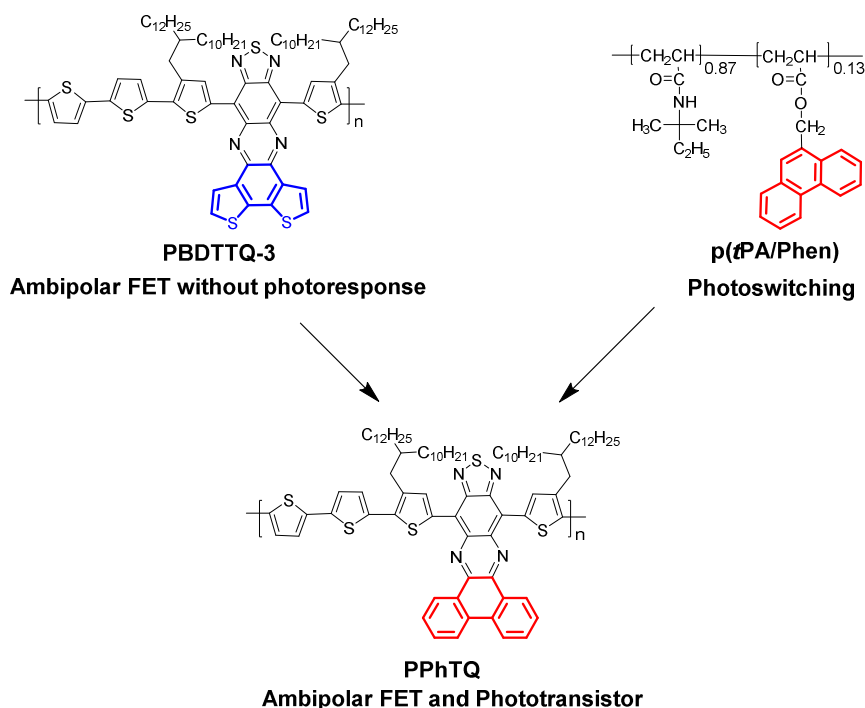
Figure 5.1 Design map for multifunctional condensed TQ polymers.

Due to the ability to easily vary the chemical structures of thiadiazoloquinoxaline (TQ) based materials, it is possible to manipulate their electronic properties. In particular, polymers containing different combinations of donors and TQ-functionalized moieties have been extremely effective in many applications, such as OPVs,[11,12] OFETs,[13,14] light emitting FETs (LEFETs),[15] polymer light emitting diodes (PLEDs),[16] near-infrared electroluminescence[17] and photoacoustic vascular imaging.[18] However, to date there has been limited efforts towards applying TQ-containing polymers in the field of OPTs.

Miyashita and coworkers have had interesting preliminary results when they attached phenanthrene group to a non-conjugated polymer (**p(*t*PA/Phen),** Figure 5.1) and used it as the active component in molecular photoswitching devices.[19-21] Inspired by this work, to enhance the practical applications of TQ polymers in organic electronics, a photosensitizer group, phenanthrene, is attached onto the TQ moiety to replace the benzodithiophene group in **PBDTTQ-3**. Polymer **PPhTQ** was, therefore, synthesized. **PhTQ** core is a known functionality that has shown promise as an active component for OPVs, and has been incorporated into oligomeric materials with low degrees of polymerization (DP) ranging from 3-9.[22-24] However, it is imperative to increase the macromolecular size of these kinds of polymers to improve their processability and optoelectronic properties. Indeed, the new polymer **PPhTQ** has a high DP as high as 28. This enabled such polymer to achieve high charge transport properties with mobilities of 0.09 cm^2 V^{-1} s^{-1} for holes and 0.06 cm^2 V^{-1} s^{-1} for electrons in OFETs. Additionally, **PPhTQ** was used as the active layer in an OPT that achieve a maximum value of 400 A/W and 0.5 for photoresponsivity (P_R) and photosensitivity (P_S), respectively.

5.2 Synthesis and Characterization

The synthesis of **PPhTQ** is shown in Scheme 5.1. The 4,7-bis(4-(2-decyltetradecyl)thiophen-2-yl)-5,6-dinitrobenzo[c][1,2,5]thiadiazole (**1**) was converted to the corresponding diamine **2**, which was directly used without purification. The monomer **PhTQ** was prepared by condensation reaction between crude compound **2** and phenanthrene-9,10-dione. Afterwards, the dibromination was carried out to obtain polymerization precursor **Br$_2$-PhTQ**. Finally, **PPhTQ** was synthesized via a Stille coupling between **Br$_2$-PhTQ** and 5,5'-bis(trimethylstannyl)-2,2'-bithiophene (**6**). **PPhTQ** exhibited a good solubility in common

solvents such as chloroform, THF and toluene. A M_n of 37.2 kg/mol and PDI of 1.88 were determined by GPC using polystyrene as standard and THF as eluent at 30 °C. Additionally, the thermal stability of this polymer was investigated by TGA. The TGA curve of **PPhTQ** is shown in Figure 5.2. **PPhTQ** exhibited an excellent thermal stability at 402 °C with 5% weight loss. The polymer side chains decomposed between 400 and 500 °C.
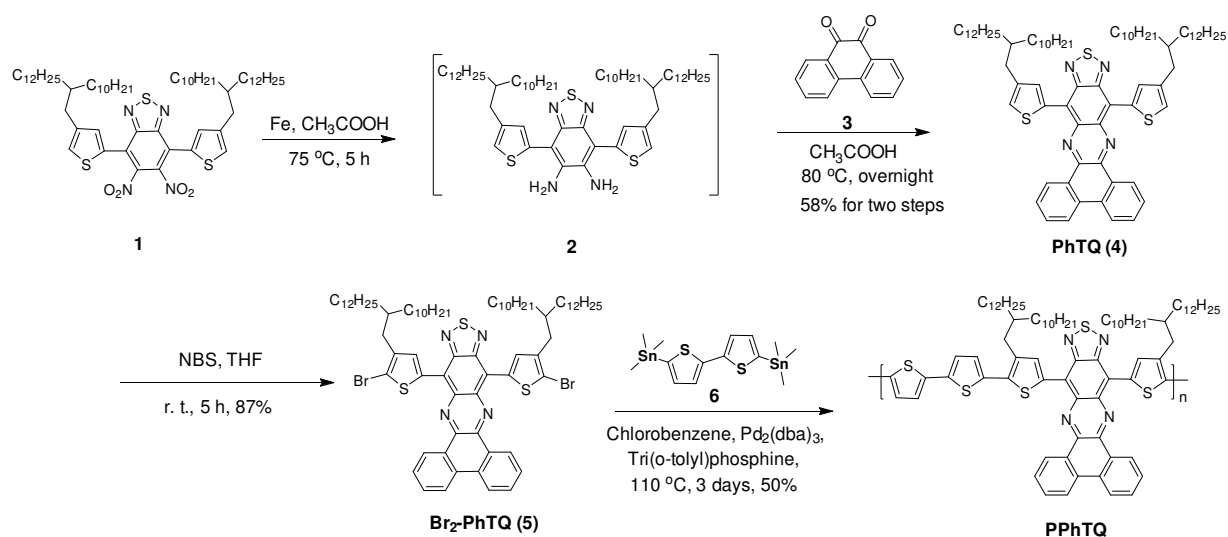
Scheme 5.1 Synthetic route for **PPhTQ**.
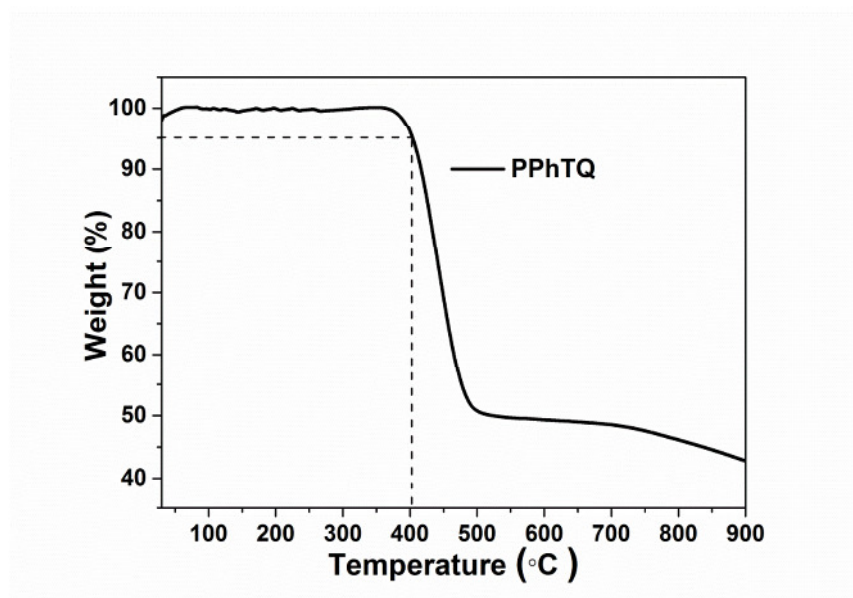
Figure 5.2 TGA curve of **PPhTQ** measured under a nitrogen atmosphere at a heating rate of 10 °C/min.

5.3 Optical and electrochemical properties

UV-vis-NIR absorption spectra of **PPhTQ** were recorded in dilute toluene solution as well as thin film as shown in Figure 5.3. A maximum absorption peak at 1143 nm in solution is significant a large red-shift of 138 nm as compared to **PAPhTQ**, while blue-shift of 127 nm in comparison with **PBDTTQ-3** (see Chapter 4). It was related to their different intramolecular charge transfer (ICT) abilities between donors and acceptors in resulting polymers. The film was prepared by drop-casting onto a glass slide from 2 mg/mL toluene solution. **PPhTQ** displayed slightly broadened bands compared to those in solution, indicating aggregation in solid state. The optical bandgap of 0.80 eV was estimated according to the absorption onset of the solid film.
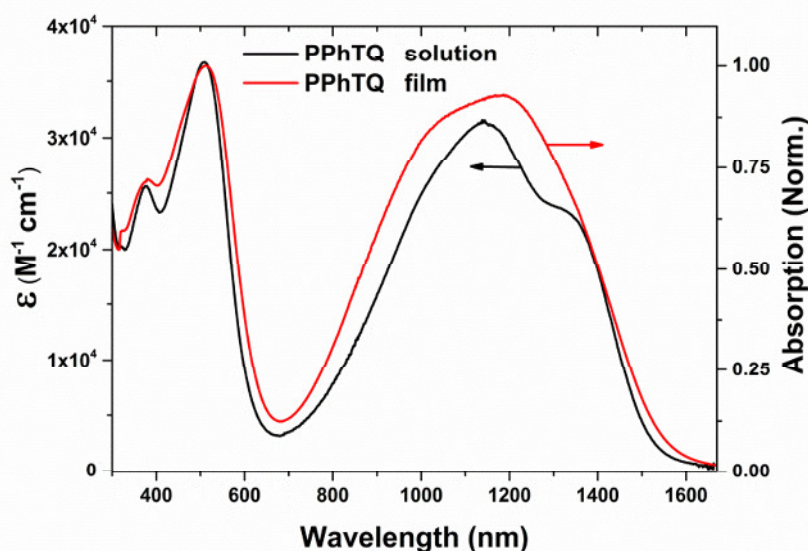
Figure 5.3 UV-vis-NIR absorption spectra of **PPhTQ** in toluene solution and thin film.

According to the first onset of reduction peaks, the electron affinity (EA) of **PhTQ** was estimated to be around -3.84 eV from cyclic voltammetry (CV) in dichloromethane solution (Figure 5.4a). This value is higher than that of **APhTQ** (-3.73 eV), but lower than that of **BDTTQ-3** (-3.92 eV), suggesting that the electron withdrawing nature of **PhTQ** was stronger than **APhTQ**, but weaker than **BDTTQ-3**. The ionization potential (IP) and EA of **PPhTQ** were calculated according to the first onsets of oxidation and reduction peaks in the CV plots,[25] with values of -5.08 and -4.01 eV, respectively (Figure 5.4b). The EA value of

PPhTQ was still in between values of **PAPhTQ** and **PBDTTQ-3**. This is in agreement with their corresponding EA values of monomers. On the other hand, density functional theory (DFT) calculations were also carried out to describe the electron density distribution along the conjugated backbone of **PPhTQ**. The HOMO and LUMO levels are shown in Figure 5.5. The electron density distributions of dimer **PPhTQ** repeat units are well delocalized over both LUMO and HOMO levels. These similar results as **PAPhTQ** and **PBDTTQ-3** indicated a potential ambipolarity for **PPhTQ** as semiconductor. In comparison with the optical bandgap, the electrochemical bandgap increases by 0.27 eV, which might result from the exciton bonding energy of the conjugated polymer.[26]
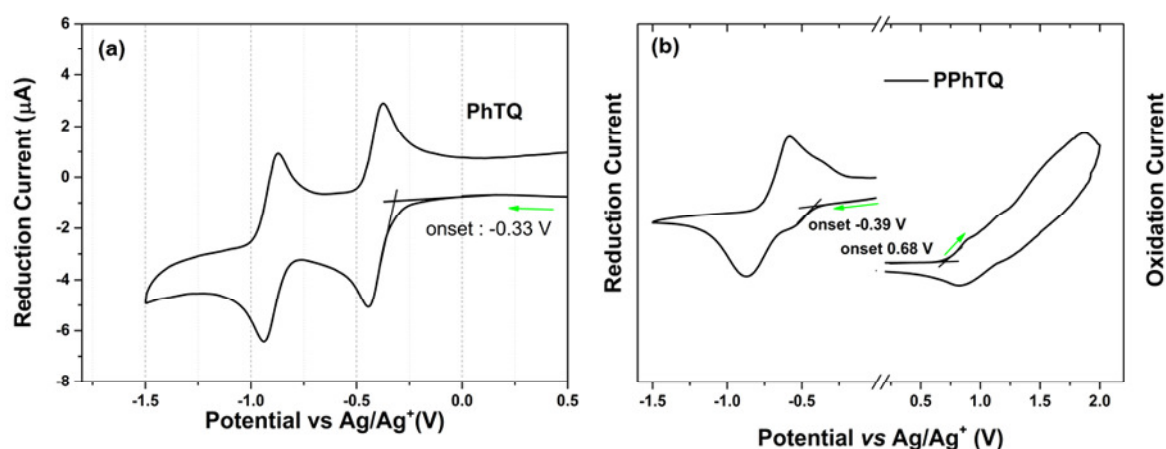
Figure 5.4 The cyclic voltammograms of **PhTQ** (a) and **PPhTQ** (b).
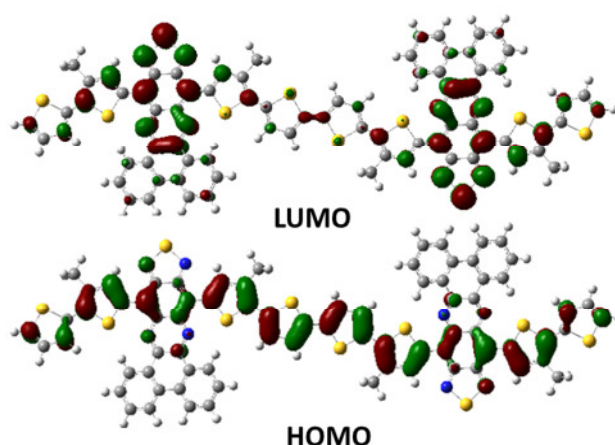
Figure 5.5 LUMO and HOMO diagrams of methyl substituted dimer of the **PPhTQ** repeat unit calculated by DFT (B3LYP, 6-31G∗).

5.4 OFET properties

To evaluate the charge carrier transport of **PPhTQ**, thin-film transistors were fabricated with bottom-gate bottom-contact configurations. This was in collaboration with ▮▮▮▮▮ (Max Planck Institute for Polymer Research, Mainz). Heavily doped silicon covered by 300 nm thick thermally grown oxide dielectric acts as gate electrode. The hexamethyldisilazane (HMDS) was employed to functionalize the dielectric surface in order to minimize interfacial trapping sites. Au was evaporated as source and drain electrodes. The thickness of 1-5 µm of **PPhTQ** films were deposited by drop-casting from 10 mg/mL chloroform solution. The transfer and output characteristics are presented in Figure 5.6, showing a typical linear/saturation behavior. More importantly, a well-balanced ambipolar charge carrier transport was evident from the transfer curve in both p- and n-type operation modes for negative and positive gate voltages. In the negative drain mode for a source-drain voltage (V_D) of -120 V, the crossover point was located at around V_G = -40 V indicating a change from electron- to hole-dominated current (Figure 5.6a). Below this gate voltage the transistor exhibited a hole transport in the accumulation mode. In the positive regime at V_D = 120 V the electrons dominate the device operation from approximately V_G = 60 V, which was slightly improved in comparison to **PBDTTQ-3** (70 V). It might result from the immobile Si–O⁻ ions at the semiconductor/dielectric interface caused by electrochemically trapping the injected electrons.[27] Although the charge trapping could be reduced by HMDS, it did not completely eliminate. It has been proven that this negative effect influences only the threshold voltage, but not the mobility.[28] On the other hand, at low V_D the output plots exhibited a nonlinear behavior clearly indicating contact resistance and charge injection limitation, as shown in Figure 5.6b.[29] The field-effect mobilities of **PPhTQ** reached 0.09 cm^2 V^{-1} s^{-1} for holes and 0.04 cm^2 V^{-1} s^{-1} for electrons, which are among the best transistor performances in TQ-containing polymers. In addition, the electron transport was slightly enhanced reaching a mobility of 0.06 cm^2 V^{-1} s^{-1} when chlorobenzene was used as solvent. The on/off ratio of the devices was as low as 10-10^2, which could be ascribed to the adventitious doping due to the high IP value of this polymer.[13] Because glovebox conditions consist of an oxygen concentration from 0.5 to 1 ppm and moisture concentration of around 0.2 ppm. As recently reported, moderate doping of organic semiconductors by "dilute air" (O_2 ~1 ppm and H_2O ~1 ppm) dramatically decreased the field-effect performance.[30]
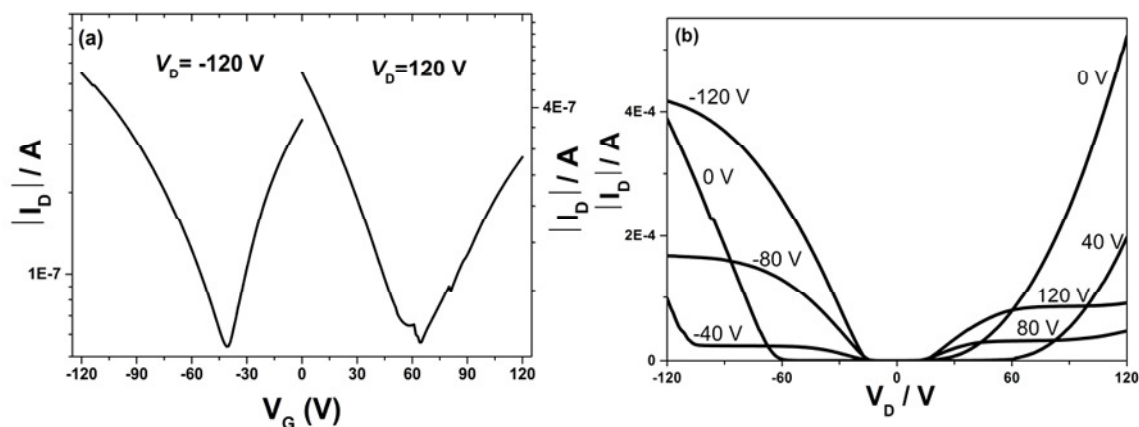
Figure 5.6 Transfer (a) and output (b) curves of **PPhTQ**.

5.5 Self-organization

In order to elucidate the **PPhTQ** organization in thin films, the grazing-incidence wide-angle X-ray scattering (GIWAXS) was performed by ▇▇▇▇▇▇▇▇▇▇ (Max Planck Institute for Polymer Research, Mainz), as shown in Figure 5.7.
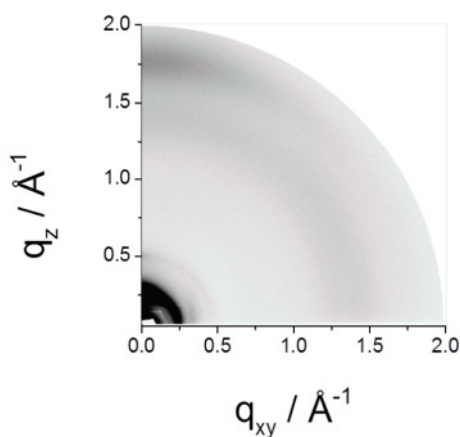
Figure 5.7 GIWAXS pattern for **PPhTQ** thin films on a HMDS-modified substrate.

The GIWAXS pattern exhibits a pronounced order which was evident from reflections up to second order appearing in the out-of-plane pattern. From the first order peak at $q_z = 0.25$ Å^{-1} and $q_{xy} = 0$ Å^{-1} an interlayer distance of 2.51 nm was determined. Additional reflections at $q_z = 0$ Å^{-1} and $q_{xy} = 0.32$ Å^{-1} correspond to a d-spacing of 1.96 nm, which was assigned to the length of the repeating unit along the backbone. The reflection at the wide-angle out-of-plane was related to the π-stacking distance of 0.375 nm. The appearance of the interlayer and π-

stacking reflection on the same plane indicates the coexistence of the face- and edge-on organization, whereby the first type of arrangement revealed a π-stacking peak in the GIWAXS pattern. However, the similar structures **PAPhTQ** and **PBDTTQ-3** possess poor ordering in thin films (Chapter 4), it was related to the different acceptor cores of these three polymers, considering they differ only in the acceptor units.

5.6 Phototransistor properties

Based on previous design concept (Chapter 3 and 4), the **PPhTQ** exhibited good ambipolar transistor performance. More interesting, the introduction of the phenanthrene group resulted in an additional high photoresponsivity opening great potential for OPT applications as expectation. This was in collaboration with ███████████ (Max Planck Institute for Polymer Research, Mainz).
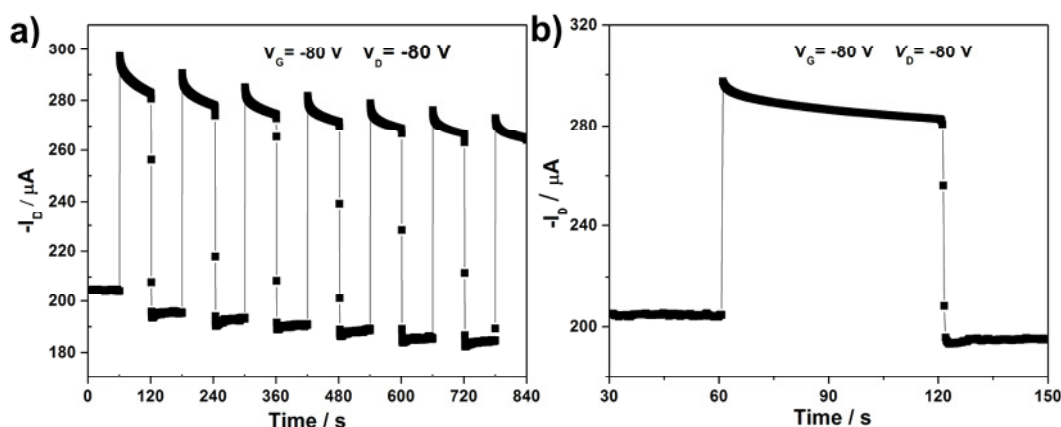
Figure 5.8 (a) On-off characteristics of the phototransistor at V_G= -80 V and V_D= -80 V. "On" and "off" are related to light switching. (b)The single cycle of the photoresponse of phototransistor at V_G= -80 V and V_D= -80 V.

Figure 5.8a exhibits its device performance as a phototransistor. At V_G=V_D= -80 V, the absolute value of the drain current is around 200 μA in the dark. When light was switched on, the absorption of the light generates hole-electron pairs. The photogenerated holes could easily move to the drain electrode under the action of the electrical field between source and drain.[31] As reported in the literature,[31] the photogenerated electrons were trapped under the source electrode. Interestingly, the electrons lower the potential barrier between the source

and channel could consequently facilitate the injection of excess holes from the source electrode into the organic semiconductor layer. As a result, a photocurrent (I_{ph}) of ~100 µA was generated so that -I_D increased to ~300 µA. After switching off the light, the drain current recovered to the original level. The stability of **PPhTQ** phototransistors was confirmed by 7 on-off cycles (Figure 5.8a). A single cycle of the photoresponse behavior is presented in Figure 5.8b.

P_R and P_S are key parameters for assessing the performance of phototransistors. The values of P_R and P_S are typically defined as: $P_R= (I_{inc}-I_{dark})/P_{inc} = I_{ph}/P_{inc}$, $P_S= (I_{inc}-I_{dark})/I_{dark} = I_{ph}/I_{dark}$, where P_{inc} is the incident illumination power on the device channel, I_{inc} and I_{dark} are the drain current under the incident illumination and in the dark, respectively. P_R is plotted as a function of the gate voltage (V_G) with V_D = -80 V in Figure 5.9a. At V_G< 0 V, P_R is only around 0.1 A/W, while this parameter significantly grows to 400 A/W with increasing V_G to -80 V. To the best of our knowledge, this value exceeds that of single-crystal silicon and is among the highest photoresponsivity for thin film phototransistors based on conjugated polymers. The high performance of **PPhTQ** was attributed to (1) the wide absorption feature from 250 to 1600 nm which is beneficial for generating carriers, (2) the high mobility of thin film which make transistor efficient collection and transportation carriers.[8] In addition, the value of P_S is comparably low, with a maximum value of about 0.5 (Figure 5.9b), which is primarily attributed to the high off-current and subsequent low on/off ratio of **PPhTQ**. Considering previous **PAPhTQ** and **PBDTQ-3** without photoresponse behavior, it is assumed that such photoelectric property of this polymer originates from the phenanthrene condensed TQ moiety.
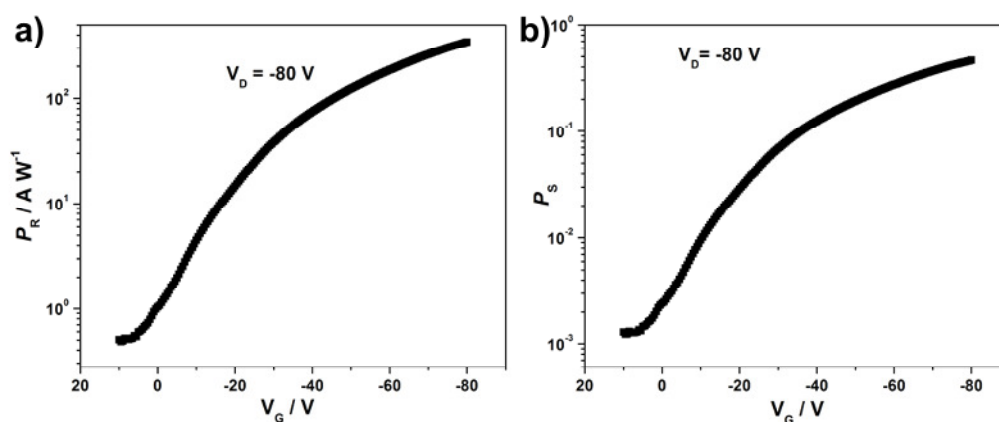
Figure 5.9 (a) Variation of photoresponsivity P_R with V_G at V_D= -80 V. (b) Variation of photosensitivity P_S with V_G at V_D= -80 V.

5.7 Summary

A new TQ-based conjugated polymer, **PPhTQ**, was synthesized. **PPhTQ** exhibited a well-balanced ambipolor field-effect behavior with mobilities of 0.09 $cm^2 V^{-1} s^{-1}$ for holes and 0.06 $cm^2 V^{-1} s^{-1}$ for electrons. It had only a slight influence on the charge carrier transport in comparison to **PAPhTQ** and **PBDTTQ-3**. Interestingly, introduction of a phenanthrene group into the TQ moiety made **PPhTQ** as an active layer in OPT devices. The resulting thin film phototransistor showed a maximum photoresponsivity of 400 A/W, which not only exceeds that of single-crystal silicon-based OPTs (~300 A/W), but is also among the best OPT performances for conjugated polymers.

Additionally, interestingly, **PPhTQ** has the best ordered arrangement in films, **PAPhTQ** has slightly higher ordered film than **PBDTTQ-3** among these three polymers as confirmed by GIWAXS. It is very important to investigate this question by studying the arrangement of the monomeric subunits, because these polymers differ only in the acceptor cores. Such work is investigated in Chapter 7.

5.8 Synthetic details

The intermediate compounds 4,7-bis(4-(2-decyltetradecyl)thiophen-2-yl)-5,6-dinitrobenzo[c][1,2,5]thia diazole (**1**) and 5,5'-bis(trimethylstannyl) -2,2'-bithiophene (**6**) were prepared as descripted in Chapter 3.

10,14-Bis(4-(2-decyltetradecyl)thiophen-2-yl)dibenzo[a,c][1,2,5]thiadiazolo[3,4-i]phenazine (PhTQ)
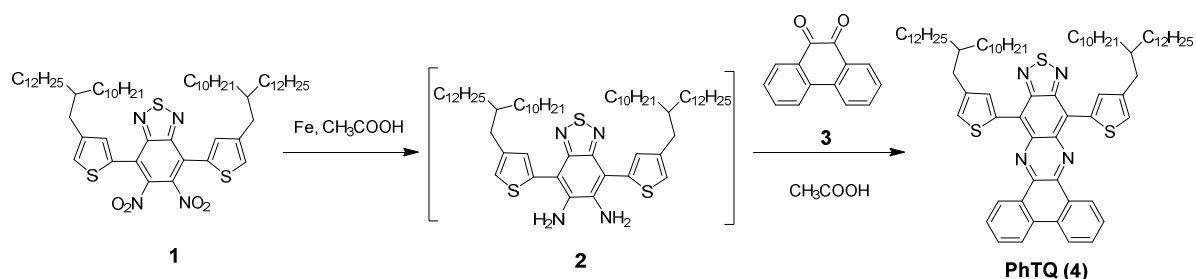
A mixture of compound **1** (0.5 g, 0.47 mmol) and fine iron powder (311 mg, 5.55 mmol) in acetic acid (15 mL) was stirred for 5 h at 75 °C under argon. The reaction mixture was cooled to room temperature, precipitated in 5% aqueous NaOH and extracted with diethyl ether (3×20 mL). The combined organic layers were washed with brine, dried with $MgSO_4$. The solvent was removed under reduced pressure to give corresponding diamine **2** with deep dark oil. This crude product was added into acetic acid (15 mL) solution of phenanthrene-9,10-dione (**3**, 98 mg, 0.47 mmol). The resulting mixture was heated to 80 °C overnight under argon. After cooling to room temperature, the mixture was poured into 100 mL 5% aqueous NaOH and extracted with dichloromethane (3×20 mL). The combined organic phases were dried with $MgSO_4$ and filtered. The filtrate was concentrated and purified by column chromatography eluting with hexane dichloromethane (3:1) to give 0.32 g (green solid, two steps 58%) of **PhTQ**: ^{1}H NMR (250 MHz, CD_2Cl_2, ppm) δ 9.30 (dd, *J* = 2.5 Hz, *J* = 7.5 Hz, 2H), 8.78 (s, 2H), 8.38 (dd, *J* = 2.5 Hz, *J* = 7.5 Hz, 2H), 7.74-7.61 (m, 4H), 7.27 (d, *J* = 2.5 Hz, 2H), 2.70 (d, *J* = 7.50 Hz, 4H), 1.80 (br, 2H), 1.40-1.22 (br, 80H), 0.87-0.82 (m, 12H). ^{13}C NMR (62.5 MHz, CD_2Cl_2, ppm) δ 151.58, 143.65, 141.82, 136.07, 135.88, 135.85, 133.17, 131.33, 130.61, 129.15, 128.49, 127.95, 123.20, 121.06, 39.49, 35.26, 32.34, 30.59, 30.21, 30.19, 30.16, 30.14, 30.12, 30.08, 29.81, 29.78, 27.12, 23.10, 14.29. HRMS (ESI+): m/z calc. 1175.7971 found 1175.7993.

10,14-Bis(5-bromo-4-(2-decyltetradecyl)thiophen-2-yl)dibenzo[a,c][1,2,5]thiadiazolo[3,4-i]phenazine (Br$_2$-PhTQ)

PhTQ (4)   Br$_2$-PhTQ (5)
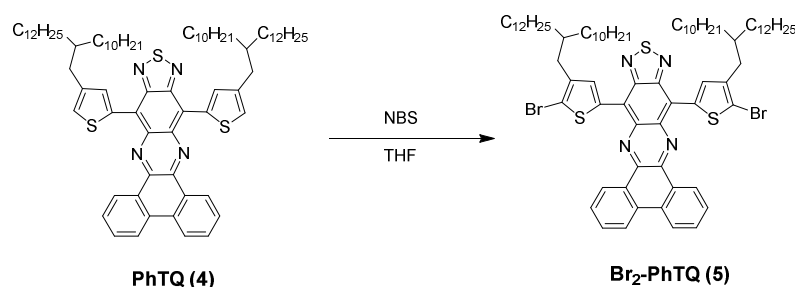
PhTQ (**4**, 284 mg, 0.24 mmol) was dissolved in 15 mL THF at room temperature. NBS (94 mg, 0.53 mmol) was carefully added into the solution in small batches in dark. The mixture was stirred for 5 h. After removing the solvent under reduced pressure, the residue was purified by column chromatography with dichloromethane/hexane (1:3) as the eluent to

give **Br₂-PhTQ** as a green solid (280 mg, 87%). ^{1}H NMR (250 MHz, CD$_2$Cl$_2$, ppm) δ 8.48 (d, *J* = 5.0 Hz, 2H), 8.34 (s, 2H), 7.84 (s, 2H), 7.30 (t, *J* = 7.5 Hz, 2H), 7.12 (t, *J* = 7.5 Hz, 2H), 2.36 (d, *J* = 7.5 Hz, 4H), 1.71 (m, 2H), 1.36-1.24 (br, 80H), 0.87 (t, *J* = 7.50 Hz, 12H). ^{13}C NMR (62.5 MHz, CD$_2$Cl$_2$, ppm) δ 150.38, 142.95, 140.40, 135.20, 135.01, 134.75, 132.46, 130.85, 129.51, 128.92, 127.81, 122.46, 119.22, 118.74, 38.95, 34.16, 33.76, 32.41, 32.38, 30.72, 30.32, 30.29, 30.25, 30.22, 30.20, 30.15, 29.88, 29.84, 27.02, 23.15, 23.13, 14.35. HRMS (ESI+): m/z calc. 1331.6181, found 1331.6171.

Synthesis of PPhTQ
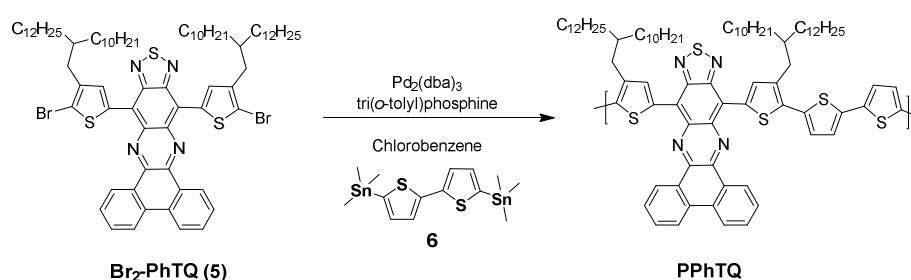
Br₂-PhTQ (**5**, 0.1 mmol), 5,5'-bis(trimethylstannyl)-2,2'-bithiophene (**6**, 0.1 mmol), and chlorobenzene (8 mL) were placed in a 50 mL Schlenk tube. The mixture was purged with argon for 5 min, and then 5.5 mg of tris(dibenzylideneacetone)dipalladium(0) (Pd$_2$(dba)$_3$) and 7.3 mg of tri(o-tolyl)phosphine (P(o-tolyl)$_3$) were added. Then the mixture was heated up to 110 °C under argon for 3 days. The polymer was end-capped with tributylphenylstannane and bromobenzene in sequence. After cooling to room temperature, the reaction mixture was poured into methanol. The crude polymer was filtered and subjected to Soxhlet extraction with methanol, acetone, hexane, dichloromethane and chloroform. The chloroform fraction was collected and added 30 mL of sodium diethyldithiocarbamate aqueous solution (1 g/100 mL) to remove residual palladium catalyst, the mixture was heated to 60 °C with vigorous stirring for 2 h. The mixture was separated and organic phase was washed with water for 3 times. The chloroform solution was concentrated and precipitated in methanol. The target polymer was collected by filtration and dried in vacuum to afford a black solid 61 mg (50%).

Molecular weight by GPC: Mn = 37.2 kg mol^{-1}, PDI = 1.88.

Elemental analysis: Calcd. For C$_{84}$H$_{112}$N$_4$S$_5$: C, 75.42; H, 8.44; N, 4.19; S, 11.95. Found: C, 75.08; H, 9.41; N, 3.91; S, 11.56.

5.9 References

(1) Yu, H.; Bao, Z.; Oh, J. H. *Adv. Funct. Mater.,* **2013**, *23*, 629-639.

(2) Narayan, K. S.; Kumar, N. *Appl. Phys. Lett.,* **2001**, *79*, 1891-1893.

(3) Cho, M. Y.; Kim, S. J.; Han, Y. D.; Park, D. H.; Kim, K. H.; Choi, D. H.; Joo, J. *Adv. Funct. Mater.,* **2008**, *18*, 2905-2912.

(4) Sun Kim, Y.; Young Bae, S.; Hwan Kim, K.; Wan Lee, T.; Hur, J. A.; Ha Hoang, M.; Ju Cho, M.; Kim, S.-J.; Kim, Y.; Kim, M.; Lee, K.; Joong Lee, S.; Hoon Choi, D. *Chem. Commun.,* **2011**, *47*, 8907-8909.

(5) Johnson, N. M.; Chiang, A. *Appl. Phys. Lett.,* **1984**, *45*, 1102-1104.

(6) Kim, K. H.; Bae, S. Y.; Kim, Y. S.; Hur, J. A.; Hoang, M. H.; Lee, T. W.; Cho, M. J.; Kim, Y.; Kim, M.; Jin, J.-I.; Kim, S.-J.; Lee, K.; Lee, S. J.; Choi, D. H. *Adv. Mater.,* **2011**, *23*, 3095-3099.

(7) Hoang, M. H.; Kim, Y.; Kim, M.; Kim, K. H.; Lee, T. W.; Nguyen, D. N.; Kim, S.-J.; Lee, K.; Lee, S. J.; Choi, D. H. *Adv. Mater.,* **2012**, *24*, 5363-5367.

(8) Dong, H.; Zhu, H.; Meng, Q.; Gong, X.; Hu, W. *Chem. Soc. Rev.,* **2012**, *41*, 1754-1808.

(9) Liu, Y.; Dong, H.; Jiang, S.; Zhao, G.; Shi, Q.; Tan, J.; Jiang, L.; Hu, W.; Zhan, X. *Chem. Mater.,* **2013**, *25*, 2649-2655.

(10) Li, H.; Wu, Y.; Wang, X.; Kong, Q.; Fu, H. *Chem. Commun.,* **2014**, *50*, 11000-11003.

(11) Inganäs, O.; Zhang, F.; Tvingstedt, K.; Andersson, L. M.; Hellström, S.; Andersson, M. R. *Adv. Mater.,* **2010**, *22*, E100-E116.

(12) Keshtov, M. L.; Marochkin, D. V.; Kochurov, V. S.; Khokhlov, A. R.; Koukaras, E. N.; Sharma, G. D. *Poly. Chem.,* **2013**, *4*, 4033-4044.

(13) Zhang, X.; Steckler, T. T.; Dasari, R. R.; Ohira, S.; Potscavage, W. J.; Tiwari, S. P.; Coppee, S.; Ellinger, S.; Barlow, S.; Bredas, J.-L.; Kippelen, B.; Reynolds, J. R.; Marder, S. R. *J. Mater. Chem.,* **2010**, *20*, 123-134.

(14) Dallos, T.; Beckmann, D.; Brunklaus, G.; Baumgarten, M. *J. Am. Chem. Soc.,* **2011**, *133*, 13898-13901.

(15) Steckler, T. T.; Lee, M. J.; Chen, Z.; Fenwick, O.; Andersson, M. R.; Cacialli, F.; Sirringhaus, H. *J. Mater. Chem. C,* **2014**, *2*, 5133-5141.

(16) Steckler, T. T.; Fenwick, O.; Lockwood, T.; Andersson, M. R.; Cacialli, F. *Macromol. Rapid Commun.,* **2013**, *34*, 990-996.

(17) Steckler, T. T.; Henriksson, P.; Mollinger, S.; Lundin, A.; Salleo, A.; Andersson, M. R. *J. Am. Chem. Soc.,* **2014**, *136*, 1190-1193.

(18) Liu, J.; Geng, J.; Liao, L.-D.; Thakor, N.; Gao, X.; Liu, B. *Poly. Chem.,* **2014**, *5*, 2854-2862.

(19) Matsui, J.; Mitsuishi, M.; Aoki, A.; Miyashita, T. *Angew. Chem. Int. Ed.,* **2003**, *42*, 2272-2275.

(20) Matsui, J.; Mitsuishi, M.; Aoki, A.; Miyashita, T. *J. Am. Chem. Soc.,* **2004**, *126*, 3708-3709.

(21) Mitsuishi, M.; Matsui, J.; Miyashita, T. *J. Mater. Chem.,* **2009**, *19*, 325-329.

(22) Hai, J.; Shi, G.; Yu, J.; Zhu, E.; Bian, L.; Ma, W.; Tang, W. *New J. Chem.,* **2014**, *38*, 4816-4822.

(23) Qin, C.; Fu, Y.; Chui, C.-H.; Kan, C.-W.; Xie, Z.; Wang, L.; Wong, W.-Y. *Macromol. Rapid Commun.,* **2011**, *32*, 1472-1477.

(24) Hai, J.; Yu, W.; Zhu, E.; Bian, L.; Zhang, J.; Tang, W. *Thin Solid Films,* **2014**, *562*, 75-83.

(25) Bredas, J.-L. *Mater. Horiz.,* **2014**, *1*, 17-19.

(26) Sariciftci, N. S. *Primary Photoexcitations in Conjugated Polymers:Molecular Excitons vs Semiconductor Band Model; World Scientific: Singapore, 1997.*

(27) Chua, L.-L.; Zaumseil, J.; Chang, J.-F.; Ou, E. C. W.; Ho, P. K. H.; Sirringhaus, H.; Friend, R. H. *Nature,* **2005**, *434*, 194-199.

(28) Braga, D.; Horowitz, G. *Adv. Mater.,* **2009**, *21*, 1473-1486.

(29) Zhang, W.; Smith, J.; Watkins, S. E.; Gysel, R.; McGehee, M.; Salleo, A.; Kirkpatrick, J.; Ashraf, S.; Anthopoulos, T.; Heeney, M.; McCulloch, I. *J. Am. Chem. Soc.,* **2010**, *132*, 11437-11439.

(30) Lu, G.; Blakesley, J.; Himmelberger, S.; Pingel, P.; Frisch, J.; Lieberwirth, I.; Salzmann, I.; Oehzelt, M.; Di Pietro, R.; Salleo, A.; Koch, N.; Neher, D. *Nat. Commun.,* **2013**, *4*, 1588.

(31) Huang, W.; Yang, B.; Sun, J.; Liu, B.; Yang, J.; Zou, Y.; Xiong, J.; Zhou, C.; Gao, Y. *Org. Electron.,* **2014**, *15*, 1050-1055.

Chapter 6. Tuning Optoelectronic Properties of Dual-acceptor Based Low Bandgap Ambipolar Polymers by Thiophene-bridge Length
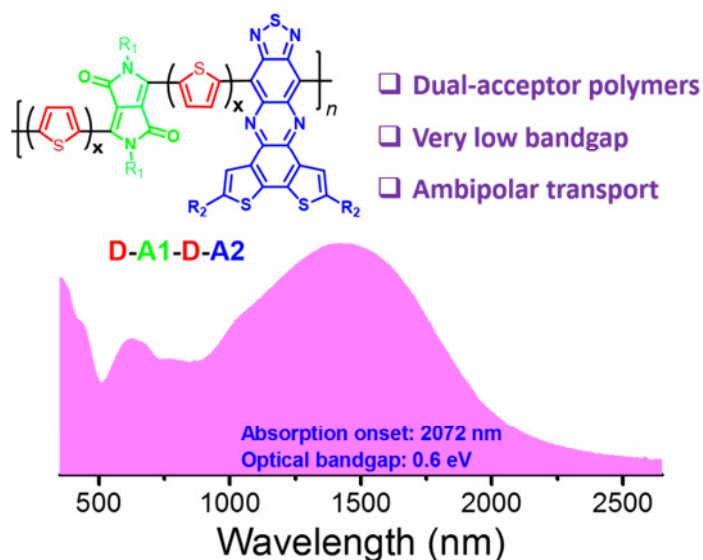
In this chapter, three DPP-TQ-based very low bandgap polymers were prepared. Both acceptors of these polymers were separated by one, two, and three thiophenes. Only inserting one thiophene between **DPP** and the benzodithiophene condensed **TQ**, polymer **PDPP-T-TQ** has a very low optical bandgap of 0.60 eV. When increasing the thiophene bridge length between both acceptors, the optical bandgaps of the polymer were enlarged. From polymers **PDDP-T-TQ** to **PDPP-3T-TQ**, the coplanarity were significantly improved as confirmed by GIWAXS, thereby the **PDPP-3T-TQ** has the best ambipolar device performance with 5.0×10^{-4} cm^2 V s^{-1} for holes and 5.0×10^{-5} cm^2 V s^{-1} for electrons among these polymers.

Note: Large part of this chapter has been submitted to *Polym. Chem.*, **2015**, Revision.

6.1 Introduction

Conjugated polymers with a very low bandgap ($\leq$ 1 eV) have been drawing substantial attention due to their broad and near-infrared (NIR) absorption, multiple redox states in a small potential window, ambipolar charge carrier transport, and potential use in sensors, batteries, and supercapacitors.[1] As a significant breakthrough work, Wudl and coworkers reported a poly(isothianaphthene) with an energy bandgap of ~1 eV due to a strong quinoid character in the thiophene ring.[2,3] Recently, tailoring donor-acceptor interactions in D-A copolymers has proven to be an effective strategy for developing very low bandgap polymers. The combination of strong donors and acceptors with quinoidal character has produced many soluble polymers with optical bandgaps (E_g^{opt}) lower than 0.70 eV, such as **P(DTP-BThBTT)** and **P(CPDT-TQ)** (Figure 6.1).[4-7]
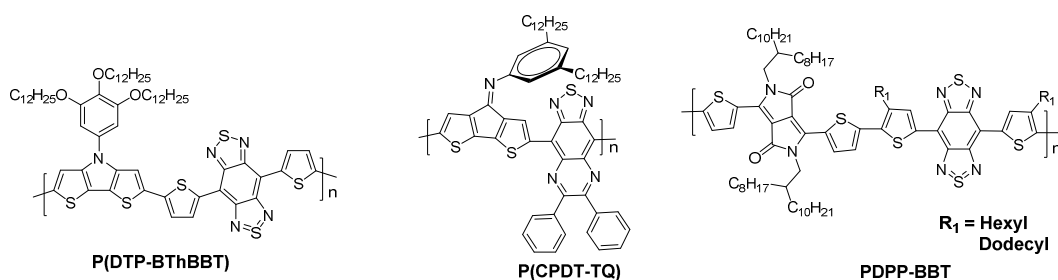
Figure 6.1 The very low bandgap polymer structures were reported in the literatures.

However, many low bandgap polymers containing one strong acceptor have higher hole than electron mobility, such as those derived from benzobisthiadiazole (**BBT**)[4,6] and diketopyrrolopyrrole (**DPP**)[8,9]. To improve electron transport and thus obtain balanced charge carrier transport, a dual-acceptor design strategy has been proposed to construct D-A1-D-A2 polymers.[10-14] For example, **PDPP-BBT** (Figure 6.1) exhibited an E_g^{opt} of around 0.65 eV and well-balanced ambipolar charge transporting behavior with mobilities of 1.17 cm^2 V^{-1} s^{-1} for holes and 1.32 cm^2 V^{-1} s^{-1} for electrons.[15] Compared to the polymers composed of only one strong acceptor, dual-acceptor polymers with very low bandgap and balanced charge carrier transport are rarely studied.

In this chapter, we report two high electron affinity acceptors, **DPP** and new condensed **TQ** derivative (compound **3** in Scheme 6.1), as building blocks which are combined in one polymer backbone. As previously demonstrated (Chapter 2 and 4), this new **TQ** derivative is

a new strong acceptor, the corresponding D-A copolymer exhibits a very low E_g^{opt} of 0.76 eV and hole-dominant ambipolar behavior. On the other hand, **DPP** has been widely studied as a strong acceptor in low bandgap polymers because numerous DPP-based polymers have revealed excellent performance as ambipolar semiconductor.[16,17] Therefore, it can be expected that the combination of the two acceptors could endow the resulting dual-acceptor polymers the desired characteristics of both very low bandgap and balanced ambipolarity. Three copolymers (**PDPP-T-TQ**, **PDPP-2T-TQ** and **PDPP-3T-TQ** in Scheme 6.1) were designed and synthesized, in which the two acceptors are separated in the polymer backbone by oligothiophene bridges with varying lengths in order to elaborately tune the optoelectronic properties and charge carrier transport.

6.2 Synthesis and characterization
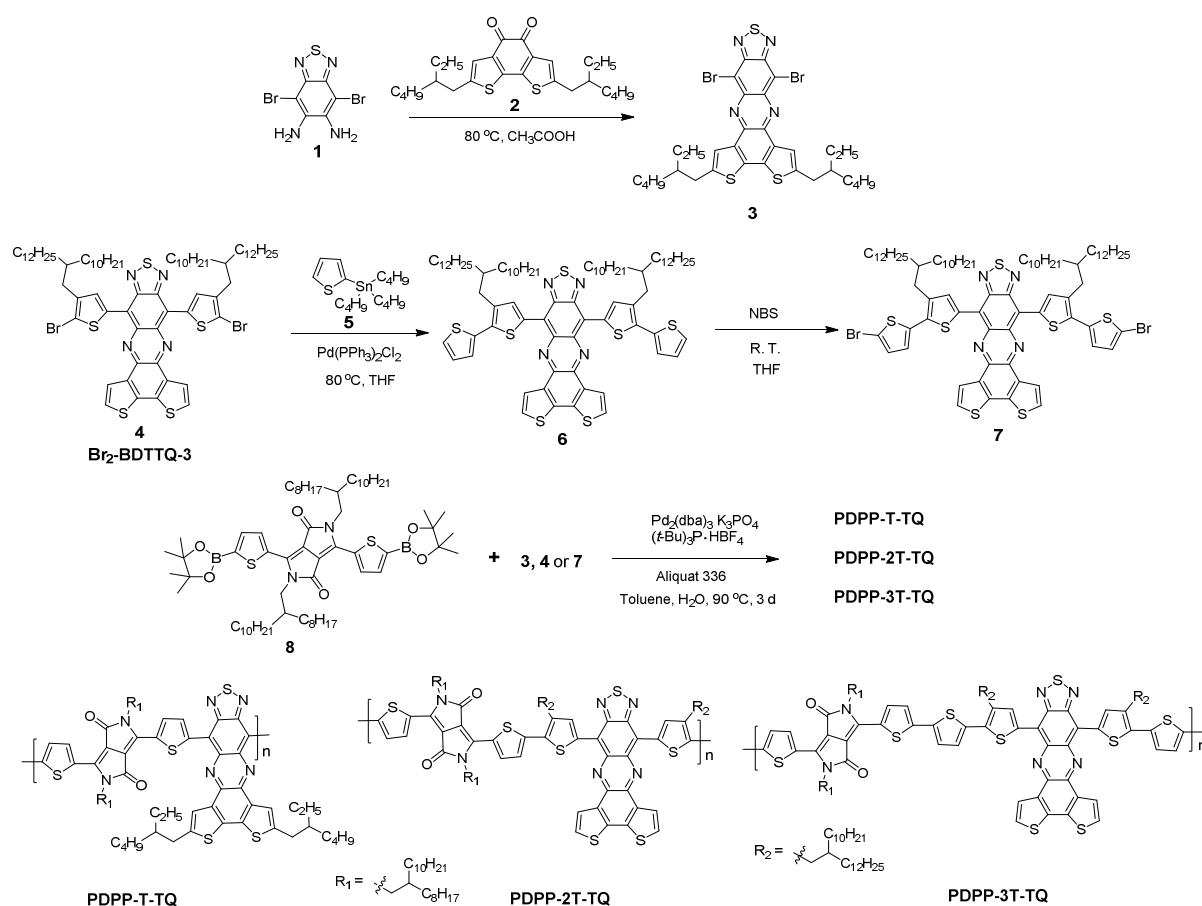
Scheme 6.1 Synthetic routes for the three polymers.

The synthesis of the three polymers is outlined in Scheme 6.1. In order to introduce different oligothiophenes between **DPP** and condensed **TQ** derivative, the three TQ precursors (**3**, **4** and **7**) were synthesized by flanking thiophenes onto condensed **TQ** at both sides. Monomer **3** was synthesized from 4,7-dibromobenzo[c][1,2,5]thiadiazole-5,6-diamine (**1**) and 7-bis(2-ethylhexyl)benzo[2,1-b:3,4-b']dithiophene-4,5-dione (**2**) via a condensation reaction. Monomer **4** was obtained as description in Chapter 4. Monomer **7** was prepared from **Br$_2$-BDTTQ-3** after two-steps reaction, Stille coupling and bromination. Suzuki coupling reactions were carried out between precursors **3**, **4** and **7**, and 3,6-bis-(5-(4,4,5,5-tetramethyl-1,3,2-dioxaborolan-thiophen-2-yl))-N,N-bis(octyldodecyl)-1,4-dioxo-pyrrolo[3,4-c]pyrrole (**8**)[18] to give corresponding **PDPP-T-TQ**, **PDPP-2T-TQ** and **PDPP-3T-TQ**, respectively. The number-average molecular weight (M$_n$) and polydispersity index (PDI) of the three polymers were determined by GPC method using polystyrene as standard and tetrahydrofuran as eluent at 30 °C. The data are listed in Table 1. **PDPP-T-TQ** and **PDPP-2T-TQ** have the low M$_n$ of 7.4 and 7.3 kDa, respectively, which might arise from the low reaction activity and the steric hindrance preventing to produce higher M$_n$ during polymerization. Similar low M$_n$ (8.7 kg mol^{-1}) reported for **PDPP-BBT** (Figure 6.1).[15] After introducing one more electron-rich thiophene onto monomer **4** at both sides, the steric hindrance between **DPP** and compound **7** was reduced so that the **PDPP-3T-TQ** possessed a higher M$_n$ than the other two polymers.
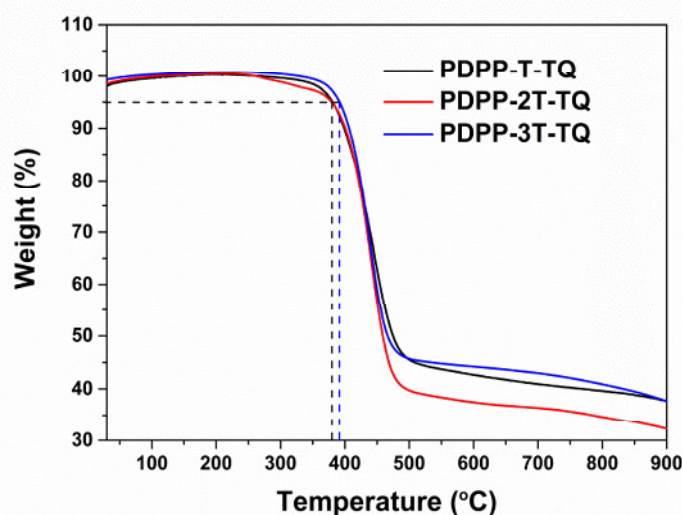
Figure 6.2 TGA curves for **PDPP-T-TQ, PDPP-2T-TQ** and **PDPP-3T-TQ** measured under a nitrogen atmosphere at a heating rate of 10 ºC/min.

The three polymers exhibited excellent solubility in common organic solvents such as chloroform and tetrahydrofuran at room temperature. Additionally, the thermal stability of three polymers was measured by thermogravimetric analysis (TGA) (Figure 6.2). They exhibited good stability with 5% weight loss up to 380 °C for **PDPP-T-TQ** and **PDPP-2T-TQ**, and 390 °C for **PDPP-3T-TQ**. When the temperature was raised to 500 °C, the side chains of three polymers were decomposed as previously discussed in Chapter 2.

6.3 Optical properties

UV-vis-NIR absorption spectra of the polymers were recorded in chloroform solutions (c = 10^{-5} M) as well as in films. The relevant data are summarized in Table 6.1. In dilute chloroform solutions, all polymers exhibit three absorption bands as shown in Figure 6.3a. The first intense band, between 300 and 500 nm, contains double peaks which were typical for many **TQ** polymers,[7,19,20] suggesting that this band could be contributed by the **TQ** moiety. The second one ranges from 500 to 800 nm, similar to the region of long wavelength absorption profile in **DPP**-based polymers,[21,22] it could origin from the intramolecular interaction between **DPP** and adjacent thiophene units. The last band broadly covers from 800 to 2250 nm, which was attributed to the intramolecular charge transfer (ICT) between donors and acceptors in the polymer main chains. **PDPP-T-TQ** exhibited inconspicuous **TQ** and **DPP** absorption characters but had a λ_{max} value up to 1343 nm, indicating a very strong ICT process within this polymer. Increasing the thiophene bridge to two units between the **DPP** and **TQ** led to a blue shift of 324 nm in λ_{max} for **PDPP-2T-TQ**. Meanwhile, the absorption profile is much more dominated by the **TQ** and **DPP** moieties. When introducing another thiophene between **DPP** and **TQ**, the λ_{max} of **PDPP-3T-TQ** further shifted to 970 nm and more remarkable **TQ** and **DPP** absorption features were observed. Thin films were prepared by drop-casting chloroform solutions of the three polymers onto glass slides. The films displayed slightly broadened spectra but with only small red-shifts of 1, 5 and 25 nm at λ_{max} compared with those in solutions (Figure 6.3b), indicating that the obvious red-shift occurs along with the increased backbone coplanarity of the polymers. The optical bandgaps of **PDPP-T-TQ**, **PDPP-2T-TQ** and **PDPP-3T-TQ** were calculated to be 0.60, 0.75 and 0.88 eV, according to the onset of solid absorption spectra, respectively, which stems from the electronic changes in the HOMO and LUMO (see DFT calculations). These results

demonstrate that changing the distance between **DPP** and **TQ** acceptors by the oligothiophene bridge length is an effective strategy for tuning the optoelectronic properties of the **DPP-TQ** dual-acceptor polymers.
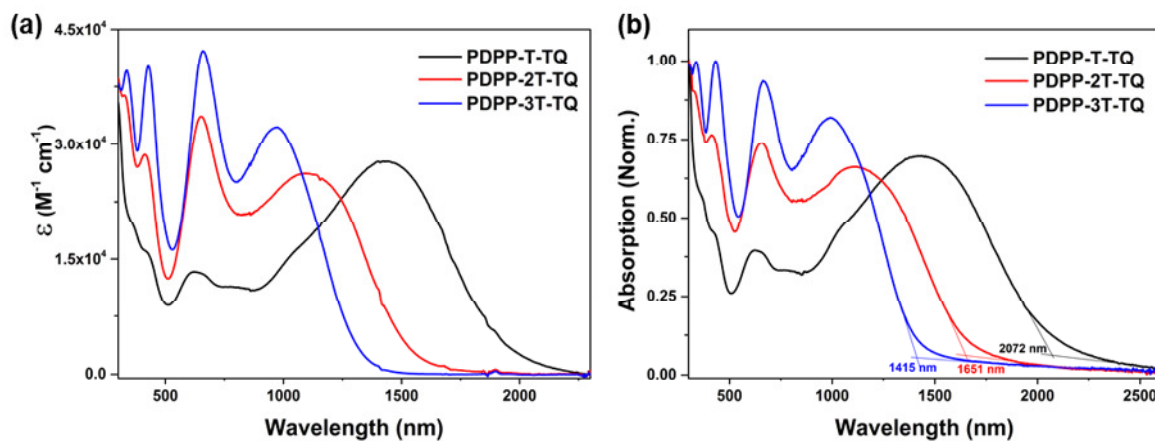
Figure 6.3 UV-visible-NIR absorption spectra of three polymers (a) in chloroform solutions and (b) in films.

6.4 Electrochemical properties

The electrochemical properties of three polymers were determined by cyclic voltammetry (CV). The films were drop-casted from chloroform solutions of these polymers onto glassy carbon electrode. Cyclic voltammograms of these polymers are presented in Figure 6.4. The corresponding data are summarized in Table 6.1. The electron affinities (EA) and ionization potentials (IP) of the polymers were calculated according the onset of first reduction and oxidation potentials.[23] The values of EA are -4.23, -4.13 and -4.07 eV for **PDPP-T-TQ**, **PDPP-2T-TQ** and **PDPP-3T-TQ**, respectively, while the corresponding IP values are -5.12, -5.06, and -5.08 eV. Interestingly, the different thiophene numbers can significantly alter the EA values compared to their similar IP values. The **PDPP-T-TQ** had a lowest EA level, which was related to its strongest ICT ability, led to a narrowest HOMO-LUMO bandgap among these three polymers. The electrochemical bandgap of three polymers were calculated to be 0.89, 0.93 and 1.01 eV for **PDPP-T-TQ**, **PDPP-2T-TQ** and **PDPP-3T-TQ**, respectively. It is the same tendency with their optical bandgap. The only difference is that the electronic

bandgaps are larger than their optical bandgaps, which is attributed to the exciton binding energy of conjugated polymers.[24]
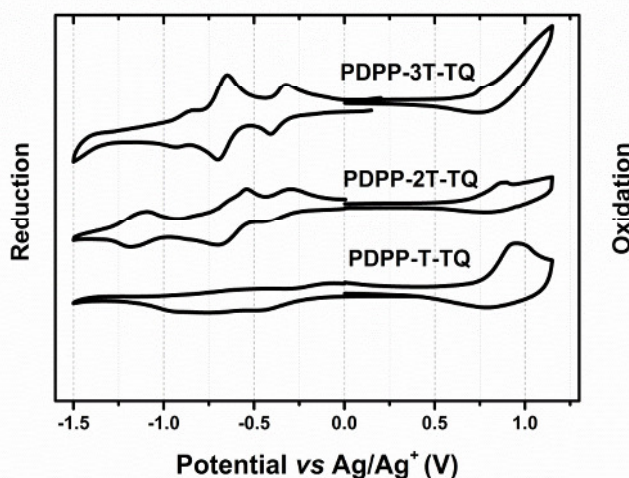
Figure 6.4 Cyclic voltammograms of **PDPP-T-TQ**, **PDPP-2T-TQ** and **PDPP-3T-TQ** in films.

Table 6.1 Molecular weights, decomposition temperature, optical absorption, electrochemical properties and field-effect mobilities of **PDPP-T-TQ**, **PDPP-2T-TQ** and **PDPP-3T-TQ**.

Polymer	M_w/M_n (kg/mol)[a]	T_d (°C)[b]	λ_{abs} (nm) soln.[c]	λ_{abs}(nm) film[d]	E_g^{opt} (eV)[d]	IP (eV)[e]	EA (eV)[e]	μ_h (cm^2 V^{-1} s^{-1})	μ_e (cm^2 V^{-1} s^{-1})
PDPP-T-TQ	26.3/7.4	380	1434	1435	0.60	-5.12	-4.23	2×10^{-5}	3×10^{-5}
PDPP-2T-TQ	23.1/7.3	380	1110	1115	0.75	-5.06	-4.13	1×10^{-5}	4×10^{-5}
PDPP-3T-TQ	43.9/13.2	390	970	995	0.88	-5.08	-4.07	5×10^{-4}	5×10^{-5}

[a]Determined by GPC in THF using polystyrene standards; [b]Temperature of decomposition corresponding to 5% weight loss from TGA analysis under N_2 with the heating rate of 10 °C/min; [c]Dissolved in chloroform (c = 10^{-5} M); [d]Drop-cast from chloroform solution (2 mg/mL); [e]IP and EA were estimated from the onsets of the first oxidation and reduction peak, while the potentials were determined using ferrocene (Fc) as standard by empirical formulas $E_{IP/EA} = - (E_{Ox/Red}^{onset} - E_{Fc/Fc+}^{1/2} + 4.8)$ eV, wherein $E_{Fc/Fc+}^{1/2} = 0.40$ eV.

6.5 OFET properties

In order to evaluate the charge transport properties of all three polymers, bottom-gate bottom-contact field effect transistors were fabricated in collaboration with ██████████

███████ (Max Planck Institute for Polymer Research, Mainz). All polymers were deposited by drop-casting 5 mg/mL chloroform solution on silicon/silicone dioxide (SiO_2) substrates in nitrogen atmosphere, followed by annealing at 150 °C for 1 h. The 300 nm thick SiO_2 dielectric covering the highly doped Si and acting as the gate electrode was functionalized with hexamethyldisilazane (HMDS) to minimize interfacial trapping sites.
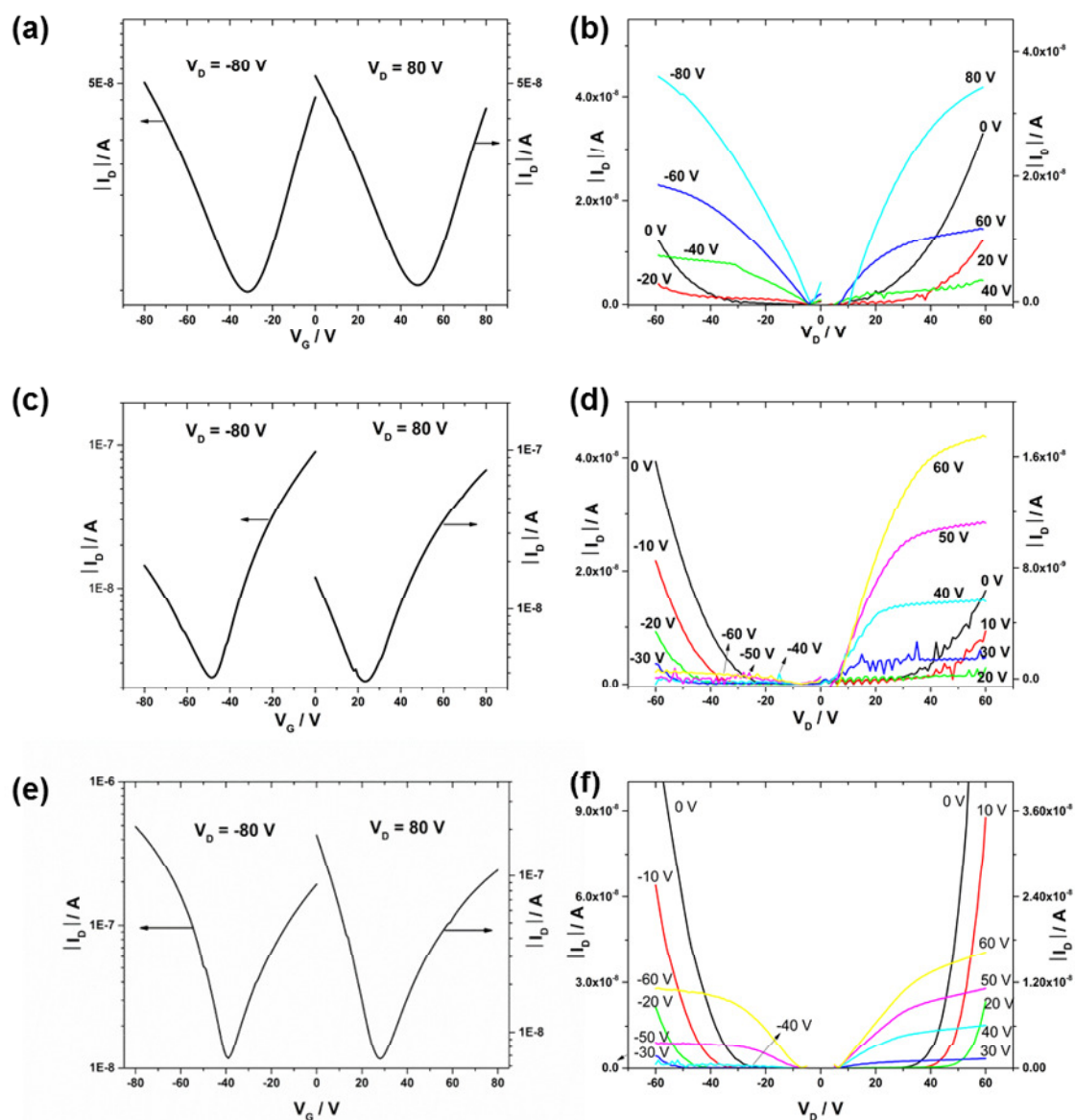
Figure 6.5 The transfer and output curves of (a and b) **PDPP-T-TQ**, (c and d) **PDPP-2T-TQ** and (e and f) **PDPP-3T-T**Q.

The transfer and output characteristics of three polymers are shown in Figure 6.5. The corresponding data are collected in Table 6.1. All the polymers exhibited ambipolar device

behavior. Polymer **PDPP-T-TQ** possessed balanced charge transport with hole and electron mobilities of 2×10^{-5} cm^2 V^{-1} s^{-1} and 3×10^{-5} cm^2 V^{-1} s^{-1}. One more thiophene units in the bridge between **DPP** and condensed **TQ** acceptors (**PDPP-2T-TQ**) did not influence polymer hole and electron mobility in comparison to **PDPP-T-TQ**. A significant difference in transport behavior was observed for **PDPP-3T-TQ**, which exhibited a hole-dominant ambipolar behavior with 5×10^{-4} cm^2 V^{-1} s^{-1} for holes and 5×10^{-5} cm^2 V^{-1} s^{-1} for electrons, the hole mobility was one order of magnitude higher than for the other polymers **PDPP-T-TQ** and **PDPP-2T-TQ**. These results implied that the thiophene bridge length between **DPP** and condensed **TQ** can transform the **DPP-TQ** based polymers from well-balanced ambipolar to hole-dominant ambipolar behavior. Additionally, for all polymers a contact resistance is observed in the transfer and output curves. This effect is probably caused by the disorder at the semiconductor/electrode interface which significantly reduces the injection of the charge carriers from metal electrode to the active layers.

6.6 Self-organization in films

To understand the molecular organization of **PDPP-T-TQ**, **PDPP-2T-TQ** and **PDPP-3T-TQ** in thin films, grazing incident X-ray wide angle scattering (GIWAXS) was carried out in collaboration with █████████████████ (Max Planck Institute for Polymer Research, Mainz). For these measurements the same procedure for the film preparation was used as for the transistor devices. Figure 6.6 presents the GIWAXS patterns of the three polymers**.** The GIWAXS patterns revealed slight variations between **PDPP-T-TQ** and **PDPP-2T-TQ**. For both polymers, an interlayer distance of 1.60 nm and 2.17 nm was determined from the position of the main reflection in small-angle range. The larger interlayer spacing for **PDPP-2T-TQ** was directly related to longer side chains. The isotropic distribution of these reflections suggested a lack of long-range order and a random arrangement of the crystallites towards the surface. A characteristic π-stacking reflection was missing indicating a disordered organization of the polymer chains within the layer structures. In contrast, the GIWAXS pattern of **PDPP-3T-TQ** (Figure 6.6c) exhibited more distinct reflections. In the small-angle region, the maximum intensity of the reflection was located on the equatorial plane of the pattern, whereby an interlayer distance of 2.65 nm was found. This reflection position in the

pattern was indicative for a face-on orientation of the polymer on the surface. This conclusion was verified by the appearance of a π-stacking scattering intensity on the meridional plane at q = 1.7 Å^{-1} (0.36 nm). The π-stacking reflection implied a better order arrangement of thin films for **PDPP-3T-TQ** in comparison to the other two polymers. This was the main reason that **PDPP-3T-TQ** has better charge carrier mobilities. However, it could not provide an explanation why increasing the thiophene bridge length made the polymer transformation from well-balanced ambipolar to hole-dominant ambipolar behavior. Therefore, density functional theory (DFT) calculations were carried out.
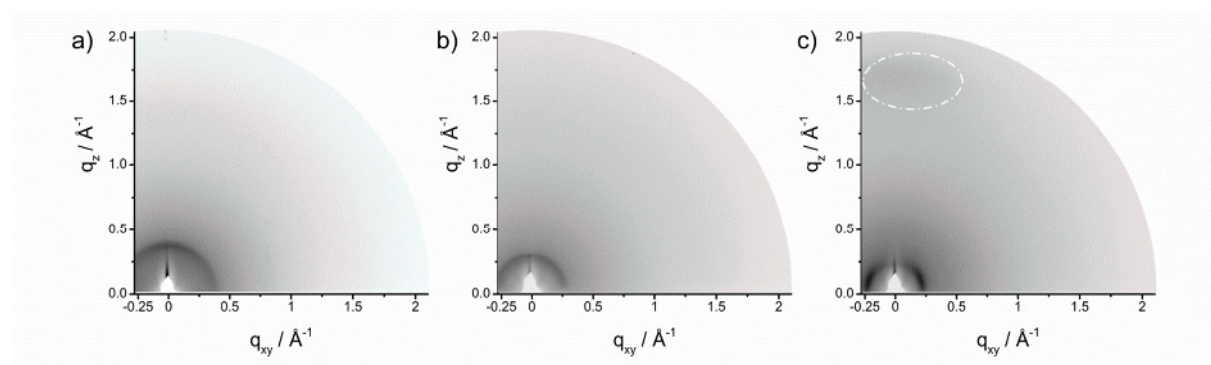
Figure 6.6 GIWAXS patterns of a) **PDPP-T-TQ**, b) **PDPP-2T-TQ** and c) **PDPP-3T-TQ** thin films. Reflections corresponding to π-stacking are indicated by dashed circles.

6.7 Density functional theory calculations

DFT calculations were carried out based one repeat unit of polymer, named **DPP-T-TQ**, **DPP-2T-TQ** and **DPP-3T-TQ**, carrying methyl substituents. The electron density distributions of the LUMO and HOMO of geometry optimized structures are shown in Figure 6.7. All HOMO levels of three monomeric units were very similar with delocalization over the conjugated repeat unit. However, the electron density distribution decreased in LUMO levels of the **DPP** segment as we increased thiophene bridge length. As found in previous discussion in Chapter 2, the distribution of electron density in HOMO and LUMO levels of polymers are very important for their hole and electron carrier mobilities. Therefore, the electron density of **DPP-3T-TQ** was further reduced in its LUMO levels, it can be explained why hole charge transport was dominant in this polymer. In addition, the results from DFT calculations were well consistent with the observations from CV results, demonstrating that the thiophene bridge length can significantly alter the EA in comparison with IP. It can hence

be concluded that the thiophene bridge length not only tune the organization behavior in thin films but also can strongly influence the ratio of electron and hole carrier mobilities.
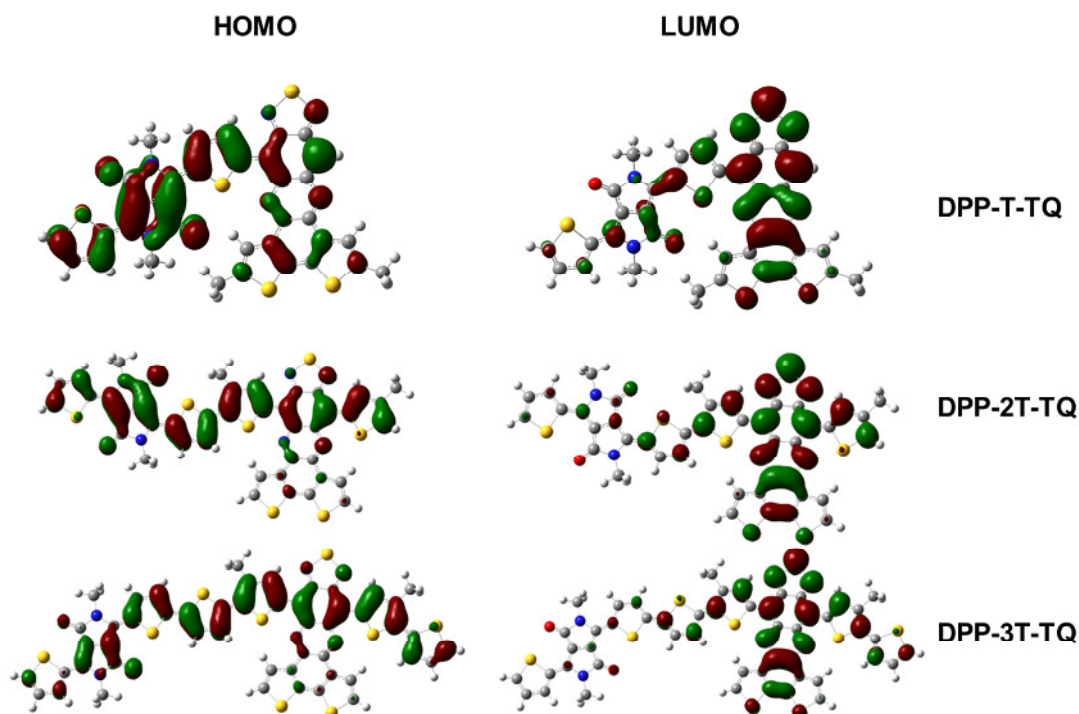
Figure 6.7 DFT calculation (B3LYP, 6-31G), the electron density distribution on one repeat unit of **PDPP-T-TQ, PDPP-2T-TQ** and **PDPP-3T-TQ.**

6.8 Summary

In this chapter, we have successfully synthesized three D-A1-D-A2 architecture polymers with very low optical bandgaps. The two acceptors of these polymers were separated by one, two and three thiophenes. Three polymers exhibited excellent thermal stability and solubility. These polymers possessed very low optical bandgaps, in particular, the optical band gap of **PDPP-T-TQ** achieved 0.60 eV! To the best of our knowledge, it is one of lowest optical bandgap among TQ-based polymers. By increasing the thiophene bridge length between both acceptors, the optical bandgaps of polymers were significant enlarged.

The cyclic voltammetry indicated their high electron affinity (from -4.07 to -4.23 eV), they are deeper than their single acceptor based polymers. From polymers **PDDP-2T-TQ** to

PDPP-3T-TQ, although the intramolecular charge transfer abilities of polymers were decreased, the coplanarities of polymers were significantly improved as confirmed by GIWAXS. **PDPP-3T-TQ** exhibited a hole-dominant ambipolar behavior with 5×10^{-4} cm^2 V^{-1} s^{-1} for holes and 5×10^{-5} cm^2 V^{-1} s^{-1} for electrons, the hole mobility is one order of magnitude higher than for the other polymers **PDPP-2T-TQ**. These results implied improvement of coplanarity of polymer is more important than enhancement of ICT of polymers in improving the molecular charge transport.

6.9 Synthetic details

The intermediate compounds 4,7-dibromobenzo[c][1,2,5]thiadiazole-5,6-diamine (**1**),[25] 2,7-bis(2-ethylhexyl)benzo[2,1-b:3,4-b']dithiophene-4,5-dione (**2**) and Br$_2$-BDTTQ-3 (**4**) were according to Chapter 2 and 4. 3,6-bis-(5-(4,4,5,5-tetramethyl-1,3,2-dioxaborolan-thiophen-2-yl))-N,N-bis(octyldodecyl)-1,4-dioxo-pyrrolo[3,4-c] pyrrole (**8**) were prepared according to the literature procedure as shown in scheme below.
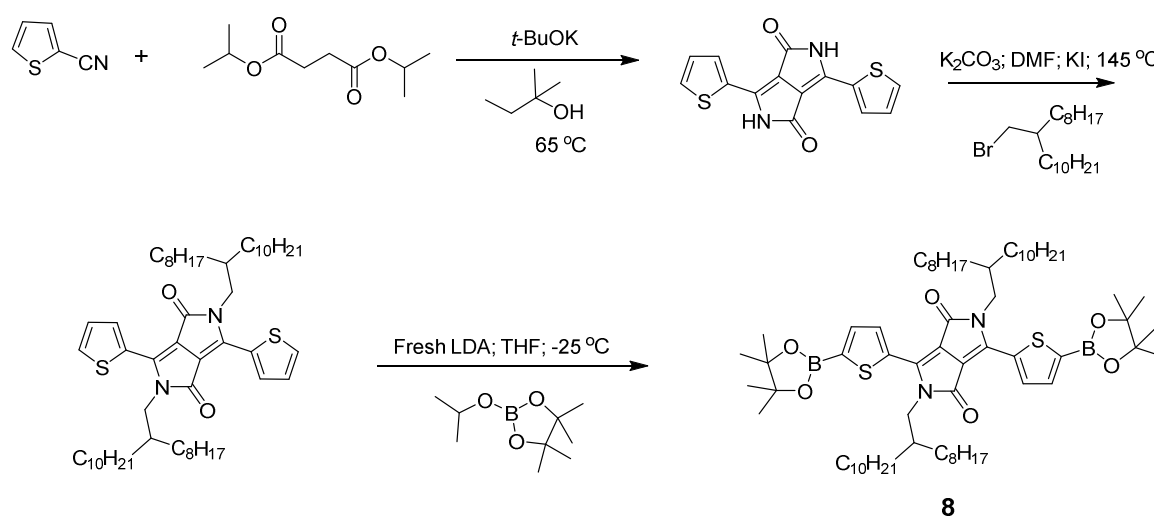
Scheme 6.2 Synthetic route for compound **8**.[18,26]

8,12-Dibromo-2,5-bis(2-ethylhexyl)-[1,2,5]thiadiazolo[3,4-i]dithieno[3,2-a:2',3'-c]phenazine (3)
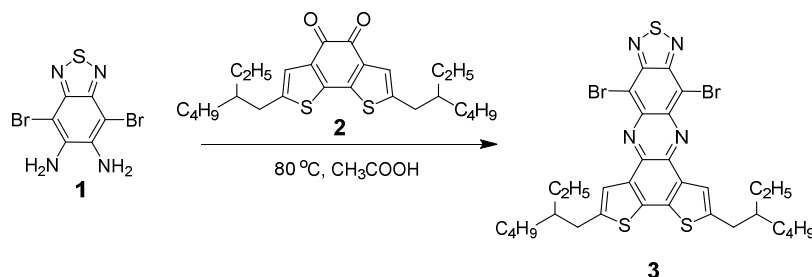
A suspension of **1** (0.40 g, 1.23 mmol), **2** (0.55 g, 1.23 mmol) and 35 mL acetic acid were placed into a 50 mL Schlenk tube. The mixture was heated to 80 ℃ and stirred overnight. After cooling to room temperature, the product was filtered and washed with methanol, then purified by column using hexane/dichloromethane (2:1) as eluent to give 0.77 g of compound **3** (dark green solid, 85%). ^{1}H NMR (250 MHz, CD$_2$Cl$_2$) δ 8.03 (s, 2H), 3.00 (dd, J = 2.5 Hz, J = 5.0 Hz, 4H), 1.76 (m, 2H), 1.41 (br, 16H), 0.95 (br, 12H). ^{13}C NMR (62.5 MHz, CDCl$_3$) δ 151.65, 145.10, 142.45, 137.39, 137.66, 133.30, 123.47, 113.40, 41.74, 34.87, 32.63, 29.09, 25.76, 23.19, 14.35, 11.03. HRMS (ESI+): m/z calcd 731.0547, found 731.0541.

8,12-bis(3-(2-decyltetradecyl)-[2,2'-bithiophen]-5-yl)-[1,2,5]thiadiazolo[3,4-i]dithieno[3,2-a:2',3'-c]phenazine (6)
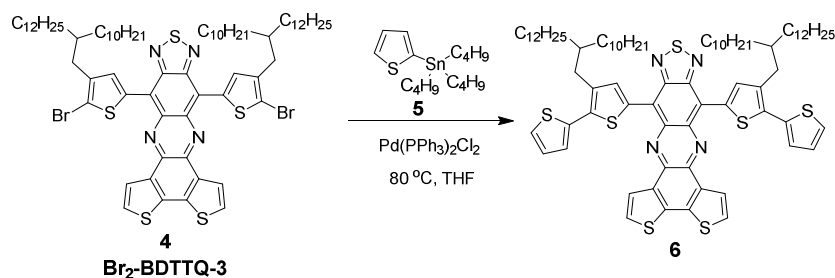
Br$_2$-BDTTQ-3 (**4**, 0.35g, 0.26 mmol), 2-tributylstanylthiophene (**5**, 0.30 g, 0.78 mmol) and Pd(PPh$_3$)$_2$Cl$_2$ (21 mg, 0.026 mmol) were dissolved in 15 mL of anhydrous THF under argon. The resulting solution was stirred for 16 h at 80 °C. The solvent was removed under reduced pressure to afford a dark-red oil, which was purified by column chromatography using hexane/dichloromethane (4:1) as eluent to give 0.29 g (dark-green solid, 82%) of

compound **6**. ^{1}H NMR (250 MHz, CD$_2$Cl$_2$, ppm) δ 8.62 (s, 2H), 7.79 (d, J = 5.0 Hz, 2H), 7.33 (t, J = 5.0 Hz, J = 2.5 Hz, 2H), 7.08 (m, 6H), 2.67 (d, J = 7.50 Hz, 4H), 1.80 (m, 2H), 1.38-1.23 (m, 80H), 0.89-0.84 (m, 12H). ^{13}C NMR (62.5 MHz, CD$_2$Cl$_2$, ppm) δ 150.67, 138.82, 137.89, 137.85, 137.77, 137.72, 137.04, 134.68, 134.45, 134.35, 127.92, 126.88, 125.29, 125.13, 124.40, 119.14, 38.77, 34.43, 33.77, 32.40, 32.37, 30.76, 30.32, 30.28, 30.25, 30.20, 30.15, 29.87, 29.83, 26.82, 23.13, 14.33. HRMS (ESI+): m/z calc. 1351.6854, found 1351.6850.

8,12-bis(5'-bromo-3-(2-decyltetradecyl)-[2,2'-bithiophen]-5-yl)-[1,2,5]thiadiazolo[3,4-i]dithieno[3,2-a:2',3'-c]phenazine (7)
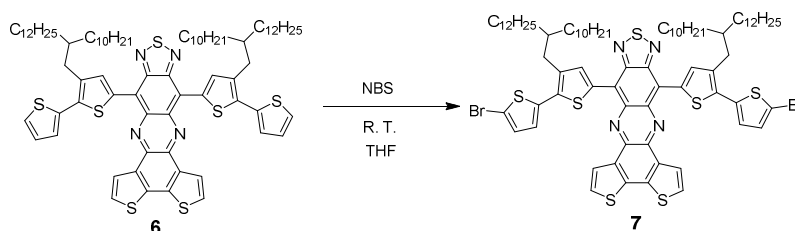
Compound **6** (0.25 g, 0.18 mmol) was dissolved in 15 mL THF at the room temperature. NBS (72.4 mg, 0.41 mmol) was carefully added into the solution in small batches under dark. The mixture was stirred for 5 h. After removing the solvent under reduced pressure, the residue was purified by column chromatography using hexane/dichloromethane (4:1) as eluent to give monomer **7** as a dark-green solid (0.24 g, 86%). ^{1}H NMR (250 MHz, CD$_2$Cl$_2$) ^{1}H NMR (250 MHz, THF-d_8, ppm) δ 8.66 (s, 2H), 7.93 (d, J = 5.0 Hz, 2H), 7.38 (d, J = 5.0 Hz, 2H), 7.11 (d, J = 2.5 Hz, 2H), 6.92 (d, J = 5.0 Hz, 2H), 2.67 (d, J = 7.50 Hz, 4H), 1.81 (br, 2H), 1.39-1.22 (m, 80H), 0.88-0.83 (m, 12H). ^{13}C NMR (62.5 MHz, THF-d_8, ppm) δ 150.97, 139.75, 139.48, 138.51, 138.13, 138.10, 137.79, 137.27, 135.12, 134.94, 131.38, 127.24, 126.00, 125.44, 119.47, 112.10, 39.21, 34.84, 34.22, 32.76, 32.73, 31.11, 30.67, 30.62, 30.57, 30.51, 30.24, 30.19, 27.26 (overlap by THF-d_8) 23.41, 14.33. HRMS (ESI+): m/z calcd 1507.5063, found 1507.5059.

Synthesis of PDPP-T-TQ
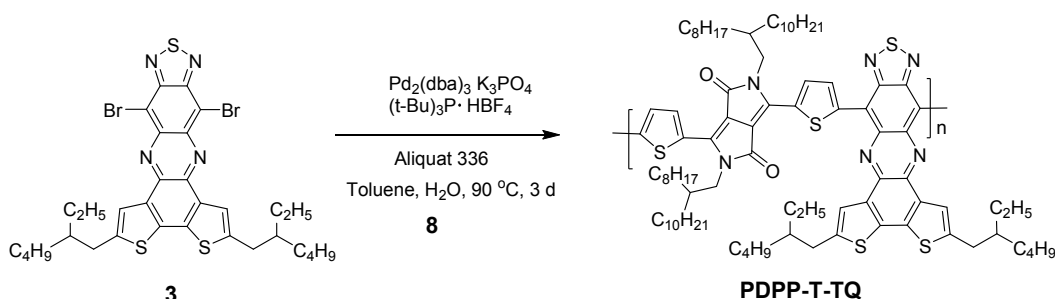
To a solution of monomer **3** (0.05 mmol) and diboronyl ester-**DPP** (**8**, 0.05 mmol), tri-tertbutylphosphoniumtetrafluoborate ((t-Bu)$_3$P·HBF$_4$, 0.0067 mmol), tris(dibenzylideneacetone)dipalladium(0) (Pd$_2$(dba)$_3$, 0.00335 mmol) and aliquat 336 (2 drops) in 6 mL of toluene was added a solution of potassium phosphate (0.074 g, 0.35 mmol) in 0.46 mL of degassed water. The mixture was vigorously stirred at 90 °C for 3 days. The polymer was end-capped with phenyl units by adding phenyl boronic acid and bromobenzene in sequence. After cooling to room temperature, the reaction mixture was poured into vigorously stirred methanol (100 mL). The polymer was filtered and subjected to Soxhlet extraction with methanol, acetone and hexane. The hexane fraction was collected and added 30 mL of sodium diethyldithiocarbamate aqueous solution (1g/100 mL) to remove residual palladium catalyst, the mixture was heated to 60 °C with vigorous stirring for 2 h. The mixture was separated and organic phase was washed with water for 3 times. The hexane solution was concentrated and precipitated in methanol. The resulting solid was collected by filtration and dried in vacuum to afford black solid (55 mg, 77%). Molecular weight by GPC (30 °C): M$_n$ = 7.4 kg mol^{-1}, PDI = 3.54. Elemental analysis: Calcd. for C$_{86}$H$_{122}$N$_6$O$_2$S$_5$: C 72.12, H 8.59, N 5.87, S 11.19; found: C 72.00, H 8.82, N 5.92, S 10.92.

Synthesis of **PDPP-2T-TQ** and **PDPP-3T-TQ**

PDPP-2T-TQ and **PDPP-3T-TQ** were prepared using monomer **4** and **7** instead of monomer **3** in similar procedure and workup to **PDPP-T-TQ**.

4
Br$_2$-BDTTQ-3
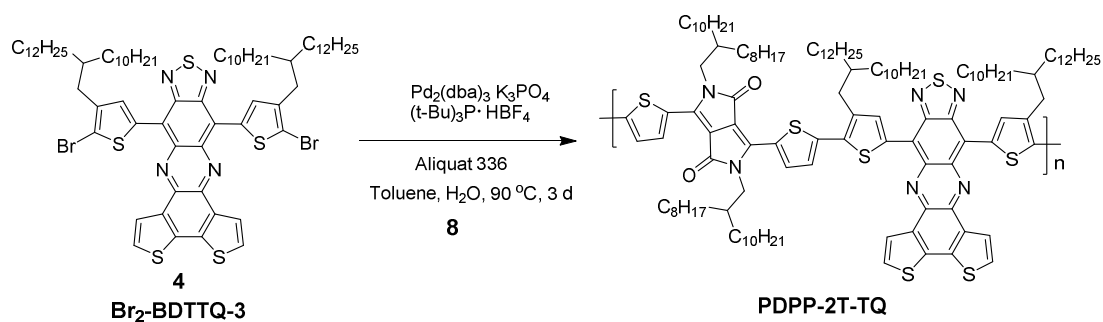
PDPP-2T-TQ

PDPP-2T-TQ (black solid, 75 mg, 74%). Molecular weight by GPC (30 °C): M$_n$ = 7.3 kg mol^{-1}, PDI = 3.18. Elemental analysis: Calcd. for C$_{126}$H$_{190}$N$_6$O$_2$S$_7$: C 73.99, H 9.36, N 4.11, S 10.97; found: C 73.60, H 9.65, N 3.99, S 10.92.

4
Br$_2$-BDTTQ-3
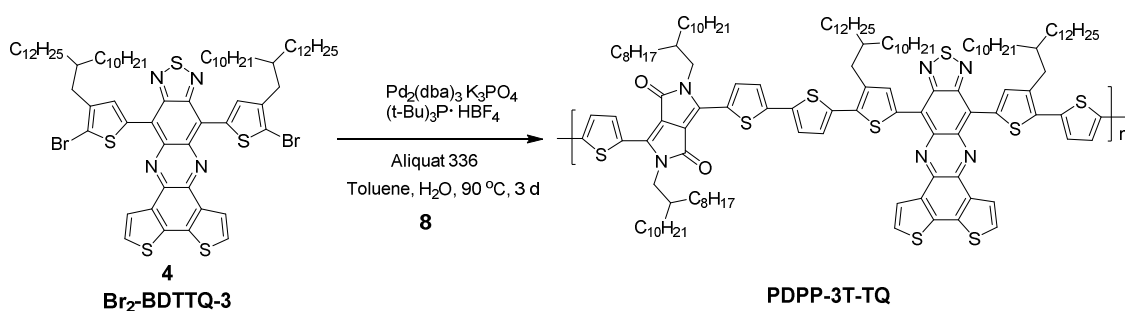
PDPP-3T-TQ

PDPP-3T-TQ (black solid, 88 mg, 80%). Molecular weight by GPC (30 °C): M$_n$ = 13.2 kg mol^{-1}, PDI = 3.31. Elemental analysis: Calcd. for C$_{134}$H$_{194}$N$_6$O$_2$S$_9$: C 73.84, H 8.85, N 3.80, S 13.06; found: C 72.55, H 9.15, N 3.73, S 12.88.

6.10 References

(1) Skotheim, T. A.; Reynolds , J. R. *Handbook of conducting polymers, Third ed.; Conjugated Polymers: Theory, Synthesis, Properties, and Characterization*; CRC press LLC: Boca Raton, FL, 2007.

(2) Wudl, F.; Kobayashi, M.; Heeger, A. J. *J. Org. Chem.,* **1984**, *49*, 3382-3384.

(3) Brédas, J. L.; Heeger, A. J.; Wudl, F. *J. Chem. Phys.,* **1986**, *85*, 4673-4678.

(4) Yuen, J. D.; Kumar, R.; Zakhidov, D.; Seifter, J.; Lim, B.; Heeger, A. J.; Wudl, F. *Adv. Mater.,* **2011**, *23*, 3780-3785.

(5) Fan, J.; Yuen, J. D.; Cui, W. B.; Seifter, J.; Mohebbi, A. R.; Wang, M. F.; Zhou, H. Q.; Heeger, A.; Wudl, F. *Adv. Mater.,* **2012**, *24*, 6164-6168.

(6) Fan, J.; Yuen, J. D.; Wang, M. F.; Seifter, J.; Seo, J. H.; Mohebbi, A. R.; Zakhidov, D.; Heeger, A.; Wudl, F. *Adv. Mater.,* **2012**, *24*, 2186-2190.

(7) Steckler, T. T.; Henriksson, P.; Mollinger, S.; Lundin, A.; Salleo, A.; Andersson, M. R. *J. Am. Chem. Soc.,* **2014**, *136*, 1190-1193.

(8) Yun, H.-J.; Choi, H. H.; Kwon, S.-K.; Kim, Y.-H.; Cho, K. *Chem. Mater.,* **2014**, *26*, 3928-3937.

(9) Bürgi, L.; Turbiez, M.; Pfeiffer, R.; Bienewald, F.; Kirner, H.-J.; Winnewisser, C. *Adv. Mater.,* **2008**, *20*, 2217-2224.

(10) Sonar, P.; Singh, S. P.; Li, Y.; Soh, M. S.; Dodabalapur, A. *Adv. Mater.,* **2010**, *22*, 5409-5413.

(11) Cho, S.; Lee, J.; Tong, M.; Seo, J. H.; Yang, C. *Adv. Funct. Mater.,* **2011**, *21*, 1910-1916.

(12) Ashraf, R. S.; Kronemeijer, A. J.; James, D. I.; Sirringhaus, H.; McCulloch, I. *Chem. Commun.,* **2012**, *48*, 3939-3941.

(13) Kronemeijer, A. J.; Gili, E.; Shahid, M.; Rivnay, J.; Salleo, A.; Heeney, M.; Sirringhaus, H. *Adv. Mater.,* **2012**, *24*, 1558-1565.

(14) Sonar, P.; Foong, T. R. B.; Singh, S. P.; Li, Y. N.; Dodabalapur, A. *Chem. Commun.,* **2012**, *48*, 8383-8385.

(15) Yuen, J. D.; Fan, J.; Seifter, J.; Lim, B.; Hufschmid, R.; Heeger, A. J.; Wudl, F. *J. Am. Chem. Soc.,* **2011**, *133*, 20799-20807.

(16) Lee, J.; Han, A. R.; Yu, H.; Shin, T. J.; Yang, C.; Oh, J. H. *J. Am. Chem. Soc.,* **2013**, *135*, 9540-9547.

(17) Chen, Z. Y.; Lee, M. J.; Ashraf, R. S.; Gu, Y.; Albert-Seifried, S.; Nielsen, M. M.; Schroeder, B.; Anthopoulos, T. D.; Heeney, M.; McCulloch, I.; Sirringhaus, H. *Adv. Mater.,* **2012**, *24*, 647-652.

(18) Guo, X.; Puniredd, S. R.; Baumgarten, M.; Pisula, W.; Müllen, K. *Adv. Mater.,* **2013**, *25*, 5467-5472.

(19) Dexter Tam, T. L.; Salim, T.; Li, H.; Zhou, F.; Mhaisalkar, S. G.; Su, H.; Lam, Y. M.; Grimsdale, A. C. *J. Mater. Chem.,* **2012**, *22*, 18528-18534.

(20) Keshtov, M. L.; Marochkin, D. V.; Kochurov, V. S.; Khokhlov, A. R.; Koukaras, E. N.; Sharma, G. D. *Poly. Chem.,* **2013**, *4*, 4033-4044.

(21) Li, W.; Roelofs, W. S. C.; Wienk, M. M.; Janssen, R. A. J. *J. Am. Chem. Soc.,* **2012**, *134*, 13787-13795.

(22) Son, S. K.; Kim, B. S.; Lee, C.-Y.; Lee, J. S.; Cho, J. H.; Ko, M. J.; Lee, D.-K.; Kim, H.; Choi, D. H.; Kim, K. *Sol. Energy Mater. Sol. Cells,* **2012**, *104*, 185-192.

(23) Bredas, J.-L. *Mater. Horiz.,* **2014**, *1*, 17-19.

(24) Sariciftci, N. S. *Primary Photoexcitations in Conjugated Polymers:Molecular Excitons vs Semiconductor Band Model; World Scientific: Singapore, 1997.*

(25) Li, H.; Zhou, F.; Tam, T. L. D.; Lam, Y. M.; Mhaisalkar, S. G.; Su, H.; Grimsdale, A. C. *J. Mater. Chem. C,* **2013**, *1*, 1745-1752.

(26) Huo, L.; Hou, J.; Chen, H.-Y.; Zhang, S.; Jiang, Y.; Chen, T. L.; Yang, Y. *Macromolecules,* **2009**, *42*, 6564-6571.

Chapter 7. Condensed Derivatives of Thiadiazoloquinoxaline as Strong Acceptors
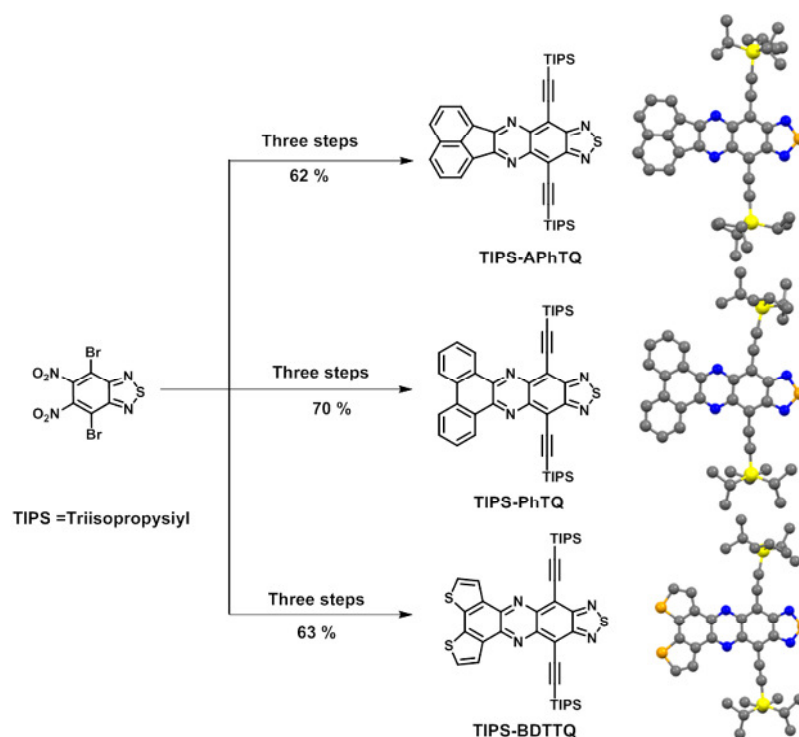
In this chapter, three novel condensed thiadiazoloquinoxaline (TQ) derivatives, **TIPS-APhTQ**, **TIPS-PhTQ** and **TIPS-BDTTQ**, were synthesized by introducing two triisopropylsilylethynyl groups and upon altering the aromatic-ring units in the condensed moiety of TQ. The synthetic route is very efficient providing high yields. Cyclic voltammetry suggested high electron affinity value of them. Single crystal X-ray diffraction revealed that three molecules form corresponding dimers by intermolecular S-N interaction and have very similar two-dimensional (2D) π stacking. The π-stacking distance of them are as close as 3.34-3.46 Å.

Note: Large part of this chapter has been published in *Cryst. Growth Des.*, **2015**, *15*, 1934-1938.

7.1 Introduction

Since the first report on the synthesis of [1,2,5]thiadiazolo[3,4-*g*]quinoxalines (TQs)[1] as an *o*-quinoid strong acceptor unit, this buliding block has been explored in conjugated D-A copolymers for electronics.[2-4] In chapter 4 and 5, we have synthesized and studied three condensed TQ-based polymers as shown in Figure 7.1. They exhibited excellent ambipolar behaviour in OFET. Interestingly, GIWAX measurements suggested that **PAPhTQ** displayed more orderly morphology than **PBDTTQ-3**, while **PPhTQ** showed the best orderly arrangment among these three copolymers. It should be attributed to their different TQ cores, considering that the structures of three copolymers differ only in condensed TQ cores. Therefore, the fundamental question arised as to whether it is possible to design and synthesize new TQ monomers with strong crystallization ability, meanwhile they only differ in these three TQ cores. In the past few years, TQs have been widely expanded by the condensation reaction,[5-8] but the crystal structures of TQs with analysis of the molecular ordering were rarely reported and studied. It is thus vital to develop new TQ small molecules and study their π-π stacking in these crystals. Additionally, developing new TQ materials is also important to broaden our understanding of their characteristics.
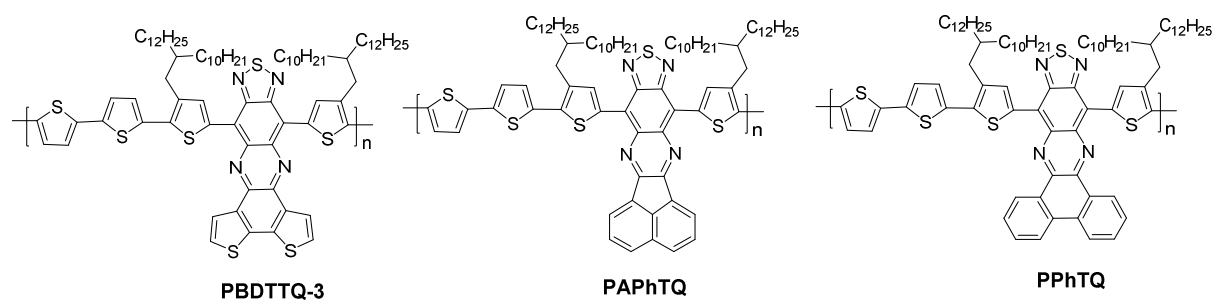
Figure 7.1 Condensed TQ-based copolymers in our previous work.

Introducing triisopropylsilyl (TIPS)-ethynyl groups has proven to be successful not only in improving solubility and stability of acenes and heteroacenes, but also in enhancing their capability for π-stacked arrays.[9-12] Two familiar methods were used to introduce TIPS-ethynyl groups into acenes and heteroacenes. The first is the nucleophilic addition of TIPS-ethynyl anion, which proceeds via the corresponding dione precursors.[9,13] The second method is the

Sonogashira coupling reaction which is carried out between the (triisopropylsilyl)acetylene and corresponding dibromo precursors.[14] The first method was employed and produced a TQ molecule with four TIPS-ethynyl groups (Scheme 7.1, **B1**) by Bunz and his coworkers. The problem here is that the dione precursor had a complex synthetic procedure from commercial material 1, 4-dimethoxybenzene as shown in Scheme 7.1.[15,16] Recently, substituted benzene condensed TQ (Scheme 7.2, **B2**) with strong π-π stacking were reported, although the steps of synthesis were signifiacntly reduced, the step of introducing the TIPS-ethynyl group was only achieved in a yield of 21%.[17,18] Previously, our group also grafted the ethynyl groups into a TQ core by a Sonogashira coupling reaction between 2-ethylnylthiophene and dibromo TQ molecules as shown in Scheme 7.3. However, as a drawback after the coupling reaction was finished, the palladium acted as a hydrogen-transfer catalyst, reducing the triple bonds.[19,20] It is, therefore, still a challenge to introduce TIPS-ethynyl groups into TQs aromatic backbone to promote strong π-π stacking structures.
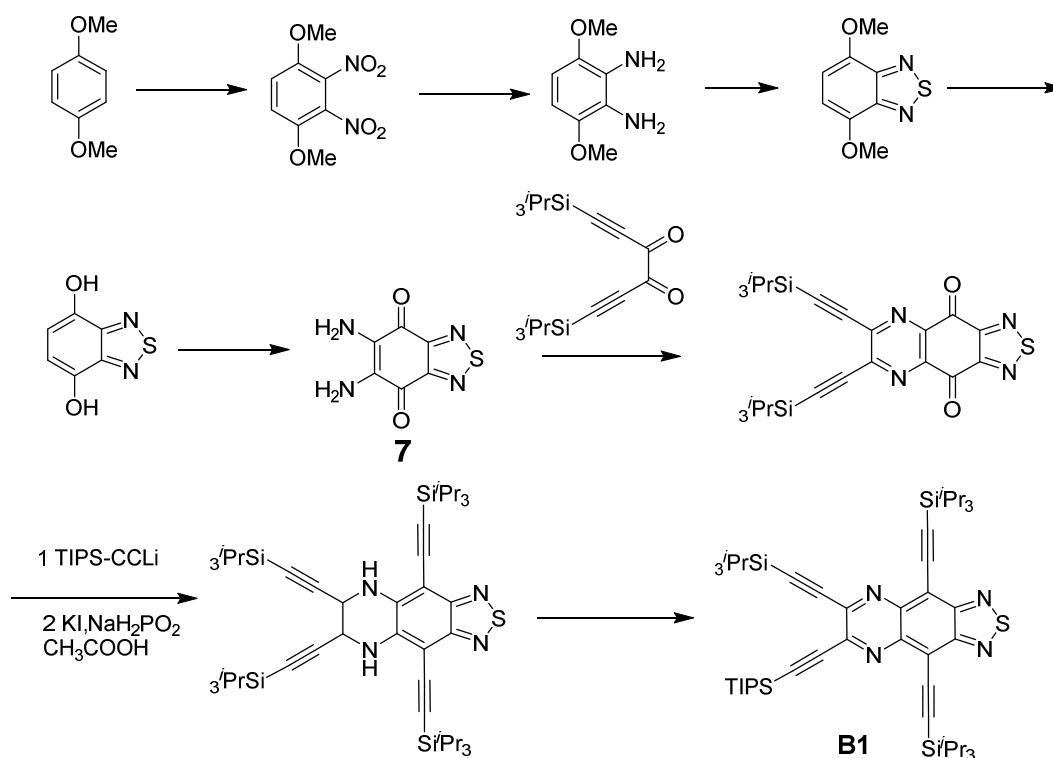
Scheme 7.1 Synthesis route of compound **B1**.
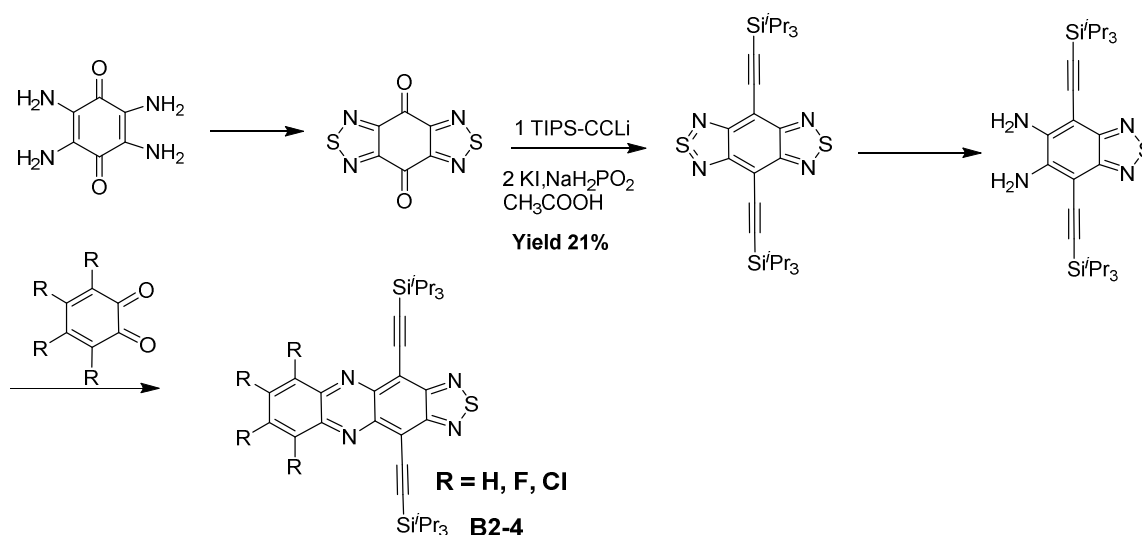
Scheme 7.2 Synthesis route of compounds **B2-4**.
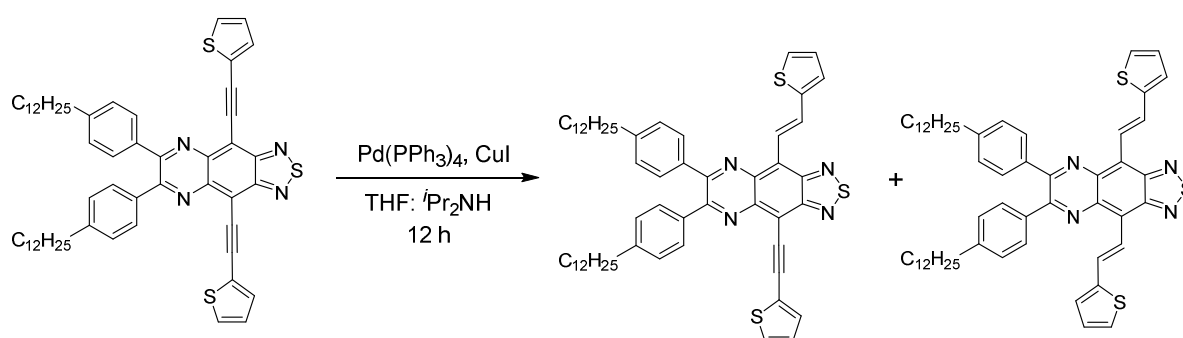
Scheme 7.3 The route of reducing the triple bonds in TQ molecules.

In this chapter, we describe the synthesis and characterization of TQ derivatives with a pair of TIPS-ethynyl groups, **TIPS-APhTQ**, **TIPS-PhTQ** and **TIPS-BDTTQ** (Scheme 7.4), which are attached to the TQ core by acenaphthylene, phenanthrene and benzo[2,1-b:3,4-b']dithiophene (**BDT**) groups, respectively. A new approach is first used to graft TIPS-ethynyl groups onto the 4,7-dibromo-5,6-dinitrobenzothiadizole (**1**) precusor. The ease of synthesis and information about their π-π stacking structures are appealing features of this study.

7.2 Synthesis and characterization
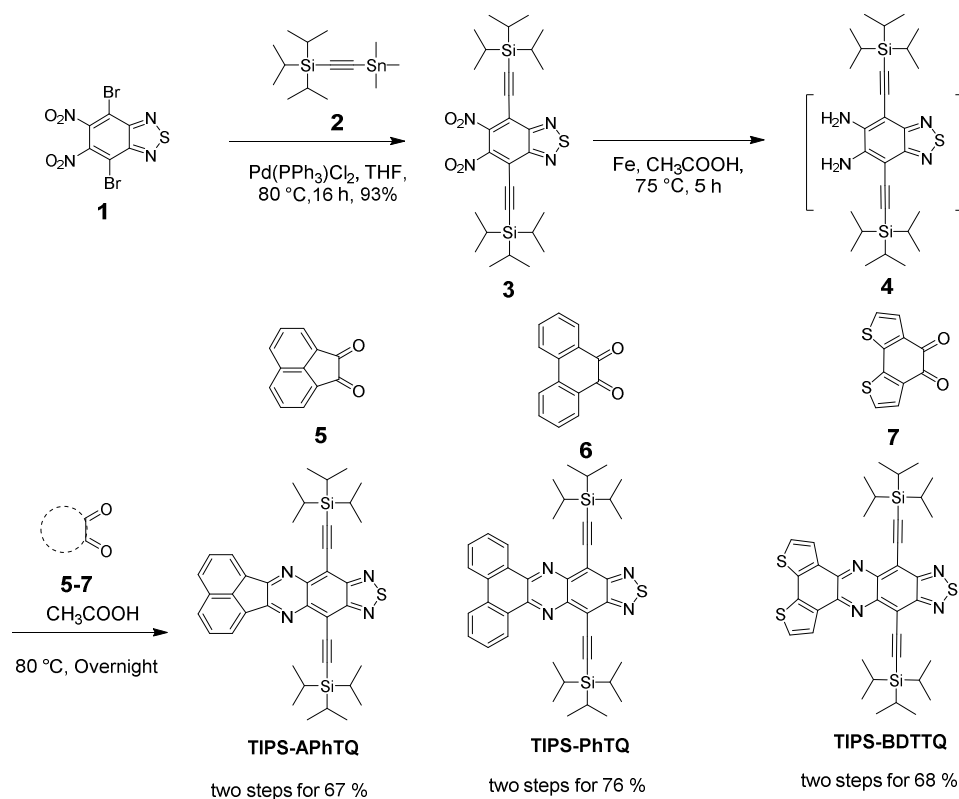
Scheme 7.4 Synthesis of **TIPS-APhTQ**, **TIPS-PhTQ** and **TIPS-BDTTQ**.

A facile synthetic route is illustrated in Scheme 7.4 for the three target molecules. The 4,7-dibromo-5,6-dinitrobenzothiadizole (**1**) was synthesized from commercial 4,7-dibromo benzothiadizole,[21] which was reacted with 1-trimethylstannyl-2-triisopropylsilylethyne (**2**)[22] by Stille coupling to produce compound **3** in high yield of 93%. After reduction, the corresponding diamine **4** was obtained, which was directly converted via a condensation with the corresponding diones **5**-**7** without purification to give the desired final molecules **TIPS-APhTQ**, **TIPS-PhTQ**, and **TIPS-BDTTQ**, respectively. In our previous methods,[19] a key issue was that diisopropylammonium salt can provide a hydrogen source for reducing triple bonds in Sonogashira coupling under palladium catalyst involvement. While it is impossible to find hydrogen source for reducing triple bonds in Stille coupling, it thereby avoids the reduction of the triple bonds. In combination with good yields, it is easy to achieve gram scale for these three compounds. Additionally, these molecules have good solubility in common organic solvents (>10 mg/mL in dichloromethane) and exhibit excellent thermal stability as shown in Figure 7.2, with 5% weight loss upon heating up to 360 °C for **TIPS-APhTQ** and

TIPS-PhTQ, and 380 °C for **TIPS-BDTTQ**.
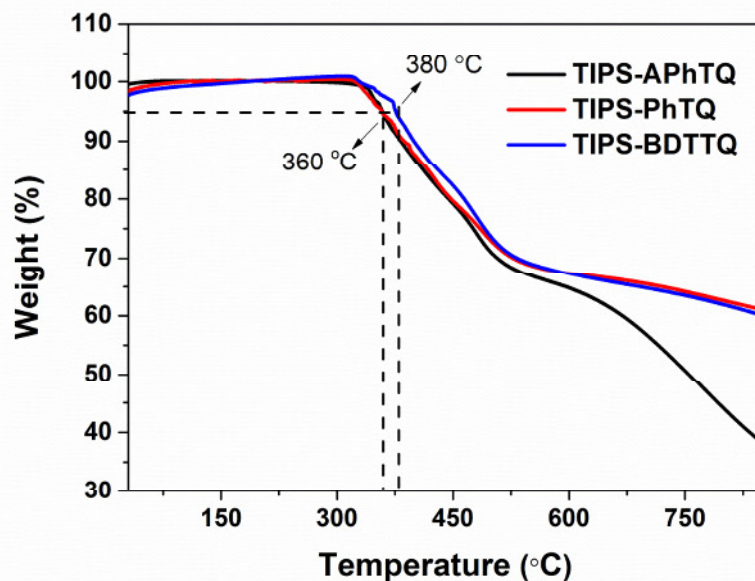
Figure 7.2 TGA curves for **TIPS-APhTQ**, **TIPS-PhTQ** and **TIPS-BDTTQ** measured under a nitrogen atmosphere at a heating rate of 10 ºC/min.

7.3 Optical properties

The absorption and emission spectra of these three molecules were recorded in dilute dichloromethane solution (c= 10^{-5} M, Figure 7.3) and the corresponding data are summarized in Table 7.1. The absorption profile of the three molecules is composed of three absorption band regions, which are designated as band I, II and III in Figure 7.3. The first band covers from 250 to 390 nm. The band II is between 340 and 515 nm. The last band ranges from 460 to 685 nm. The absorption profiles of these molecules are similar to the *β, p* and *α* bands of polycyclic hydrocarbons as described by Clar.[23,24] The bands I and II are attributed to the π-π* and n-π* transitions of the conjugated aromatic segments.[25] In the band III, the absorption maximum (λ_{max}) was red-shifted from **TIPS-APhTQ** (544 nm), **TIPS-PhTQ** (592 nm), to **TIPS-BDTTQ** (632 nm). Considering that three molecules differ only in the aromatic-ring units, this is attributed to the fused aromatic structures, led to different electron delocalization and conjugation within the extended fused-ring system. The fused aromatic units also strongly affect the molecular optical gaps, which were 2.17, 2.00 and 1.86 eV for **TIPS-APhTQ**, **TIPS-PhTQ** and **TIPS-BDTTQ**, respectively, as determined from the absorption onset of the

dichloromethane solutions. From acenaphthylene to phenanthrene, the optical gap is reduced by 0.17 eV. It can be further reduced by 0.14 eV upon introducing **BDT** to replace phenanthrene. This is in agreement with corresponding **APhTQ**, **PhTQ** and **BDTTQ** containing polymers, the optical gaps of them were reduced by 0.23 eV from acenaphthylene to **BDT** unit (Chapter 4 and 5). However, no significant changes in the long wavelength absorption coefficients were observed.
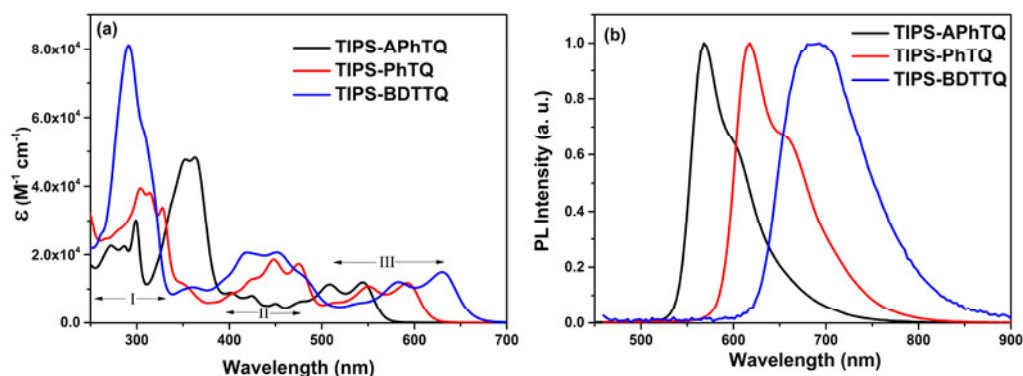
Figure 7.3 UV-vis absorption (a) and fluorescence (b) spectra of **TIPS-APhTQ**, **TIPS-PhTQ** and **TIPS-BDTTQ** in dichloromethane.

The three molecules demonstrate a corresponding bathochromic shift in their solution emission curves (Figure 7.3b). Emission quantum yields decreased within the series from **TIPS-APhTQ** (Φ_{em} = 0.25), **TIPS-PhTQ** (Φ_{em} = 0.14) to **TIPS-BDTTQ** (Φ_{em} = 0.03). Attaching a **BDT** group into the TQ core significantly reduced the fluorescence quantum yield due to efficient intersystem crossing induced by the heavy atom effect of sulfur.[26] The Stokes shifts are 26 nm for **TIPS-APhTQ** and **TIPS-PhTQ**, and 51 nm for **TIPS-BDTTQ.** These values are far smaller than those of nonplanar conjugated TQ, which were flanked by two tetraphenylethene moieties due to their rigid planar conjugated structures.[27]

7.4 Electrochemical properties

The electron affinities (EA) of these three molecules were studied by cyclic voltammetry (CV).[28] The corresponding data are collected in Table 7.1. All three compounds exhibited two reversible reduction peaks in dichloromethane solution (Figure 7.4). The EA values of the molecules were calculated from the onset of the first reduction peak. The acenaphthylene

containing **TIPS-APhTQ** had the highest EA value (-3.82 eV), while **TIPS-PhTQ** has additional two π-electrons in comparison to **TIPS-APhTQ**. As a result, **TIPS-PhTQ** displays a lower potential of reduction, with EA value of -3.95 eV. The extension of the conjugated TQ core via thiophene-enriched **BDT** group (**TIPS-BDTTQ**) provided the lowest EA value of -3.99 eV. These results suggest that by attaching different fused-ring groups the electron deficient nature of the TQ molecules can be easily tuned. This is the same sequence as for our previously reported monomers **APhTQ** (-3.73 eV), **PhTQ** (-3.84 eV) and **BDTTQ-3** (-3.92 eV) in Chapter 4 and 5.
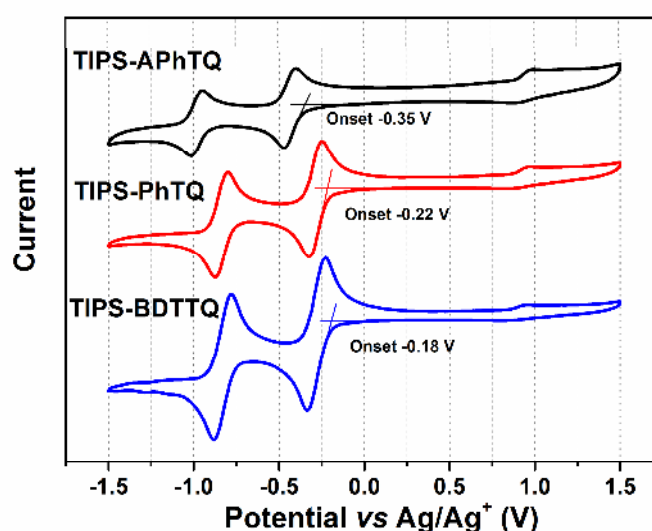
Figure 7.4 The cyclic voltammograms of three compounds in dichloromethane.

Table 7.1 Photophysical and electrochemical properties of three compounds.

Compounds	Band I (nm) [a]	Band II (nm) [a]	Band III (nm) [a]	λ_{abs} / nm (log ε)[a]	λ_{em} / nm [a,b] (Φem)[b]	Stokes shift / nm	EA / eV [c]
TIPS-APhTQ	250-390	395-460	460-580	544 (4.08)	570 (0.25)	26	-3.82
TIPS-PhTQ	250-380	385-500	500-630	592 (4.07)	618 (0.14)	26	-3.95
TIPS-BDTTQ	250-335	340-515	530-685	632 (4.17)	683 (0.03)	51	-3.99

[a]Dissolved in dichloromethane (c = 10^{-5} M); [b] Excitation wavelengths for the emission measurements are 514, 488 and 451 nm for **TIPS-APhTQ**, **TIPS-PhTQ** and **TIPS-BDTTQ**, respectively. In dichloromethane estimated by using the comparative method with fluorescein (0.1 M NaOH, Φ_{em} = 0.91 at 514 and 488 nm, 0.90 at 451 nm.),[29,30] [c]EA were estimated from the onsets of the first reduction peaks, while the potentials were determined using ferrocene (Fc) as standard by empirical formulas E_{EA} = - ($E_{Red\ onset}$- $E_{Fc/Fc+(1/2)}$+4.8) eV , wherein $E_{Fc/Fc+(1/2)}$ = 0.63 eV.

7.5 Density functional theory calculations

In order to combine these results with theoretical predictions, the density functional theory (DFT, B3LYP, 6-31G) calculations were carried out as shown in Figure 7.5. The DFT calculations provided the LUMO levels of -3.58, -3.77 and -3.92 eV, and the energy gaps (ΔE_g(LUMO-HOMO)) of 2.19, 1.98, 1.79 eV for **TIPS-APhTQ**, **TIPS-PhTQ** and **TIPS-BDTTQ**, respectively. These results demonstrate that theoretical predictions exhibit the same tendency as the experimental data by analyzing LUMO *vs* EA, and ΔE_g(LUMO-HOMO) *vs.* E_{opt}. It is beneficial for us to predict the electronic properties for such new TQ derivatives in line with the experimental finding.
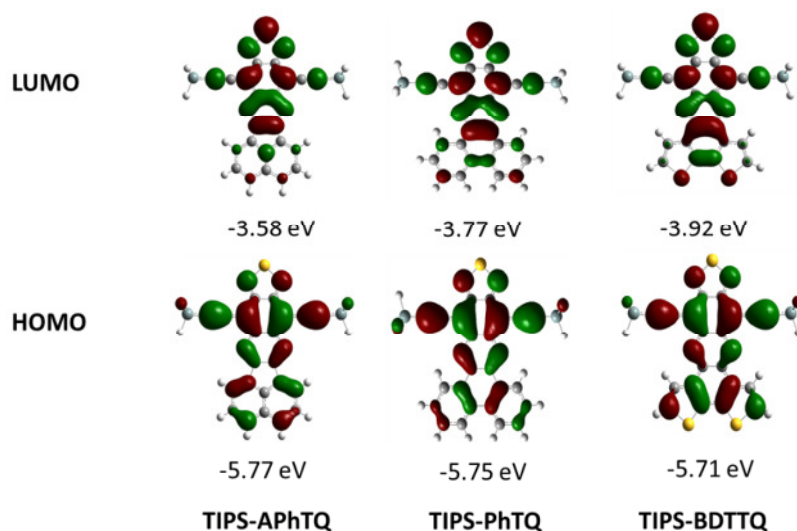
Figure 7.5 DFT (B3LYP, 6-31g) calculation of LUMO and HOMO levels of **TIPS-APhTQ**, **TIPS-PhTQ** and **TIPS-BDTTQ,** the isopropyl groups were replaced by hydrogens.

7.6 Crystal packing properties

Single crystal analysis of molecules is a vital requirement to understand their electron structure properties. The crystals of three molecules were obtained by slow evaporation from dichloromethane at room temperature. The X-ray crystal structure analysis was carried out by ███████████████ (Johannes Gutenberg-University, Mainz). The X-ray crystallographic data for the molecules were collected on a STOE IPDS 2T diffractometer using a graphite monochromator Mo-Kα radiation source (**TIPS-APhTQ,**

TIPS-BDTTQ), and a Smart CCD difractometer using a graphite monochromator Mo-Kα radiation source (**TIPS-PhTQ**). The structures were solved by direct method (SIR-97) and refined by SHELXL-97 (full matrix)[31] 445 refined parameters (**TIPS-APhTQ**), 454 refined parameters (**TIPS-PhTQ**) and 436 refined parameters (**TIPS-BDTTQ**).
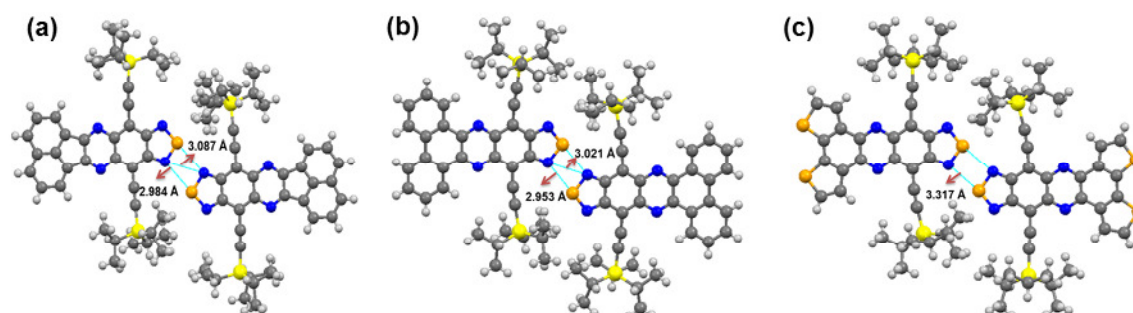
Figure 7.6 S-N and N-N distances of thiadiazole moietis of dimer for **TIPS-APhTQ (a)**, **TIPS-PhTQ (b)** and **TIPS-BDTTQ (c)**. Van der Waals radius: S 1.8 Å; N 1.55 Å.
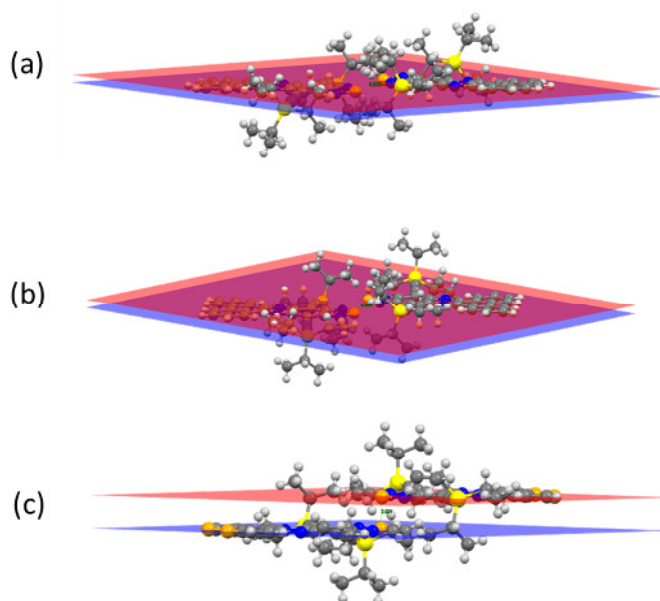
Figure 7.7 The vertical offset (red plane to blue plane) within the dimer 0.53 Å for **TIPS-APhTQ (a)**, 0.67 Å for **TIPS-PhTQ (b)** and 2.02 Å for **TIPS-BDTTQ (c)**.

These molecules showed dimer features by close head-to-head contacts of the thiadiazole moieties with N-S interaction, where the distances are shorter than the

combined van der Waals radii of sulfur and nitrogen (Figure 7.6). **TIPS-APhTQ** and **TIPS-PhTQ** also yield a weak N-N interaction, with the distances of 3.09 Å and 3.02 Å. The vertical offset with the dimers (Figure 7.7) was 0.53, 0.67 and 2.02 Å, for **TIPS-APhTQ**, **TIPS-PhTQ** and **TIPS-BDTTQ**, respectively. The significantly large intermolecular distance of **TIPS-BDTTQ**, might be attributed to its weak S-N interaction and the N-N interaction between adjacent thiadiazole moieties were lost.
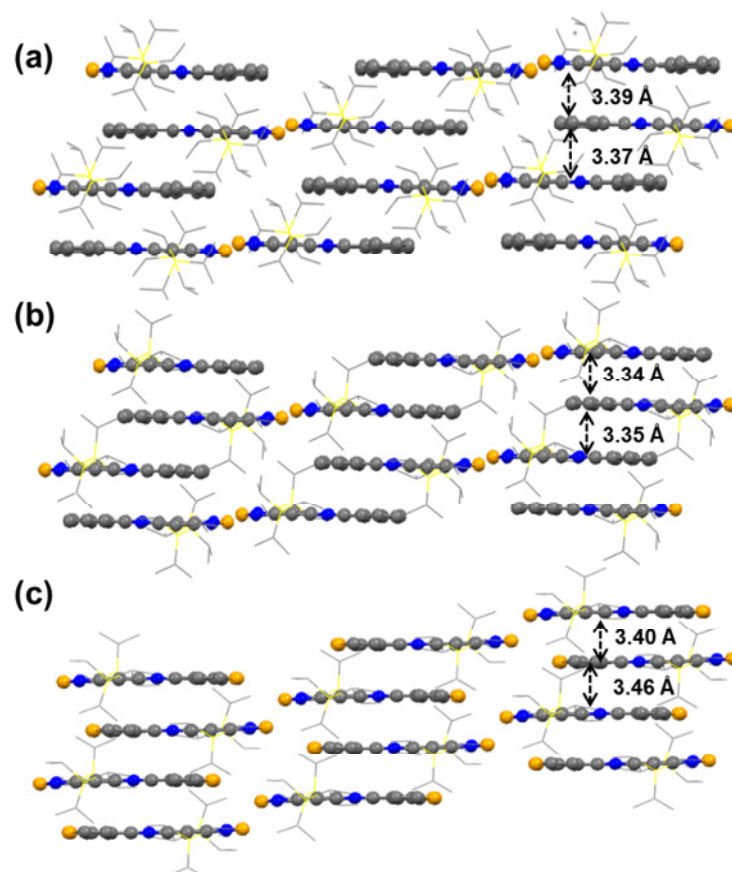
Figure 7.8 The packing of **TIPS-APhTQ** (a), **TIPS-PhTQ** (b), **TIPS-BDTTQ** (c). The TQ cores are shown with ball-stick models and the TIPS-ethynyl substituents are shown with wireframe models. Hydrogen atoms are removed for clarification. Carbon, nitrogen, sulfur and silicon atoms are shown in grey, blue, orange and yellow, respectively.

The packing of these three molecules was similar (Figure 7.8), due to the same unit cell. The dimers form a brick wall packing style. **TIPS-PhTQ** has the shortest π-stacking distances of 3.34 and 3.35 Å, suggesting it has the strongest π-π interaction. Introducing the acenaphthylene unit, slightly increases the π-π distances to 3.37 and

3.39 Å. The largest distances of 3.40 and 3.46 Å for **TIPS-BDTTQ** indicate that it possesses the weakest π-π interaction among these molecules. Grazing incidence wide angle X-ray scattering (GIWAXS) for our previous polymer systems revealed that **PAPhTQ** was slightly higher ordered in thin films than **PBDTTQ-3**. **PPhTQ** exhibited best ordered thin films. Considering the different substituents of polymers and monomer units the molecular packing may already be altered, and for sure there will be a difference between crystal packing and arrangement in thin films. Although the condensed TQ cores' π-stacking ability cannot provide direct evidence for the ordering of corresponding polymers, some correlation should exist for the same acceptor core between small molecules and corresponding polymers.

The bond lengths of extended benzene (green) in **TIPS-PhTQ** and **TIPS-BDTTQ** are obtained from their crystal analysis as shown in Figure 7.9. Compared to the benzene part of **TIPS-PhTQ**, the bonds C1-C2 and C3-C4 of benzene in **TIPS-BDTTQ** exhibit siginificant shortening, while other four bonds show slightly decrease. As a result, the average bond length alternation (BLA) of benzene in **TIPS-BDTTQ** (0.020 Å) is only a half of benzene in **TIPS-PhTQ** (0.042 Å). This result inplied the BDT group condensed TQ has stronger delocalization and conjugation within the extened fused-ring system than phenanthrene unit. This can then explain why **TIPS-BDTTQ** has a smaller optical gap than **TIPS-PhTQ**.
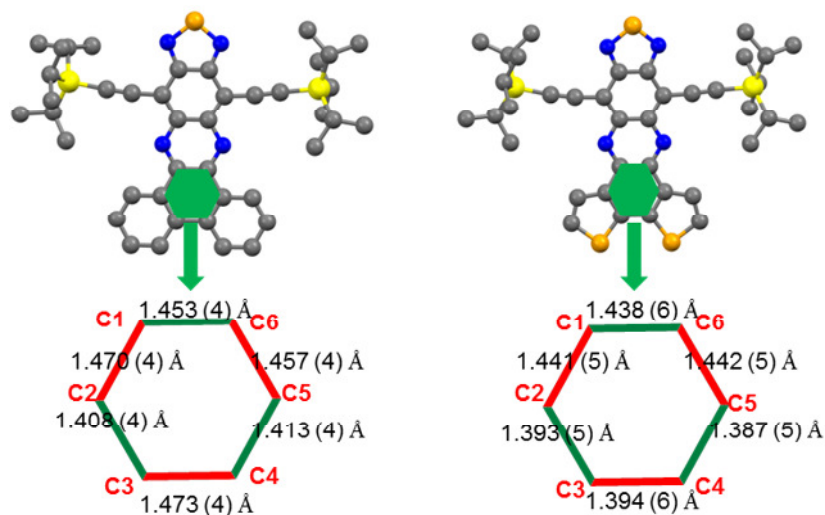
Figure 7.9 Experimental bond lengths for fused benzene of condensed TQs (**TIPS-PhTQ** and **TIPS-BDTTQ**)

7.7 Summary

We report a facile and highly efficient approach to synthesize three TQ derivatives with two TIPS-ethynyl groups, **TIPS-APhTQ**, **TIPS-PhTQ** and **TIPS-BDTTQ**, which had good solubility and high electron affinities. Changing the fused aromatic unit in the TQ core significantly affected the molecular opoelectronic properties and crystal packing. **TIPS-BDTTQ** possesses a very low EA value of -3.99 eV, without strong withdrawing groups like fluorine, chlorine and cyano groups. All three molecules demonstrate a brick wall packing motif through their dimer interactions. Among these molecules, **TIPS-PhTQ** possesses the shortest distances with 3.34 and 3.35 Å. On the other hand, it has to be emphasized that the key intermediate **3** could be reduced to the corresponding tetraamine, which is promising to synthesize centrosymmetric large azaacenes by condensation reaction with two equivalents of corresponding diones. Further investigation of such reactions are carried out in Chapter 8.

7.8 Synthetic details

Intermediates 4,7-dibromo-5,6-dinitro-2,1,3-benzothiadiazole (**1**) and benzo[2,1-b:3,4-b']dithiophene-4,5-dione (**8**) were prepared according to Chapter 2. 1-trimethylstannyl-2-triisopropysiylethyne (**2**)[22] was synthesized according to the literature procedure as shown in Scheme 7.5.
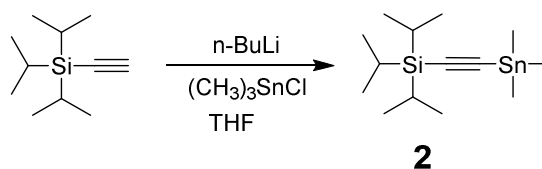
Scheme 7.5 Synthetic route for compound **2**.[22]

5,6-Dinitro-4,7-bis((triisopropylsilyl)ethynyl)benzo[c][1,2,5]thiadiazole (3)
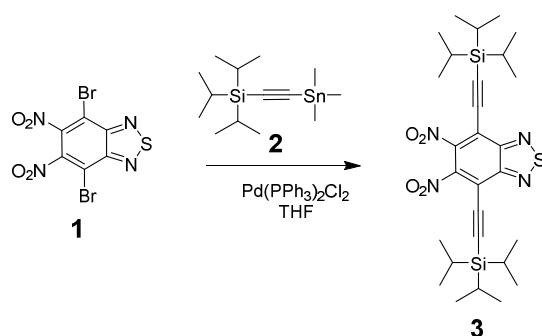
4,7-Dibromo-5,6-dinitrobenzothiadiazole (**1**, 1.23g, 3.2 mmol), compound **2** (2.55 g, 7.40 mmol), and Pd(PPh$_3$)$_2$Cl$_2$ (225 mg, 0.32 mmol) were dissolved in 40 mL of anhydrous THF under argon. The resulting solution was stirred at 80 °C for 16 h. After removal of the solvent, the crude product was purified by column chromatography using dichloromethane/ hexane (1:4) as the eluent to give 1.74 g (yellowish solid, 93%) of compound **3**. ^{1}H NMR (250 MHz, CD$_2$Cl$_2$, ppm) δ 1.19 (m, broad, 42H) ^{13}C NMR (175 MHz, CD$_2$Cl$_2$, ppm) δ 153.53, 146.05, 115.48, 113.07, 95.33, 18.73, 11.62. HRMS (ESI+ Na): m/z calc. 609.2363, found 609.2355.

General procedure for the preparation of TIPS-APhTQ, TIPS-PhTQ and TIPS-BDTTQ

A mixture of compound **3** (100 mg, 0.171 mmol) and fine iron powder (113 mg, 2.018 mmol) in acetic acid (10 mL) was stirred at 75 °C for 5 h under argon. The reaction mixture was poured into 50 mL of water after cooling to room temperature. Subsequently, the pH was adjusted to 6–7 using 5% aqueous NaOH. The solution was extracted with diethyl ether (3×20 mL). The combined organic layers were washed with brine, dried with MgSO$_4$. The solvent was removed under reduced pressure to give corresponding diamine **7** with deep red oil. This crude product was directly added into acetic acid (10 mL) solutions of corresponding diones (**5**-**7**, 0.256 mmol). The mixtures were heated to 80 °C overnight under argon. After cooling to room temperature, each mixture was poured into 100 mL 5% aqueous NaOH and extracted with dichloromethane (3×50 mL). The combined organic phases were dried with MgSO$_4$ and filtered. The solution was concentrated and purified by column chromatography eluting with hexane dichloromethane (from 4:1 to 2:1) to give corresponding final products.

8,12-Bis((triisopropylsilyl)ethynyl)acenaphtho[1,2-b][1,2,5]thiadiazolo[3,4-g]quinoxaline (**TIPS-APhTQ**)
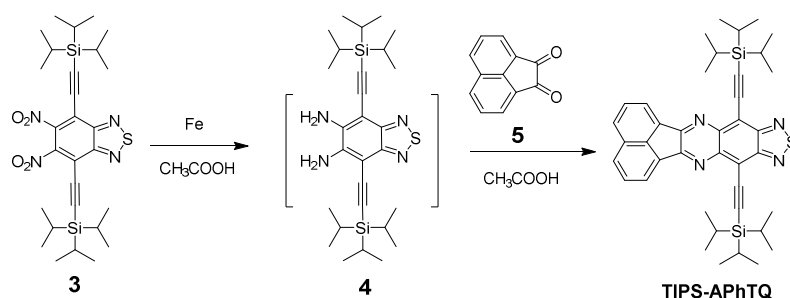
Red solid (77 mg, 67% for two steps), ^{1}H NMR (250 MHz, CD_2Cl_2, ppm) δ 8.41 (d, J = 5.0 Hz 2H), 8.22 (d, J = 7.5 Hz, 2H), 7.95 (dd, J = 7.5 Hz, J = 2.5 Hz, 2H), 1.34 (m, broad, 42H). ^{13}C NMR (62.5 MHz, CD_2Cl_2, ppm) δ 156.44, 154.61, 142.94, 139.94, 131.64, 130.74, 130.63, 129.42, 122.60, 115.16, 109.06, 101.66, 19.07, 11.99. HRMS (ESI+): m/z calc. 673.3217 found 673.3201.

10,14-Bis((triisopropylsilyl)ethynyl)dibenzo[a,c][1,2,5]thiadiazolo[3,4-i]phenazine (**TIPS-PhTQ**)
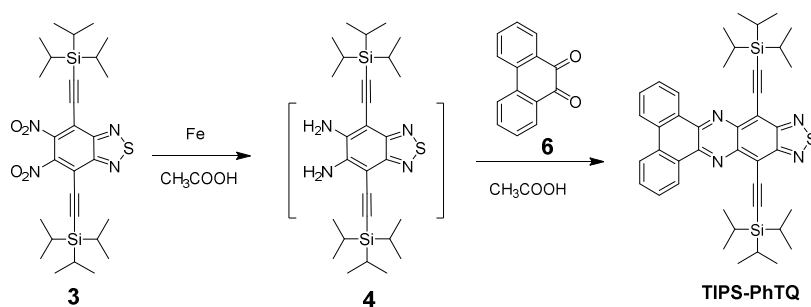
Deep red solid (91 mg, 76% for two steps), ^{1}H NMR (250 MHz, CD_2Cl_2, ppm) δ 9.49 (dd, J = 2.5 Hz, J = 2.5 Hz, 2H), 8.52 (d, J = 7.5 Hz, 2H), 7.88 (m, 2H), 7.73 (m, 2H), 1.35 (m, broad, 42H). ^{13}C NMR (62.5 MHz, CD_2Cl_2, ppm) δ 155.05, 145.48, 142.39, 133.48, 132.34, 130.36, 128.66, 127.76, 123.67, 114.42, 109.96, 102.09, 19.04, 12.03; HRMS (ESI+): m/z calc. 699.3373 found 699.3366.

8,12-Bis((triisopropylsilyl)ethynyl)-[1,2,5]thiadiazolo[3,4-i]dithieno[3,2-a:2',3'-c]phenazine (TIPS-BDTTQ)
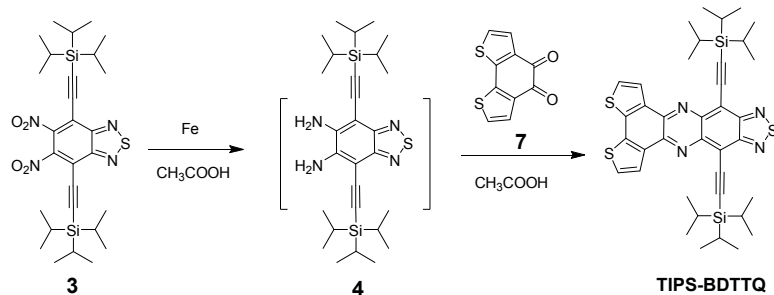
Dark green solid (90 mg, 74% for two steps), ^{1}H NMR (250 MHz, CD$_2$Cl$_2$, ppm) δ 8.45 (d, *J* = 5.0 Hz 2H), 7.63 (d, *J* = 5.0 Hz, 2H), 1.34 (m, broad, 42H). ^{13}C NMR (62.5 MHz, CD$_2$Cl$_2$, ppm) δ 154.94, 142.67, 141.81, 138.42, 135.16, 125.90, 125.61, 114.23, 110.27, 102.30, 19.09, 11.99. HRMS (ESI+): m/z calc. 711.2501 found 711.2491.

7.9 References

(1) Kitamura, C.; Tanaka, S.; Yamashita, Y. *Chem. Mater.,* **1996**, *8*, 570-578.

(2) Chen, M. X.; Crispin, X.; Perzon, E.; Andersson, M. R.; Pullerits, T.; Andersson, M.; Inganas, O.; Berggren, M. *Appl. Phys. Lett.,* **2005**, *87*, 252105.

(3) Zhang, X.; Steckler, T. T.; Dasari, R. R.; Ohira, S.; Potscavage, W. J.; Tiwari, S. P.; Coppee, S.; Ellinger, S.; Barlow, S.; Bredas, J.-L.; Kippelen, B.; Reynolds, J. R.; Marder, S. R. *J. Mater. Chem.,* **2010**, *20*, 123-134.

(4) Cheng, K.-F.; Chueh, C.-C.; Lin, C.-H.; Chen, W.-C. *J. Polym. Sci., Part A: Polym. Chem.,* **2008**, *46*, 6305-6316.

(5) Luo, M.; Shadnia, H.; Qian, G.; Du, X.; Yu, D.; Ma, D.; Wright, J. S.; Wang, Z. Y. *Chem. Eur. J.,* **2009**, *15*, 8902-8908.

(6) Li, H.; Tam, T. L.; Lam, Y. M.; Mhaisalkar, S. G.; Grimsdale, A. C. *Org. Lett.,* **2011**, *13*, 46-49.

(7) Tam, T. L.; Li, H.; Lam, Y. M.; Mhaisalkar, S. G.; Grimsdale, A. C. *Org. Lett.,* **2011**, *13*, 4612-4615.

(8) Li, H.; Zhou, F.; Tam, T. L. D.; Lam, Y. M.; Mhaisalkar, S. G.; Su, H.; Grimsdale, A. C. *J. Mater. Chem. C,* **2013**, *1*, 1745-1752.

(9) Anthony, J. E.; Brooks, J. S.; Eaton, D. L.; Parkin, S. R. *J. Am. Chem. Soc.,* **2001**, *123*, 9482-9483.

(10) Lindner, B. D.; Engelhart, J. U.; Tverskoy, O.; Appleton, A. L.; Rominger, F.; Peters, A.; Himmel, H.-J.; Bunz, U. H. F. *Angew. Chem. Int. Ed.,* **2011**, *50*, 8588-8591.

(11) Tang, M. L.; Reichardt, A. D.; Miyaki, N.; Stoltenberg, R. M.; Bao, Z. *J. Am. Chem. Soc.,* **2008**, *130*, 6064-6065.

(12) Tang, M. L.; Reichardt, A. D.; Wei, P.; Bao, Z. *J. Am. Chem. Soc.,* **2009**, *131*, 5264-5273.

(13) Miao, S.; Smith, M. D.; Bunz, U. H. F. *Org. Lett.,* **2006**, *8*, 757-760.

(14) He, Z.; Mao, R.; Liu, D.; Miao, Q. *Org. Lett.,* **2012**, *14*, 4190-4193.

(15) Miao, S.; Schleyer, P. V.; Wu, J. I.; Hardcastle, K. I.; Bunz, U. H. F. *Org. Lett.,* **2007**, *9*, 1073-1076.

(16) Lei, T.; Zhou, Y.; Cheng, C.-Y.; Cao, Y.; Peng, Y.; Bian, J.; Pei, J. *Org. Lett.,* **2011**, *13*, 2642-2645.

(17) Lindner, B. D.; Paulus, F.; Appleton, A. L.; Schaffroth, M.; Engelhart, J. U.; Schelkle, K. M.; Tverskoy, O.; Rominger, F.; Hamburger, M.; Bunz, U. H. F. *J. Mater. Chem. C,* **2014**, *2*, 9609-9612.

(18) Neidlein, R.; Tran-Viet, D.; Gieren, A.; Kokkinidis, M.; Wilckens, R.; Geserich, H.-P.; Ruppel, W. *Chem. Ber.,* **1982**, *115*, 2898-2904.

(19) Dallos, T.; Hamburger, M.; Baumgarten, M. *Org. Lett.,* **2011**, *13*, 1936-1939.

(20) STELZIG, T. Donor-Acceptor System in the Quest for Organic Semiconductors. Ph. D. Dissertation, Johannes Gutenberg-University Mainz, 2012.

(21) Wang, E.; Hou, L.; Wang, Z.; Hellström, S.; Mammo, W.; Zhang, F.; Inganäs, O.; Andersson, M. R. *Org. Lett.,* **2010**, *12*, 4470-4473.

(22) DeCicco, R. C.; Black, A.; Li, L.; Goroff, N. S. *Eur. J. Org. Chem.,* **2012**, *2012*, 4699-4704.

(23) Clar, E. *Ber. Deuts. Chem. Ges.,* **1936**, *69*, 607-614.

(24) Clar, E.; Schoental, R. *Polycyclic Hydrocarbons*; Springer: London, 1964; Vol. 1.

(25) Qian, G.; Zhong, Z.; Luo, M.; Yu, D.; Zhang, Z.; Ma, D.; Wang, Z. Y. *J. Phys. Chem. C,* **2009**, *113*, 1589-1595.

(26) Seixas de Melo, J.; Burrows, H. D.; Svensson, M.; Andersson, M. R.; Monkman, A. P. *J. Chem. Phys.,* **2003**, *118*, 1550-1556.

(27) Du, X.; Qi, J.; Zhang, Z.; Ma, D.; Wang, Z. Y. *Chem. Mater.,* **2012**, *24*, 2178-2185.

(28) Bredas, J.-L. *Mater. Horiz.,* **2014**, *1*, 17-19.

(29) Magde, D.; Wong, R.; Seybold, P. G. *Photochem. Photobiol.,* **2002**, *75*, 327-334.

(30) Cheknlyuk, A.; Fadeev, V.; Georgiev, G.; Kalkanjiev, T.; Nickolov, Z. *Spectrosc. Lett.,* **1982**, *15*, 355-365.

(31) Sheldrick, G. M. SHELX 97, Program for Crystal Structure Solution and Refinement; Göttingen Unviersity: Germany, 1997.

Chapter 8. A Highly Ordered Phenanthroline-Fused Azaacene
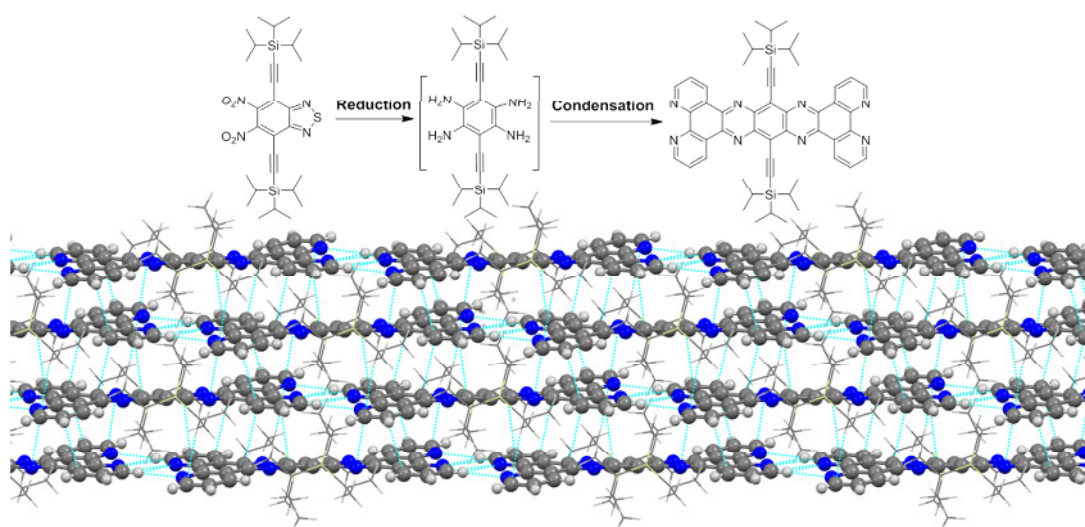
In this chapter, a new synthetic route to prepare a centrosymmetric phenanthroline-fused azaacene derivative, **TIPS-BisPhNPQ**, is described. Another axialsymmetric phenanthroline-fused azaacene derivative, **TIPS-PhNTQ**, is also synthesized for comparison. Both molecules were investigated for optical and electrochemical properties and solid-state packing.

Note: Large part of this chapter has been submitted to *Cryst. Growth Des.*, **2015**.

8.1 Introduction

Large acenes, particularly exemplified by pentacene, have been paid great attention in organic field-effect transistors (OFET).[1-5] The molecular size and structure of acenes are very important for their optoelectronic properties,[6] but their solubility and stability gradually decrease with increasing numbers of aromatic fused ring.[7-9] Three strategies are usually used to stabilize large linear acenes. (1) Introducing special substituents into the acenes backbone, like triisopropylsily (TIPS) acetylene[10] and tritertbutylsilyl (TTBS) acetylene[11], which can stabilize the LUMO level and prevent singlet oxygen sensitization by lowering the molecular triplet energy.[12] (2) Replacing tertiary carbon atom (C-H) moieties using imine nitrogen atoms (-N=) in acenes backbone increases the stabilization of their HOMO and LUMO levels to obtain linear extended azaacenes.[13-17] (3) Expanding laterally the conjugation of the linear aromatic backbone using aromatic rings, such as pyrene-fused azaacenes.[18-22] where the sextet of π electrons are localized on the external rings, Additionally, previous computational studies by Winkler and Houk[23] indicated that replacing a CH moiety by a nitrogen atom or grafting one cyano group onto the terminal ring at both sides can help formation of intermolecular interconnection by hydrogen bonds (C−H···N). More interestingly, combination of these features with molecular π-π stacking can create a highly ordered two-dimensional (2D) arrangement. However, such azaacene molecules are rarely synthesized because of a lack of effective synthetic protocols.

Currently, a very common approach for preparing soluble TIPS-azaacences is the nucleophilic addition between TIPS-ethynyl anion and corresponding dione azaazcenes.[13,24,25] However, it suffers from a difficulty in synthesizing the key dione azaacenes for further extension of conjugation of TIPS-azaacenes due to their very poor solubility. Ideally, for the purpose of synthesizing highly conjugated centrosymmetric TIPS-azaacences, it would be desirable to use a TIPS-ethynyl containing intermediate compound as a reactant, which yields directly soluble TIPS-azaacenes during the condensation step, without a post-functionalization.

With all of the above reasons in mind, in this chapter we report a convenient synthetic route for preparing a key intermediate compound, 3,6-bis((triisopropylsilyl)ethynyl)benzene-1,2, 4,5-tetraamine (**3**) (Scheme 8.1), which can be directly used to produce TIPS-azaacenes by condensation reaction with corresponding *o*-dione derivatives. Considering that the imine

N atoms in 1, 10-phenanthroline offer a great opportunity to form intermolecular hydrogen bonds (C–H···N),[26,27] 1,10-phenanthroline-5,6-dione was, therefore, chosen to be condensed with tetraamine **3**. It can be expected that the resulting **TIPS-BisPhNPQ** (Scheme 1) will be a soluble and stable centrosymmetric azaacene molecule with potentially ordered arrangement in the solid state. For contrast, an axialsymmetric **TIPS-PhNTQ** (Scheme 1) was also synthesized. For both functionalized azaacene derivatives, we investigate the effect of different symmetric structures on both the electronic properties and solid-state packing in their crystals.

8.2 Synthesis and characterization
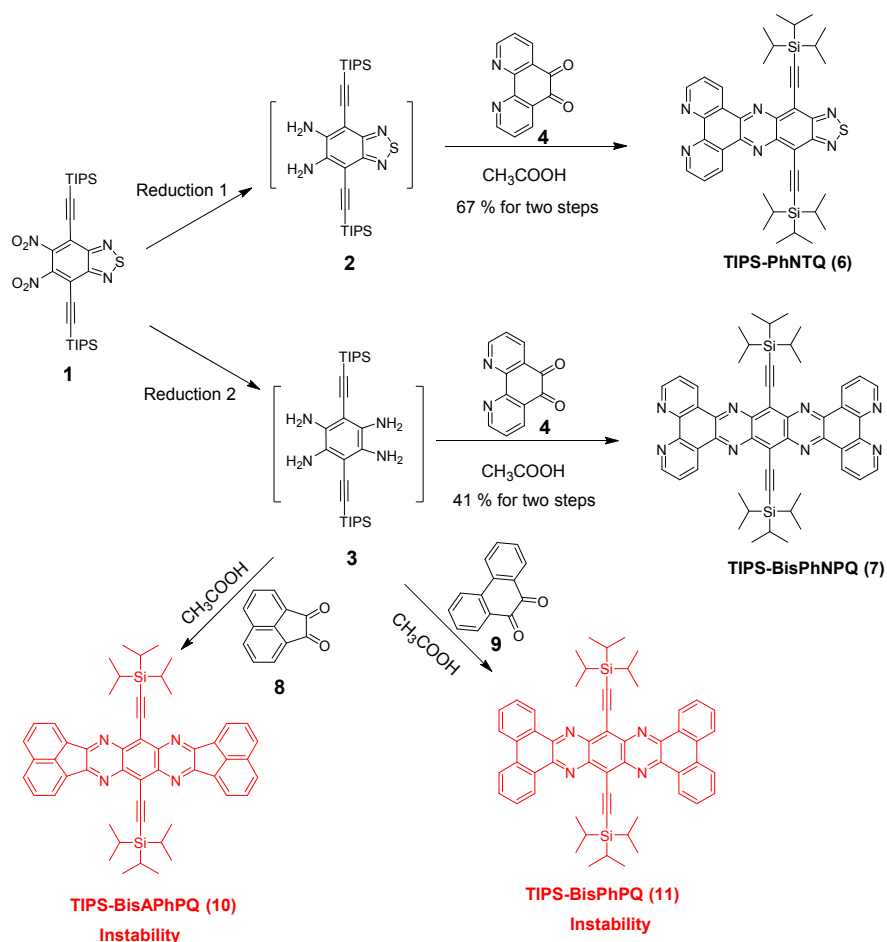
Scheme 8.1 Synthetic route for **TIPS-PhNTQ** and **TIPS-BisPhNPQ.**

The synthesis of the two small molecules is illustrated in Scheme 8. 1. **TIPS-PhNTQ** was

synthesized from 5,6-dinitro-4,7-bis((triisopropylsilyl)ethynyl)benzo[c][1,2,5]thiadiazole (**1**) in a high yield of 67% for two-steps as described in Chapter 7. It has good solubility in common solvents, such as dichloromethane, chloroform and THF.

Table 8.1 The list of different reaction conditions for reduction of compound **1** into compound **3**.

No.	Conditions (100 mg compound **1** ; Argon protect)	The signal of compound **3** (detected by FD-MS)
1	dry 10 ml THF; 10 eq NaBH$_4$; 50 °C; 12 h.	Didn't find
2	dry 10 ml THF; 10 eq LiAlH$_4$; room temperature; 12 h.	Didn't find
3	10 ml acetic acid; 3-5 drops water; 20 eq Zn; 50 °C; 12 h.	Didn't find
4	Continue No. 3, 70 °C for another 6 h.	Didn't find
5	Continue No. 4, 90 °C for another 12 h.	weak signal
6	8 ml ethanol; 2 ml acetic acid; 0.4 ml HCl (1N); 20 eq Zn; 90 °C; 16 h.	strong signal
7	8 ml ethanol; 2 ml acetic acid; 1 ml HCl (1N); 20 eq Zn; 90 °C; 9 h.	strong signal

In order to obtain key intermediate 3,6-bis((triisopropylsilyl)ethynyl)benzene-1,2,4,5-tetraamine (**3**), many reduction systems were attempted from starting material **1** as shown in Table 8.1. Firstly, the method 3 was tried according to previous literature[28], due to their similar structures (reduction 5,6-dinitro-4,7-di(thiophen-2-yl)benzo[c][1,2,5]thiadiazole into 3,6-di(thiophen-2-yl)benzene-1,2,4,5-tetraamine). Another consideration is that the TIPS-ethynyl group could be more sensitive than thienyl group under reducing conditions. Therefore the initial temperature was controlled at 50 °C. But the peak of compound **3** was not observed by FD-MS, even when the reaction time was extended to 12 hours, the starting material signal was clearly observed during this reaction period. When the temperature was raised to 70 °C for 12 hours (method 4), the signal of compound **3** was not still found by FD-MS. Until the temperature was further increased to 90 °C for another 12 hours (method 5), the very weak signal of compound **3** was observed by FD-MS. The methods 1 and 2 were reported to reduce the benzothiadiazole into the corresponding diamine.[29,30] This combination, however, also failed to obtain the desired compound **3** in our reaction system. In order to find

the best conditions for reduction of compound **1**, the reducing agent was optimized based on methods 3, 4, 5. Finally, an optimal reduction system (method 7) was successfully discovered to achieve compound **3** using zinc, HCl, acetic acid and ethanol. The mixture was filtered to remove extra zinc, and then was directly used in next step without purification.

The linear azaacenes **TIPS-BisAPhPQ** and **TIPS-BisPhPQ** were firstly tried to be prepared by condensation reaction between the crude compound **3** and acenaphthylene-1,2-dione (**8**), phenanthrene-9,10-dione (**9**). Unfortunately, both compounds decomposed when they were purified by the silicon or aluminium oxide column chromatography. Taking **TIPS-BisAPhPQ** for an example, the signal of target molecule (molecular weight: 791.2 g mol^{-1}) was determined by FD-MS when the condensation reaction was done before workup. But after separation using silicon or aluminium oxide column chromatography, this signal wasn't observed using FD-MS, which implies that the **TIPS-BisAPhPQ** could decompose. The same unstable problem was also found in **TIPS-BisPhPQ**. Those unstable molecules usually possess high-lying HOMO levels.
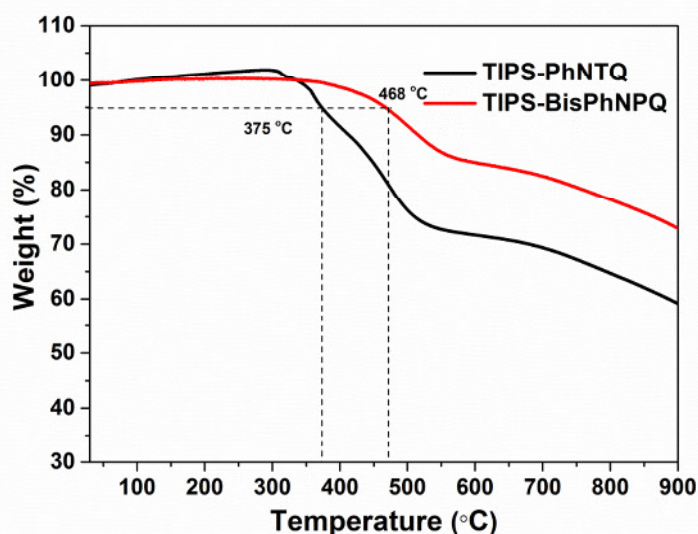
Figure 8.1 TGA curves for **TIPS-PhNTQ** and **TIPS-BisPhNPQ** measured under a nitrogen atmosphere at a heating rate of 10 ℃/min.

The electron-withdrawing nature of the 1,10-phenanthroline can stabilize the HOMO and LUMO energy levels of the resulting molecule.[31] In order to develop stable azaacene derivatives, we designed and synthesized a new azaacene **TIPS-BisPhNPQ**. The crude product **3** was condensed with two equivalents of 1,10-phenanthroline-5,6-dione **4** to give the

desired molecule **TIPS-BisPhNPQ** with a yield of 41% for two-steps. Additionally, both molecules have good solubility in common solvents such as chloroform and tetrahydrofuran. **TIPS-PhNTQ** exhibits good thermal stability with 5% weight loss around 375 °C, and even better thermal stability is observed for **TIPS-BisPhNPQ** with 5% weight loss at 468 °C (Figure 8.1).

8.3 Optical properties
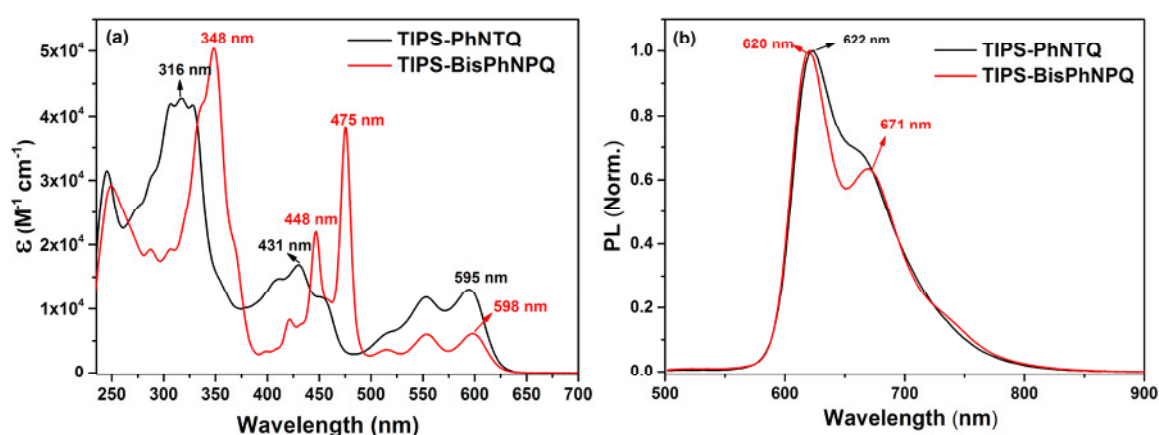
Figure 8.2 UV-vis absorption (a) and fluorescence (b) spectra of **TIPS-PhNTQ** and **TIPS-BisPhNPQ** in dichloromethane solutions.

UV-vis absorption and emission spectra of both molecules were recorded in dilute dichloromethane solutions (10^{-5} M Figure 8.2). Short-wavelength bands covering 250-500 nm are attributed to the π-π* and n-π* transitions of the conjugated aromatic moieties.[32] Both molecules display similar absorption bands at long wavelength between 500 and 650 nm, the only difference is that the molar extinction coefficient of **TIPS-BisPhNPQ** is twice than that of **TIPS-PhNTQ**. The optical gaps were estimated from the absorption onset of the solution to be 2.0 eV for both molecules. Additionally, both compounds exhibit similar emission spectra, but **TIPS-BisPhNPQ** has a more pronounced shoulder at 671 nm (Figure 8.2b). The Stokes shifts are 27 nm and 22 nm for **TIPS-PhNTQ** and **TIPS-BisPhNTQ.** Due to the rigid coplanar conjugated structures of both materials, these values are far smaller than those of nonplanar conjugated TQ derivatives with two flanked tetraphenylethene moieties.[32]

Fluorescence quantum yield measurements were performed in dichloromethane using a cuvette with a 1 cm path length at room temperature. The absorption spectra were measured within a maximum wavelength between 0 and 0.05. **TIPS-PhNTQ** and **TIPS-BisPhNPQ** were excited at 453 and 475 nm in dichloromethane solutions, respectively. Quantum yields were estimated to be 0.29 and 0.20, respectively, by using the comparative method with fluorescein (0.1 M NaOH, Φ_{em} = 0.90 at 453 nm)[33] for **TIPS-PhNTQ** and rhodamine 110 (Ethanol, Φ_{em} = 0.91 at 475 nm)[32] for **TIPS-BisPhNPQ**.

8.4 Electrochemical properties
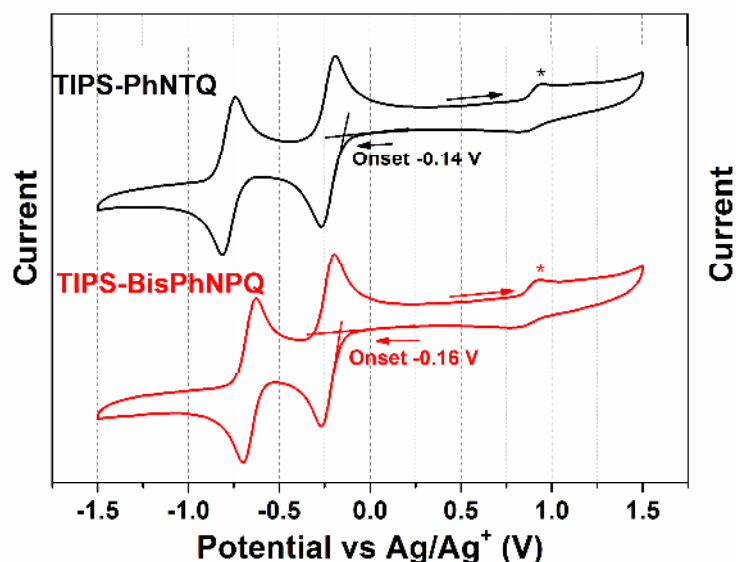
Figure 8.3 The cyclic voltammograms of **TIPS-PhNTQ** and **TIPS-BisPhNPQ** in dichloromethane solutions. *Lost upon dilution.

The electron affinities (EA) and ionization potentials (IP) of both molecules were investigated in dichloromethane solutions by cyclic voltammetry. Both of them exhibit two reversible reduction peaks and one irreversible oxidation peak (Figure 8.3). The values of EA were calculated to be -4.03 eV for **TIPS-PhNTQ** and -4.01 eV for **TIPS-BisPhNPQ**, according to their onsets of the first reduction peak. These values are lower than those of pyrene-fused azaacenes, which were provided to be a range from -3.18 to -3.78 eV, [18,20-22]

suggesting phenanthroline is a more effective group for increasing the electron affinity.

8.5 Crystal packing properties

The single crystals of **TIPS-PhNTQ** and **TIPS-BisPhNPQ** were grown by slow evaporation from solutions in dichloromethane at room temperature. The X-ray crystal structure analysis experimental was carried out by ▉▉▉▉▉▉▉▉ (Johannes Gutenberg-University, Mainz). X-ray crystallographic data for the molecules were collected on an IPDS 2T diffractometer using a Mo-Kα IμS mirror system radiation for **TIPS-PhNTQ**, and a STOE IPDS 2T diffractometer using a graphite monochromator Mo-Kα radiation source for **TIPS-BisPhNPQ**. The structures were solved by direct methods (SIR-97)[34] and refined for **TIPS-PhNTQ** by SHELXL-2014 (full matrix) 524 refined parameters, and for **TIPS-BisPhNPQ** by SHELXL-97 (full matrix), 290 refined parameters.
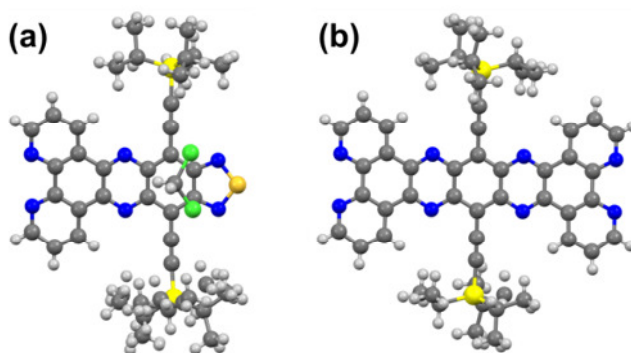
Figure 8.4 Single crystal X-ray structure of **TIPS-PhNTQ (a)** and **TIPS-BisPhNPQ (b)**. Carbon, nitrogen, sulfur, silicon and chloride atoms are shown in grey, blue, orange, yellow, and green, respectively.

Their crystal structures are shown in Figure 8.4. Both molecules have near planar conjugated backbone, which is in agreement with their small Stokes shifts. The one molecule of **TIPS-PHNTQ** includes one dichloromethane molecule in the unit cell, the dichloromethane is removed for clarity. The interaction between two adjacent molecules of **TIPS-PhNTQ** and **TIPS-BisPhNPQ** are shown in Figure 8.7a and 8.9b. **TIPS-PhNTQ** demonstrates dimer features by close head-to-head contact of thiadiazole moieties with N-S (3.14 Å) and N-N (3.07 Å) interations. However, **TIPS-BisPhNPQ** exhibits a ribbon which

extends in two directions by eight C−H···N H-bonds and four weak C···N interactions. The intermolecular distances of H-to-N and C-to-N are 2.64 and 3.24 Å, respectively, which are shorter than the combined van der Waals radii of nitrogen-hydrogen (2.75 Å), and carbon-nitrogen (3.25 Å).
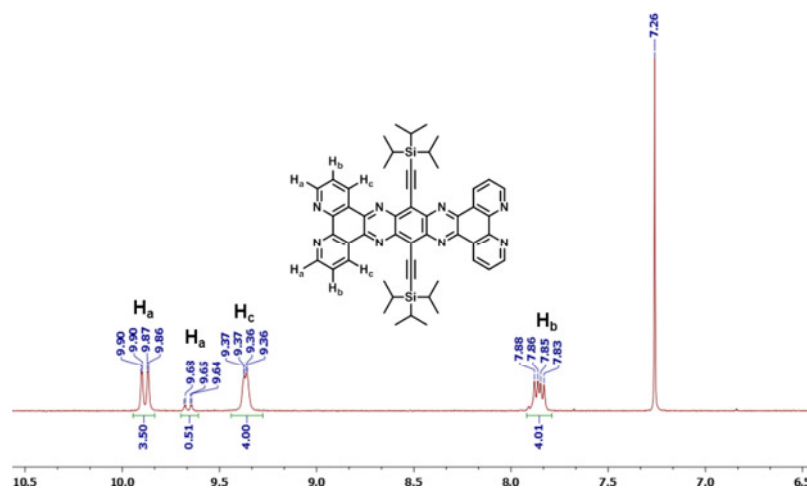
Figure 8.5 ^{1}H NMR spectrum of **TIPS-BisPhNPQ** in CDCl$_3$ solution (aromatic region).
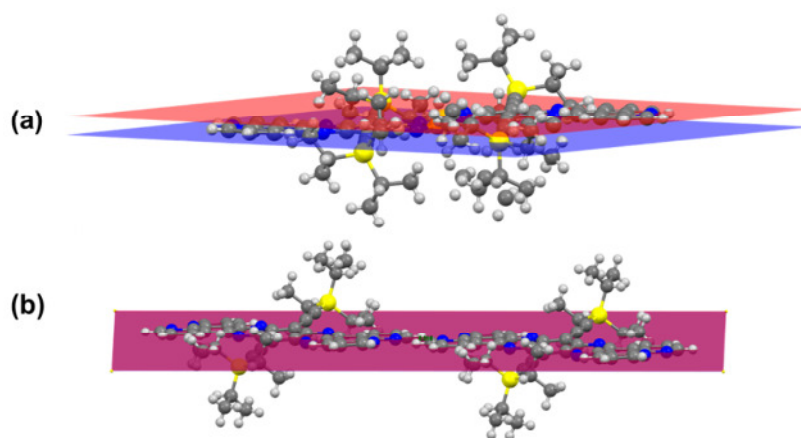
Figure 8.6 The vertical offset (red plane to blue plane) within the adjacent molecules 1.00 Å for **TIPS-PhNTQ (a)** and 0.02 Å for **TIPS-BisPhNPQ (b)**.

On the other hand, in the ^{1}H-NMR spectra (Figure 8.5), the proton signals (C−H···N) of **TIPS-BisPhNPQ** are significantly different in C$_2$D$_2$Cl$_4$ (9.86 ppm) and CDCl$_3$ (9.90 and 9.68 ppm), indicating that the H-Bonds of **TIPS-BisPhNPQ** exist in chloroform solution. These results reveal that the H-bonds of **TIPS-BisPhNPQ** can form in solid-state as well as in solutions. The vertical offset within the adjacent molecules (Figure 8.6) are 1.00 and 0.02 Å

for **TIPS-PhNTQ** and **TIPS-BisPhNPQ**, respectively. The significantly small distance of **TIPS-BisPhNPQ** is related to its centrosymmetric structure and intermolecular H-bonds.
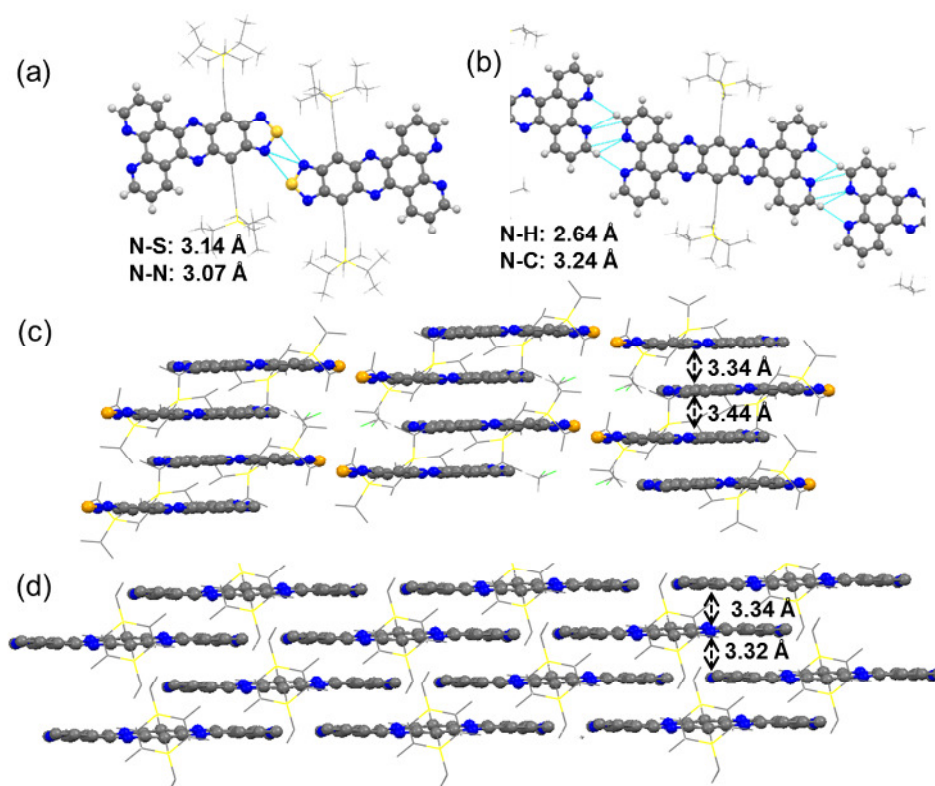
Figure 8.7 The intermolecular interaction in **TIPS-PhNTQ** (a) and **TIPS-BisPhNPQ** (b). The packing of **TIPS-PhNTQ** (c) and **TIPS-BisPhNPQ** (d). The conjugated cores are shown with ball-stick models and the TIPS-ethynyl substituents are shown with wireframe models. Hydrogen atoms are removed for clarity. Carbon, nitrogen, sulfur and silicon atoms are shown in grey, blue, orange and yellow, respectively. Van der Waals radius: H 1.20 Å; C 1.70 Å; N 1.55 Å; S 1.80 Å.

Although both molecules have the same unit cell, their packing pattern are very different, which is related to their different symmetric structures. The packing patterns of both molecules are provided in Figure 8.7c and 8.7d. **TIPS-PhNTQ** displays a 2-D arrangement with π-π stacking distances of 3.34 and 3.44 Å.[35] **TIPS-BisPhNPQ** exhibits a 2D brickwork arrangement, which is typical of TIPS-pentacene and TIPS-tetraazapentacene.[10,13,25] The distances between π planes in the molecule of **TIPS-BisPhNPQ** are 3.32 and 3.34 Å, which are shorter than those in TIPS-pentacene (3.47 Å).[10] Additionally, compared to two π-π stacking distances of TIPS-tetraazapentacene (3.28 and 3.38 Å),[25] the difference of vertical offset in **TIPS-BisPhNPQ** is only 0.02 Å due to its intermolecular H-bonds, suggesting that

this molecule could have a better ordered arrangement in the solid-state.

8.6 Summary

In this chapter, we have successfully synthesized two new phenanthroline-fused azaacenes derivatives, **TIPS-BisPhNPQ** and **TIPS-PhNTQ**, by a novel synthetic route. Both of them exhibit good solubility and high stabilities. Although both molecules possess similar optical bandgap and electrochemical properties, they have different packing styles. **TIPS-BisPhNPQ** shows a π-stacking of 2D brickwork arrangement. More interesting, this molecule forms the intermolecular H-bonds by phenanthroline as end capping groups, which leads to a highly ordered solid-state arrangement. On the other hand, it has to be emphasized that the key intermediate **3** provides a chance to synthesize more centrosymmetric large azaacenes.

8.7 Synthetic details

Intermediate of 5,6-dinitro-4,7-bis((triisopropylsilyl)ethynyl)benzo[c][1,2,5]thiadiazole (**1**) was prepared according to Chapter 7.

10,14-Bis((triisopropylsilyl)ethynyl)dipyrido[3,2-a:2',3'-c][1,2,5]thiadiazolo[3,4-i]phenazine (TIPS-PhNTQ)
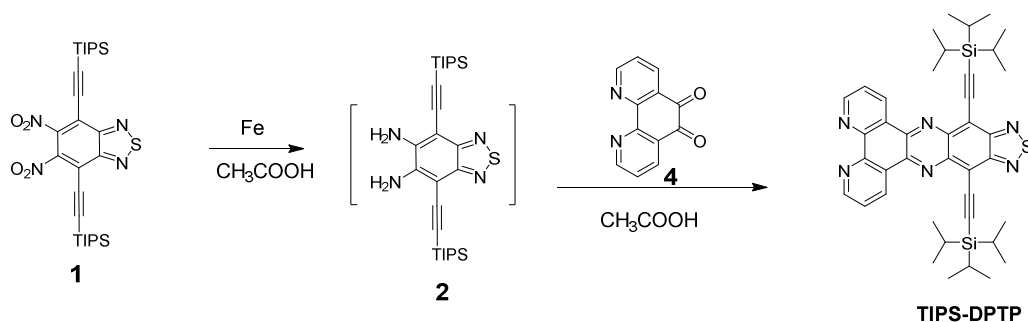
A mixture of compound **1** (100 mg, 0.171 mmol) and fine iron powder (113 mg, 2.018 mmol) in acetic acid (10 mL) was stirred at 75 °C for 5 h under argon. After cooling to the

room temperature, the mixture was poured into water and extracted with diethyl ether (3 × 20 mL). The combined organic layers were washed with brine, dried with MgSO$_4$. The solvent was removed under reduced pressure to give the corresponding diamine **2** with deep red oil. This crude product was directly added into acetic acid (10 mL) solution of 1,10-phenanthroline-5,6-dione (**4**) (0.256 mmol). The mixture was heated to 80 °C overnight under argon. After cooling to room temperature, the mixture was poured into 100 mL 5% aqueous NaOH and extracted with dichloromethane (3×20 mL). The combined organic phases were dried with MgSO$_4$ and filtered. The filtrate was concentrated and purified by column chromatography eluting with hexane dichloromethane (4:1) and 5% triethylamine to **TIPS-PhNTQ**. Red solid (80 mg, 67% for two steps), ^{1}H NMR (250 MHz, CD$_2$Cl$_2$, ppm) δ 9.71 (dd, *J* = 2.5 Hz, *J* = 5.0 Hz, 2H), 9.24 (dd, *J* = 2.5 Hz, *J* = 2.5 Hz, 2H), 7.79 (dd, *J* = 2.5 Hz, *J* = 5.0 Hz, 2H), 1.35 (m, broad, 42H). ^{13}C NMR (125 MHz, CD$_2$Cl$_2$, ppm) δ 155.35, 153.87, 150.17, 144.22, 142.26, 134.72, 127.91, 124.72, 115.05, 111.00, 101.90, 19.08, 12.07; HRMS (ESI+): m/z calc. 701.3278 found 701.3294.

10,21-Bis((triisopropylsilyl)ethynyl)dipyrido[3',2':5,6;2'',3'':7,8]quinoxalino[2,3-i]dipyrido[3,2-a:2',3'-c]phenazine (TIPS-BisPhNPQ)
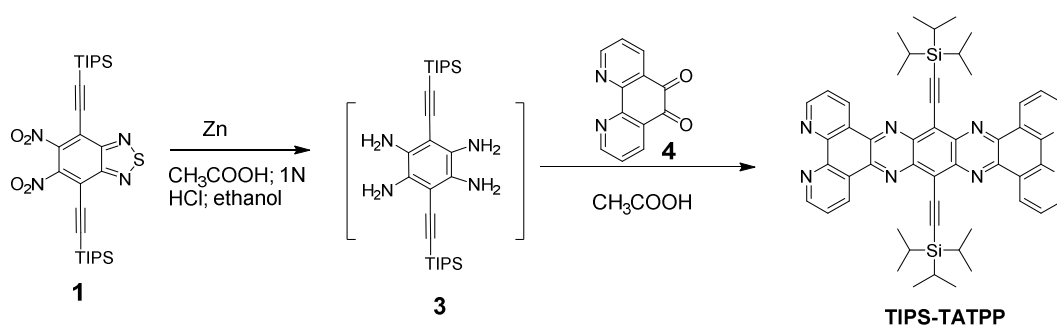
Compound **1** (100 mg, 0.171 mmol) and zinc (222 mg, 3.42 mmol) were dissolved in a mixture solvent (8 mL ethanol, 2 mL acetic acid and 1mL HCl (1N)) and stirred at 90 °C for 9 h under argon. After being cooled to the room temperature, the mixture was poured into 50 mL of water and extracted with diethyl ether (3×20 mL). The combined organic layers were dried with MgSO$_4$. The solvent was removed under reduced pressure to give the key

intermediate 3,6-bis((triisopropylsilyl)ethynyl)benzene-1,2,4,5-tetraamine (**3**) with deep red oil. This crude product was directly added into acetic acid (10 mL) solution of compound **4** (0.256 mmol). The mixture was heated to 80 °C overnight under argon. After cooling to room temperature, the mixture was poured into 100 mL 5% aqueous NaOH and extracted with dichloromethane (3×50 mL). The combined organic phases were dried with $MgSO_4$ and filtered. The filtrate was concentrated and purified by column chromatography eluting with hexane dichloromethane (3:1) and 5% triethylamine to give **TIPS-BisPhNPQ**. Red solid (59 mg, 41% for two steps), ^{1}H NMR (250 MHz, $C_2D_2Cl_4$, ppm) δ 9.86 (dd, *J* = 2.5 Hz, *J* = 5.0 Hz, 4H), 9.29 (dd, *J* = 2.5 Hz, *J* = 2.5 Hz, 4H), 7.84 (dd, *J* = 2.5 Hz, *J* = 5.0 Hz, 4H), 1.44 (m, broad, 42H). ^{13}C NMR (62.5 MHz, $C_2D_2Cl_4$, ppm) δ 153.65, 149.54, 143.59, 142.60, 135.12, 127.93, 124.79, 123.19, 111.33, 102.10, 19.38, 12.08; HRMS (ESI+): m/z calc. 847.4088 found 847.4072.

8.8 References

(1) Bendikov, M.; Wudl, F.; Perepichka, D. F. *Chem. Rev.,* **2004**, *104*, 4891-4946.

(2) Bailey, W. J.; Madoff, M. *J. Am. Chem. Soc.,* **1953**, *75*, 5603-5604.

(3) Payne, M. M.; Parkin, S. R.; Anthony, J. E.; Kuo, C.-C.; Jackson, T. N. *J. Am. Chem. Soc.,* **2005**, *127*, 4986-4987.

(4) Anthony, J. E. *Angew. Chem. Int. Ed.,* **2008**, *47*, 452-483.

(5) Giri, G.; Verploegen, E.; Mannsfeld, S. C. B.; Atahan-Evrenk, S.; Kim, D. H.; Lee, S. Y.; Becerril, H. A.; Aspuru-Guzik, A.; Toney, M. F.; Bao, Z. *Nature,* **2011**, *480*, 504-508.

(6) Gierschner, J.; Cornil, J.; Egelhaaf, H. J. *Adv. Mater.,* **2007**, *19*, 173-191.

(7) Payne, M. M.; Odom, S. A.; Parkin, S. R.; Anthony, J. E. *Org. Lett.,* **2004**, *6*, 3325-3328.

(8) Duong, H. M.; Bendikov, M.; Steiger, D.; Zhang, Q.; Sonmez, G.; Yamada, J.; Wudl, F. *Org. Lett.,* **2003**, *5*, 4433-4436.

(9) Einholz, R.; Bettinger, H. F. *Angew. Chem. Int. Ed.,* **2013**, *52*, 9818-9820.

(10) Anthony, J. E.; Brooks, J. S.; Eaton, D. L.; Parkin, S. R. *J. Am. Chem. Soc.,* **2001**, *123*, 9482-9483.

(11) Payne, M. M.; Parkin, S. R.; Anthony, J. E. *J. Am. Chem. Soc.,* **2005**, *127*, 8028-8029.

(12) Maliakal, A.; Raghavachari, K.; Katz, H.; Chandross, E.; Siegrist, T. *Chem. Mater.,* **2004**, *16*, 4980-4986.

(13) Miao, S.; Appleton, A. L.; Berger, N.; Barlow, S.; Marder, S. R.; Hardcastle, K. I.; Bunz, U. H. F. *Chem. Eur. J.,* **2009**, *15*, 4990-4993.

(14) Lindner, B. D.; Engelhart, J. U.; Tverskoy, O.; Appleton, A. L.; Rominger, F.; Peters, A.; Himmel, H.-J.; Bunz, U. H. F. *Angew. Chem. Int. Ed.,* **2011**, *50*, 8588-8591.

(15) Engelhart, J. U.; Lindner, B. D.; Tverskoy, O.; Rominger, F.; Bunz, U. H. F. *Org. Lett.,* **2012**, *14*, 1008-1011.

(16) Bunz, U. H. F.; Engelhart, J. U.; Lindner, B. D.; Schaffroth, M. *Angew. Chem. Int. Ed.,* **2013**, *52*, 3810-3821.

(17) Engelhart, J. U.; Tverskoy, O.; Bunz, U. H. F. *J. Am. Chem. Soc.,* **2014**, *136*, 15166-15169.

(18) Gao, B.; Wang, M.; Cheng, Y.; Wang, L.; Jing, X.; Wang, F. *J. Am. Chem. Soc.,* **2008**, *130*, 8297-8306.

(19) Mateo-Alonso, A.; Kulisic, N.; Valenti, G.; Marcaccio, M.; Paolucci, F.; Prato, M. *Chem. Asian J.,* **2010**, *5*, 482-485.

(20) Kulisic, N.; More, S.; Mateo-Alonso, A. *Chem. Commun.,* **2011**, *47*, 514-516.

(21) More, S.; Bhosale, R.; Choudhary, S.; Mateo-Alonso, A. *Org. Lett.,* **2012**, *14*, 4170-4173.

(22) Feng, X.; Iwanaga, F.; Hu, J.-Y.; Tomiyasu, H.; Nakano, M.; Redshaw, C.; Elsegood, M. R. J.; Yamato, T. *Org. Lett.,* **2013**, *15*, 3594-3597.

(23) Winkler, M.; Houk, K. N. *J. Am. Chem. Soc.,* **2007**, *129*, 1805-1815.

(24) Liang, Z.; Tang, Q.; Mao, R.; Liu, D.; Xu, J.; Miao, Q. *Adv. Mater.,* **2011**, *23*, 5514-5518.

(25) Liang, Z.; Tang, Q.; Xu, J.; Miao, Q. *Adv. Mater.,* **2011**, *23*, 1535-1539.

(26) Shuku, Y.; Suizu, R.; Awaga, K. *Inorg. Chem.,* **2011**, *50*, 11859-11861.

(27) Bhat, S. S.; Kumbhar, A. A.; Heptullah, H.; Khan, A. A.; Gobre, V. V.; Gejji, S. P.; Puranik, V. G. *Inorg. Chem.,* **2010**, *50*, 545-558.

(28) Zhang, F. L.; Bijleveld, J.; Perzon, E.; Tvingstedt, K.; Barrau, S.; Inganas, O.; Andersson, M. R. *J. Mater. Chem.,* **2008**, *18*, 5468-5474.

(29) Patel, D. G.; Feng, F.; Ohnishi, Y.-y.; Abboud, K. A.; Hirata, S.; Schanze, K. S.; Reynolds, J. R. *J. Am. Chem. Soc.,* **2012**, *134*, 2599-2612.

(30) Appleton, A. L.; Brombosz, S. M.; Barlow, S.; Sears, J. S.; Bredas, J.-L.; Marder, S. R.; Bunz, U. H. F. *Nat. Commun.,* **2010**, *1*, 91.

(31) Nietfeld, J. P.; Schwiderski, R. L.; Gonnella, T. P.; Rasmussen, S. C. *J. Org. Chem.,* **2011**, *76*, 6383-6388.

(32) Du, X.; Qi, J.; Zhang, Z.; Ma, D.; Wang, Z. Y. *Chem. Mater.,* **2012**, *24*, 2178-2185.

(33) Galanin, M. D.; Kufénko, A. A.; Smorchkov, V. N.; Timofee, Y. P.; Chizhikov, Z. A. *Opt. Spektrosk.,* **1982**, *53*, 683-689.

(34) Sheldrick, G. M. SHELX 97, Program for Crystal Structure Solution and Refinement; Göttingen Unviersity: Germany, 1997.

(35) Lindner, B. D.; Paulus, F.; Appleton, A. L.; Schaffroth, M.; Engelhart, J. U.; Schelkle, K. M.; Tverskoy, O.; Rominger, F.; Hamburger, M.; Bunz, U. H. F. *J. Mater. Chem. C,* **2014**, *2*, 9609-9612.

Chapter 9. Conclusion and Outlook

The main aim of this work was the synthesis, characterization and application of aromatic rings condensed thiadiazolo[3,4-*g*]quinoxalines (TQs) based copolymers and small molecules for organic electronics. Such acceptors have planar, quinoidal structure and high electron deficient nature.

This work began with the systhesis of benzodithiophene condensed TQ (**BDTTQ,** Chapter 2) based polymers formed from different reactive sites, and expanded it towards novel synthetic protocols that were used to prepare new TQs and azaacenes small molecules with strong crystallization characteristics. We focused on molecular rational design. Within this direction of work, several important achievements are summarized as below:

The copolymers **PBDTTQ-1** and **PBDTTQ-2** (Chapter 2) with different linkage between acceptor **BDTTQ** and donor alkylated bithiophene were synthesized. UV-vis-NIR spectra and cyclic voltammetry indicated that **PBDTTQ-2** showed narrower optical bandgap and lower EA value than that for **PBDTTQ-1**. Interestingly, **PBDTTQ-1** did not show any field-effect response, while **PBDTTQ-2** exhibited ambipolar transport behaviour. This was in good agreement with DFT calculations.

The structure and charge transport correlations of **TQ-2T**-based polymers were investigated in Chapter 3. Two crucial modifications were found in enhancing the charge transport of TQ-based polymers. Firstly, the unsubstituted donor units combined with **TQ-2T** into polymer conjugated backbone, like polymers **P1-P4**. Such strategy improved the molecular arrangement in the fibers and films. Therefore, the hole mobilities of **P1**-**P4** were achieved higher than for previously reported TQ polymers. Secondly, four dodecyl side chains of **P4** were regrouped into a pair of branched 2-decyl-tetradecyl alkyl chains and yielded **P6**. In comparison with **P4**, the planarity of **P6** did not significantly change, but its molecular weight and solubility were remarkably improved. Meanwhile, the crystallinity was

further enhanced. Therefore, **P6** exhibited the highest hole charge carrier mobility of 0.24 cm^2 V^{-1} s^{-1} among these polymers.

Subsequently, a pair of 2-decyl-tetradecyl alkyl chains was grafted on **BDTTQ** and **APhTQ** cores and two high performance ambipolar polymer semiconductors (**PBDTTQ-3** and **PAPhTQ**, Chapter 4) were obtained. In comparison with redundant side chains of **PBDTTQ-2**, **PBDTTQ-3** exhibited very low optical bandgap and higher electron deficient nature. Meanwhile, the mobilities are two orders of magnitude higher than for **PBDTTQ-2**. Changing the fused aromatic rings from acenaphthylene to benzodithiophene in the TQ moiety also played a significant role on the optoelectronic properties and the device performances of these polymers. **PAPhTQ** exhibited a larger optical bandgap and a weaker EA compared to **PBDTTQ-3**. Although both polymers had quite disordered films, **PBDTTQ-3** still exhibited well-balanced ambipolar charge carrier transport with mobilities up to 0.22 cm^2 V^{-1} s^{-1} for holes and 0.21 cm^2 V^{-1} s^{-1} for electrons. **PAPhTQ** revealed also ambipolarity with slightly lower average mobilities.

A photosensitizer group, phenanthrene, was condensed onto TQ moiety to yield a new acceptor **PhTQ** (Chapter 5). It expanded a new application of **PhTQ**-based polymers in organic phototransistor (OPT). The corresponding polymer **PPhTQ** exhibited a balanced ambipolor field-effect behavior. As expected, **PPhTQ** as an active layer in OPT device showed a maximum photoresponsivity of 400 A/W, which not only exceeds that of single-crystal silicon-based OPTs (~300 A/W), but is also among the best OPT performances for conjugated polymers.

Dual-acceptor-based copolymers, **PDPP-T-TQ**, **PDPP-2T-TQ**, and **PDPP-3T-TQ,** were designed and synthesized based on two acceptors TQ and DPP (Chapter 6). **PDPP-T-TQ** showed a surprisingly low optical bandgap with 0.60 eV. From polymers **PDDP-2T-TQ** to **PDPP-3T-TQ**, the intramolecular charge transfer abilities of polymers were decreased, while the coplanarities of the polymers were significantly improved. Meanwhile, as ambipolar copolymers, the hole mobility of **PDPP-3T-TQ** was one order of magnitude higher than for **PDDP-2T-TQ.** These results implied that improvement of intramolecular coplanarities could be a more efficient strategy in improving charge transport than the enhancement of their ICT for DPP-TQ based copolymers.

Althogh the chargr carrier mobilities of the TQ-based polymers have been achieved up to 0.2 cm^2 V^{-1} s^{-1} in our work, it is still possible to further improve mobilities via molecular design. Some proposed TQ polymer structures are shown in Chart 9.1. Firstly, the benzene units replace the benzodithiophene in **BDTTQ**, shuch as **TQ3-5**, the introduction of fluorine and chlorine atoms in benens units can enhance the intermolecular interactions. The DFT (6-31G) calculations indicated that **TQ1** has a similar LUMO level (-3.72 eV) as **BDTTQ** (-3.70 eV), However, the LUMO levels of **TQ2** and **TQ3** are surpurisingly decreased to -4.16 and -4.17 eV, respectively, which are lower than dithienyl-benzobisthiadiazole (-4.02 eV **DT-BBT**). These results implied that the corresponding polymers **P1-P3** could have highly ordered arrangement in films and exhibit high performance ambipolar or n-type device behaviors. Secondly, the branched alkyl chains of **PBDTTQ-3** can be replaced by tuning the distance of the branching point (**P4-Y**) or siloxane-terminated (**P5**). It could improve molecular packing in films, leading to better ambipolar charge carrier transport.
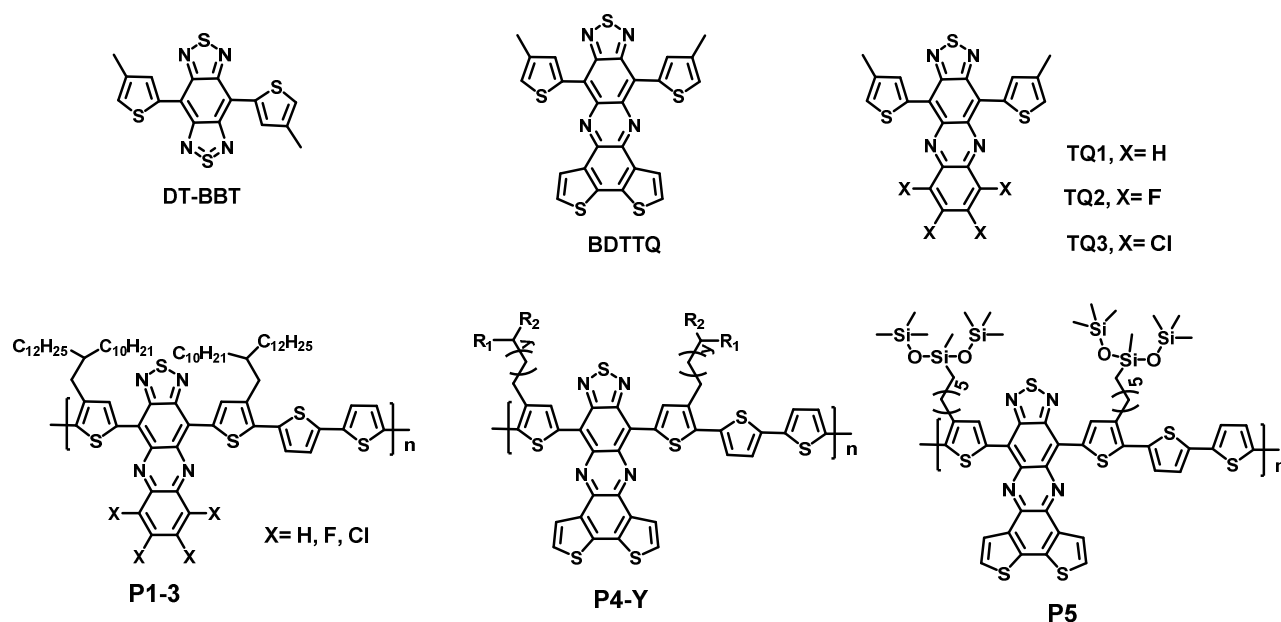
Chart 9.1 The structures of small molecles and proposed condensed TQ-based polymer structures for the future investigations.

The results that were mentioned in the polymer parts also encouraged us to study some small moleucles. Therefore, three target molecules, **TIPS-APhTQ**, **TIPS-PhTQ,** and **TIPS-BDTTQ**, were synthesized via a facile and highly efficient route (Chapter 7). **TIPS-BDTTQ** exhibited a very low EA value of -4.0 eV. All three molecules

demonstrated a brick wall packing motif through their dimer interactions. Among these molecules, **TIPS-PhTQ** and **TIPS-BDTTQ** possessed shortest and largest π-stacking distances, respectively. Interesting, It was in good agreement with the polymers morphology where **PPhTQ** had the best ordered arrangement in films, **PAPhTQ** exhibited slightly higher order than **PBDTTQ-3** among these three polymers in films.

The synthetic route was further modified and successfully synthesized a centrosymmetric phenanthroline-fused azaacene, **TIPS-BisPhNPQ** (Chapter 8). In comparison with axialsymmetric phenanthroline-fused azaacene derivative, **TIPS-PhNTQ**, **TIPS-BisPhNPQ** shows a π-stacking of 2D brickwork arrangement. More interestingly, this molecule formed the intermolecular H-bonds by phenanthroline as end capping groups, which led to a highly ordered arrangement in solid states.
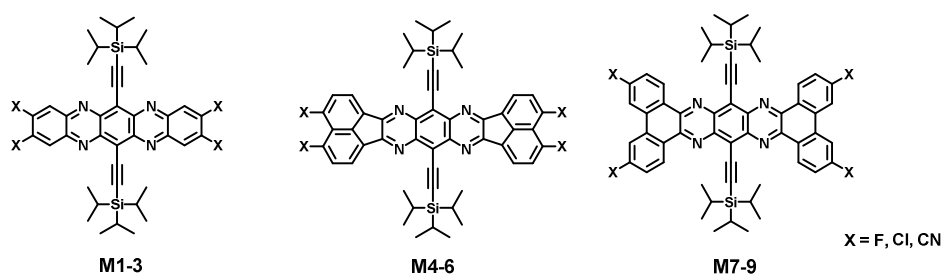
Chart 9.2 Proposed new azaacenes for the future investigations in OFETs.

It should be noted that the key intermediate 3,6-bis((triisopropylsilyl)ethynyl)benzene-1,2,4,5-tetraamine (**3** in Chapter 8) provides a chance to synthesize more large azaacenes. The new molecules (**M1-9**) are designed as shown in Chart 9.2. These molecules could show some advantages for application in OFETs. Firstly, the introduction of fluorine, chlorine, and cyano groups will enable to enhance molecular π-stacking ability and stabilize molecular HOMO energy levels. Secondly, the TIPS-ethynyl groups were attached to new molecules, which are beneficial for improving molecular crystallization ability and solubility. Besides these new molecules, we believe that this new synthetic protocol can produce more azaacenes which possess excellent electron charge transport in OFETs.

Appendix

Appendix-I General methods

Chemicals and solvents

All chemicals and reagents were used as received from commercial sources (Sigma-Aldrich, Acros Organics, Fluka, Merck, Tokyo Chemical Industry) without further purification. Solvents for chemical synthesis were used as received from Sigma-Aldrich and Acros Organics, unless stated otherwise.

Chromatography

Preparative column chromatography was carried out on silica 60 with a grain size of 0.063-0.2 mm or 0.04-0.063 mm (flash silica gel), which were received from Macherey-Nagel. Some special preparative column chromatography was performed using neutral and base aluminum oxide (Fluka). The analytical thin layer chromatography (TLC), 0.2 mm silica gel with fluorescent indicator, was used from Macherey-Nagel. Compounds were detected by fluorescence quenching at 254 nm, self-fluorescence at 366 nm. For eluents, the analytical grade solvents were used directly, and technical grade solvent (hexane) was distilled prior to the use.

Microwave assisted synthesis

The microwave assisted synthesis was performed for some Stille coupling reactions in a CEM discover TM system, in a closed 10 mL vial equipped with temperature and pressure sensor and magnetic stirring.

Appendix-II Analytical techniques

NMR spectroscopy

^{1}H NMR and ^{13}C NMR spectra were recorded in deuterated solvents on a Bruker DPX 250, 500 and 700 spectrometers. Chemical shifts (δ) were given in parts per million (ppm) with tetramethylsilane as internal standard. The measurements were carried out at room temperature (293 K), unless stated otherwise.

Mass spectrometry

Field-desorption mass spectra (FD-MS) were recorded on a VG Instruments ZAB 2-SE0FPD spectrometer (range 100-3300). High Resolution Mass Spectra (HRMS) were carried out by the Microanalytical Laboratory of Johannes Gutenberg-University, Mainz. UV–Vis-NIR absorption spectra were measured on a Perkin-Elmer Lambda 9 spectrophotometer at room temperature.

UV-vis-NIR and steady sate fluorescence spectroscopy

Solution and solid state UV-vis-NIR spectra were recorded on a Perkin Elmer Lambda 15 spectrophotometer. Unless otherwise noted, a concentration of 10^{-5} mol L^{-1} was used in solvents of spectroscopic grade at room temperature. The quantum corrected steady state fluorescence spectra were registered on a SPEX-Fluorolog II (212) spectrometer. Fluorescence quantum yields were determined by the comparative method (the references were mentioned in text) and corrected for the refractive index of the solvent of the probe. The solutions were prepared with an absorbance between 0 and 0.1 at the wavelength region of experimental interest. Conversion into an absolute quantum yield is obtained by solving the following equation:

$$\Phi_{Fl,Sample} = \Phi_{Fl,Reference} \times (OD_{Reference} / OD_{Sample}) \times (A_{Sample} / A_{Reference}) \times (\eta_{Sample} / \eta_{Reference})^2$$

wherein:

Φ : fluorescence quantum yield of the sample and reference;

OD : The absorption intensity of the sample and reference;

A : The area of under fluorescence intensity;

η: Refractive index of the solvent.

Cyclic voltammetry

Cyclic voltammetry (CV) was carried out on a computer-controlled GSTAT12 in a three-electrode cell in anhydrous solvents solution of Bu_4NPF_6 (0.1 M) with a scan rate of 50 mV/s at room temperature under argon (dichloromethane for monomers and acetonitrile for polymers). A Pt wire, a silver wire, and a glassy carbon electrode were used as the counter electrode, the reference electrode, and the working electrode, respectively. For the monomers, the measurements were carried out using a 0.1 mol L^{-1} dichloromethane solution of n-Bu_4NPF_6 as electrolyte, while the analytes were dissolved in concentrations of 10^{-3} mol L^{-1}. EA were estimated from the onsets of the first reduction peak, while the potentials were determined using ferrocene (Fc) as standard by empirical formulas $E_{EA} = - (E_{Red}^{onset} - E_{Fc/Fc+}^{1/2} + 4.8)$ eV wherein $E_{Fc/Fc+}^{1/2} = 0.63$ eV.

Thermogravimetric analysis and differential scanning calorimetry

Thermogravimetric analysis (TGA) were carried out on a Mettler 500 Thermogravimetry Analyzer with heating rates of 10 K/min. Differential scanning calorimetry (DSC) were measured on a Mettler DSC 30 with heating and cooling rates of 10 K/min.

Gel permeation chromatography

The molecular weights were determined by PSS-WinGPC (PSS) (pump: alliance GPC 2000) GPC equipped with an UV or RI detector running in tetrahydrofuran at 30 ^{o}C or 1,2,4-trichlorobenzene at 135 °C using a PLgel MIXED-B column (particle size: 10 mm, dimension: 0.8×30 cm) calibrated against polystyrene standards.

Elemental analysis

Elemental analysis of solid samples was carried out on a Foss Heraeus Vario EL as a service of the Institute for Organic Chemistry, Johannes Gutenberg-University of Mainz.

Computational methods

The geometry optimizations were performed using Gaussian 03, 2 Revision B.04 quantum chemistry program at the B3LYP level of theory.[1] All calculations were carried out using the 6-31G, 6-31G* or 6-31G** basis sets.[2,3] For all compounds the lowest energy conformers, found by conformational search, were subjected to full geometry optimization (Gaussian, Inc., Pittsburgh PA, 2003).

OFET devices fabrication and measurements

All FETs were fabricated employing the bottom-gate, bottom-contact architecture. The 200 nm thick SiO_2 dielectric covering the highly doped Si acting as the gate electrode was functionalized with hexamethyldisilazane (HMDS) to minimize interfacial trapping sites. Polymer thin films were deposited by spin-coating or drop-casting in different solutions with different concentrations (Mentioned in text) on FET substrates under nitrogen atmosphere, followed by annealing. The channel lengths and widths are 20 and 1400 μm, respectively. All the electrical measurements (using Keithley 4200 SCS) were performed in a glovebox under nitrogen atmosphere.

Organic Phototransistors (OPTs) fabrication and measurements

Bottom-gate bottom-contact architecture was utilized for devices. The source and drain electrodes with 60 nm in thickness were deposited by Au evaporation. Before measurement, annealing at 180 ^{o}C was carried out to remove residual solvent. A Keithley 4200-SCS was used for all electrical measurements in a glovebox under nitrogen atmosphere. The white light of a Nikon microscope (SMZ1000, ~15 mW cm^{-2}) was directly used for irradiation.

OPV devices fabrication and measurements

The photovoltaic devices were prepared using the common fabrication process. The active layer was deposited by spin-coating a solution of the donor-acceptor mixture onto indium thin oxide (ITO) glass substrates, which were precoated with poly(ethylenedioxythiophene) doped with polystyrene sulfonic acid (PEDOT:PSS, a conducting polymer); then a typically 100 nm thick Al layer was vapor deposited onto the active layer. The photovoltaic response of the device was determined using an AM 1.5G standard, operating with an illumination intensity of 100 mW cm^{-2}.

X-ray diffraction

Film X-ray diffraction was performed on a theta-theta Philips PW 1820 Kristalloflex diffractometer with a graphite-monochromized Cu-Kα X-ray beam (Cu Kα, λ = 1.5418 Å)hitting the thin film deposited as described in each case. The diffraction patterns were recorded in the 2θ range from 0 to 30.

Two-dimensional wide-angle X-ray scattering

2DWAXS measurements were performed using a custom setup consisting of the Siemens Kristalloflex X-ray source (copper anode X-ray tube, operated at 35 kV/20 mA), Osmic confocal MaxFlux optics, two collimating pinholes (1.0 and 0.5 mm Owis, Germany) and an antiscattering pinhole (0.7 mm – Owis, Germany). The patterns were recorded on a MAR345 image plate detector (Marresearch, Germany). The samples were prepared by filament extrusion using a home-built mini-extruder.

Grazing incidence wide-angle X-ray scattering

GIWAXS measurements were performed using a custom setup consisting of rotating anode X-ray source (Rigaku Micromax). By orienting the substrate surface at or just below the critical angle for total reflection with respect to the incoming X-ray beam (~0.2°), scattering from the deposited film was maximized with respect to scattering from the substrate. The GIWAXS data were acquired using a camera comprising an evacuated sample chamber with an X-ray photosensitive image plate. A rotating Cu-anode operating at 42 kV and 20 mA (Cu Kα, λ = 1.5418 Å) was used as X-ray source, focused, and monochromatized by a 1D multilayer. Diffraction patterns were recorded on a MAR345 image plate detector.

Scanning force microscopy

The scanning force microscopy (SFM) analysis was performed in intermittent contact mode (MFP-3D, Asylum Research, Santa Barbara, USA). The SFM was operated in a glove box filled with dry N2 at room temperature. Silicon cantilevers (OMCL AC 240 TS, Olympus, Japan) with a nominal resonance frequency of 70 kHz and a spring constant of 2 N/m were used. All SFM images were flattened and analyzed by using the Gwyddion 2.30 software (http://gwyddion.net/).

References:

(1) Frisch, M. J. et al. Gaussian 03, Revision B.04: Gaussian, Inc., Pittsburgh PA, 2003.

(2) Becke, A. D. *J. Chem. Phys.,* **1993**, *98*, 5648-5652.

(3) Lee, C. T.; Yang, W. T.; Parr, R. G. *Phys. Rev. B,* **1988**, *37*, 785-789.

Appendix-III Crystallographic table

Compound	TIPS-APhTQ	TIPS-PhTQ	TIPS-BDTTQ
CCDC number	1035450	1035451	1035452
Chemical formula	$C_{40}H_{48}N_4Si_2S$	$C_{42}H_{50}N_4Si_2S$	$C_{38}H_{46}N_4Si_2S_3$
Formula Mass (g mol^{-1})	673.06	699.1	711.15
Crystal system	triclinic	triclinic	triclinic
Space group	$P\bar{1}$	$P\bar{1}$	$P\bar{1}$
Crystal size (mm^3)	$0.03 \times 0.14 \times 0.48$	$0.02 \times 0.19 \times 1.3$	$0.06 \times 0.18 \times 1.0$
a (Å)	7.818(7)	8.0002(14)	7.5790(10)
b (Å)	14.4719(2)	14.350(3)	14.4202(16)
c (Å)	18.6562(16)	17.786(3)	17.562(2)
α (°)	67.602(6)	105.315(4)	105.750(9)
β (°)	78.490(7)	93.718(5)	94.034(10)
γ (°)	82.794(7)	99.307(5)	90.134(10)
Z	2	2	2
Unit cell volume / Å^3	1909.4(3)	1931(1)	1842.2(4)
Temperature (°C)	-60	-100	-60
Absorption (mm^{-1})	0.18	0.18	0.300
Radiation	Mo-K$_a$	Mo-K$_a$	Mo-K$_a$
Diffractometer	STOE IPDS 2T	Smart CCD	STOE IPDS 2T
No. of reflections measured	19744	26315	19063
R$_{int}$	0.0792	0.0828	0.0961
wR2	0.1453	0.1637	0.2233
Goodness of fit	0.878	0.971	0.922

Compound	TIPS-PhNTQ	TIPS-BisPhNPQ
CCDC number	1054330	1054329
Chemical formula	$C_{40}H_{48}N_6Si_2S$, CH_2Cl_2	$C_{52}H_{54}N_8Si_2$
Formula Mass (g mol^{-1})	786.01	847.21
Crystal system	triclinic	triclinic
Space group	$P\bar{1}$	$P\bar{1}$
Crystal size (mm^3)	$0.03 \times 0.04 \times 0.6$	$0.05 \times 0.1 \times 0.45$
a (Å)	8.0609(14)	8.2898(8)
b (Å)	16.2948(11)	9.0365(8)
c (Å)	17.4620(12)	15.893(2)
α (°)	70.798(5)	84.845(8)
β (°)	85.053(6)	84.909(8)
γ (°)	82.202(6)	74.567(8)
Z	2	1
Unit cell volume / Å^3	2143.9(3)	1140.4(2)
Temperature (°C)	-80	-80
Absorption (mm^{-1})	2.63	0.12
Radiation	$C_u\text{-}K_a$	$Mo\text{-}K_a$
Diffractometer	IPDS 2T	STOE IPDS 2T
No. of reflections measured	25974	11788
R_{int}	0.1508	0.0501
wR2	0.3425	0.1386
Goodness of fit	1.805	0.981

List of Publications

1. **C. An**, S. R. Puniredd, X. Guo, T. Stelzig, Y. Zhao, W. Pisula and M. Baumgarten, Benzodithiophene−Thiadiazoloquinoxaline as an Acceptor for Ambipolar Copolymers with Deep LUMO Level and Distinct Linkage Pattern, *Macromolecules*, **2014**, *47*, 979-986.

2. **C. An**, M. Li, T. Marszalek, D. Li, R. Berger, W. Pisula and M. Baumgarten, Thiadiazoloquinoxaline-Based Low-Bandgap Conjugated Polymers as Ambipolar Semiconductors for Organic Field Effect Transistors, *Chem. Mater.*, **2014**, *26*, 5923-5929.

3. M. Li, **C. An**, W. Pisula and K. Müllen, Alignment of Organic Semiconductor Microstripes by Two-Phase Dip-Coating, *small*, **2014**, *10*, 1926–1931.

4. X. Guo, H. N. Tsao, P. Gao, D. Xia, **C. An**, M. K. Nazeeruddin, M. Baumgarten, M. Gratzel and K. Müllen, Dithieno[2,3-d;2',3'-d']benzo[1,2-b;4,5-b']-dithiophene based organic sensitizers for dyesensitized solar cells, *RSC Adv.,* **2014**, *4*, 54130–54133.

5. **C. An**, M. Li, T. Marszalek, X. Guo, W. Pisula and M. Baumgarten, Investigation of the structure–property relationship of thiadiazoloquinoxaline-based copolymer semiconductors via molecular engineering, *J. Mater. Chem. C*, **2015**, *3*, 3876—3881.

6. **C. An**, S. Zhou and M. Baumgarten, Condensed Derivatives of Thiadiazoloquinoxaline as Strong Acceptors, *Cryst. Growth Des.*, **2015,** *15*, 1934−1938.

7. M. Li, **C. An (co-first)**, T. Marszalek, X. Guo, Y.-Z. Long, H. Yin, C. Gu, M. Baumgarten, W. Pisula and K. Müllen, Phenanthrene Condensed Thiadiazoloquinoxaline Donor−Acceptor Polymer for Phototransistor Applications, *Chem. Mater.,* **2015**, *27*, 2218–2223.

8. S. Zhou, **C. An**, T. Stelzig, S. R. Puniredd, X. Guo, W. Pisula and M. Baumgarten, Strengthening the Acceptor Properties of Thiadiazoloquinoxalines via Planarization, *New J. Chem.*, **2015**, Doi: 10.1039/C5NJ00517E.

9. **C. An,** X. Guo and M. Baumgarten, A Highly Ordered Phenanthroline Fused Azaacene. (Submitted to **Crystal Growth & Design, 2015**).

10. **C. An**, T. Marszalek (co-first), X. Guo, S. R. Puniredd, W. Pisula and M. Baumgarten, Tuning Optoelectronic Properties of Dual-Acceptor Based Low-Bandgap Ambipolar Polymers by Thiophene-Bridge Length, *Polym. Chem.,* **2015**, revision.

11. M. Li, **C. An**, T. Marszalek, Y. Zheng, I. Lieberwirth, M. Baumgarten, K. Müllen and W. Pisula, Impact of interfacial microstructure on charge carrier transport in solution-processed organic field-effect transistors, *Nat. Commun.,* **2015**, revision.

Curriculum Vitae

Personal Details

Name: Cunbin An

E-mail: ancunbin2011@gmail.com

Date of birth: 11 November, 1985

Place of birth: Henan, China

Nationality: China

Marital status: Married

Education

September 2011 – May 2015: PhD studies, Max Planck Institute for Polymer Research, Mainz, Germany.

Research adviser: █████████████████

Group Director: █████████

September 2008 – July 2011: M.Sc. in Organic Chemistry, Department of Chemistry, Renmin University of China, Beijing, China.

Research adviser: █████████████████

Group Director: █████████████

September 2004 – July 2008: B.Sc. in Chemistry, Department of Chemistry, Zhengzhou University, Zhengzhou, China

Thesis adviser: █████████████

Awards and Fellowships

September 2011– September 2014: China Scholarship Council provided a 3-years-scholarship for PhD Study in Max-Planck Institute for Polymer Research, Germany.

September 2008 – July 2011: Renmin University of China offered a 3-years-scholarship for Master study.

September 2005 – July 2006 Outstanding young volunteer, Zhengzhou University.

Acknowledgments

First and foremost, I would like to express my sincere gratitude to ███████████ ████████, who gave me the unique opportunity to work in his research group and entrusted me with a very interesting and challenging research topic on synthesis of conjugated polymers. Furthermore, I really appreciate his continuous and kind support, inspiring and fruitful suggestions in my research, as well as careful corrections on my publications and thesis. Finally, I am very grateful for his big help besides the scientific work.

I also deeply acknowledge ████████████████, who allows me to join his unique research group and gave me many important scientific suggestions on quarterly reports.

My thanks go to:

████████████████ for prior developments of condensed TQ small molecules. She also provided some fruitful suggestions when I started this project.

██████████████ for prior developments of condensed TQ small molecules.

███████████████ for help in molecular devices and self-organization measurements.

████████████████████████ and ███████████████ for OFETs devices, 2DWAXs and GIWAXs measurements.

██████████████ for fabrication of OFETs and phototransistor devices.

██████████████ for fabrication of OPV devices.

████████████████ and ██████ for SPM measurements and discussion.

█████████████████████ for the single crystal X-ray measurements.

███████████████ for discussion and corrections on my publications.

██████████ for giving me many help, when I first came here.

██████████ and ██████████ for GPC measurements.

██████████ for the out-of-plane X-ray measurements.

████████ for TGA and DSC measurements.

████████ for technical support in the lab.

████████ and ██████████ for 500 and 700 MHz NMR measurements.

I would like to thank all my past and present colleagues ████████████████████ ████████████████ for exciting discussions, encouragements, and creating first-class working environment.

Finally, I want to express my very cordial gratitude to my parents, my parents in law, my wife and my daughter for their endless encouragement and all kinds of support.